



Mathematisch-Naturwissenschaftliche Fakultät

**Role of the Rab GTPase activating proteins
TBC1D1 and TBC1D4 in the regulation of
skeletal muscle fatty acid metabolism**

Inaugural-Dissertation

zur Erlangung des Doktorgrades
der Mathematisch-Naturwissenschaftlichen Fakultät
der Heinrich-Heine-Universität Düsseldorf

vorgelegt von

Tim Benninghoff

geboren am 06. März 1986 in Duisburg

Düsseldorf, März 2019

Aus dem Institut für Klinische Biochemie und Pathobiochemie
des Deutschen Diabetes-Zentrums,
Leibniz-Zentrum für Diabetesforschung
an der Heinrich-Heine-Universität Düsseldorf

Gedruckt mit der Genehmigung der
Mathematisch-Naturwissenschaftlichen Fakultät der
Heinrich-Heine-Universität Düsseldorf

Berichtersteller:

1. Prof. Dr. Hadi Al-Hasani
2. Prof. Dr. Michael Feldbrügge

Tag der mündlichen Prüfung: 05.12.2019

Table of Contents

Table of Contents	III
Summary	VIII
Zusammenfassung	IX
1 Introduction	1
1.1 <i>Diabetes mellitus</i>	1
1.1.1 Type 1 <i>diabetes mellitus</i> (T1DM).....	1
1.1.2 Obesity, insulin resistance, type 2 <i>diabetes mellitus</i> (T2DM) and the role of skeletal muscle tissue	2
1.2 Skeletal muscle anatomy, development and energy metabolism.....	3
1.2.1 Skeletal muscle insulin signaling, GLUT4 translocation and glucose metabolism	4
1.2.2 Skeletal muscle lipid metabolism.....	6
1.2.2.1 Regulated uptake of long-chain fatty acids	7
1.2.2.2 Regulated uptake of long-chain fatty acids	9
1.3 Fatty acid metabolism, lipid accumulation and <i>diabetes mellitus</i>	10
1.3.1 Metabolic flexibility and fuel selection.....	11
1.3.2 Lipid accumulation, ectopic lipid deposition and <i>diabetes mellitus</i>	12
1.4 Genes involved in regulating skeletal muscle fatty acid metabolism.....	14
1.4.1 Genes regulating fatty acid uptake	15
1.4.2 Genes involved in regulating lipid degradation and biosynthesis	15
1.4.3 Genes encoding for skeletal muscle transcription factors	15
1.4.4 Genes with implications in mitochondrial energy metabolism	15
1.4.5 Lipid droplet formation and lipid storage associated genes.....	16
1.5 Small Rab GTPases	16
1.5.1 Small Rab GTPases in vesicle trafficking with relation to energy metabolism.....	17
1.6 Rab GTPase activating proteins (RabGAP)	18
1.6.1 TBC1D1 and TBC1D4/AS160 as prominent RabGAPs in energy metabolism.....	18
1.6.2 Impact of <i>Tbc1d1</i> - and <i>Tbc1d4</i> -deficiency on skeletal muscle lipid metabolism	19
1.6.3 RabGAPs and the link to human metabolic phenotypes and diseases.....	20
2 Aim of the current study	22

3	Material and Methods	24
3.1	Material	24
3.1.1	Animal experiments	24
3.1.1.1	Experimental animals	24
3.1.1.2	Animal housing.....	24
3.1.2	Cell culture experiments	25
3.1.2.1	C2C12 myoblast cell line.....	25
3.1.3	Chemicals.....	25
3.1.4	Radiochemicals	26
3.1.5	Reaction kits	27
3.1.6	Machines and Devices	27
3.1.7	Software	29
3.1.8	Buffers, Culturing Media and Solutions	29
3.1.9	siRNA oligonucleotides.....	30
3.1.10	Western Blot Antibodies	31
3.1.11	Disposable material	31
3.1.12	qRT-PCR (quantitative real-time PCR) primers.....	32
3.1.13	Genotyping primers	35
3.2	Methods.....	35
3.2.1	Animal experimental methods	35
3.2.1.1	<i>In vivo</i> electrotransfection (IVE)	36
3.2.1.2	<i>Ex vivo</i> fatty acid uptake assay	37
3.2.1.3	<i>Ex vivo</i> fatty acid oxidation assay.....	38
3.2.1.4	<i>Ex vivo</i> determination of skeletal muscle malonyl-CoA and acetyl-CoA levels	38
3.2.2	Cell culture experiments	39
3.2.2.1	Cell culture of C2C12 myoblasts.....	39
3.2.2.1.1	Freezing, thawing and maintaining of C2C12 cells	40
3.2.2.1.2	Chemical siRNA transfection.....	41
3.2.2.2	<i>In vitro</i> assays	42
3.2.2.2.1	<i>In vitro</i> fatty acid uptake assay	42
3.2.2.2.2	<i>In vitro</i> fatty acid oxidation assay	42
3.2.3	Methods of molecular biology	44
3.2.3.1	Isolation of genomic DNA from mouse tail tips.....	44
3.2.3.2	Determination of nuclei acid concentration	45
3.2.3.3	Genotyping of experimental animals	45

3.2.3.4	Agarose gel electrophoresis.....	47
3.2.4	Biochemical methods	47
3.2.4.1	Protein isolation from cell culture and isolated murine skeletal muscle samples	47
3.2.4.2	Determination of protein concentration	47
3.2.4.3	Western Blot analysis.....	48
3.2.4.3.1	Sample preparation and SDS-polyacrylamide gel electrophoresis.....	48
3.2.4.3.2	Tank Western Blotting and protein detection	49
3.2.4.4	GC-analysis of skeletal muscle fatty acid composition.....	49
3.2.4.4.1	GC data analysis and calculations	50
3.2.4.5	Gene expression analysis	53
3.2.4.5.1	RNA isolation.....	53
3.2.4.5.2	cDNA synthesis	54
3.2.4.5.3	Quantitative real-time PCR (qRT-PCR).....	54
3.2.5	Statistical analysis	55
4	Results	57
4.1	Impact of RabGAPs TBC1D1 and TBC1D4/AS160 on fatty acid uptake in C2C12 myotubes	57
4.1.1	C2C12 myotube differentiation status.....	57
4.1.2	Palmitic acid uptake into C2C12 myotubes after siRNA-mediated <i>Tbc1d1</i> and <i>Tbc1d4</i> knockdown	58
4.2	Impact of RabGAPs TBC1D1 and TBC1D4/AS160 on C2C12 skeletal muscle cell fatty acid oxidation	60
4.3	Lipid substrate specificity of the TBC1D1 and TBC1D4 effect on C2C12 myotube fatty acid uptake	60
4.3.1	Impact of TBC1D1 and TBC1D4 on the uptake of short-chain and unsaturated long-chain fatty acids in C2C12 skeletal muscle cells	61
4.4	Expression analysis of genes involved in skeletal muscle mitochondrial biogenesis, lipid metabolism and vesicle trafficking under <i>Tbc1d1</i> knockdown conditions in C2C12 myotubes.....	62
4.4.1	Validation of <i>Tbc1d1</i> knockdown specificity after transfection with <i>Tbc1d1</i> -targeting siRNA	63
4.4.2	Analysis of mRNA expression of genes involved in fatty acid binding and uptake under <i>Tbc1d1</i> knockdown conditions in C2C12 myotubes	63
4.4.3	Analysis of mRNA expression of genes involved in lipid degradation and biosynthesis under <i>Tbc1d1</i> knockdown conditions in C2C12 myotubes	64

4.4.4	Analysis of mRNA expression of transcriptional regulator genes under <i>Tbc1d1</i> knockdown conditions in C2C12 myotubes	65
4.4.5	Analysis of mRNA expression of genes implicated in mitochondrial energy metabolism under <i>Tbc1d1</i> knockdown conditions in C2C12 myotubes	66
4.4.6	Analysis of mRNA expression of genes encoding for proteins involved in lipid storage and lipid droplet formation under <i>Tbc1d1</i> knockdown conditions in C2C12 myotubes	67
4.4.7	Analysis of mRNA expression of genes encoding for direct targets of TBC1D1 under <i>Tbc1d1</i> knockdown conditions in C2C12 myotubes	68
4.5	Analysis of the influence of TBC1D1 deficiency on the fatty acid profile of mouse skeletal muscle	69
4.5.1	Total fatty acid content of <i>Gastrocnemius</i> muscle from wildtype and D1KO mice.....	69
4.5.2	Fatty acid profile of wildtype and <i>Tbc1d1</i> -deficient <i>Gastrocnemius</i> muscles.....	70
4.5.3	Fraction differences of fatty acid species classes with regard to saturation grade between wildtype and <i>Tbc1d1</i> -deficient mouse skeletal muscles.....	71
4.5.4	FA-desaturation activities in WT and <i>Tbc1d1</i> -deficient mouse <i>Gastrocnemius</i> muscles.....	72
4.5.5	FA elongation and elongase indexes of WT and TBC1D1 KO mouse <i>Gastrocnemius</i> muscles.....	74
4.5.6	Thioesterase and <i>de novo</i> lipogenesis indexes of WT and TBC1D1 KO mouse <i>Gastrocnemius</i> muscles.....	74
4.6	Malonyl- and acetyl-CoA levels of wildtype and <i>Tbc1d1</i> -deficient <i>Gastrocnemius</i> muscles	75
4.7	Role of Rab GTPases as protein downstream targets of TBC1D1 and TBC1D4 in <i>in vitro</i> C2C12 myotube fatty acid uptake	76
4.7.1	FA elongation and elongase indexes of WT and TBC1D1 KO mouse <i>Gastrocnemius</i> muscles.....	76
4.7.2	Impact of distinct Rab GTPases on <i>in vitro</i> fatty acid uptake in C2C12 myotubes	77
4.7.3	Impact of insulin-stimulation on C2C12 myotube fatty acid uptake (FAU) after independent single silencing of <i>Rab8a</i> , <i>Rab10</i> and <i>Rab14</i>	79
4.8	The Role of Rab GTPases as protein downstream targets of TBC1D1 and TBC1D4 in <i>ex vivo</i> mouse <i>EDL</i> and <i>Soleus</i> muscle fatty acid oxidation	80
4.8.1	Role of Rab8a in <i>ex vivo</i> <i>EDL</i> and <i>Soleus</i> fatty acid oxidation (FAO)	81

4.8.2	Role of Rab10 in <i>ex vivo</i> EDL and Soleus fatty acid oxidation (FAO)	82
4.9	Role of fatty acid transport proteins FATP1, FATP4 and FAT/CD36 in fatty acid uptake (FAU) in C2C12 myotubes	83
4.10	TBC1D1 and its influence on the expression of fatty acid metabolism-relevant proteins	84
4.10.1	Influence of <i>Tbc1d1</i> -deficiency on FATP4, PDK4 and FAT/CD36 protein expression in mouse EDL muscles under palmitate stimulation	85
4.10.2	Influence of <i>Tbc1d1</i> -deficiency on FATP4, PDK4 and FAT/CD36 protein expression in mouse EDL muscles under fasting and refeeding conditions	87
4.11	The connection of TBC1D1 and TBC1D4 with the fatty acid translocase FAT/CD36 in <i>ex vivo</i> skeletal muscle fatty acid uptake (FAU)	89
4.12	Interplay of TBC1D1, TBC1D4 and FATP4 with regard to C2C12 myotube fatty acid uptake.....	90
5	Discussion	92
5.1	TBC1D1 and TBC1D4 regulate skeletal muscle fatty acid metabolism, depending on fatty acid chain length, by promoting fatty acid transport protein translocation, but also by altering gene expression.....	92
5.2	<i>Tbc1d1</i> -deficiency has an influence on skeletal muscle cell lipid composition, lipid processing, but not lipid storage and the content of the AMPK-malonyl-CoA signaling axis for β -oxidation	97
5.3	Small Rab GTPases as direct downstream targets of TBC1D1 and TBC1D4 have a direct impact on skeletal muscle cell fatty acid metabolism	101
5.3.1	FATP4, rather than CD36 is mainly responsible for the observed lipid-preferring metabolic switch caused by <i>Tbc1d1</i> -deficiency in skeletal muscle	104
5.4	Conclusion and Outlook	107
6	Literature.....	110
7	Appendix.....	135
7.1	Index of figures	135
7.2	Index of tables	138
7.3	Abbreviations.....	139
7.4	Contribution to publications	143
7.5	Acknowledgements	145
	Eidesstattliche Erklärung.....	146

Summary

Metabolic flexibility is a key feature of skeletal muscle tissue to adapt to changing energy demands and substrate availability. The Rab GTPase-activating protein (RabGAP) TBC1D1 has previously been described to play a critical role in skeletal muscle and whole-body lipid and glucose metabolism, respectively. *Tbc1d1*-deficient mice exhibit a disturbed glucose uptake into skeletal muscle under insulin-stimulated conditions and after exposure to the AMPK activator AICAR (5-aminoimidazole-4-carboxamide-1- β -D-ribofuranoside). In addition, both, *in vivo* lipid utilization as well as fatty acid uptake and oxidation in skeletal muscle cells are enhanced upon *Tbc1d1*-deficiency. Thus, it was concluded that TBC1D1 represents a molecular switch between glucose and lipid utilization, primarily acting in the skeletal muscle.

In the present study, it could be demonstrated that TBC1D1 and its closely related RabGAP TBC1D4 (= AKT substrate of 160 kDa, AS160) mediate their metabolic action by directly regulating the activity of small Rab GTPases in skeletal muscle cells. Knockdown of the previously described RabGAP downstream targets *Rab8a*, *Rab8b*, *Rab10*, *Rab14* and *Rab40b* in C2C12 myotubes resulted in decreased long-chain-fatty acid uptake. Moreover, data obtained in isolated murine skeletal muscles and cultivated C2C12 myotubes indicated that the RabGAP-mediated processes are predominantly dependent on changes in the translocation of fatty acid transport protein FATP4. Besides the direct impact of TBC1D1 and TBC1D4 on skeletal muscle lipid metabolism, additional indirect alterations of skeletal muscle physiology could be shown. *Tbc1d1*-depleted C2C12 myotubes exhibit increased mRNA expression of *Fatp4* and pyruvate dehydrogenase kinase 4 (*Pdk4*), and FATP4 as well as PDK4 protein abundance is increased in skeletal muscle from *Tbc1d1*-deficient mice. In addition, investigation of skeletal muscle lipid composition reveals alterations of lipid distribution and potentially activity of key enzymes responsible for the cellular lipid composition.

Further studies will focus on the mechanisms underlying the molecular connection between RabGAP action and expression as well as activity of enzymes controlling lipid metabolism in skeletal muscle and, as a consequence, whole-body energy metabolism.

Zusammenfassung

Metabolische Flexibilität ist eine besondere Eigenschaft von Skelettmuskelgewebe, um sich an einen verändernden Energiebedarf, sowie an eine sich verändernde Energiesubstratverfügbarkeit anzupassen. Für das Rab GTPase-aktivierende Protein (RabGAP) TBC1D1 konnte gezeigt werden, dass es eine entscheidende Rolle im Lipid- und Glukosestoffwechsel, sowohl von Skelettmuskeln, als auch des gesamten Körpers, spielt. Mäuse mit einer *Tbc1d1*-Defizienz weisen eine gestörte Glukoseaufnahme in Skelettmuskeln nach Insulinstimulation, sowie nach Stimulation mit dem AMPK-Aktivator AICAR (5-Aminoimidazol-4-Carboxyamid-1- β -D-Ribofuranosid) auf. Darüber hinaus sind sowohl der in vivo Fettverbrauch, als auch die Aufnahme und Oxidation von Fettsäuren in Skelettmuskelzellen unter *Tbc1d1*-defizienten Bedingungen erhöht. Daraus wurde geschlussfolgert, dass TBC1D1 vornehmlich in Skelettmuskeln als molekularer Schalter zwischen Glukose- und Fettstoffwechsel fungiert.

In der vorliegenden Studie konnte gezeigt werden, dass sowohl TBC1D1, als auch dessen nahe verwandtes RabGAP TBC1D4 (= AKT Substrate of 160 kDa, AS160) ihre Wirkung auf den Stoffwechsel von Skelettmuskelzellen durch eine direkte Regulation der Aktivität von kleinen Rab GTPasen vermitteln. Ein *siRNA*-vermittelter Knockdown von bereits bekannten Substraten der RabGAPs TBC1D1 und TBC1D4 aus der Familie der kleinen Rab GTPase *Rab8a*, *Rab8b*, *Rab10*, *Rab14* und *Rab40b* in differenzierten C2C12 Skelettmuskelzellen führte zu einer Verminderung der Aufnahme langkettiger Fettsäuren. Darüber hinaus lassen Ergebnisse aus Versuchen an isolierten murinen Skelettmuskeln und kultivierten C2C12 Skelettmuskelzellen darauf schließen, dass die RabGAP-vermittelten Veränderungen des Fettstoffwechsels vornehmlich auf eine veränderte Translokation des Fettsäuretransportproteins 4 (FATP4) zurückzuführen sind. Neben einem direkten Einfluss von TBC1D1 und TBC1D4 auf den Fettstoffwechsel von Skelettmuskelzellen konnten auch indirekt vermittelte Veränderungen der Muskelphysiologie nachgewiesen werden. In differenzierten C2C12 Myotuben führt eine *siRNA*-vermittelte Reduktion von *Tbc1d1* zu einer verstärkten mRNA-Expression von *Fatp4* und der Pyruvatdehydrogenasekinase 4 (*Pdk4*). Darüber hinaus weisen Skelettmuskeln von *Tbc1d1*-defizienten Mäusen eine verstärkte Proteinexpression von FATP4 und PDK4 auf. Zusätzlich konnte durch Untersuchungen des Lipidprofils von murinen Skelettmuskeln gezeigt werden, dass sich die Zusammensetzung von Fettsäuren in Abhängigkeit von TBC1D1 verändert, möglicherweise durch eine veränderte Aktivität von Enzymen der Lipidprozessierung.

Weiterführende Untersuchungen sollen sich auf den Mechanismus konzentrieren, der der Verbindung von RabGAP-Effekten und der Expression und Aktivität von Enzymen zugrunde liegt, die den Lipidstoffwechsel von Skelettmuskeln und letztendlich den Energiestoffwechsel des gesamten Körpers beeinflussen.

1 Introduction

1.1 *Diabetes mellitus*

Diabetes mellitus is defined as a group of metabolic disorders that result from a diverse etiology (WHO, 2016) and which are essentially characterized by chronic hyperglycemia, disturbances in carbohydrate, lipid and protein metabolism. These defects either derive from a defective secretion of the peptide hormone insulin, defective insulin action, or a combination of both (ADA, 2016).

Common secondary complications of manifested *Diabetes mellitus* are microvascular diseases such as retinopathy, neuropathy and nephropathy, as well as macrovascular defects such as atherosclerosis (Gibbons & Goebel-Fabbri, 2017). With regard to the cause of the manifestation of Diabetes, a general differentiation into Type 1 and Type 2 *Diabetes mellitus*, gestational *Diabetes* and other specific forms of *Diabetes* has been defined. However, over the years, more complexity has been added to the distinct classifications of *Diabetes*, distinguishing a) monogenic *Diabetes*, which itself summarizes a large subset of causes deriving from single nucleotide mutations at distinct loci, b) drug – associated *Diabetes* and other disease-associated *Diabetes*-causing events (e.g. cystic fibrosis, pancreatitis) (Thomas & Philipson, 2015), and c) polygenic *Diabetes* that is a result of a combination of multiple coding allelic variants of several genes (Langenberg & Lotta, 2018; Sharp et al., 2018). *Diabetes* is nowadays seen as a global health burden with growing economical meaning, since the general *Diabetes* prevalence was predicted to increase from 177 million affected people in the year 2000 to estimated 366 people suffering from the disease worldwide in the year 2030 (Wild et al. 2004). These numbers estimated in 2004 had to be raised as the *World Health Organization* (WHO) reported already 422 million people with *Diabetes* worldwide in the year 2014 (WHO, 2016).

1.1.1 Type 1 *diabetes mellitus* (T1DM)

Type 1 *diabetes mellitus* accounts for approximately 5–10 % of all cases of Diabetes (ADA, 2010, 2016). It is considered a T-cell associated autoimmune disease that is characterized by a primary loss of insulin-secreting β -cells within the pancreatic islets of Langerhans (Eiselein et al., 2004). As a consequence, people affected by Type 1 *Diabetes mellitus* suffer from an absolute lack of insulin due to the proceeding loss of insulin-secreting cells (Precechtelova et al., 2014). It has been reported that the manifestation of the disease occurs at a stage of approximately 90 % of β -cell loss and at an average age of 14 years (Eiselein et al., 2004). People suffering from this type of *Diabetes* depend on a lifelong gavage of exogenous insulin to compensate for the absolute lack of endogenous insulin. Besides an inherited genetic predisposition for developing T1DM, environmental factors and virus infections can also

contribute to the onset of the disease (Craighead, 1978; van Belle et al., 2011; Van Belle et al., 2010).

1.1.2 Obesity, insulin resistance, type 2 *diabetes mellitus* (T2DM) and the role of skeletal muscle tissue

Peripheral insulin resistance is a physiological disturbance that is characterized by an improper reaction of insulin-sensitive tissues such as skeletal muscle, adipose tissue and liver to physiological insulin concentrations. Thus, insulin resistance is accompanied by impaired glucose uptake into these tissues and consequently super-physiological levels of glucose in the blood. It is a major predictor for the development of T2DM (Lillioja et al., 1993). Obesity is strongly associated with the development of type 2 diabetes, as obesity can induce insulin resistance. In 2008, the WHO stated that worldwide 35 % of the adults older than 20 were overweight defined by a *Body Mass Index* (BMI) greater than 25 kg/m². Further, it was reported that more than 500 million people over 20 years of age were considered as being obese (BMI > 30 kg/m²). Since approximately 90 % of patients suffering from Type 2 diabetes are found to be overweight or obese, body weight may be a major contributing factor to onset and development of the disease (Hossain et al., 2007; Whitmore, 2010). Obesity is a result of excessive accumulation of fat primarily in adipose tissue. The adipose tissue plays a central role in the development of insulin resistance. Adipokines as well as free fatty acids released from the adipose cells have the ability to interfere with normal insulin signaling resulting in an impaired response of insulin-target tissues (e.g. skeletal muscle, liver), followed by hyperglycemia and hyperinsulinemia (Holland et al., 2007; Schenk et al., 2008). Obesity also leads to adipose tissue macrophage infiltration. The resulting inflammation can also contribute to the development of insulin resistance and T2DM (Weisberg et al., 2003; Xu et al., 2003). Additionally, the ectopic accumulation of lipids in non-adipose tissues may contribute to disturbances in insulin signaling and glucose clearance (Larson-Meyer et al., 2011; Samuel & Shulman, 2016). In recent years the term “diabesity” was used to stress the linkage between obesity and the development of type 2 diabetes mellitus (Chadt et al., 2018; Kalra, 2013). However, it needs to be said that only a small portion of obese and insulin resistant patients develop diabetes (Chadt et al., 2018).

Hyperglycemia as main consequence of insulin resistance due to an impaired uptake of glucose from the blood into insulin-target tissues leads to increased insulin production by pancreatic β -cells that ultimately causes β -cell hyperplasia, failure and retrogression. The concept of glucose toxicity was established in this context due to the cytotoxic effects of hyperglycemia on the functionality and viability of pancreatic β -cells.

The majority of diabetic patients suffer from the type 2 form of the disease (90-95 %). Nevertheless, since only a low percentage of obese, insulin resistant people develop diabetes

mellitus, there need to exist several other factors to take into consideration in order to explain the diabetes manifestation. The onset and development of T2DM and the pathophysiological progression of the malady seem to involve genetic, epigenetic and environmental factors (e.g. lifestyle, nutrition, physical activity) (Prasad & Groop, 2015). The combination of a mono- or polygenic predisposition in combination with risk factors such as obesity, increased blood pressure, super physiological levels of triglycerides, fasting plasma glucose or high-density lipoproteins (HDL) drives the processing of T2DM (Lebovitz, 1999; Y. Wu et al., 2014).

1.2 Skeletal muscle anatomy, development and energy metabolism

Skeletal muscle tissues account for about 35-40 % of total body weight in humans (Janssen et al., 2000; Zurlo et al., 1990). It represents the largest organ in the human body (Pedersen, 2013). Due to the complex nature of the muscle, the following paragraph will present a brief summary on muscle development and muscle organization from the single cell to a multi-layer organ. Development of skeletal muscles begins with embryonic mesenchymal cells that differentiate into mononucleated myoblasts (Kim et al. 2015). These myoblasts aggregate and fuse with each other to become multinucleated myotubes with centralized nuclei. The syncytial myotubes increase their length by further fusing with myoblasts (Gerhart et al., 2006). With the appearance of muscle-specific proteins such as myosin and actin, the myotubes become myofibrils (Demonbreun et al., 2015; Yasa et al., 2015). The formerly centralized nuclei become located to the periphery of the myofibril (Mitchell et al., 2010). The presence of actin and myosin leads to the striated pattern that is characteristic for skeletal muscles. Myofibrils contain the protein machinery that is responsible for muscle contraction. This structure is known as myofilament. Several myofilaments arranged in parallel form the myofibrils (Ottenheijm & Granzier, 2010). The fibrils are surrounded by a network of the muscle cell-specific sarcoplasmic reticulum (Lamboley et al., 2014). Several myofibrils are bundled and connected by the intermediate filament desmin to form a muscle fiber. The myofibrils are surrounded by the sarcoplasm in which mitochondria and other cellular structures are located. The nuclei of the muscle cell syncytium are located in the periphery of the muscle fibers.(Greising et al., 2012). A single muscle fiber is surrounded by a muscle-specific cell membrane named sarcolemma. The sarcolemma is covered with a basal lamina that builds tubular structures (T-tubules) orthogonal to the longitudinal axis of the muscle cells. These T-tubules stand in contact with the sarcoplasmic reticulum and are involved in the calcium ion influx that is important for regulating muscle cell contraction (Jayasinghe & Launikonis, 2013; Jayasinghe et al., 2013). Several bundles of muscle fibers, the so-called muscle fascicles in parallel build up the muscle as physiological and anatomic macro structure. Skeletal muscles are connected to bones by

tendons. These tendons transduce the contractive energy produced by the muscle into movement of the bone (Zierath & Hawley, 2004).

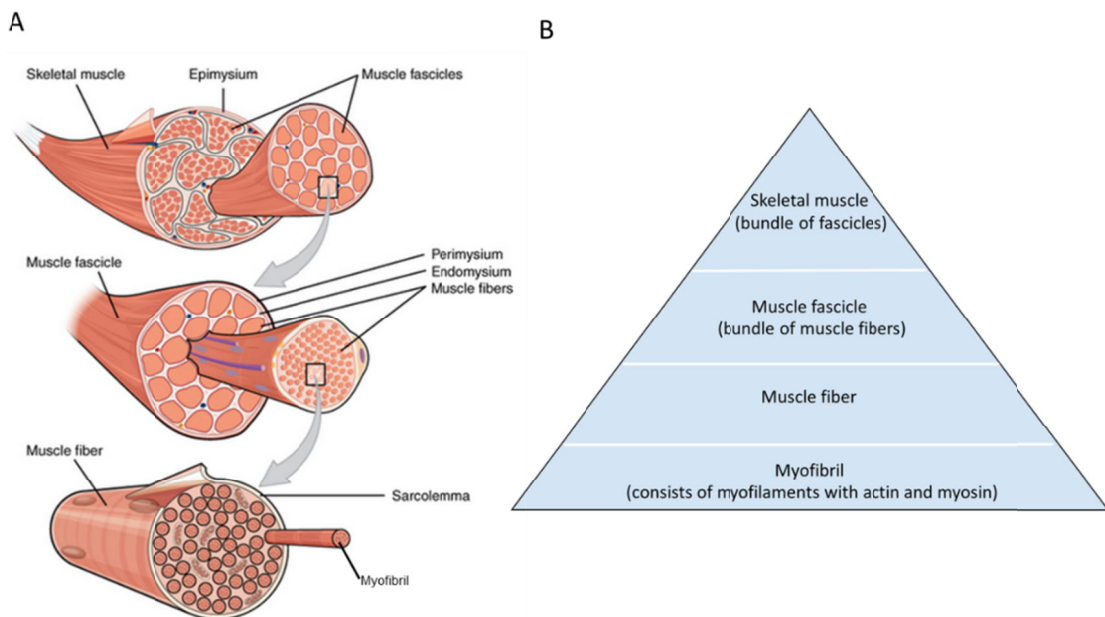


Figure 1: Structural composition of skeletal muscles. Schematic overview of skeletal muscle anatomy (A) and muscle subunit hierarchy (B). Skeletal muscle consists of a complex set of functional subunits, beginning with the myofilaments that build up the myofibril. A bundle of myofibrils is surrounded by the sarcolemma and named muscle fiber. Muscle fibers are surrounded by the endomysium and bundled by an external layer of perimysium to create a muscle fascicle. Several fascicles together are collectively bundled and surrounded by the epimysium to create a skeletal muscle. Figure modified after <https://opentextbc.ca/anatomyandphysiology/chapter/10-2-skeletal-muscle>.

The main energy substrates for skeletal muscle cells are glucose and fatty acids (Kraegen et al., 2008). It was reported that skeletal muscles are the main sink of the body for both, glucose and lipids (Minokoshi et al., 2012; Morales et al., 2017). Data suggest in terms of glucose that skeletal muscle is responsible for 25 % of glucose clearance from the blood plasma under basal and fasting conditions (Cersosimo et al., 2000) and 70-85 % in the postprandial state (DeFronzo et al., 1981; Ferrannini et al., 1985). The uptake and metabolism of energy substrates are highly conserved and tightly regulated cellular processes.

1.2.1 Skeletal muscle insulin signaling, GLUT4 translocation and glucose metabolism

Glucose and fatty acids are seen as the main energy source for skeletal muscle. After food intake the majority of glucose circulating in the blood is taken up by skeletal muscle, and, to a lower extent by adipose tissue and liver. To clear glucose from the bloodstream proteins from a family of 14 facilitative glucose transporters (GLUTs) are engaged, that selectively allow the transport mainly of glucose through an ATP-independent diffusion mechanism from the blood into target tissue cells (Hruz & Mueckler, 2001; Mueckler & Thorens, 2013). Only a few

members of the GLUT family exhibit different or additional transportation specificities: GLUT1 and GLUT3 were shown to transport glucose and dehydroascorbic acid (Rumsey et al., 1997), GLUT2 can transport glucose and also mannose, fructose and galactose, however with a low affinity (Mueckler & Thorens, 2013). GLUT5 was reported to possess a specifically high affinity for fructose (Burant et al., 1992). Among the members of the GLUT family, GLUT4 is reported to be the only transport protein that shows a sequestration in intracellular storage compartments and at the cell surface membrane. The supply of skeletal muscle and other insulin-sensitive tissues with glucose involves the facilitative transport protein GLUT4 (Capilla et al., 2010). It is postulated that under basal conditions about 5 % of total GLUT4 in a cell are located at the cell surface to promote a constant uptake of glucose from the extracellular space into the cell. The majority (95 %) of the GLUT4 transporters have been described to reside in an endosomal storage compartment within the cell. Under unstimulated conditions, there is a constant and slow translocation and internalization of GLUT4 molecules between the storage site and the cell surface.

Elevated postprandial blood glucose levels are sensed by the pancreas that in turn secretes insulin. Insulin binds to its receptor at the membrane of insulin-sensitive cells and initiates a signaling cascade. Especially skeletal muscle cells are to consider in terms of insulin-stimulated glucose disposal, as these cells account for approximately 60-80 % of the increase in glucose uptake after insulin signaling (Ng et al., 2012). This insulin cascade involves a series of consecutive phosphorylation events of the insulin receptor substrate (IRS), phosphatidylinositol-3-kinase (PI3K), and 3-phosphoinositide-dependent protein kinase 1 (PDK1), which causes the phosphorylation and activation of AKT (also known as protein kinase B) and results in the promotion of an acceleration of GLUT4-containing vesicle exocytosis and an accumulation of approximately 20-50 % of GLUT4 at the cell surface while 50-80 % remain at the storage site (Stockli et al., 2011; Wieringa et al., 2012). This is the reason why GLUT4 is seen as insulin-responsive GLUT (Wasik & Lehtonen, 2018). Besides insulin, physical activity in the form of muscle contraction also leads to the translocation of GLUT4-containing vesicles towards the cell surface. The contraction-induced GLUT4 trafficking is not mediated by AKT phosphorylation, but in part by the phosphorylation of AMP-activated protein kinase (AMPK) (Richter & Hargreaves, 2013). It has also been published that there may exist an alternative mechanism for contraction-stimulated GLUT4 translocation, because even without functional AMPK Mu and colleagues could monitor GLUT4 trafficking (Mu et al., 2001) A model for insulin signaling and insulin- and contraction-stimulated GLUT4 translocation is depicted in Fig. 2. The translocation of GLUT4 has been studied extensively and has not been revealed completely yet. After the clearance of glucose from the blood, insulin levels drop and an increased internalization of GLUT4 occurs until the basal status is reset.

Glucose in the muscle becomes phosphorylated by hexokinase IV (glucokinase) before it enters glycolysis, or is being stored as energy reserve in the form of glycogen. Pyruvate

generated by glycolysis is then further metabolized in the mitochondria by the pyruvate dehydrogenase complex (PDC) to generate acetyl-CoA that is then used in the Krebs cycle to generate substrates for the respiratory chain.

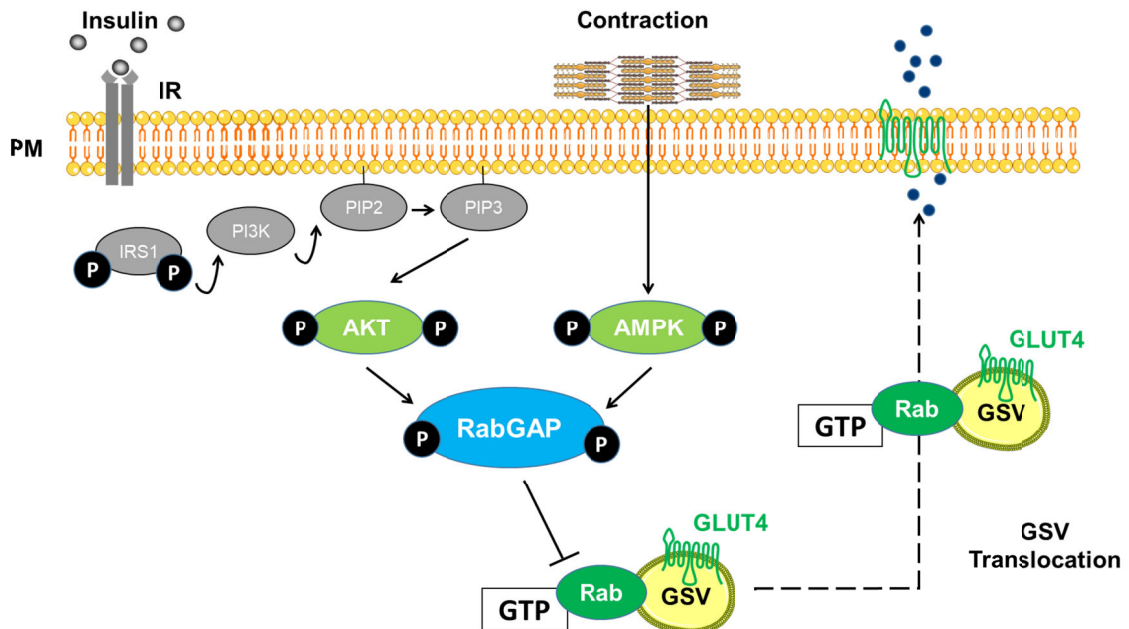


Figure 2: Model representation of insulin signaling and insulin- and contraction induced GLUT4 translocation. Upon physiological stimulation via insulin or muscle cell contraction insulin binds the insulin receptor (IR) which in turn induces a phosphorylation cascade that finally leads to the activation of AKT. Muscle contraction leads to a phosphorylation-driven activation of AMPK. The contraction and insulin-signaling pathway converge at the level of the Rab GTPase-activating proteins (RabGAP), independently cause its phosphorylation and lead to the inactivation of the GAP. The GAP can no longer act on downstream Rab GTPases which leads to an increase in activated (GTP-bound) Rab proteins. These active Rabs interact with glucose transporter storage vesicles (GSV) and promote their translocation towards the cell surface where the vesicles fuse with the plasma membrane (PM) and cause an accumulation of GLUT4. This in turn endorses cellular glucose uptake. IRS: insulin receptor substrate, PI3K: phosphatidylinositol-3-kinase, PIP2: Phosphatidylinositol 4,5-bisphosphate, PIP3: Phosphatidylinositol (3,4,5)-trisphosphate

1.2.2 Skeletal muscle lipid metabolism

Besides glucose, lipids are of great importance for maintaining energy supply (Eaton, 2002; Sylow et al., 2017). The biggest proportion of dietary lipids consists of triglycerols (TG). Triglycerols can be stored in adipose tissue and, to a smaller extend, in skeletal muscle, liver and other tissues. After ingestion, hydrophobic lipids become emulsified by bile acids (Albaugh et al., 2017). In the small intestine, pancreatic lipase cleaves TAGs into free fatty acids (FFA), glycerol, and monoacylglycerols (MAG). Enterocytes resorb the pancreatic lipase products. Inside the intestinal epithelial cells, a re-synthesis of TAGs takes place. The TAGs are then sequestered with apolipoproteins to chylomicrons that are delivered into the blood stream via lymphatic vessels and transported to their respective target, such as muscle and adipose tissue. Endogenously produced and secreted very low density lipoproteins (VLDL) that also contain

triglycerides represent also an energy source for muscle and fat tissue. Lipoprotein lipases (LPL) located at the endothelial surface of blood vessels in muscle and fat tissue catalyze hydrolysis of triglycerides from lipoproteins into fatty acids and monoacylglycerols. These fatty acids are taken up by the skeletal muscle cells and further processed to become oxidized. Oxidation products are then used for ATP generation in the TCA cycle and the respiratory chain.

1.2.2.1 Regulated uptake of long-chain fatty acids

Long-chain fatty acids represent a specific class of metabolically relevant lipid molecules. Besides glucose, fatty acids serve as a large source of energy substrates, especially for skeletal and cardiac muscle tissue. The chemical properties of fatty acid molecules require specific mechanisms for transportation and uptake of the molecules. In aqueous solutions, such as blood plasma or the cytosol, they have a low solubility of 1-10 nM (Vorum et al., 1992). The presence of proteins with the chemical properties to bind fatty acids can highly increase fatty acid solubility is required. Albumin in plasma and the cytosolic fatty acid binding protein FABP_C were shown to occur in physiological concentrations of 300-600 μ M, and 150-300 μ M, respectively, have the ability to bind high concentrations of fatty acids and to act as extra- or intracellular fatty acid buffers (Richieri et al., 1993; Vork et al., 1993). As the concentrations and functions of fatty acid-solubilizing proteins were described as buffers and intracellular sinks for incoming lipids, they are thought to be rather important for keeping fatty acids in the cells but not to force cellular fatty acid uptake (Schwenk et al., 2010). Although the nature of fatty acid molecules is amphipathic with a non-polar carbon chain and a polar head group that potentially enables the molecules to enter the lipid bilayer of the cell membrane and to diffuse into a cell or out of a cell, it is thought that physiological matters require a regulation of cellular fatty acid provision (Schwenk et al., 2010). It was also postulated for enterocytes that fatty acid uptake occurs in part as passive diffusion and as a regulated and balanced process to meet cellular demands. However, the model of free diffusion of fatty acids into cells has been proposed to be the most likely and exclusive mechanism of short-chain fatty acid uptake, while, in contrast, diffusion is proposed to be part of the long-chain fatty acid uptake machinery, and evidences arose that a complex and regulated process of transporter-facilitated long-chain fatty acid uptake exists as well (Charney et al., 1998; Kamp & Hamilton, 2006; Schwenk et al., 2010). It is believed that long-chain fatty acid uptake is mediated by transmembrane proteins. They are assumed to trap and collect specific long-chain fatty acids from extracellular liquids and enrich their concentration at the outer cell surface. Subsequently, the fatty acids are assumed to passively diffuse through the lipid bilayer (Luiken, Bonen, et al., 2002). However, the exact mechanism how fatty acids pass the cell membrane is controversially discussed. It was reported that passive diffusion is not exclusively driving the cellular supply with long-chain fatty acids, but, that at least in part, carrier-mediated processes may be involved (Turcotte et al., 2000).

The fatty acid transport protein most extensively studied in the past is FAT/CD36 (cluster of differentiation 36). Already in 1993, it was found that CD36 is able to bind oxidized LDL, and that it is capable of facilitating the transportation of fatty acids across the plasma membrane (Abumrad et al., 1993; Endemann et al., 1993). CD36 is widely, but not ubiquitously expressed in mammalian cell types, including adipocytes, cardiac and skeletal muscle cells. Physiologically, the function of CD36 in those cells is lipid storage in adipose tissue and lipid supply of myocytes, but it seems also to be implicated in metabolic malfunctioning involved in the development of obesity and diabetes (J. F. C. Glatz & Luiken, 2018). In the context of lipid utilization, it could be shown that CD36 is exclusively involved in long-chain fatty acid uptake, since it does not bind short-chain fatty acids (J. F. Glatz et al., 2010). Besides CD36, at least two other fatty acid uptake facilitating proteins have been described to be expressed in skeletal muscle cells, FATP1 and FATP4 (Anderson & Stahl, 2013; Stahl et al., 2002). Both of these proteins belong to the SCL27 family of fatty acid transport proteins (FATP). FATP1, encoded by the *Slc24a1* gene, has been described to promote the uptake of long-chain fatty acids into several insulin-responsive tissues, including skeletal muscle (Wu et al., 2006). It was shown that FATP1 has a higher affinity towards long-chain fatty acids than to shorter fatty acids as endogenous substrates (Gimeno et al., 2003; Schaffer & Lodish, 1994). FATP4, which is encoded by the *Slc27a4* gene, was also described to be responsible for long-chain fatty acid uptake into skeletal muscle cells in both, rodents and humans (Jain et al., 2009; Nickerson et al., 2009). Similar to FATP1, FATP4 also shows only minor transport activity towards short-chain fatty acids and seems to exclusively facilitate the uptake of long-chain fatty acids (Gimeno et al., 2003; Stahl et al., 1999). In recent years evidences arose that led to the assumption that for some facilitative cellular fatty acid transport proteins a certain translocation machinery exists that shows similarities to the extensively studied mechanism of GLUT4 translocation (Chabowski et al., 2005; Jain et al., 2015). Especially the groups of Joost Luiken, Arend Bonen and Jan Glatz could show in skeletal and cardiac muscle that CD36, FATP1 and FATP4 seem to be shuttled between the cell surface and a certain intracellular storage site (J. F. Glatz et al., 2016; Jain et al., 2015; Jain et al., 2012; Nickerson et al., 2009). For CD36, it could be shown in HL-1 cardiomyocytes that it seems to be recruited from an intracellular storage site to accumulate at the cell surface upon insulin or stimulation with the AMPK activator AICAR (5-aminoimidazole-4-carboxamide-1- β -D-ribofuranoside) while involving a similar transportation system as GLUT4 (Samovski et al., 2012). Another protein that was described to be critical for skeletal muscle fatty acid uptake is the plasma membrane fatty acid binding protein (FABP_{PM}). This protein is thought to be a superficial capturer of fatty acids at the cell surface. As there is little known about the uptake of short-chain fatty acids despite the observations that their uptake is partially independent of fatty acid transport proteins, membrane-embedded fatty acid translocases and cytosolic fatty acid binding proteins, it seems likely that supply with these fatty acid species is less regulated by carrier proteins than the supply of target tissues with long-chain fatty acids (Schonfeld & Wojtczak, 2016). A group of tissue-specific proteins that seem to

control fatty acid uptake was discovered. It became evident that for skeletal muscle cells, a cluster of several facilitative transport proteins is responsible for regulated fatty acid uptake (see Table 1).

Table 1: Skeletal and cardiac muscle fatty acid binding and transport proteins.

Protein	Molecular mass	Tissue expression
FAT/CD36	88 kDa (53 kDa nonglycosylated)	cardiac muscle skeletal muscle
FABP _{PM}	~40 kDa	
FATP1	71 kDa	
FATP4	72 kDa	

The following paragraph summarizes an overview on the essential reaction steps of cellular fatty acid degradation by β -oxidation.

1.2.2.2 Regulated uptake of long-chain fatty acids

The catabolism of fatty acids mainly takes place in the mitochondria and peroxisomes. In both organelles, β -oxidation requires a similar set of enzymes that catalyze the degradation of lipids. Some enzymes, however, are special for the peroxisomal fatty acid oxidation. It is assumed that long- and very-long-chain fatty acids with a chain length of 20 or more carbon atoms undergo an initial chain-shortening oxidation in peroxisomes before the final oxidation takes place in mitochondria (Reddy & Hashimoto, 2001). However, since peroxisomes are metabolically less relevant in skeletal muscle cells this chapter focusses on mitochondrial β -oxidation. The term β -oxidation summarizes a series of biochemical reactions in eukaryotic mitochondria that lead to a subsequent shortening of a fatty acid chain resulting in the production of acetyl-CoA, NADH and FADH₂. Acetyl-CoA is then further metabolized in the citric acid cycle, NADH and FADH₂ function as co-enzymes in the electron transport chain (Houten & Wanders, 2010). Cytosolic fatty acids become activated by esterifying them with co-enzyme A to fatty acyl-CoA ester. Subsequently, fatty acyl-CoA is shuttled into the mitochondrial matrix involving the action of carnitine palmitoyltransferase I and II (CPT1, CPT2). It was reported that malonyl-CoA inhibits carnitine palmitoyltransferase 1 (CPT1), member of a protein cluster responsible for transportation of activated CoA-coupled fatty acids into the mitochondria. Thus, malonyl-CoA is able to decrease the fatty acid oxidation. Acetyl-CoA can be converted into malonyl-CoA by acetyl-CoA carboxylase (ACC) and vice versa back to acetyl-CoA by malonyl-CoA decarboxylase (MCD). Generally, fatty acid oxidation in the mitochondrial matrix is subdivided into 4 steps: The fatty acid is dehydrogenated by acyl-CoA dehydrogenase (ACAD) to create a double-bond between C2 and C3 of the fatty acid chain to produce trans- Δ^2 enoyl-CoA. This is hydrated at the site of the double-bond by enoyl-CoA hydratase and forms β -hydroxyacyl-CoA (or 3-L-hydroxyacyl-CoA). This molecule is dehydrogenated by 3-L, or β -

hydroxyacyl-CoA dehydrogenase (β -HAD) to generate β -ketoacyl-CoA. Subsequently 2 C-atoms are released from the fatty acid chain by a nucleophilic attack of CoA on C3 in form of acetyl-CoA (Adeva-Andany et al., 2018). This 4 step mechanism is continued until the last carbon atoms have been turned into acetyl-CoA. The general steps of β -oxidation are summarized in Fig. 3. Each acetyl-CoA molecule is further oxidized in the citric acid cycle, releasing CO_2 and reducing equivalents for oxidative phosphorylation.

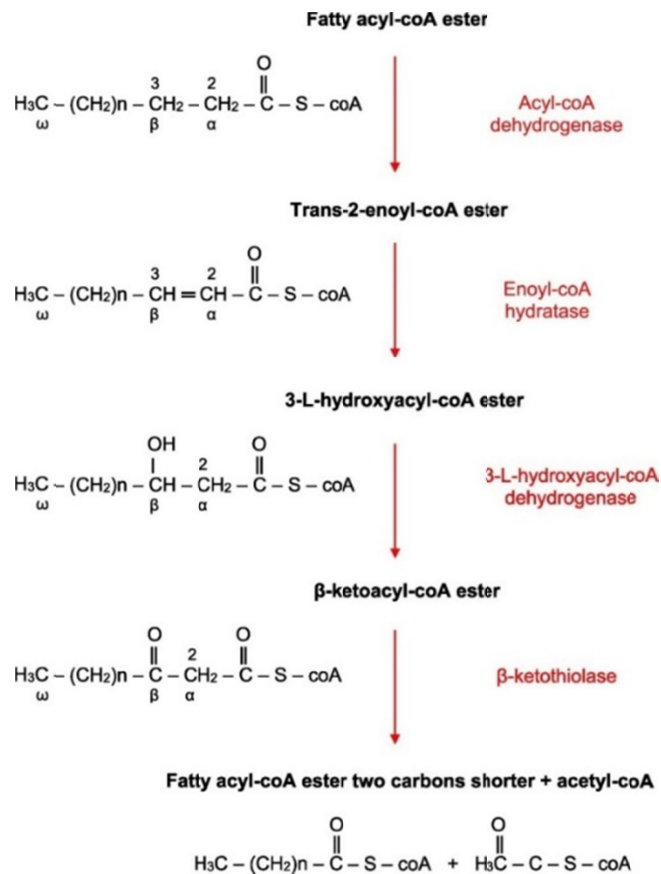


Figure 3: Key reactions of fatty acid β -oxidation. Fatty acyl-CoA esters are dehydrogenated by acyl-CoA dehydrogenase to form trans-2-enoyl-CoA. This is hydrated between C2 and C3 by enoyl-CoA hydratase and generates 3-L, or β -hydroxyacyl-CoA. The hydroxyacyl-CoA molecule is oxidized or dehydrated by 3-L, or β -hydroxyacyl-CoA dehydrogenase and forms a molecule of β -ketoacyl-CoA by converting the C3-hydroxy group into a keto group. In a thiolytic reaction, catalyzed by β -ketothiolase, one molecule of acetyl-CoA is cleaved from the fatty acyl-CoA. The fatty acid carbon chain is shortened by 2 C atoms per β -oxidation cycle. (Adeva-Andany et al., 2018).

1.3 Fatty acid metabolism, lipid accumulation and *diabetes mellitus*

The development of diabetes in children and adults has been stated to be strongly associated to obesity (Campbell & Carlson, 1993; Gower et al., 1999; Kahn et al., 2006). Nevertheless, only a small portion of obese people develop diabetes (Chadt et al., 2018). In

contrast, it is assumed, that 90 % of diabetic patients are obese (Hossain et al., 2007; Whitmore, 2010). The influence of visceral adipose tissue on the development of insulin resistance was studied extensively in the past (Albu et al., 1997; Banerji et al., 1995; Goodpaster et al., 2003). Moreover, it is assumed that body fat distribution and peripheral lipid accumulation, e.g. in the skeletal muscle, contributes to the development of insulin resistance and type 2 diabetes (Befroy et al., 2007; Petersen et al., 2005). The following paragraphs summarize the main effects of energy substrate selection and lipid deposition on the development of peripheral insulin resistance and *diabetes mellitus*.

1.3.1 Metabolic flexibility and fuel selection

Metabolic flexibility is defined as the functional ability of an organism to respond and react to changes in energy demand and to constantly adhere to certain conditions (Galgani et al., 2008; Goodpaster & Sparks, 2017). Skeletal muscles have to permanently adapt to fast fluctuations in nutrient fluxes and energy demands. For instance, with regard to glucose and fatty acid utilization, skeletal muscle cells switch substrate oxidation involving insulin signaling (Chomentowski et al., 2011). The muscle cell transition from glucose to fat oxidation is a consequence of either a reduction in energy intake (fasting) or an increased energy expenditure during physical activity (Henriksson, 1995). Upon insulin stimulation, glucose oxidation is promoted, while lipid oxidation is inhibited (Chomentowski et al., 2011). The failure to adjust fuel substrate oxidation to nutrient source accessibility has also been referred to as metabolic inflexibility. This metabolic state often goes along with insulin resistance, ectopic lipid accumulation, obesity and mitochondrial dysfunction (S. Zhang et al., 2014). Studies found evidence that problems in metabolic adaptations to suitable energy substrates and metabolic switching between these substrates are primary events for the development of obesity and insulin resistance. Obese and individuals suffering from type 2 diabetes also show a defect in switching between fuels in response to insulin-stimulation (Kelley, 2005; Kelley et al., 1999) (Fig. 4).

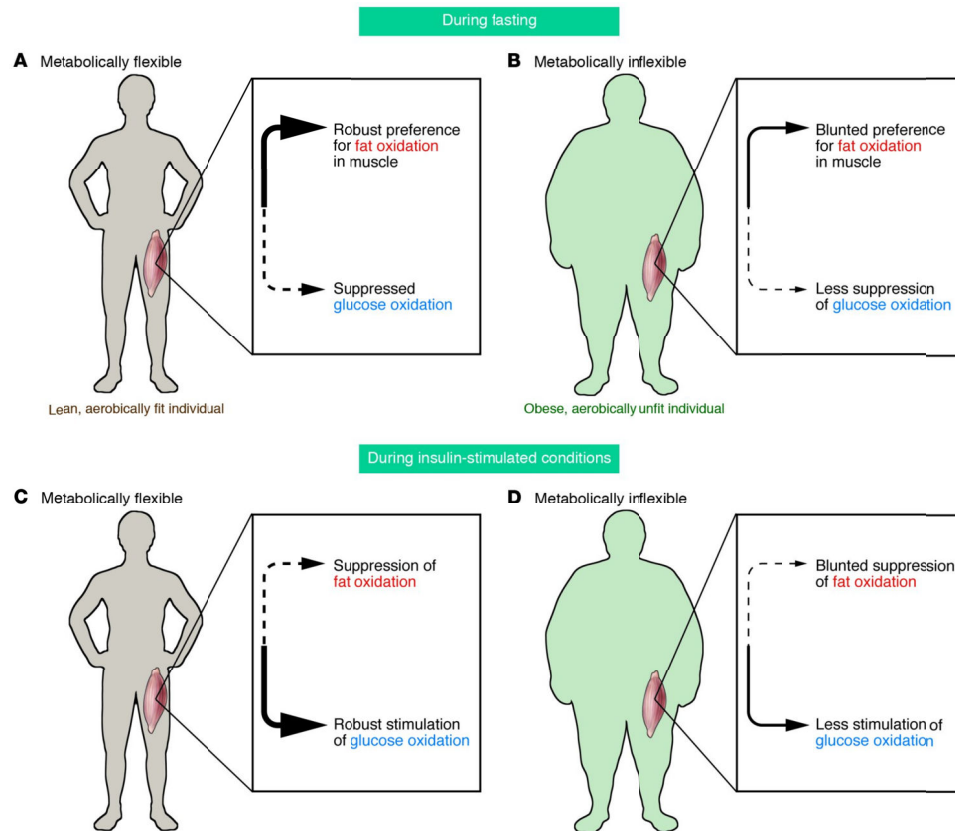


Figure 4: Skeletal muscle metabolic flexibility. A) Lean, aerobically healthy individuals suppress glucose oxidation and prefer to oxidize fat under fasting conditions. B) Fasting obese individuals exhibit a decreased fat oxidation and an only mildly decreased glucose oxidation. C) Insulin stimulation causes a suppression of fat oxidation and a remarkable induction of glucose oxidation in lean, aerobically fit individuals. D) In obese and aerobically unfit people, the suppression of lipid oxidation is blunted, while the glucose oxidation is only stimulated to a low extent after insulin stimulation (Kelley, 2005).

During fasting, lean and metabolically fit individuals suppress glucose oxidation and mainly rely on lipid oxidation, while fasting metabolically inflexible obese individuals have a diminished lipid oxidation preference and a weaker suppression of glucose breakdown. Under insulin-stimulated conditions, lean healthy subjects reduce lipid metabolism to cope with the glucose concentrations that under physiological conditions have caused the rise in insulin levels by considerably increasing glucose catabolism. In contrast, obese, metabolically inflexible subjects exhibit no suppression of lipid oxidation and only a mild increase in insulin-stimulated glucose oxidation, likely because of a substantial insulin resistance (Kelley, 2005; Kelley & Mandarino, 2000). Besides the sheer ability to select the fuel, the capacity to use the fuel as substrate also is thought to contribute to the characterization of the state of metabolic flexibility (Kelley et al., 2002).

1.3.2 Lipid accumulation, ectopic lipid deposition and *diabetes mellitus*

Most of the TGs are stored in adipose tissue, in both, lean and obese conditions. Despite that, TGs are also found to be deposited in other tissues than adipose depots, such as liver,

skeletal and heart muscle or the pancreas (van Herpen & Schrauwen-Hinderling, 2008). Lipolysis leads to the release of non-esterified fatty acids (NEFA) from the adipose tissue into circulation. From here, lipids are taken up by other tissues (e.g. skeletal muscle, liver, kidney, pancreas) to primarily serve as energy substrates, but maybe also as a short-term buffer for excessive lipids entering the body (Zacharewicz et al., 2018). Almost all eukaryotic cells have the ability to store triglycerides (TG) in form of intracellular lipid droplets (LD). These are seen as lipid stores, but furthermore also as a sort of cellular organelle that is assumed to be implicated in several essential cellular processes (Henne et al., 2018; Martin & Parton, 2006; C. Zhang & Liu, 2017). The structure of LDs is highly conserved among bacteria and eukaryotes with only small individual differences (Chitraju et al., 2012). Generally, lipid droplets consist of a neutral lipid core that mainly contains TGs or cholesterol (Barbosa & Siniossoglou, 2017). The core is surrounded by a phospholipid monolayer. Fatty acids that have been transported into a muscle cell get bound to acyl-CoA and are subsequently either metabolized by oxidation or processed to lipid storage (Bosma, 2016). The main source pathway to generate TGs in muscle cells is the monoacyl-diacylglycerol (MAG-DAG) pathway (Han et al., 2013), where MAGs are converted into DAGs which is then acylated to form TGs. The MAG-TG conversion is catalyzed by enzymes of the DAG-acyltransferase (DGAT) family that are predominantly catalyzing the coupling of a third fatty acid to the TG glycerol backbone (Wendel et al., 2009). Lipid droplets bud from the endoplasmic reticulum (ER) (Welte, 2015). They are coated with several proteins, including members of the perilipin family. It was reported that all LDs contain at least one perilipin family member in the phospholipid coat (Sztalryd & Kimmel, 2014). For skeletal muscle it was found that the intramyocellular lipid droplets predominantly exhibit PLIN2, PLIN3 and PLIN5 (Bosma, 2016; Daemen et al., 2018; Gemmink et al., 2016; Sztalryd & Brasaemle, 2017).

In skeletal muscle cells lipid droplets serve as energy depots that, additionally to the glycogen stores represent substrate sinks to constantly provide energy to the muscle (Bosma, 2016; Zacharewicz et al., 2018). The reasons for ectopic lipid deposition can be an increased uptake of fatty acids, an augmented fatty acid synthesis, or a diminished lipid oxidation (Shulman, 2000). Intramyocellular lipid (IMCL) accumulation is a commonly observed characteristic in skeletal muscles. These IMCLs serve as energy source during prolonged physical activities and endurance exercise (Stellingwerff et al., 2007). Goodpaster and colleagues found elevated levels of IMCLs in highly trained athletes. It became evident that the IMCL levels of professional athletes are comparably high as the elevated muscle lipid concentrations that are found in patients suffering from diabetes (Goodpaster et al., 2001). This phenomenon of excessive ectopic fat accumulation in healthy individuals was termed "athletes paradox" (Zacharewicz et al., 2018). Amassing of fatty acids in non-adipose tissues such as liver or skeletal muscle can have severe consequences for the physiology of these organs (Fig. 5).

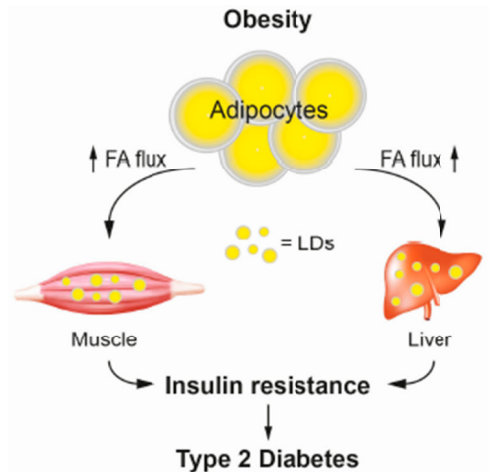


Figure 5: Peripheral lipid accumulation and the development of diabetes. Metabolic energy substrates that are beyond the actual energy demand are stored in lipid droplets (LD) in the form of triglycerides in adipocytes. In case of a chronic oversupply of the organism with nutrients (mainly lipids) the body is provoked to redistribute fatty acid (FA) fluxes to clear lipids from the circulation. This is achieved by an increased uptake of FAs into non-adipose tissues (e.g. skeletal muscle, liver). Here, surplus lipids that exceed the tissues oxidative capacity are stored in TG-containing LDs. Lipid intermediates, reactive oxygen species and other factors can interfere with physiological insulin-signaling and cause peripheral insulin resistance which may result in the onset of Type 2 Diabetes (Markgraf et al., 2016).

Morbid obesity, a state in which the available energy exceeds the capacity of the adipose tissue to store energy as lipids, increases ectopic lipid accumulation and deposition (Samuel & Shulman, 2016). This condition is commonly referred to as lipotoxicity. Through an increase in intracellular lipid intermediates (i.e. DAGs, ceramides) organelles can become damaged which in turn may affect intracellular metabolic regulation (Brons & Grunnet, 2017). The cellular functional impairments are caused by several mechanisms, such as generation of reactive oxygen species (ROS), lipid-induced apoptosis, and disturbances of intracellular signaling (Samuel et al., 2010). Therefore, the alterations resulting from lipotoxicity and lipid intermediates can cause skeletal muscle insulin resistance, which may ultimately result in the manifestation of type 2 *Diabetes mellitus*.

1.4 Genes involved in regulating skeletal muscle fatty acid metabolism

Cellular energy homeostasis is a tightly regulated and complex transaction. Several different genes that can be clustered in terms of the level of their cellular action govern the processes of lipid metabolism, from the uptake, the storage and the biosynthesis and degradation of fatty acids.

1.4.1 Genes regulating fatty acid uptake

It was shown that FAT/CD36, FATP1 and FATP4 are the fatty acid transport proteins that are mainly involved in the regulated uptake of lipids into skeletal muscle cells (Jain et al., 2015). The genes *Cd36*, *Slc27a1* (FATP1) and *Slc27a4* (FATP4) encode these transporters. The *Fabp3* and *Fabp4* genes encode for the two fatty acid binding proteins FABP3 and FABP4, both described to be expressed in skeletal muscle cells and to be important for cell surface fatty acid capturing (Smathers & Petersen, 2011).

1.4.2 Genes involved in regulating lipid degradation and biosynthesis

Several candidate genes were described to encode for proteins that play critical roles in the breakdown and synthesis of fatty acids in muscle cells. The expression of *Fasn* (fatty acid synthase), *Fads1* and *Fads2* (fatty acid desaturase 1/2, also known as Δ 5-desaturase, respectively Δ 6-desaturase) was measured as these proteins are of importance for the synthesis of long-chain fatty acids from malonyl-CoA and acetyl-CoA and the generation of highly unsaturated fatty acids from essential polyunsaturated fatty acids (Nakamura et al., 2014; Ponnampalam et al., 2015). Expression of *Lipe* (hormone-sensitive lipase) and *Lpl* (lipoprotein lipase) was investigated because these enzymes are critical for hydrolysis of triglycerides to free fatty acids and the hydrolysis of triglycerides from lipoproteins (Bazhan et al., 2017).

1.4.3 Genes encoding for skeletal muscle transcription factors

Due to the complexity of cellular energy homeostasis, a strict regulation of expression of genes involved is required. Many transcription factors were described to be involved in directing skeletal muscle lipid metabolism. *Pparg* and *Ppard* are two transcription factors that have been found to be activated by lipid metabolites and to regulate the expression of fatty acid utilization genes such as *Cd36* or *Fabp3* (Luquet et al., 2005). *Hif1a* and *Ppargc1a* (PGC1 α) are transcriptional regulators that have been described to be expressed in muscle and to regulate muscle cell energy metabolism. The expression of class I histone deacetylases *Sirt1*, *Sirt2* and *Sirt3* can be assessed in the context of energy homeostasis, because it could be shown that these proteins regulate the expression of genes involved in lipid metabolism (Hirschey et al., 2010; Schwer et al., 2006; Wang & Tong, 2009; Ye et al., 2017). Since the lack of TBC1D1 leads to changes in fatty acid oxidation the expression of mitochondrial transcription factor A (*Tfam*) can be evaluated as well.

1.4.4 Genes with implications in mitochondrial energy metabolism

Besides *Cpt1b*, the muscle isoform of carnitine palmitoyltransferase 1 (Henique et al., 2010), the expression of the two β -oxidation enzymes *Acadl* (acyl-CoA decarboxylase, long chain) and *Hadh* (3-hydroxyacyl-CoA dehydrogenase) was assessed (Maher et al., 2014). In

addition to that, the expression of the mitochondrial matrix protein pyruvate dehydrogenase kinase 4 (*Pdk4*), an enzyme that has been shown to play a role in cellular energy substrate shift from glucose to fatty acid metabolism (S. Zhang et al., 2014) and uncoupling protein isoform 3 (*Ucp3*) was determined (Abe et al., 2016; Toledo et al., 2018).

1.4.5 Lipid droplet formation and lipid storage associated genes

Several genes could be identified to regulate lipid droplet generation and size, but also the surface structure of the droplets. *Cidec*, a member of the cell death-inducing DFF45-like effector protein family was described to be a determining factor of lipid droplet size (Boren et al., 2013) was together with the perilipins *Plin2* and *Plin3* reported to be expressed as coating proteins of in lipid droplets (Greenberg et al., 2011). The two fat storage-inducing transmembrane proteins 1 and 2 (FITM1, FITM2) are encoded by the genes *Fitm1* and *Fitm2* and have been described to be involved in skeletal muscle lipid storage in lipid droplets and budding of lipid droplets from the endoplasmic reticulum (Gross et al., 2011; Hayes et al., 2017). The diacylglycerol transferases DGAT1 (*Dgat1*) and DGAT2 (*Dgat2*), were described to be two proteins that play crucial roles in lipid droplet formation (Markgraf et al., 2016; Markgraf et al., 2014). *Hspa8*, also known as heat shock cognate protein of 70 kDa (*Hsc70*), encodes for a protein that has been described to be implicated in chaperon-mediated lipid droplet degradation (Kaushik & Cuervo, 2015). *Hilpda* was published to encode for a hypoxia-inducible lipid droplet associated protein (de la Rosa Rodriguez & Kersten, 2017).

1.5 Small Rab GTPases

Eukaryotic cells with their extreme internal specialization of different cellular compartments and organelles, that fulfill every sort of action that is essential for the wellbeing and survival of a single cell, need to strictly regulate the interplay of compartments with each other or with the environment (Stenmark, 2009). One class of G proteins, the so-called small Rab (**R**as-related in **b**rain) GTPases, stands out in regulating the organized intracellular vesicle transportation system. This protein class is the largest subfamily within the Ras superfamily of small G proteins, consisting of more than 60-70 family members identified in the human genome (Colicelli, 2004; Kiral et al., 2018; S. Pfeffer, 2005; Shi et al., 2017). It represents a group of master switches that are massively involved in cellular trafficking events. Each Rab GTPase is typically associated with the control of several steps of membrane traffic by recruiting effector proteins such as motor proteins, kinases, phosphatases, or vesicle fusion, budding and tethering proteins (Eathiraj et al., 2005; Novick, 2016; Stenmark, 2009). An important characteristic of the Rab GTPases is that family members exhibit distinct distribution and localization patterns within the cell (Chavrier et al., 1990). The distinct targeting of a certain membrane by a Rab protein seems to depend on several Rab protein regions (Ali et al., 2004).

As small G proteins, the activity of the Rab GTPases strongly depends on their GTP/GDP binding status (Araki et al., 1990). This binding status goes along with substantial conformational changes in the switch I and switch II regions of the Rab protein (S. R. Pfeffer, 2005). In their GTP-bound conformation, the Rab proteins are described to be more active and can mediate their key action, the transportation of cellular vesicles. The Rab activation by exchanging GDP with GTP is catalyzed by proteins of the guanine nucleotide exchange factor (GEF) family (Delprato et al., 2004; Marat et al., 2011). To inactivate Rab proteins, GTPase activating proteins (GAP) hydrolyze GTP themselves, but also enhance GTP hydrolysis activity of Rab proteins to catalyze the cleavage of GTP to GDP + P_i (Stenmark, 2009). A schematic overview over the activation and inactivation of small Rab-GTPases is depicted in Fig. 6.

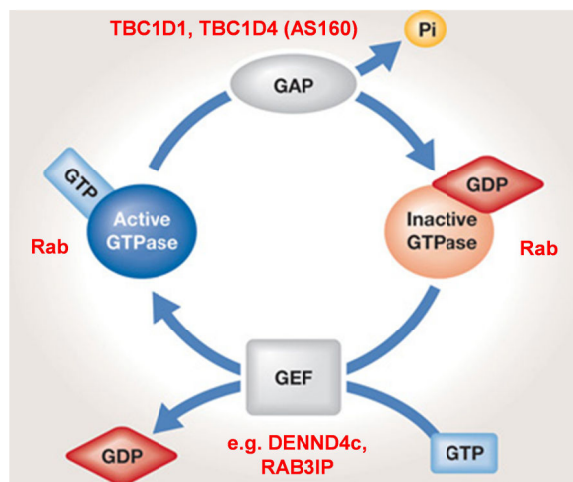


Figure 6: Activity regulation of small Rab-GTPases. A GTPase-activating protein (GAP), such as TBC1D1 or TBC1D4 (AS160) stimulates the hydrolysis of one inorganic phosphate from a GTP-bound Rab protein into a GDP-bound Rab to inactivate the small GTPase. In turn, a guanine nucleotide exchange factor (GEF) catalyzes the replacement of a GDP with a GTP attached to a Rab GTPase, thereby activating the GTPase. Modified image (Duran & Hall, 2012).

1.5.1 Small Rab GTPases in vesicle trafficking with relation to energy metabolism

Metabolically relevant tissues, such as skeletal muscle or adipose tissue, strongly depend on a regulated and well balanced control of energy substrate supply. The translocation of the insulin-sensitive glucose transporter 4 (GLUT4) has been studied intensively. As models suggest that the GLUT4 proteins cycle between an intracellular storage compartment and the cell surface, it seems likely that the trafficking of GLUT4-containing vesicles is depending on the action Rab GTPases. It has been reported that several Rab proteins regulate GLUT4 translocation in muscle and adipose cells under several physiological conditions. It was reported that RAB8a, RAB13 and RAB14 are responsible for insulin-stimulated GLUT4 surface recruitment in skeletal muscle cells (Ishikura et al., 2007; H. Li et al., 2017; Sun et al., 2014; Sun et al., 2016). A novel Rab GTPase that is important for insulin-stimulated GLUT4 translocation in skeletal is RAB20 (Gorgens et al., 2017). Also, it was reported that RAB8a,

RAB13 and RAB14 not only seem to be important for insulin signaling, but also mediate contraction-induced translocation of GLUT4 (Deng et al., 2018; Z. Li et al., 2017). For RAB28, our working group could recently publish that it is involved in basal GLUT4 surface recruitment in isolated murine skeletal muscle cells and primary adipocytes (Zhou et al., 2017). RAB10 is described to regulate insulin-stimulated GLUT4 translocation in adipocytes (Bruno et al., 2016; Sano et al., 2008). RAB14 was addressed to participate in adipocyte GLUT4 sorting (Brewer et al., 2016).

1.6 Rab GTPase activating proteins (RabGAP)

The action of Rab proteins as regulatory molecules within the cellular transportation system requires the presence of a strict activation and inactivation system that acts directly on the Rab GTPases. Two classes of proteins are responsible for the activity state of Rab proteins: guanine nucleotide exchange factors (GEFs) and GTPase activating proteins (GAPs) (Barr & Lambright, 2010). What most of the regulatory relevant RabGAPs, except RAB3GAP (Kern et al., 2015), have in common is the presence of a highly conserved Tre-2/Bub2/Cdc16 (TBC) domain (Fukuda, 2011; Pan et al., 2006). It was predicted that the family of Rab-specific TBC domain-consisting proteins comprises of 44 members (Frasa et al., 2012). Together with the information that approximately 60-70 Rab GTPases have been identified in mammals, this leads to the conclusion that one RabGAP may regulate the activity of several Rab GTPases. Indeed, it was reported that for example the RabGAPs TBC1D1 and TBC1D4 (AS160) confer *in vitro* GAP activity towards Rab8a, 8b, 10 and 14 (Roach et al., 2007; Sano et al., 2008). Among the RabGAPs, both TBC1D1 and TBC1D4 seem to be the two Rab GTPase activating proteins with the largest importance for energy homeostasis and energy substrate turnover, because these RabGAPs seem to be important regulators for energy fuel selection, e.g. in skeletal muscle tissue (Chadt et al., 2015; Chadt et al., 2008).

1.6.1 TBC1D1 and TBC1D4/AS160 as prominent RabGAPs in energy metabolism

Numerous studies have established the concept that TBC1D1 and TBC1D4 (also referred to as AS160) are crucial for the regulation of insulin- and contraction-stimulated GLUT4 translocation (Hargett et al., 2016; Mafakheri et al., 2018; Zhou et al., 2017). Human studies conducted in the Greenlandic Inuit population revealed a loss-of-function mutation in the *TBC1D4* gene leading to increased plasma glucose and serum insulin levels of allele carriers compared to non-carriers or individuals heterozygous for this variant (Moltke et al., 2014).

Both RabGAPs, TBC1D1 and TBC1D4, have a common domain structure with partial differences in total protein length and domain size (Sakamoto & Holman, 2008). Both RabGAPs consist of two N-terminal phosphotyrosine-binding domains (PTB), a calmodulin binding domain

(CBD) and the C-terminal functional TBC (GAP) domain which is responsible for catalyzing GTP hydrolysis (Cartee, 2015; S. Y. Park et al., 2011). With regard to the total protein the RabGAPs have been described to be 61-69 % identical, with the highest degree of homology in the GAP domains (identical to 91 %) (Miinea et al., 2005; Roach et al., 2007). In the course of the insulin signaling cascade or the contraction-mediated pathway, the kinases AKT or AMPK phosphorylate TBC1D1 and TBC1D4 at GAP- and kinase-specific residues. These phosphorylation events inactivate the GAP activity and transduce the signal to provoke GLUT4 vesicle translocation. An overview of the known AMPK and AKT phosphorylation sites of mouse TBC1D1 and TBC1D4 is depicted in Fig. 7.

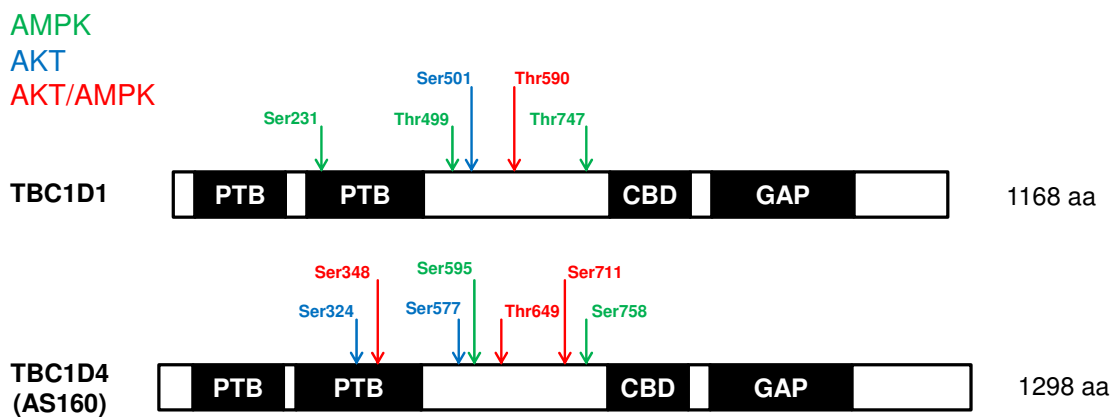


Figure 7: Domain structure and AKT/AMPK phosphorylation sites of mouse TBC1D1 and TBC1D4.

The domain structure of TBC1D1 and TBC1D4 is similar. Both GAPs have two phosphotyrosine-binding domains (PTB), a calmodulin-binding domain and a catalytically active GAP domain, responsible for GTP hydrolysis. Both RabGAPs can be phosphorylation by the upstream kinases AKT and AMPK. Phosphorylation occurs at serine (Ser) or threonine (Thr) positions. AMPK phosphorylation sites are represented in green, AKT sites in blue and shared AKT/AMPK sites in red. Mouse TBC1D1 can be phosphorylated by AMPK at Ser²³¹, Thr⁴⁹⁹ and Thr⁷⁴⁷. D1 AKT phosphorylation happens at Ser⁵⁰¹. Both kinases phosphorylate D1 at Thr⁵⁹⁰. TBC1D4 can be phosphorylated by AMPK at Ser⁵⁹⁵ and Ser⁷⁵⁸, by AKT at Ser³²⁴, Ser⁵⁷⁷ and by both kinases at Ser³⁴⁸, Thr⁶⁴⁹ and Ser⁷¹¹ (Mafakheri et al., 2018).

Several isoforms and splicing variants of the two RabGAPs have been described (Baus et al., 2008; Chadt et al., 2008; Taylor et al., 2008). To date only little is known about their specific functions in metabolic regulation. It was described that the different isoforms show differing phosphorylation sides (Dash et al., 2010; Dash et al., 2009; Taylor et al., 2008).

1.6.2 Impact of *Tbc1d1*- and *Tbc1d4*-deficiency on skeletal muscle lipid metabolism

Besides the role that TBC1D1 and TBC1D4 play in basal and insulin- or muscle contraction-stimulated GLUT4 translocation and glucose uptake (Cartee, 2015; Chadt et al., 2008), the two proteins seem to represent a critical step in cellular physiology that may be decisive for the choice of the energy substrate the cell is going to metabolize. In terms of lipid metabolism it was shown that mice with a global *Tbc1d1*-deficiency showed a preferential usage of lipids as

energy substrate, represented by a reduced respiratory quotient (RQ) (Chadt et al., 2015; Chadt et al., 2008; Dokas et al., 2013). Moreover, it was shown that mice with a knockout of TBC1D1, TBC1D4 and the double knockout of both GAPs exhibited a significantly reduced RQ and an increased whole-body fatty acid oxidation. Moreover, the basal *ex vivo* lipid oxidation in intact *EDL* (*Extensor digitorum longus*) muscles from D1KO, D4KO and D1/4KO mice was significantly increased compared to wildtype control animals (Chadt et al., 2015). Early *in vitro* studies conducted in C2C12 myotubes also showed that siRNA-mediated ablation of *Tbc1d1* caused a significant increase in cellular fatty acid uptake (Chadt et al., 2008). In the past, several studies were conducted to further elucidate how the RabGAPs alter lipid metabolism. An overexpression study found that TBC1D1 reduces palmitate oxidation in skeletal muscle cells by decreasing the activity of β -HAD, a key enzyme of mitochondrial β -oxidation (Maher et al., 2014). Another study performed *in vitro* in cardiomyocytes demonstrated that TBC1D4 and its downstream Rab GTPases are directly involved in insulin- and AICAR-stimulated surface recruitment of FAT/CD36, a protein described to be a key fatty acid uptake facilitator (Samovski et al., 2012).

Unpublished data from our lab show that the citrate synthase activity is not different between WT and D1KO mouse muscles. Overexpression of TBC1D1 in mouse skeletal muscles did not alter mitochondrial content compared to non-overexpressing wildtype muscles (Maher et al., 2014). Additionally, unpublished data revealed no difference in the total amount of mitochondrial DNA between D1KO and WT mice, measured by expression analysis of the mitochondrially encoded NADH dehydrogenase 2 gene (mt-ND2). Interestingly, the effect of *Tbc1d1*-deficiency on lipid uptake and oxidation seems not to be restricted to skeletal muscle tissue, but could also be found in isolated primary pancreatic islets. In contrast to the data obtained for skeletal muscle, mitochondrial copy number was found to be higher in D1KO islets of Langerhans (Stermann et al., 2018).

Summarizing this, there is still uncertainty on how the RabGAPs TBC1D1 and TBC1D4 influence uptake and breakdown of fatty acids in skeletal muscles. According to the available data it seems likely that there are more than one pathways that may be involved.

1.6.3 RabGAPs and the link to human metabolic phenotypes and diseases

Most of the data on TBC1D1 and TBC1D4 and their function in whole-body and in particular skeletal muscle metabolism were generated cell lines or tissues from rodent model organisms. Here, studies revealed that a lack of the RabGAPs has a crucial impact on energy metabolism (Chadt et al., 2008; Dokas et al., 2016; Dokas et al., 2013). Besides numerous publications linking the RabGAPs to GLUT4 trafficking in different tissues, it could also be shown that it may regulate the translocation of fatty acid uptake facilitating proteins such as CD36 (Samovski et

al., 2012). In contrast, only few studies found evidence that *TBC1D1* and *TBC1D4* are also relevant for human metabolic and pathogenic phenotypes. A whole exome sequencing of patients suffering from Congenital anomalies of the kidneys and urinary tract (CAKUT) yielded in the identification of different missense mutations of *TBC1D1* that were predicted to confer pathogenicity (Kosfeld et al., 2016). The authors reported that some of the clinical characteristics of CAKUT could also be found in the kidneys in *Tbc1d1*-deficient mice. Similar as reported for D1KO skeletal muscles (Chadt et al., 2015), Kosfeld and colleagues also found reduced GLUT4 protein levels in the kidneys of these animals. One patient carrying a truncated mutation of *TBC1D1* displayed characteristics of insulin resistance. Thus, the authors concluded that *TBC1D1* may contribute to the development of kidney anomalies and pathogenesis, eventually by influencing glucose homeostasis (Kosfeld et al., 2016).

A study performed in the lab of Torben Hansen in Denmark found an interesting linkage of *TBC1D4* and the development of metabolic disease. In a historically isolated native Inuit population in Greenland, it was recorded that the Type 2 *Diabetes mellitus* (T2DM) prevalence rose between the 1960s and the beginning of this century by 10 % (Jorgensen et al., 2013). A mapping of quantitative traits related to T2DM and an exome sequencing approach revealed nonsense p.Arg684Ter mutation within the *TBC1D4* gene. Homozygous carriers of this mutant variant exhibited higher plasma glucose and serum insulin levels and lower fasting plasma glucose concentrations (Moltke et al., 2014). In muscle biopsies lower mRNA expression levels of *SLC2A4* (encoding for GLUT4) were found (Moltke et al., 2014). The described findings co-occurred with significantly decreased insulin-stimulated glucose uptake in skeletal muscles, postprandial hyperglycemia and the onset of the metabolic syndrome and T2DM (Moltke et al., 2014). One explanation for an accumulation of mutant *TBC1D4* alleles may be a positive selection favoring allele carriers. The *TBC1D4* mutation was associated with hyperglycemia and decreased skeletal muscle insulin sensitivity. Traditionally, the nutrition of the Inuit consisted of protein- and fat rich sea food and seal meat, but lower amounts of carbohydrates (Bjerregaard et al., 2000; Grarup et al., 2015). Evolutionary, the genetic accumulation may have been an adaptation to the Greenlandic environment that predominantly forced the native people to consume a protein- and fat-rich diet with rather low amounts of carbohydrates. The phenotype of *Tbc1d4*-deficient C2C12 and L6 and D4KO mouse muscles of taking up and oxidizing increased amounts of fatty acids instead of metabolizing glucose (Chadt et al., 2015; Miklosz et al., 2016) could be a necessary modification of energy metabolism to cope with prevailing dietary habits. The increased T2DM prevalence among the isolated Inuit population in the past 50 years may be a result of globalization. The availability of carbohydrate- and fat-rich diets (Western Style Diet) in combination with a switch towards a more sedentary lifestyle may be less compatible to the metabolic preferences of Inuit. As a consequence, this may lead to hyperglycemia and insulin-resistance in carriers of the *TBC1D4* p.Arg684Ter mutation and could lead to an increase in *Diabetes* prevalence.

2 Aim of the current study

In previous publications it was shown that both Rab-GTPase activating proteins (GAP), TBC1D1 and TBC1D4 influence glucose homeostasis of skeletal muscle cells and tissues by regulating the translocation of the glucose transporter isoform 4 (GLUT4). Moreover, an implication of the GAPs in the development of diseases was postulated. However, there is only limited information available on how TBC1D1 and TBC1D4 mediate their functional involvement in the regulation of cellular lipid metabolism. The GAPs seem to act as key switches deciding which energy substrate (glucose vs. fat) shall be metabolized. It was described that the skeletal muscles of *Tbc1d1*-deficient mice exhibit a decrease in insulin-stimulated glucose uptake *ex vivo*, while the basal fatty acid oxidation was significantly increased (Chadt et al., 2015; Chadt et al., 2008). How the effect on fatty acid metabolism is conferred remains not understood completely. A study performed *in vitro* in murine cardiomyocytes could link the action of the GAP TBC1D4 to its regulatory function towards Rab GTPases and stated that the GAP and its downstream targets regulate the surface recruitment of fatty acid transport protein CD36 (Samovski et al., 2012). Another study stated that TBC1D1 is involved in the regulation of the β -oxidation enzyme β -hydroxyacyl-CoA dehydrogenase (β -HAD) (Maher et al., 2014). However, the explanation for an increased lipid metabolism upon *Tbc1d1*- and *Tbc1d4*- deficiency still remains intermittent. To further reveal the underlying regulatory mechanisms that drive the observed TBC1D1 and TBC1D4 knockout effect, the following key questions were addressed in this study:

1. Is the effect of increased fatty acid utilization of skeletal muscle cells upon RabGAP-deficiency specific for a certain fatty acid species?
2. Does the knockdown of *Tbc1d1* alter the mRNA expression of key metabolic regulator genes?
3. Does a TBC1D1 knockout influence murine skeletal muscle total lipid content and the lipid profile and does it alter the expression of metabolic factors that may contribute to the observed changes in lipid utilization?
4. Which D1 and D4 downstream Rab GTPase targets and fatty acid transport facilitating proteins are important for *in vitro* and *in/ex vivo* skeletal muscle cell lipid uptake?

To work on these research questions, a complex set of both, *in vitro* and *ex vivo* experiments involving murine C2C12 myotubes, as well as a defined group of genetically manipulated mice (*Mus musculus*) was utilized. *In vitro*, the impact of certain expression manipulations on FA uptake and oxidation was performed. *Ex vivo*, the fatty acid utilization as well as the overall skeletal muscle lipid composition was analyzed. Additionally, several

approaches on mRNA and protein expression analysis were conducted in samples derived either from cultured myotubes, or dissected mouse skeletal muscles.

3 Material and Methods

3.1 Material

3.1.1 Animal experiments

3.1.1.1 Experimental animals

All *ex vivo* data presented in this study have been generated with tissue samples of mice. For this study, several mouse models carrying different genetic modifications were used (Tab. 2). Briefly, recombinant congenic *Tbc1d1*-deficient mice on C57BL/6J background (D1KO) were generated as previously described (Chadt et al. 2008). Mice with a targeted whole-body deletion of *Tbc1d4* (D4KO) were obtained from Texas A&M Institute for Genomic Medicine (Houston, TX) and crossed with the D1KO strain as described by Chadt et al. 2015 to generate double-deficient *Tbc1d1*-, *Tbc1d4* and *Tbc1d1/4*-deficient mice (D1/4KO). *Cd36*-deficient mice were initially generated by Dr. Maria Febbraio (Febbraio et al., 1999) to study the impact of the fatty acid transport protein FAT/CD36 on murine lipid metabolism and were obtained from her lab. These mice were in-house intercrossed with the previously mentioned RabGAP-deficient mice to generate *D1/4KO-Cd36* double and triple knockout mice. The following table summarizes the mouse models with their respective working designation that were utilized during this study.

Table 2: Summary over the utilized experimental mouse strains

Systemic strain name	Designation	Genetic modification
C57BL/6J	WT	Wildtype gene expression
RCS.B6.SJL. <i>Nob1.10</i>	D1KO	<i>Tbc1d1</i> -deficient
<i>Tbc1d4</i> -KO	D4KO	<i>Tbc1d4</i> -deficient
RCS.B6.SJL. <i>Nob1.10</i> x KO- <i>Tbc1d4</i>	D1/4KO	<i>Tbc1d1-Tbc1d4</i> -deficient
<i>Cd36</i> -KO	CD36KO	<i>Cd36</i> -deficient
-	D1-CD36 KO	<i>Tbc1d1-Cd36</i> -deficient
-	D4-CD36 KO	<i>Tbc1d4-Cd36</i> -deficient

3.1.1.2 Animal housing

All experimental mouse strains were bred and housed in the in-house animal facility. Mice were kept in groups of up to six mice per cage under a 12:12 hours light-dark regiment. After weaning at the age of 3 weeks, mice received a chow diet (Ssniff, Soest, Germany) (33 kcal % from protein, 58 kcal % from carbohydrates, 9 % kcal from fat) and water *ad libitum*. At an age of three weeks, the animal caretakers collected tail-tip biopsies for genotyping. For all experiments, male mice at an age of 10-25 weeks were used. For some experiments mice were

fasted for 4 or 16 hours prior to the experimental intervention. The animal experiments performed during this project were approved by the ethics committee of the state agency for nature, environment and consumer protection (LANUV) of North Rhine-Westphalia, Germany (Reference numbers 84-02.04.2012.A296, 84-02.04.2013.A352, 84-02.04.2015.A442 and 84-02.04.2017.A345).

3.1.2 Cell culture experiments

3.1.2.1 C2C12 myoblast cell line

The C2C12 myoblast cell line was purchased from ATCC (Manassas VA, USA) and stored at -196 °C upon arrival until further experimental use.

3.1.3 Chemicals

Table 3: Chemicals

Compound	Supplier
5-aminoimidazole-4-carboxamide-1- β -D-ribofuranoside (AICAR)	Toronto Research Chemicals, North York ON, Canada
Acetyl chloride ≥ 99.5 %	Sigma Aldrich, Steinheim, Germany
Acrylamide	AppliChem, Darmstadt, Germany
Agar-Agar, Kobe I	Carl Roth, Karlsruhe, Germany
Agarose	Biozym, Hessisch Oldendorf, Germany
Ammoniumpersulfate (APS)	Serva, Heidelberg, Germany
BSA Fraction V, fatty acid free	Carl Roth, Karlsruhe, Germany
Butyric Acid	Sigma Aldrich, Steinheim, Germany
cOmplete protease inhibitor cocktail	Roche Diagnostics, Mannheim, Germany
D(+)-Glucose, ≥ 99.5 %	Sigma Aldrich, Steinheim, Germany
Dimethylsulfoxide (DMSO)	AppliChem, Darmstadt, Germany
Dithiothreitol (DTT)	VWR, Darmstadt, Germany
D-Mannitol	AppliChem, Darmstadt, Germany
dNTP set, PCR grade (100 mM each)	Roche, Mannheim, Germany
Dulbecco's modified eagle medium (DMEM), high glucose, L-Glutamine, sodium pyruvate, phenol red, w/o HEPES	Gibco at Thermo Fisher Scientific, Darmstadt, Germany
Ethidium bromide	MP Biochemicals, Illkirch, France
Ethylendiaminetetraacetic acid (EDTA)	Carl Roth, Karlsruhe, Germany
Ethylene glycol tetraacetic acid (EGTA)	Serva, Heidelberg, Germany
Fetal Bovine Serum (FBS)	Thermo Fisher Scientific, Darmstadt,

Compound	Supplier
	Germany
Horse Serum (HS)	ATCC at LGC Standards, Wesel, Germany
Hyaluronidase (Type I-S)	Sigma-Aldrich, Steinheim, Germany
Methanol (MeOH)	AppliChem, Darmstadt, Germany
n-hexane	AppliChem, Darmstadt, Germany
Oleic Acid	Sigma Aldrich, Steinheim, Germany
Palmitic Acid Sigma Ultra approx. 99 %	Sigma Aldrich, Steinheim, Germany
Penicillin/Streptomycin solution (P/S)	Thermo Fisher Scientific, Darmstadt, Germany
Pentadecanoic acid	Sigma Aldrich, Steinheim, Germany
Peptone ex casein	Carl Roth, Karlsruhe, Germany
PhosSTOP phosphatase inhibitor cocktail	Roche Diagnostics, Mannheim, Germany
Potassium chloride (KCl)	Merck, Darmstadt, Germany
Powdered milk, blotting grade	Carl Roth, Karlsruhe, Germany
Rotiszint® eco plus LSC-Universalcocktail	Carl Roth, Karlsruhe, Germany
Sodium chloride (NaCl), ≥99.5 %	Carl Roth, Karlsruhe, Germany
Sodium hydroxide (NaOH) pellets	AppliChem, Darmstadt, Germany
Tetraethylethyldiamine (TEMED)	Carl Roth, Karlsruhe, Germany
Yeast extract	Carl Roth, Karlsruhe, Germany
Phosphate-buffered saline (PBS), 1x	Gibco at Thermo Fisher Scientific, Darmstadt, Germany
Trypsin-EDTA, 1x	Sigma-Aldrich, Steinheim, Germany

3.1.4 Radiochemicals

Following radiolabeled chemicals were used for *in vitro* and *ex vivo* experiments to investigate skeletal muscle cell fatty acid uptake and oxidation.

Table 4: Radiochemicals

Compound	Concentration [mCi/ml]	Specific activity [Ci/mmol]	Supplier
[1- ¹⁴ C]-Palmitic Acid	0.1	0.056	Hartmann Analytic, Braunschweig, Germany
[9,10- ³ H(N)]-Oleic Acid	5	60	American Radiolabeled Chemicals, St. Louis MO, USA
n-[2,3- ³ H]-Butyric Acid	1	120	American Radiolabeled Chemicals, St. Louis MO, USA
[9,10- ³ H(N)]-Palmitate	1	50	Hartmann Analytic,

Compound	Concentration [mCi/ml]	Specific activity [Ci/mmol]	Supplier
			Braunschweig, Germany

3.1.5 Reaction kits

Table 5: Commercial reaction kits

Kit	Supplier
100 bp + 1 kb DNA ladder	Thermo Scientific, Peqlab, Wilmington MA, USA
10x DreamTaq green buffer	Thermo Scientific, Peqlab, Wilmington MA, USA
5x Phusion HF buffer	Thermo Scientific, Peqlab, Wilmington MA, USA
6x Gel loading dye	Thermo Scientific, Peqlab, Wilmington MA, USA
Custom designed oligonucleotide primer pairs	Eurogentech, Seraing, Belgium
DreamTaq DNA Polymerase	Thermo Scientific, Peqlab, Wilmington MA, USA
GoScript™ Reverse Transcriptase Kit	Promega, Madison WI, USA
GoTaq® qPCR Master Mix	Promega, Madison WI, USA
Hexanucleotide Primer	Roche, Mannheim, Germany
Invisorb® Genomic DNA Kit II	Stratec Molecular GmbH, Berlin, Germany
Phusion High-Fidelity DNA Polymerase	Thermo Scientific, Peqlab, Wilmington MA, USA
Pierce BCA Protein Assay Kit	Thermo, Rockford IL, USA
RNeasy Mini Kit	Qiagen, Hilden, Germany
Western Lightning ECL Pro	Perkin Elmer, Waltham MA, USA
Western Lightning ECL Ultra	Perkin Elmer, Waltham MA, USA

3.1.6 Machines and Devices

Table 6: Utilized devices and tools

Device	Supplier
Benchtop 2UV Transluminator	Ultra-Violet Products Ltd, Cambridge, UK
Cell culture water bath 12P with Thermomix 1420	B.Braun, Melsungen, Germany
ChemiDoc XRS+	Bio-Rad Laboratories, München, Germany

Device	Supplier
FS-FFAP-CB-0.25 chromatography column	CS-Chromatographie Service GmbH, Langerwehe, Germany
Gas chromatography system 6890N	Agilent Technologies, Ratingen, Germany
GelDoc XR+	Bio-Rad Laboratories, München, Germany
HERACell 240i Incubator	Thermo Scientific, Peqlab, Wilmington MA, USA
Horizontal gel electrophoresis apparatus	Biometra, Göttingen, Germany
iMark Microplate Reader	Bio-Rad Laboratories, München, Germany
Inverse microscope AE2000	Motic, Wetzlar, Germany
Laminar flow HS 12	Thermo Scientific Heraeus, Darmstadt, Germany
Liquid Szintillation Counter LS 6000LL	Beckman Coulter, Krefeld, Germany
Mini PROTEAN Tetra System	Bio-Rad Laboratories, München, Germany
NanoDrop 2000	Thermo Scientific, Peqlab, Wilmington MA, USA
Power Pac Basic	Bio-Rad Laboratories, München, Germany
Power Pac HC	Bio-Rad Laboratories, München, Germany
Reacti-Therm™ Heating/Stirring Module	Thermo Fisher Scientific, Darmstadt, Germany
Roll mixer RM 5-40	M. Zipperer GmbH, Staufen, Germany
Shaking table ST 5	M. Zipperer GmbH, Staufen, Germany
Shaking water bath	GFL mbH, Burgwedel, Germany
Short plates for SDS gels	Bio-Rad Laboratories, München, Germany
Spacer plates (1 mm, 1.5 mm) for SDS gels	Bio-Rad Laboratories, München, Germany
Standard Power Pack P25	Biometra, Göttingen, Germany
StepOnePlus™ Real-time PCR system	Applied Biosystems, Darmstadt, Germany
T100™ Thermal Cycler	Bio-Rad Laboratories, München, Germany
Tabletop centrifuge 5425 R (with rotor FA-45-24-11)	Eppendorf, Wesseling-Berzorf, Germany
Tabletop refrigerated centrifuge 5425 R (with rotor FA-45-24-11)	Eppendorf, Wesseling-Berzorf, Germany
Tankblot Eco Mini	Biometra, Göttingen, Germany
Thermomixer Compact	Eppendorf, Wesseling-Berzorf, Germany
TissueLyser II	Qiagen, Hilden, Germany
Uniprep gyrator	UniEqui, Planegg, Germany
ZOE™ Fluorescent Cell Imager	Bio-Rad Laboratories, München, Germany

3.1.7 Software

Table 7: Software used for measurements and quantifications

Software	Application	Device	Supplier
Excel 2010	Data processor	PC	Microsoft
GraphPad Prism 7	Statistical Analysis, Graphs	PC	GraphPad Software Inc.
Image Lab	Agarose gel, Western blot	GelDoc, ChemiDoc	Bio-Rad Laboratories
Microplate Manager 6	BCA	iMark Reader	Bio-Rad Laboratories
Nanodrop 2000	DNA/RNA concentration	Nanodrop 2000	Thermo Fisher
StepOne v2.3	qRT-PCR	StepOne Plus	Applied Biosystems
Word 2010	Word processor	PC	Microsoft

3.1.8 Buffers, Culturing Media and Solutions

Table 8: Buffers, cell culture media and solutions

Name	Ingredients
4x Laemmli sample buffer	20 vol % Glycerol, 8 % SDS, 10 mM EDTA, 250 mM Tris-HCl, 5 % bromphenol blue solution (2 % bromphenol blue, 4 % SDS in H ₂ O)
C2C12 culture medium	DMEM (4.5 g/L glucose), 10 vol % FCS, 1 vol % P/S
C2C12 differentiation medium	DMEM (4.5 g/L glucose), 2 vol % HS, 1 vol % P/S
C2C12 starvation medium	DMEM (4.5 g/L glucose), 1 vol % P/S
C2C12 transfection medium	DMEM (4.5 g/l glucose)
<i>Ex vivo</i> fatty acid oxidation/uptake HOT incubation buffer	KHB, 15 mM mannitol, 5 mM glucose, 0.6 mM cold palmitate, 20 % fatty acid-free BSA, 1.4 μM ³ H-palmitate
<i>Ex vivo</i> fatty acid oxidation/uptake pre-incubation buffer	KHB, 15 mM mannitol, 5 mM glucose, 3.5 mM fatty acid-free BSA
<i>In vitro</i> fatty acid oxidation HOT buffer	C2C12 differentiation medium, 11.8 μM ¹⁴ C-palmitate, 6.24 μM fatty acid-free BSA, 1 μM L-carnitine

Name	Ingredients
<i>In vitro</i> fatty acid uptake HOT buffer	KRH, 8.5 nM ³ H-palmitate/-oleate/-butyrate, 2.5 μM fatty acid-free BSA, 5 μM unlabeled cold palmitate/oleate/butyrate
<i>In vitro</i> fatty acid uptake pre-HOT buffer	KRH, 40 μM fatty acid-free BSA
<i>In vitro</i> fatty acid uptake washing buffer	KRH, 0.1 % fatty acid-free BSA
Krebs-Henseleit buffer (KHB)	<u>Stock I</u> : 118.5 mM NaCl, 0.047 mM KCl, 0.012 mM KH ₂ PO ₄ , 0.25 mM NaHCO ₃ <u>Stock II</u> : 0.025 mM CaCl ₂ , 0.012 mM MgSO ₄ , 0.05 mM HEPES
Krebs-Ringer-HEPES (KRH) buffer (pH 7.4)	136 mM NaCl, 4.7 mM KCl, 1.25 mM MgSO ₄ , 1.25 mM CaCl ₂ , 10 mM HEPES
Lysis buffer (for tissue and cell protein isolation)	20 mM Tris-HCl, 150 mM NaCl, 1 mM EDTA, 1 mM EGTA, 1 % Triton X-100 (Protease and phosphatase added freshly before use)
SDS-PAGE 1x electrophoresis buffer	25 mM Tris-HCl, 192 mM Glycine, 0.1 % (w/v) SDS
SDS-PAGE 1x separation gel buffer (pH 8.8)	500 mM Tris-HCl, 0.4 % SDS
SDS-PAGE 1x stacking gel buffer (pH 6.8)	0.5 M Tris, 0.4 % SDS
Transfer buffer (Tank blotting)	25 mM Tris-HCl, 192 mM Glycine, 20 % Methanol
Tris-buffered saline with Tween-20 (TBS-T)	10 mM Tris-HCl, 150 mM NaCl, 0.5 % Tween-20, pH 8.0

3.1.9 siRNA oligonucleotides

All siRNA oligonucleotides utilized in this study were purchased from Dharmacon (Lafayette CO, USA). The sequence and ordering information are listed in the following table.

Table 9: siRNA oligonucleotides

Designation	Sequence (5' → 3')	Ordering Number
<i>siCd36</i>	GAAAGGAUAACAUAAGCAAUU	D-062017-01
<i>siFatp1</i>	UGACGGUGGUACUGCGCAA	J-061607-09
<i>siFatp4</i>	AGACCAAGGUGCGACGGUA	J-063631-09
<i>siNT</i>	UAGCGACUAAACACAUCAAUU	D-001210-01
<i>siRab10</i>	GGGCAAAGACCUGCGUCCUU	J-040862-12
<i>siRab12</i>	GCACUACAAUCAGUGACA	J-040865-09
<i>siRab14</i>	GGUGUUGAAUUUGGUACAA	J-040866-09

Designation	Sequence (5' → 3')	Ordering Number
<i>siRab28</i>	GAGCAUAUUGCGAACAGUAA	J-040871-11
<i>siRab40b</i>	UCGAUGGAUUAAGGAGAUU	J-051754-11
<i>siRab8a</i>	CAGGAGCGGUUUCGAACAA	J-040860-09
<i>siRab8b</i>	CGAACAAUUACGACAGCAU	J-055301-10
<i>siTbc1d1</i>	GAUCAGAGGUCAUAUUUAAUU	D-040360-01
<i>siTbc1d4</i>	AAGCUAUACACCAGCAAU	J-040174-05

3.1.10 Western Blot Antibodies

Table 10: Utilized primary and secondary Western Blot antibodies

Name	Host Species	Supplier	Order. #	Dilution used in TBS-T
FAT/CD36	Rabbit	Sigma-Aldrich, St. Louis MO, USA	HPA002018	1:1,000 + 5 % BSA
FATP4	Rabbit	Abcam, Cambridge, UK	ab200353	1:1,000 + 5 % milk powder
PDK4	Rabbit	Abcam, Cambridge, UK	ab214938	1:1,000 + 5 % milk powder
RAB10	Rabbit	Cell Signaling, Danvers MA, USA	#4262	1:1,000 + 5 % milk powder
RAB8a	Mouse	BD Biosciences, Franklin Lakes NJ, USA	610845	1:2,000 + 5 % milk powder
GAPDH	Rabbit	Cell Signaling, Danvers MA, USA	#2118	1:1,000 + 5 % BSA
α -Tubulin	Mouse	Calbiochem, Darmstadt, Germany	DM1A	1:10,000 + 5 % milk powder
Anti-Rabbit-HRP	Goat	Dianova, Hamburg, Germany	111-035-003	1:10,000, 1:20,000
Anti-Mouse-HRP	Rabbit	Dianova, Hamburg, Germany	315-035-008	

3.1.11 Disposable material

Table 11: Disposable material

Material	Supplier
12-well cell culture plate	TPP Techno plastic products, Trasadingen, CH
48-well cell culture plate	Greiner bio one, Frickenhausen, Germany

Material	Supplier
6-well cell culture plate	TPP Techno plastic products, Trasadingen, CH
96-well PCR plate for quantitative Real-time PCR (qRT-PCR)	Applied Biosystems, Darmstadt, Germany
Amersham™ Protran™ 0,45 µm Nitrocellulose membrane	GE Healthcare, Little Chalfont, UK
Cell scraper	Sarstedt, Nümbrecht, Germany
Precision Plus Protein™ Dual Color Standard	Bio-Rad Laboratories, München, Germany
T150 cell culture flask	TPP Techno plastic products, Trasadingen, CH
T75 cell culture flask	TPP Techno plastic products, Trasadingen, CH
TissueLyser stainless steel beads, 5 mm	Qiagen, Hilden, Germany

3.1.12 qRT-PCR (quantitative real-time PCR) primers

The qRT-PCR primers used for mRNA expression analysis for this study were self-designed in our work group using the NCBI primer blast online tool. Primers were ordered at Eurogentec, Belgium.

Table 12: qRT-PCR Primer sequences

Target	Name	Primer sequences (5' → 3')	Product length
<i>Acadl</i>	Acyl-CoA Dehydrogenase Long Chain	Fwd: ATTGCTGAGTTGGCGATTTTC Rev: GCTGCACCGTCTGTATGTGT	112 bp
<i>Cd36</i>	Scavenger Receptor Class B, Member 3	Fwd: CCTAGTAGGCGTGGGTCTGA Rev: ACGGGGTCTCAACCATTCATC	99 bp
<i>Cidec</i>	Cell Death Inducing DFFA Like Effector C	Fwd: CCTGGCAAAGATACCATGTTCA Rev: GCTTCTGGGAAAGGGCTAGCT	104 bp
<i>Cpt1a</i>	Carnitine Palmitoyltransferase 1A	Fwd: CTCAGTGGGAGCGACTCTTCA Rev: GGCCTCTGTGGTACACGACAA	103 bp
<i>Cpt1b</i>	Carnitine Palmitoyltransferase 1B	Fwd: CAGCGCTTTGGGAACCACAT Rev: CACTGCCTCAAGAGCTGTTCTC	105 bp
<i>Dennd4c</i>	DENN Domain Containing 4C	Fwd: CCCTTCGGTTCGGCAGTTG Rev: TGGCTGTTCTACTTCCTGCG	199 bp
<i>Dennd6a</i>	DENN Domain Containing 6A	Fwd: GGGTCGTTGGACGAGGC Rev: GGATATATCACCTCCACCGCC	197 bp

Target	Name	Primer sequences (5' → 3')	Product length
<i>Desmin</i>	Intermediate Filament Protein	Fwd: AGGCTCAAGGCCAAACTACA Rev: TCTGCGCTCCAGGTCAATAC	120 bp
<i>Dgat1</i>	Diacylglycerol O-Acyltransferase 1	Fwd: AGAAGAGGACGAGGTGCGA Rev: GATGGCACCTCAGATCCCAGTAG	149 bp
<i>Dgat2</i>	Diacylglycerol O-Acyltransferase 2	Fwd: AACACGCCCAAGAAAGGTGG Rev: GTAGTCTCGGAAGTAGCGCC	75 bp
<i>Fabp3</i>	Fatty Acid Binding Protein 3	Fwd: ACCTGGAAGCTAGTGGACAG Rev: TGATGGTAGTAGGCTTGGTCAT	106 bp
<i>Fabp4</i>	Fatty Acid Binding Protein 4	Fwd: TGAAATCACCGCAGACGACA Rev: ACACATTCCACCACCAGCTT	141 bp
<i>Fads1</i>	Fatty Acid Desaturase 1	Fwd: CTCGTGATCGACCGGAAGG Rev: TGCCACAAAAGGATCCGTGG	114 bp
<i>Fads2</i>	Fatty Acid Desaturase 2	Fwd: GCCCCTTGAGTATGGCAAGA Rev: TACATAGGGATGAGCAGCGG	99 bp
<i>Fasn</i>	Fatty Acid Synthase	Fwd: TTGCTGGCACTACAGAATGC Rev: AACAGCCTCAGAGCGACAAT	192 bp
<i>Fitm1</i>	Fat Storage Inducing Transmembrane Protein 1	Fwd: CGGCAACTTCTTCAACATAAAGT Rev: GTCGTGTAGCCAGGAACACC	101 bp
<i>Fitm2</i>	Fat Storage Inducing Transmembrane Protein 2	Fwd: CGCAACGTCTCAACGTGTATT Rev: TATACCAGATGGCTGTGCCC	160 bp
<i>Hadh</i>	Hydroxyacyl-CoA Dehydrogenase	Fwd: GAGGCGATGCGTCTAAGGAA Rev: TCCATTTTCATGCCACCCGTC	136 bp
<i>Hif1a</i>	Hypoxia Inducible Factor 1 Subunit Alpha	Fwd: CAAGATCTCGGCGAAGCAA Rev: GTGAGCCTCATAACAGAAGCTTT	113 bp
<i>Hspa8</i>	Heat Shock Protein Family A (Hsp70) Member 8	Fwd: GGCCCTTCATGGTGGTGAAT Rev: TGGTAACGGTCTTTCCGAGG	153 bp
<i>Lipe</i>	Hormone-sensitive Lipase	Fwd: GGAGCTCCAGTCGGAAGAGG Rev: GTCTTCTGCGAGTGTCACCA	98 bp
<i>Lpl</i>	Lipoprotein Lipase	Fwd: CAGCTGGGCCTAACTTTGAG Rev: AATCACACGGATGGCTTCTC	206 bp
<i>Myogenin</i>	Myogenic Factor 4	Fwd: GTGCCAGTGAATGCAACTC Rev: CGAGCAAATGATCTCCTGGGT	94 bp
<i>Pdk4</i>	Pyruvate Dehydrogenase Kinase 4	Fwd: CCTTTGGCTGGTTTTGGTTA Rev: CCTGCTTGGGATACACCAGT	225 bp
<i>Plin2</i>	Perilipin 2	Fwd: GGCTGTAAACGTCTGTCTGGA Rev: AGCACACGCCTTGAGAGAAA	103 bp

Target	Name	Primer sequences (5' → 3')	Product length
<i>Plin3</i>	Perilipin 3	Fwd: ATGAACACTCCCTCGGCAAG Rev: TGGTCCACACCCTGTTTCAC	112 bp
<i>Ppard</i>	Peroxisome Proliferator Activated Receptor Delta	Fwd: ACCGAGTTCGCCAAGAACAT Rev: AGCCCGTCTTTGTTGACGAT	128 bp
<i>Pparg</i>	Peroxisome Proliferator Activated Receptor Gamma	Fwd: CGGGCTGAGAAGTCACGTT Rev: TGCGAGTGGTCTTCCATCAC	200 bp
<i>Ppargc1a</i>	PGC-1-Alpha	Fwd: GAGTCTGAAAGGGCCAAACA Rev: TGCATTCTCAATTTACCA	148 bp
<i>Rab10</i>	Ras-Related Protein Rab-10	Fwd: CGGACGATGCCTTCAATACC Rev: AGGAGGTTGTGATGGTGTGA	144 bp
<i>Rab12</i>	Ras-Related Protein Rab-12	Fwd: CAGGTCATCATCATCGGCTC Rev: ATTTTAAAGTCAACACCCACGG	113 bp
<i>Rab14</i>	Ras-Related Protein Rab-14	Fwd: GTTCAGAGCGGTTACACGGA Rev: TCCTTGCGTCTGTCAACCAG	116 bp
<i>Rab28</i>	Ras-Related Protein Rab-28	Fwd: GCACAGGGAATCCTCTTGGT Rev: TAAAGCAACCAGGGGCTGAG	123 bp
<i>Rab3ip</i>	RAB3A Interacting Protein	Fwd: AAAGCTCAGAGGGAAGCTCACA Rev: GCGATGTTGGAGAACTGGAC	157 bp
<i>Rab40b</i>	Ras-Related Protein Rab-40b	Fwd: CCGAGCAAGGTAAGTACTGAGTTT Rev: TGGCTTCTTAAGGCGACAG	107 bp
<i>Rab8a</i>	Ras-Related Protein Rab-8a	Fwd: CCAGTGCAAAGGCCAACATC Rev: CTGGTCCTCTTCTGCTGCTC	151 bp
<i>Rab8b</i>	Ras-Related Protein Rab-8b	Fwd: AGGAAAATGAACGACAGCAAT Rev: CATCAAAGCAGAGAACAGCG	104 bp
<i>Scl27a1</i>	Long-Chain Fatty Acid Transport Protein 1	Fwd: TGCTTTGGTTTCTGGGACTT Rev: CCGAACACGAATCAGAACAG	149 bp
<i>Scl27a4</i>	Long-Chain Fatty Acid Transport Protein 4	Fwd: ACTGTTCTCCAAGCTAGTGCT Rev: GATGAAGACCCGGATGAAACG	106 bp
<i>Sirt1</i>	Sirtuin 1	Fwd: GCTGACGACTTCGACGACG Rev: TCGGTCAACAGGAGGTTGTCT	101 bp
<i>Sirt2</i>	Sirtuin 2	Fwd: GCCTGGGTTCCCAAAGGAG Rev: GAGCGGAAGTCAGGGATACC	145 bp
<i>Sirt3</i>	Sirtuin 3	Fwd: ATCCCGGACTTCAGATCCCC Rev: CAACATGAAAAGGGCTTGGG	126 bp
<i>Tbc1d1</i>	TBC1 (Tre-2/USP6, BUB2, Cdc16) Domain Family, Member 1	Fwd: ACAGTGTGGGAAAAGATGCT Rev: AGGTGGAAGTCTCAGCTAG	143 bp

Target	Name	Primer sequences (5' → 3')	Product length
<i>Tbc1d4</i>	TBC1 (Tre-2/USP6, BUB2, Cdc16) Domain Family, Member 4	Fwd: CCAACAGTCTTGCCTCAGAG Rev: GAATGTGTGAGCCCGTCTTC	146 bp
<i>TBP</i>	TATA-box binding protein	Fwd: GCGGCACTGCCCATTTATTT Rev: GCGGAATGTATCTGGCACA	236 bp
<i>Tfam</i>	Mitochondrial Transcription Factor 1	Fwd: GGAATGTGGAGCGTGCTAA Rev: CAGACAAGACTGATAGACGAGGG	96 bp
<i>Ucp3</i>	Uncoupling protein isoform 3	Fwd: GTCTGCCTCATCAGGGTGTT Rev: CCTGGTCCTTACCATGCAGT	204 bp
<i>β-Actin</i>	Beta-Actin	Fwd: CCACCATGTACCCAGGCATT Rev: AGGGTGTAACGCAGCTCA	253 bp

3.1.13 Genotyping primers

Table 13: Genotyping primers

Primer	Sequence (5' → 3')	Annealing Temp
<i>Tbc1d1</i> -WT	Fwd: GGACAAGCAGCTTTCTTGTTT Rev: TCCTGGTCCAGAAGCGAG	60 °C 58 °C
<i>Tbc1d1</i> -KO	Fwd: CAACATTCTGAAGGCCTTCTG Rev: TCCCTGGCTACAAGCTGAGT	62 °C 62 °C
<i>Tbc1d4</i>	Fwd: AGTAGACTCAGAGTGGTCTTGG	50 °C
<i>Tbc1d4</i> -WT	Rev: GTCTTCCGACTCCATATTTGC	47 °C
<i>Tbc1d4</i> -KO	Rev: GCAGCGCATCGCCTTCTATC	64 °C
<i>Cd36</i>	Fwd: AGCTCATACATTGCTGTTTATGCATG	62 °C
<i>Cd36</i> -NEO	Fwd: GGTACAATCACAGTGTTTTCTACGTGG	63 °C
<i>Cd36</i>	Rev: CCGCTTCCTCGTGCTTTACGGTATC	66 °C

3.2 Methods

3.2.1 Animal experimental methods

In the following paragraphs the animal experiments that were conducted to physiologically evaluate murine skeletal muscle fatty acid metabolism related parameters are described in detail.

3.2.1.1 *In vivo* electrotransfection (IVE)

To manipulate the expression of a certain target gene of interest in murine skeletal muscles *in vivo* the IVE (in vivo electrotransfection) method was used. This method uses electrical square wave pulses to deliver siRNA (or plasmid DNA) into cells of a tissue after injection. In a first step, siRNA was pre-diluted in sterile saline to achieve a final injection volume of 30 μ l per muscle with an amount of 4 μ g siRNA. Experimental mice were separated and every mouse was solely anesthetized with isoflurane inhalation narcosis in an inhalation chamber. The numbed mouse was then bedded on an isolation pad to prevent cooling down of the body. The nose was connected to a face mask and constantly gassed with isoflurane throughout the whole procedure. Legs were electrically shaved to alleviate the access to the small hind limb muscles. Then 30 μ l saline containing 15 Units hyaluronidase (Sigma-Aldrich, Steinheim, Germany) were injected in the proximal and distal part of the front and the back of the shank (totally 4 injections to target *EDL* and *Soleus* muscle). The hyaluronidase was used to weaken up the extracellular matrix of the muscles to facilitate a later invasion of the siRNA oligonucleotides. Mice were disconnected from isoflurane and put back to their cages. The mice fully recovered quickly. After 1 h of hyaluronidase incubation, mice were anesthetized again and siRNA-saline-solutions were injected at similar positions as the hyaluronidase. The legs were then lubricated with a contact-mediating gel and grabbed with an electrode forceps connected to a square pulse generator. Eight pulses of 80 V, a duration of 20 ms and a frequency of 1 Hz were applied to each leg. Afterwards, legs were cleaned from the gel and mice were placed back into their cages. Seven days after the IVE intervention mice were subjected to *ex vivo* experiments. Following Fig. 8 summarizes the key steps of the IVE procedure.

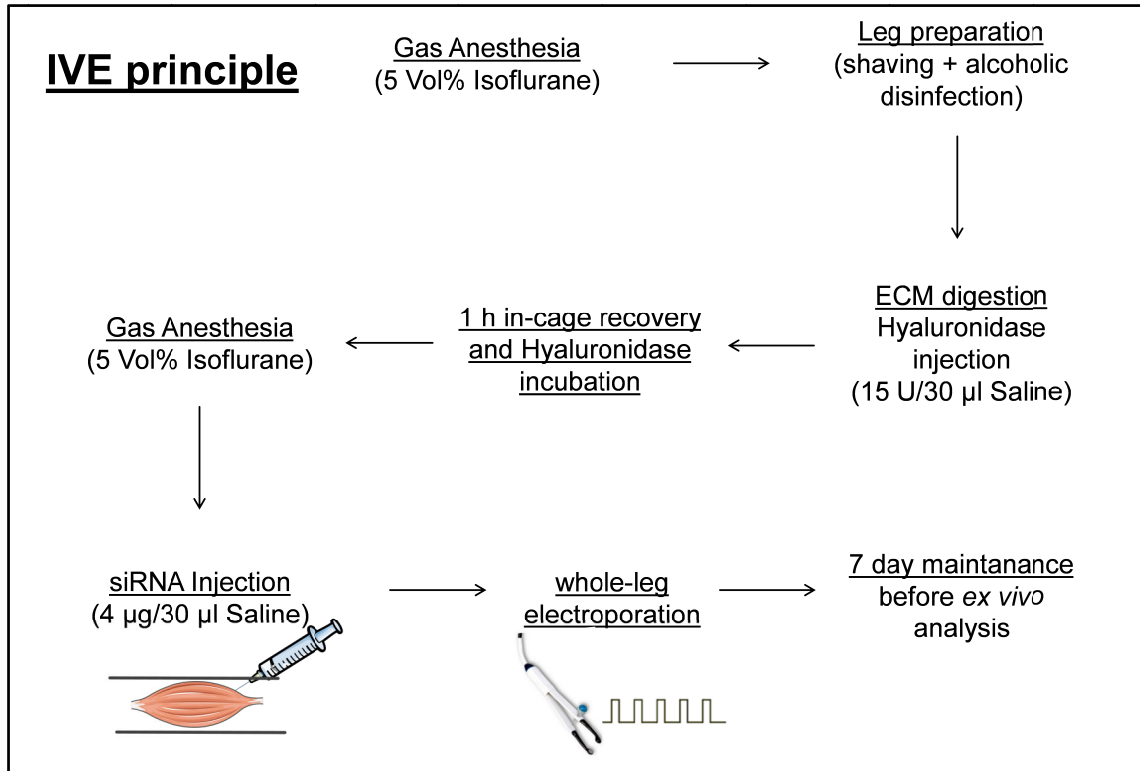


Figure 8: Schematic overview over the IVE principle: Mice were anesthetized with isoflurane, the legs shaved and disinfected and 30 µl saline containing 15 Units of hyaluronidase were injected to the mice hind limbs in the proximal and distal region of *EDL* and *Soleus* muscle. Mice were placed in their cages for 1 h for recovery and hyaluronidase incubation. Then, they were anesthetized again and 30 µl saline with 4 µg siRNA per muscle were injected in the anatomical regions of *EDL* and *Soleus*. After that the whole-leg electrotransfection was conducted by grabbing a leg with an electrode forceps and applying eight consecutive electrical pulses of 80 V for 20 ms and at a frequency of 1 Hz. After one week of mouse housing the ex vivo analysis of the expression manipulation was conducted.

3.2.1.2 *Ex vivo* fatty acid uptake assay

The animals used for the uptake assay were starved for 16 h prior to anesthesia and *EDL* or *Soleus* muscle dissection. Dissected muscles were pre-incubated for 15 min in KHB, supplemented with glucose, mannitol and fatty acid-free BSA. This was followed by two hours of incubation in the HOT buffer containing tritiated palmitate (Tab. 4). Muscles were then removed from the HOT buffer and exteriorly dried with filter papers and subsequently quick-frozen in 2 ml safe-seal reaction tubes in liquid nitrogen. For assessing *ex vivo* palmitic acid uptake, a stainless 5 mm TissueLyser steel bead (Tab. 11) and 300 µl protein lysis buffer (supplemented with phosphatase and protease inhibitors; Tab. 8) were pipetted into each safe-seal reaction tube. The muscles were then homogenized with a TissueLyser (Tab. 6) for 5 minutes at a shaking frequency of 25 Hz. Afterwards, the homogenized muscle samples were centrifuged for 10 minutes at 14,000 rcf and 4 °C to pellet the cell debris. The cleared protein supernatants were transferred to fresh 1.5 ml reaction tubes and stored at -20 °C. An aliquot of the muscle lysate was taken to determine the protein concentration of the sample by BCA assay (Tab. 5). Another aliquot of 50 µl was used for liquid scintillation counting to measure the amount of

radioactively labeled ^3H -palmitic acid that has been taken up by the muscle *ex vivo*. 50 μl of muscle lysate were mixed with 3 ml of scintillation liquid, mixed thoroughly and then subjected to the β -counter (Tab. 6). The obtained CPM values (counts per minute) of the muscle sample were normalized to the respective protein concentration of the sample. Due to inter-experiment variations the data of each single experimental day were normalized and expressed as fold of the respective reference group (e.g. wildtype mouse EDL fatty acid uptake).

3.2.1.3 *Ex vivo* fatty acid oxidation assay

The buffer compositions and incubation conditions for the oxidation assay are equal to the conditions described for the *ex vivo* fatty acid uptake assay. In contrast to the uptake assay, the animals for the oxidation assay were starved for 4 h prior to muscle dissection. The assay was essentially performed as previously described (Chadt et al., 2015). After pre- and HOT incubation (see 3.2.6.2), muscles were removed from the HOT buffer, dried with filter tissues, weighted and quick-frozen in liquid nitrogen. The Hot buffer from the vials was transferred to fresh reaction tubes. Volume of HOT buffer was determined by weighing the reaction tube (1 g = 1 ml). *Ex vivo* fatty acid oxidation was assessed indirectly by measuring the amount of $^3\text{H}_2\text{O}$ released by the muscle into the buffer as a by-product of lipid oxidation. To remove tritiated palmitate which would also contribute to the ^3H counting and to only measure the oxidation end product, the HOT buffer was filtered for 20 min in an overhead shaker through a 10 % activated charcoal slurry in Tris-HCl after the HOT muscle incubation. After centrifugation at RT for 10 min at 14.000 rcf in a table-top centrifuge to pellet the charcoal particles, the cleared filtrate was subjected to liquid scintillation counting to determine the amount of $^3\text{H}_2\text{O}$ released by the muscles as a product of β -oxidation.

3.2.1.4 *Ex vivo* determination of skeletal muscle malonyl-CoA and acetyl-CoA levels

Malonyl-CoA is a critical regulator of fatty acid oxidation and fatty acid synthesis (Foster, 2012). It was described that high levels of malonyl-CoA inhibit fatty acid oxidation and promote fatty acid synthesis. Acetyl-CoA levels can be associated with malonyl-CoA levels, as it can be converted into malonyl-CoA by acetyl-CoA carboxylase, and be generated from malonyl-CoA by malonyl-CoA decarboxylase. Determination of acetyl- and malonyl-CoA levels of WT and D1KO Soleus muscles was performed externally by the Metabolomics Unit of the Sanford Burnham Prebys medical discovery institute in Orlando FL, USA. Briefly, the metabolites were measured by an LC-MS/MS approach with electrospray ionization. For measurement, the samples are homogenized in 5 % trichloroacetic acid and supplemented with an internal standard that is labeled with a stable isotope. Extraction is achieved by solid phase extraction. The calculated amounts of malonyl- and acetyl-CoA can be expressed as pmol per mg dry muscle tissue.

3.2.2 Cell culture experiments

3.2.2.1 Cell culture of C2C12 myoblasts

The C2C12 cells represent a mouse myoblast cell line. The cells were originally isolated from mouse thigh muscle satellite cells in 1977 by Yaffe and Saxel. The cells are able to differentiate from myoblasts to myotubes after exogenous induction by serum withdrawal (McMahon et al., 1994; Yaffe & Saxel, 1977). Myogenesis is regulated by a set of myogenic regulatory factors (MRFs) (Tomczak et al., 2004). The expression pattern of the MRFs is characteristic for the stage of C212 cell differentiation on the way from myoblasts to myotubes. Differentiated myotubes develop several features that are discriminatory for skeletal muscles, including a functional contractile apparatus (Bajaj et al., 2011). C2C12 cells are often used to study differentiation events of precursor fibroblasts to skeletal muscle cells. Also, the cell line is a well-established model of skeletal muscle cells and is widely used to study muscle physiology and metabolism, as well as muscle tissue-associated diseases.

The cells were cultured in cell line-specific culture medium that harbors certain supplements to guarantee survival, growth and division of the cells (see Tab. 8). The growth and survival of the cells is depending on the adherence of the cells to the surface of the culture vessel (Ruoslahti & Reed, 1994). As an adherent cell line, the C2C12 cells only proliferate and grow when attached to the culture flask. The cells were incubated at 37 °C and 5 % CO₂ in a humidified incubator (Tab. 6). Growth, confluence and condition of cultured cells were controlled at regular intervals using an inverse cell culture microscope (Tab. 6). Cell line-specific growth medium was changed either every two to three days by carefully aspirating the old medium with a vacuum pump and adding a sufficient amount of fresh culture medium. Depending on the purpose of the experiment, the cells were either supplied with growth medium, or with differentiation medium. An overview of the media used during these experiments is depicted in Tab. 8.

When the cells reached a confluence of 70-80 % they were trypsinized and split into fresh larger flasks for maintenance or smaller multiwell plates for treatments and experiments. For splitting, the growth medium was aspirated and the cells were washed once with 1xPBS (w/o Mg²⁺/Ca²⁺) (Tab. 3). Then, a suitable volume of Trypsin-EDTA (Tab. 3) (T150 cm² flask: 3 ml, T75 cm² flask: 2 ml) was added to harvest the cells from the bottom of the culture flask. The trypsinization was performed for 3-5 min, and then fresh pre-warmed growth medium was added to inhibit trypsin and suspend the cells. The cell count was determined by counting an aliquot of cells in a Neubauer counting chamber. A desired amount of cells was seeded into the respective culture vessel for either maintenance culture or experimental culture.

3.2.2.1.1 Freezing, thawing and maintaining of C2C12 cells

A stock of cells was preserved at -196 °C in liquid nitrogen. Before removing the cells from the liquid nitrogen, a falcon tube containing growth medium was prepared and put into a 37 °C water bath. Subsequent to thawing the cells, 1 mL of the cell suspension was transferred from the freezing vial to the pre-warmed medium in the falcon tube. Then, the cells were pelleted in the tube by centrifuging at room temperature for 5 minutes at 1000 rpm. The supernatant was aspirated and cells were resuspended in fresh growth medium. The cells suspension was pipetted into the previously prepared T75 cell culture flask and transferred into a cell incubator (Tab. 6) at 37 °C and 5 % CO₂ atmosphere.

To conserve cells for further experiments and to generate a stock of undifferentiated cells, cells can be stored in cryo vials in liquid N₂. To prevent decessing, cells are frozen in growth medium supplemented with DMSO. After trypsinization, the cells were centrifuged and resuspended in freezing medium. Aliquots of the cell suspension were then pipetted carefully into cryo vials and put into a specific freezing container filled with 100 % isopropanol. This container is designed to guarantee a linear decrease if the temperature of -1 °C per minute in order to not harm the cells during the freezing procedure. After one day at -80 °C, the vials were transferred from the freezing container to a liquid N₂ storage rack.

Thawed C2C12 myoblasts are maintained in growth medium containing 10 % of fetal calf serum (FCS) and 1 % penicillin/streptomycin (P/S) (Tab. 3). It is required to split cells before they reach 100 % confluence to avoid a loss of myoblast identity of the cells. Following Table A summarizes the cell counts seeded in a certain model of culture vessel prior to differentiation.

Table 14: Seeding densities of C2C12 myoblasts prior to differentiation

Vessel	Bottom area [mm ²] per well, flask	Seeded cell count
48-well	100	2×10^4
12-well	400	4×10^4
6-well	960	2×10^5
T75	7500	5×10^5
T150	15000	1×10^6

For continuous cell maintenance, the cells were kept in T75 or T150 cell culture flasks. From these containers the cells for experimental use were harvested and divided into multiwell culture plates at the defined cell density (Tab. 14).

In the respective culture plates the C2C12 cell differentiation from myoblasts to myotubes was induced by changing the general growth medium (Tab. 8) with differentiation medium (DMEM + 2 % horse serum + 1 % penicillin/streptomycin) 24 hours after initial seeding.

Differentiation medium was renewed every second day. Figure 9 illustrates a schematic overview over the chronology of conducted cell culture steps.

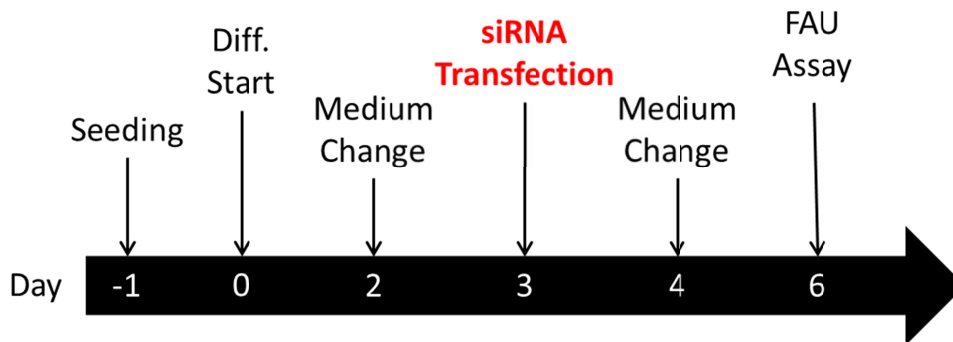


Figure 9: C2C12 cell culture and usage time line. C2C12 cells are seeded in a respective cell culture vessel on day -1. After overnight culture in a 37 °C and 5 % CO₂ incubator the cells attached to the culture flask or dish. Growth medium (DMEM + 10 % FCS + 1 % P/S) is replaced with differentiation medium (DMEM + 2 % HS + 1 % P/S) to induce cell differentiation from myoblasts to myotubes. Differentiation medium is renewed on day 2 of differentiation. On day 3 of differentiation, the C2C12 cells become chemically transfected with siRNA in transfection medium (DMEM w/o supplements). Transfection medium is changed with differentiation medium on day 4. Experiments (e.g. FAU Assay) are performed 6 days after the induction of cell differentiation. A detailed protocol of C2C12 siRNA transfection is described in the following paragraph.

3.2.2.1.2 Chemical siRNA transfection

During the course of differentiation from myoblasts to myotubes, C2C12 cells were transfected with specific siRNA oligonucleotides to selectively manipulate the expression of certain genes of interest to finally decrease the amount of a certain target protein. All C2C12 siRNA transfections for this study were performed on day 3 of cell differentiation. Since the C2C12 grow adherent and the cells massively change their morphology during differentiation, a transfection approach that would have required cells to be present in suspension was not suitable. Because of that, a chemical transfection approach was used. All siRNA oligonucleotides used were obtained from Dharmacon (Lafayette CO, USA). Since Dharmacon also offers cell line-specific transfection reagents, the Dharmafect 1 transfection solution was used to transfect the differentiating C2C12 cells. The sequence information of the siRNAs used for this study are listed in Table 9. The lyophilized siRNA was resuspended in sterile nuclease-free H₂O as recommended by the manufacturer. In brief, a defined amount of water was added to the siRNA tube to achieve a siRNA stock concentration of 250 µM. For transfection, a concentration of 50 nM of siRNA per cell well or plate was used. For every transfection, siRNA was diluted in FCS- and P/S-free DMEM. In a second reaction tube the transfection reagent was diluted with FCS- and P/S-free DMEM to achieve 2 % of DharmaFECT1 in the same volume as the siRNA dilution. Diluted siRNA and diluted DharmaFECT1 were mixed in a 1:1 ratio and incubated for 30 min at RT. In the meantime, cells were washed once with serum- and antibiotic-free DMEM medium. Then a defined volume of this medium was added to each well. Afterwards, a defined amount to finally yield 50 nM siRNA/well of siRNA-transfection reagent

solution was added dropwise to each well. Cells were incubated at 37 °C / 5 % CO₂ for 24 h. Then, medium was aspirated and changed back to differentiation medium. Cells were maintained until day 6 of differentiation before experiments were performed.

3.2.2.2 *In vitro* assays

3.2.2.2.1 *In vitro* fatty acid uptake assay

To assess the influence of certain expression manipulations on the fatty acid uptake of C2C12 myotubes, a fatty acid uptake assay was developed and established. C2C12 myoblasts were seeded in 12-well plates at a density of 4×10^4 cells/well. After the induction of differentiation and siRNA transfection where needed, the cells were maintained in differentiation medium until day 6 of differentiation. On this day the assays were performed. Cells were washed once with Krebs-Ringer-HEPES (KRH) buffer (Tab, 8) supplemented with 0.1 % fatty acid-free BSA (FA-free BSA), before they were serum-starved with DMEM (high glucose) supplemented with 1 % FA-free BSA. Subsequently, cells were washed three times with KRH + 0.1 % FA-free BSA (washing buffer), then once with pure KRH buffer. Then 1 ml of KRH supplemented with 40 μM FA-free BSA was added to the cells. This solution remained on the cells until the end of the assay. To start the uptake assay, 1 ml of a KRH-based buffer (HOT buffer) containing 8.5 nM ³H-palmitate, 2.5 μM FA-free BSA and 5 μM unlabeled cold palmitate, bound in a molar ratio of 2:1 to BSA, was added to each well. One well per plate was incubated with HOT buffer supplemented with 450 μM cold unlabeled palmitate to measure background uptake activity of the cells. The myotubes were incubated with the HOT buffer for 5 minutes in a cell culture incubator at 37 °C / 5 % CO₂. To stop the uptake, the 12-well plate was put on ice and the HOT buffer was immediately aspirated. Each well was intensively washed three times with ice-cold washing buffer. Residual washing buffer was completely aspirated and cells were lysed on ice in 300 μl/well protein lysis buffer (w/ protease- and phosphatase inhibitor cocktail). Cells were harvested with cell scrapers and the whole lysate was transferred to 1.5 ml reaction tubes. Cell debris was pelleted by centrifugation for 10 min at 4 °C and 20,000 rcf. Cleared supernatants were transferred to fresh reaction tubes. 50 μl were used for liquid scintillation counting, the rest was used for protein measurement and stored at -20 °C. Counting data were measured with a β-counter (Tab. 6) and expressed as counts per minute (CPM). The CPM value of each sample was then normalized to the respective protein concentration (3.2.4.2) to account for well-to-well cell number differences. In order to compensate for variations between experiments the final data were expressed as folds of non-treated cells.

3.2.2.2.2 *In vitro* fatty acid oxidation assay

Similar to the influence of specific expression manipulations on uptake of fatty acids, a comparable approach was conducted to evaluate the role of certain proteins of interest on the

oxidation of palmitic acid in C2C12 myotubes. The background of this assay is the trapping of $^{14}\text{CO}_2$ as a side-product of ^{14}C -palmitic acid oxidation. The acetyl-CoA from one round of β -oxidation is further metabolized in the citric acid cycle which leads to the release of CO_2 . Since one C atom in the palmitic acid chain is radioactively labeled, beside CO_2 also $^{14}\text{CO}_2$ will be released (Huynh et al., 2014). Myoblasts were seeded at a count of 2×10^4 cells/well in 48-well plates. To perform the assay, it was important to only seed cells in the first, third and fifth row of a 48-well plate because the second, fourth and sixth row were needed to measure the fatty acid oxidation later. After 24 h, cell differentiation was induced (3.2.2.1). On day 3 of differentiation, intended siRNA transfections were performed (3.2.2.2) and cells were further cultured until day 6. The fatty acid oxidation assay was basically performed as described by Lambernd et al. and Stermann et al. (Lambernd et al., 2012; Stermann et al., 2018). On the day of the experiment, the cells were washed once with fresh differentiation medium. Then 400 μl differentiation medium were added to each well. 4 cm^2 filter paper were quartered and placed into every empty well of the 48-well plate. Each filter paper was soaked with 50 μl 1 M NaOH. The 48-well plates were placed in the frame of the custom-made fatty acid oxidation chamber. 400 μl of fatty acid oxidation HOT buffer, containing 11.8 μM ^{14}C -palmitate, 6.24 μM fatty acid-free BSA and 1 μM L-carnitine in C2C12 differentiation medium were added to each well. Control wells for background oxidation measurements were supplemented with 400 μl 1 M HCl. The lid of the oxidation chamber was put on to tightly seal the wells. After an incubation time of 4 h at 37 $^\circ\text{C}$ / 5 % CO_2 , the HOT buffer was transferred to a fresh 48-well plate in the wells corresponding to the initial position on the other plate. The filter papers were transferred to the new plate as well. The adherent cells were washed once with 1xPBS and frozen at -20 $^\circ\text{C}$ for protein measurement (3.2.4.1). Then 400 μl of 1 M HCl were added to wells that contained the transferred HOT buffer. The lid of the oxidation chamber was tightly closed again and the chamber was again placed in the cell incubator overnight. Acidification of the HOT buffer with HCl caused the release of CO_2 from the liquid phase into the gas phase. The gas diffused through the pore that connects the two neighboring wells and was trapped by the NaOH-soaked filter paper. After overnight incubation, the oxidation chamber was opened, the filter papers were collected in scintillation vials and 3 ml of scintillation liquid (Tab. 3) were added. Vials were placed in a scintillation counter (Tab. 6) to measure the ^{14}C signal coming from the radioactive $^{14}\text{CO}_2$ bound to the filter papers. Normalized on protein concentrations, the fatty acid oxidation was expressed as CPM per μg of protein. Due to high variations among the experiments, the individual experiments were summarized as fold of non-treated cells. The whole procedure of the *in vitro* FAO assay is summarized in following Figure 10.

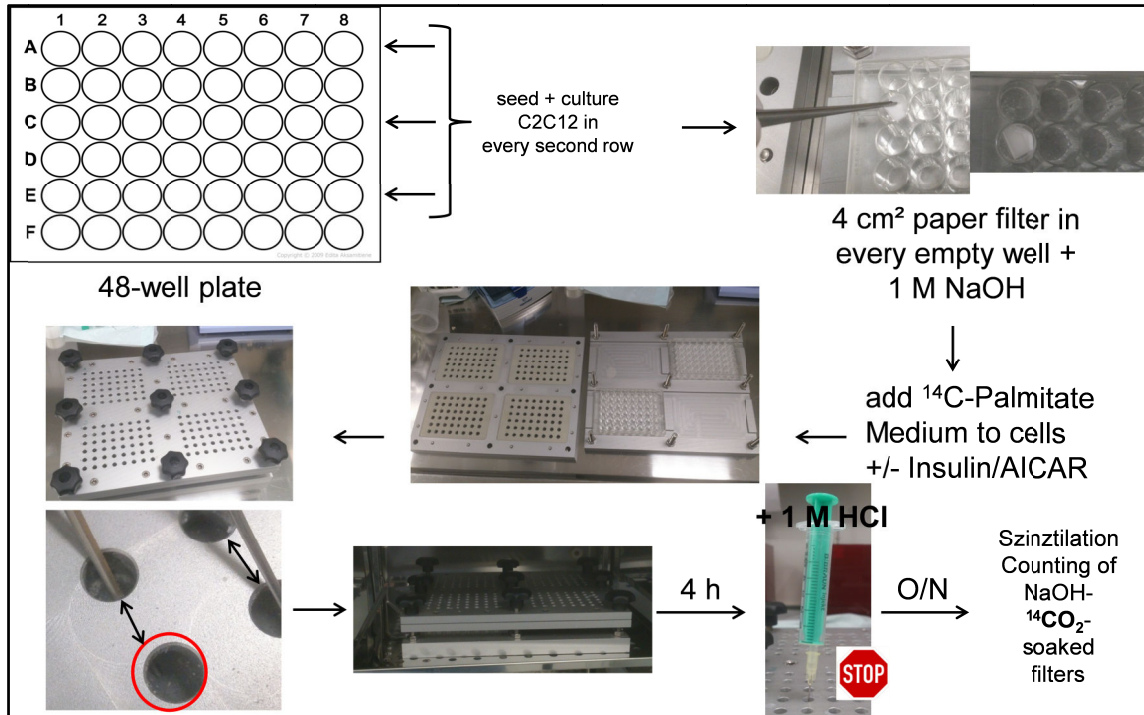


Figure 10: *In vitro* fatty acid oxidation assay. Cells were seeded at a density of 2×10^4 cells/well in every second row of a 48-well plate. Cells were differentiated for 6 days and transfected with siRNA where needed on day 3 of differentiation. On the day of the experiment a 4 cm² filter paper was placed into every empty well and soaked with 50 μ l 1 M NaOH. Then H¹⁴O buffer containing ¹⁴C-palmitic acid was added to every cell-containing well. The cell culture plates were placed in position in the custom-made oxidation chamber and the chamber was closed tightly with a lid. After 4 h of incubation at 37 °C and 5 % CO₂, 1 M HCl was injected through the gasket of the chamber lid to terminate oxidation and to acidify the buffer in order to drive out the gasses from the buffer. ¹⁴CO₂ from the buffer gets into the air and diffuses through a connective pore into the neighboring well and bind to the NaOH-soaked filter paper.

3.2.3 Methods of molecular biology

3.2.3.1 Isolation of genomic DNA from mouse tail tips

In order to determine the genotype of the experimental mice used for specific experiments and to ensure that the correct genotypes were utilized in the *ex vivo* experiments, approximately 1-2 mm of the mouse tail tip was collected in a reaction tube after weaning. Isolation of genomic DNA was performed with the Invisorb® Genomic DNA Kit II (Tab. 5) according to the manufacturer's instructions. Briefly, the tail tip biopsy was lysed in 200 μ l lysis buffer, supplemented with 10 μ l Proteinase K. For lysis, the tubes were incubated for 3 h or overnight at 60 °C and 1,200 rpm in a Thermomix (Tab. 6). To pellet the cell debris, the lysate was then centrifuged in a table centrifuge (Tab. 6) at room temperature for 1 min at 16,000 rcf. The supernatant was collected in a fresh reaction tube and supplemented with 450 μ l DNA binding buffer consisting of a silica particle slurry. To enable an effective binding of the DNA to the silica particles, the DNA-binding buffer suspension was incubated for 5 min at room temperature and then mixed thoroughly. The suspension was centrifuged for 30 seconds at 16,000 rcf and the

supernatant was discarded. The silica-DNA pellet was washed once with 650 μl ethanolic washing buffer and then re-suspended using a gyrator (Tab. 6). The washing procedure was conducted three times. After the last washing step and aspiration of the supernatant, the pellet was dried at 60 $^{\circ}\text{C}$ for approximately 10 min in a Thermomixer to evaporate any remaining ethanol (EtOH) left from the washing buffer. The sample was chilled to room temperature for 3 min before the DNA was eluted from the silica particles by adding 200 μl of pre-heated (60 $^{\circ}\text{C}$) elution buffer. The sample was mixed thoroughly with a gyrator. Then it was incubated at 60 $^{\circ}\text{C}$ for 3 min in a Thermomixer. The silica particles were sedimented by centrifugation in a table-to-centrifuge at RT for 2 min at 18,000 rcf and 180 μl of cleared supernatant were transferred to a fresh reaction tube. The DNA concentration was measured with the NanoDrop (Tab. 6) device.

3.2.3.2 Determination of nucleic acid concentration

For determining the concentration of isolated DNA and RNA samples the NanoDrop (Tab. 6) device was used. The measurement was conducted according to the instructions of the manufacturer. For DNA or RNA concentration measurements 1 μl of sample were used.

3.2.3.3 Genotyping of experimental animals

To analyze the genotype of the experimental animals, a Polymerase chain reaction (PCR) was performed to amplify a genetic region of interest. The PCR products were subsequently visualized with an ethidium bromide-stained agarose gel and a UV gel imager (GelDOC, Tab. 6).

For genotyping D1KO mice the following reaction setup with a total reaction volume of 20 μl was used:

Table 15: Reaction setup for genotyping D1KO mice

Compound	Volume [μl]	Stock Concentration
MQ-H ₂ O	5,8	/
HF-Buffer	4	/
dNTP	2	8 mM
<i>Tbc1d1</i> KO Fwd	1	10 nM
<i>Tbc1d1</i> KO Rev	1	10 nM
<i>Tbc1d1</i> WTFwd	1	10 nM
<i>Tbc1d1</i> WTRev	1	10 nM
Phusion-Polymerase	0,2	2 U/ μl
DNA	4	10 ng/ μl

Genotyping of D4KO mice was performed according to the following reaction setup:

Table 16: Reaction setup for genotyping D4KO mice

Compound	Volume [μ l]	Concentration
MQ-H ₂ O ₀	5.8	/
5x GreenGoTaq-Buffer	4	/
dNTP	2	8 mM
<i>Tbc1d4</i> Fwd	2	10 nM
<i>Tbc1d4</i> WTRev	1	10 nM
<i>Tbc1d4</i> KO Rev	1	10 nM
GoTaqPolymerase	0.2	2 U/ μ l
DNA	4	/

For CD36KO genotyping the reaction setup represented in the next Table was used:

Table 17: Reaction setup for genotyping CD36KO mice

Compound	Volume [μ l]	Concentration
MQ-H ₂ O ₀	5.8	/
5x GreenGoTaq-Buffer	4	/
dNTP	2	8 mM
<i>Cd36</i> Fwd	2	10 nM
<i>Cd36</i> KO Rev	1	10 nM
<i>Cd36</i> Rev	1	10 nM
GoTaqPolymerase	0.2	2 U/ μ l
DNA	4	/

Table 18 summarized the thermos cycling protocols that were run for genotyping PCRs:

Table 18: Genotyping thermocycler programs

Step	<i>Tbc1d1</i>		<i>Tbc1d4</i>		Repeats	<i>Cd36</i>		Repeats
	Temp.	Time	Temp.	Time		Temp.	Time	
Lid heating	105 °C	∞	105 °C	∞	Entire run	105 °C	∞	Entire run
Hot Start	98 °C	30 sec	95 °C	2 min	-	98 °C	30 sec	-
Denaturation	98 °C	10 sec	95 °C	30 sec	30x	98 °C	10 sec	33x
Annealing	65 °C	30 sec	60 °C	30 sec		66 °C	30 sec	
Elongation	72 °C	5 sec	72 °C	1 min		72 °C	1 min	
	72 °C	7 min	72 °C	5 min	-	72 °C	5 min	-
Storage	4 °C	∞	4 °C	∞	-	4 °C	∞	-

3.2.3.4 Agarose gel electrophoresis

PCR products were separated on 1 % Agarose gels that were previously supplemented with 0.005 vol% ethidium bromide. Ethidium bromide intercalates between the DNA bases and DNA bands can be visualized by UV irradiation. Staining results were documented with a GelDOC device (see Tab. 6).

3.2.4 Biochemical methods

3.2.4.1 Protein isolation from cell culture and isolated murine skeletal muscle samples

To generate protein samples that are free from cellular debris, the respective culture medium was aspirated from dishes with adherent cells. The cells were washed once with pre-warmed 1xPBS (same volume as culture medium), PBS was removed thoroughly and a distinct volume of lysis buffer supplemented with protease inhibitors and phosphatase inhibitors (Tab. 8) was added to each well (12-well plates: 100 µl/well, 6-well plate: 250 µl/well). Cells were incubated on ice for 5 min. After that, cells were detached from the bottom of each well with a cell scraper and transferred into 1.5 ml reaction tubes.

For primary muscles, each muscle was put into a 2 ml safe-seal reaction tube and incubated with 300 µl ice-cold lysis buffer (with inhibitors) on ice for 5 min. A stainless steel bead was added to each tube and the muscles were subjected to homogenization with a TissueLyser (Tab. 6) at 25 Hz for 5 min.

The cell or muscle lysates were centrifuged at 4 °C for 10 min at 21,000 rcf. The supernatant was collected and transferred into new 1.5 reaction tubes. Cleared lysates were stored at -20 °C for further use.

3.2.4.2 Determination of protein concentration

Protein concentrations of cell and tissue samples were determined using the BCA method (Smith et al. 1985) which is based on the reduction of Cu²⁺ ions by the interaction with proteins (Biuret reaction) and their subsequent complexing with bicinchoninic acid. The measurement was conducted using the BCA Protein Assay Kit (Tab. 5) with regards to the manufacturers' instructions. Extinction was measured at 562 nm using a Bio-Rad plate reader photometer (Tab.6).

3.2.4.3 Western Blot analysis

3.2.4.3.1 Sample preparation and SDS-polyacrylamide gel electrophoresis

After determination of the total protein concentration, cleared lysates were prepared for subsequent gel electrophoresis and Western blotting. The protein sample was pipetted into a fresh reaction tube and diluted with Millipore water to yield a final concentration of 1 µg total protein/µl total SDS sample. Then 4x Laemmli buffer stock (see 3.1.5) was added to yield a final 1x concentration. Depending on the respective antibody used for targeted protein detection, the protein-Laemmli buffer mixture was either heated to 95 °C for 5 min, or incubated at RT for 30 min. During Laemmli incubation the protein samples denature. Additionally the proteins become covered by negatively charged SDS molecules in an amount-dependent fashion. It is known that 1.4 g of SDS cover 1 g of protein. With this constant mass to charge ratio the proteins migrate in the electric field at a speed according to their size. The samples were ready for immediate use or storage at -20 °C.

Prepared protein samples were loaded on SDS-polyacrylamide gels. The amounts of acrylamide in the separation gels differed between 10–14 % with regard to the target protein of interest. Gels were run in the buffer chamber (Tab. 6) at 100 V for 10 min, before the voltage was increased to 200 V for 50 – 60 min, according to the percentage of the gel, which is determining the migration speed. After separation according to their molecular weight, the proteins were transferred from the gel to a nitrocellulose membrane. Gels were composed of the following chemicals and buffers. Table 19 summarizes the preparation of a 1 mm thick 10 % SDS-acrylamide gel, casted in the Bio-Rad short plate gel casting system (Tab. 6).

Table 19: SDS-polyacrylamide gel preparation

Compound	Volume
Stacking gel	
Stacking gel buffer (Table 8)	520 µl
Acrylamide (30%)	260 µl
ddH ₂ O	1.22 ml
Ammonium persulfate (APS)	4 µl
Tetraethylethylendiamine (TEMED)	2 µl
Separation Gel	
Separation gel buffer (Table 8)	1.56 ml
Acrylamide	2 ml
ddH ₂ O	2.44 ml
APS	12 µl
TEMED	6 µl

3.2.4.3.2 Tank Western Blotting and protein detection

After SDS-PAGE, the separated proteins were transferred from the polyacrylamide gel to a nitrocellulose membrane. Depending on the protein size, the transfer was performed for 4 hours or overnight. After protein transfer from the gel to the nitrocellulose membrane, the membrane was blocked for 1 h with 5 % fat-free powdered milk in TBS-T (Tab. 8) to cover unspecific antibody binding sites on the membrane surface. After washing the membrane thoroughly with TBS-T, membranes were incubated overnight with the respective primary antibody solution (see Tab. 10). After thoroughly washing the membranes with TBS-T and incubation with a specific primary antibody-dependent secondary antibody at a certain dilution (see Tab. 10), the membranes were detected with either Western Lightning ECL Pro solution, or, for more sensitive applications, Western Lightning ECL Ultra solution (Tab. 5) and visualized in the ChemiDoc Western Blot documentation system (Tab. 6). Quantitative analysis was carried out with the Image Lab software (Tab. 7).

3.2.4.4 GC-analysis of skeletal muscle fatty acid composition

For determination of skeletal muscle fatty acid composition, an experimental approach involving gas chromatography was conducted. The analysis in this work was conducted in-house with *Gastrocnemius* muscle samples of WT and D1KO mice at an age of 12 weeks. All animals were kept on chow diet prior to muscle dissection. After dissection, the *Gastrocnemius* muscle samples were quick-frozen in liquid nitrogen and subsequently stored at -80 °C for further use. On the day of experiment, the muscle samples were thawed on ice and 40-90 mg of frozen muscle were used for the measurements. Tissue samples were incubated with 200 µl pentadecanoic acid ([1 µg/µl] in n-hexane) and 1 ml 1M methanolic NaOH (4 g NaOH pellets dissolved in 100 ml MeOH) for 60 min at 90 °C in a waterbath to saponify the fatty acids in the sample. After the samples had again reached room temperature they were transferred to glass reaction tubes and supplemented with 1 ml n-hexane. Samples were vortexed for 30 sec and subsequently centrifuged for 5 min at 1,400 rcf. The upper hexane phase was discarded. The lower phase was neutralized with 1 M HCl. 4 ml n-hexane were added and the samples were vortexed. After centrifugation for 5 min at 1,400 rcf, 3 ml of the upper organic phase were transferred to a reaction tube. The total volume was inspissated with N₂ at 40 °C. Next, 110 µl derivatization solution (100 % MeOH with 0.9 M acetyl chloride) were added to each sample and tubes were incubated for 30 min at 90 °C. After cooling, the samples were inspissated completely with N₂ at 50-60 °C. Samples were reconstituted in 500 µl n-hexane by vortexing. The whole sample was transferred to a chromatography vial and used for gas chromatography. A self-prepared fatty acid standard containing 200 µg/µl defined fatty acids was subjected to GC analysis (Tab. 6) to assign the measured retention times to the respective fatty acid. The composition of the standard is summarized in Table 20.

Table 20: Fatty acid reference standard for gas chromatography.

Trivial name	Carboxyl-reference	ω -reference
Mystiric acid	C14:0	C14:0
Pentadecanoic acid	C15:0	C15:0
Palmitic acid	C16:0	C16:0
Palmitoleic acid	C16:1 Δ^9	C16:1 (ω -7)
Margaric acid	C17:0	C17:0
Stearic acid	C18:0	C18:0
Oleic acid	C18:1 Δ^9	C18:1 (ω -9)
Linoleic acid	C18:2 $\Delta^{9,12}$	C18:2 (ω -6)
α -Linoleic acid	C18:3 $\Delta^{9,12,15}$	C18:3 (ω -3)
Arachidonic acid	C20:4 $\Delta^{5,8,11,14}$	C20:4 (ω -6)

3.2.4.4.1 GC data analysis and calculations

The results of the GC fatty acid profiling are presented as peak amplitude [pA] plotted over the retention time [min]. A representative GC fatty acid profile showing the results of the fatty acid standard measurement is presented in Figure 11.

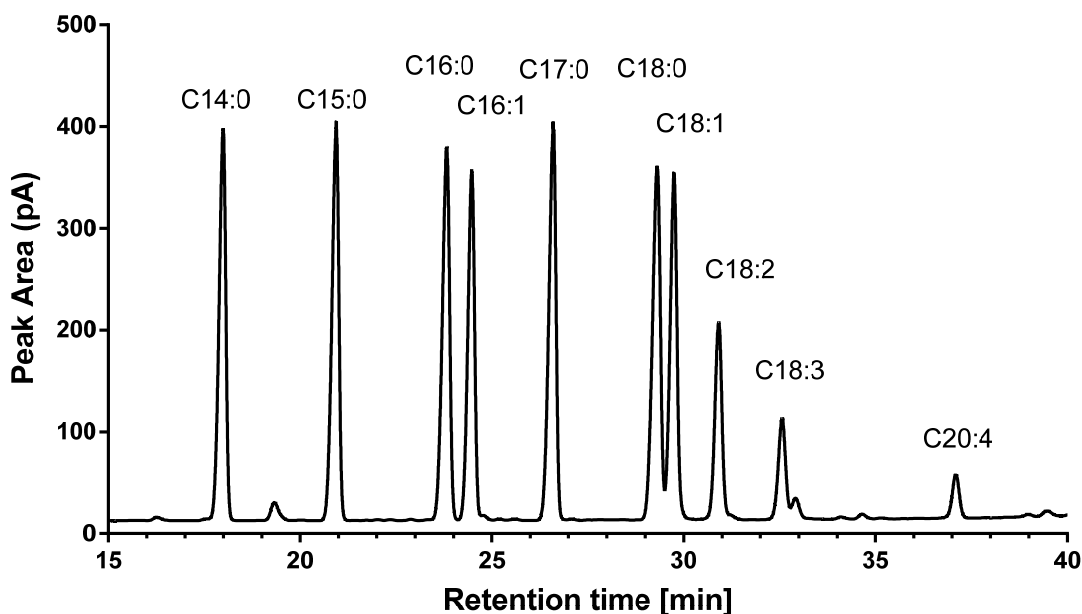


Figure 11: Representative GC fatty acid profiling result. The amplitude of the detected signal peak is plotted over the retention time. Each peak reflects a certain species of fatty acid (see Tab. 20) that is part of the fatty acid standard.

From the values of peak area of C15:0 pentadecanoic acid and the amount of C15:0 standard (200 μ g) an internal correction factor can be calculated:

$$\text{Internal correction factor } [\mu\text{g}] = \frac{\text{Amount C15:0 standard } [\mu\text{g}]}{\text{pA (C15:0)}}$$

The amount of fatty acid in μg per mg muscle can be calculated as following:

$$\text{Fatty acid } \left[\frac{\mu\text{g}}{\text{mg}} \right] = \frac{\text{pA (respective fatty acid)} \times \text{C15:0 correction factor } [\mu\text{g}]}{\text{wet muscle tissue } [\text{mg}]}$$

The total saturated fatty acid (SFA) amount in $\mu\text{g}/\text{mg}$ is calculated as the sum of C14:0, C16:0 and C18:0. Total mono and poly unsaturated fatty acid content of each sample is calculated as sum of C16:1 and 18:1, respectively C18:2, 18:3 and 20:4.

Desaturase activities:

From the measured values several indices can be calculated in order to gain detailed insight into the fatty acid handling and processing properties of the respective sample. Enzyme activity of stearoyl-CoA desaturase-1 (SCD1), an enzyme that catalyzes the conversion of C16:0 and C18:0 saturated fatty acids into the monounsaturated fatty acids into palmitoleic acid (C16:1 Δ^9) and oleic acid (C18:1 Δ^9), respectively (Flowers, 2009).

The C16 Δ^9 -desaturase index is calculated as ratio of C16:1 and C16:0 (Murakami et al., 2008):

$$\text{(C16) } \Delta^9\text{-desaturase index} = \frac{\text{C16:1 } \left[\frac{\mu\text{g}}{\text{g}} \right]}{\text{C16:0 } \left[\frac{\mu\text{g}}{\text{g}} \right]}$$

Analog to this, the C18 Δ^9 -desaturase index is calculated as ratio of C18:1 and C18:0 (Alarcon et al., 2016; Murakami et al., 2008):

$$\text{(C18) } \Delta^9\text{-desaturase index} = \frac{\text{C18:1 } \left[\frac{\mu\text{g}}{\text{g}} \right]}{\text{C18:0 } \left[\frac{\mu\text{g}}{\text{g}} \right]}$$

Δ^5 -desaturase catalyzes the reaction to introduce a double bond at the fifth carbon atom of the fatty acid chain, counted from the carboxyl terminus (Murakami et al., 2008). The activity of Δ^5 -desaturase was calculated as the ratio of arachidonic acid (C20:4) and α -Linoleic acid (C18:3):

$$\Delta 5\text{-desaturase index} = \frac{\text{C20:4} \left[\frac{\mu\text{g}}{\text{g}} \right]}{\text{C18:3} \left[\frac{\mu\text{g}}{\text{g}} \right]}$$

In analogy to the previously mentioned desaturases, $\Delta 6$ -desaturase introduces a double bond at carbon six, counted from the carboxyl terminus. The $\Delta 6$ -desaturase activity was expressed as the ratio of α -Linoleic acid (C18:3) and linoleic acid (C18:2) (Araya et al., 2010):

$$\Delta 6\text{-desaturase index} = \frac{\text{C18:3} \left[\frac{\mu\text{g}}{\text{g}} \right]}{\text{C18:2} \left[\frac{\mu\text{g}}{\text{g}} \right]}$$

Another index that can be described as a cumulative $\Delta 5$ - $\Delta 6$ -desaturase index was calculated by dividing the amount of arachidonic acid (C20:4) by the amount of linoleic acid (C18:2):

$$\text{cumulative } \Delta 5\text{-}\Delta 6\text{-desaturase index} = \frac{\text{C20:4} \left[\frac{\mu\text{g}}{\text{g}} \right]}{\text{C18:2} \left[\frac{\mu\text{g}}{\text{g}} \right]}$$

Elongase activities:

Elongases are by name enzymes that elongate fatty acid chains by catalyzing the addition of two additional carbon atoms to an existing chain. Indexes to assess elongation and elongase activity can be calculated in several ways. A C16:0 specific elongation index can be calculated by dividing the sum of the amount of C18:0 and C18:1 by the amount of C16:0 (Green et al., 2010):

$$\text{C16:0 elongation index} = \frac{(\text{C18:0} \left[\frac{\mu\text{g}}{\text{g}} \right] + \text{C18:1} \left[\frac{\mu\text{g}}{\text{g}} \right])}{\text{C16:0} \left[\frac{\mu\text{g}}{\text{g}} \right]}$$

The saturated fatty acid (SFA) elongation index was calculated by the ratio of stearic acid (C18:0) to palmitic acid (C16:0) (Dal Bosco et al., 2012):

$$\text{SFA elongation index} = \frac{\text{C18:0} \left[\frac{\mu\text{g}}{\text{g}} \right]}{\text{C16:0} \left[\frac{\mu\text{g}}{\text{g}} \right]}$$

Similarly, the monounsaturated fatty acid (MUFA) elongation index was calculated as ratio of oleic acid (C18:1) to palmitoleic acid (C16:1) (Kotronen et al., 2010):

$$\text{MUFA elongation index} = \frac{\text{C18:1} \left[\frac{\mu\text{g}}{\text{g}} \right]}{\text{C16:1} \left[\frac{\mu\text{g}}{\text{g}} \right]}$$

De novo lipogenesis (DNL) index:

Lipogenesis is not only occurring in adipose tissue. It can only be found in skeletal muscle cells. Fatty acid synthase (FAS) is for instance required to synthesize palmitic acid from products of the citric acid cycle, thus contributing to DNL (Funai et al., 2013; Maier et al., 2008). To estimate *de novo* lipogenic activity, an index was calculated of the ratio of palmitic acid (C16:0) and linoleic acid (C18:2) (Collins et al., 2011):

$$\text{de novo lipogenesis index} = \frac{\text{C16:0} \left[\frac{\mu\text{g}}{\text{g}} \right]}{\text{C18:2} \left[\frac{\mu\text{g}}{\text{g}} \right]}$$

Thioesterase activity index:

Thioesterases are a group of hydrolases that are part of the fatty acid synthase (Chirala et al., 2001). Its activity is calculated as the ratio of palmitic acid (C16:0) and myristic acid (C14:0) (Martino et al., 2014):

$$\text{Thioesterase activity index} = \frac{\text{C16:0} \left[\frac{\mu\text{g}}{\text{g}} \right]}{\text{C14:0} \left[\frac{\mu\text{g}}{\text{g}} \right]}$$

3.2.4.5 Gene expression analysis

To evaluate if certain treatments, knockdowns or knockouts have an impact on mRNA expression levels of certain target genes of interest, expression profiling with defined candidate genes was performed. For that purpose, the total RNA of skeletal muscles or cells was isolated, transcribed into complementary DNA (cDNA) and was then subjected to gene expression analysis via quantitative real-time PCR (qRT-PCR).

3.2.4.5.1 RNA isolation

Total RNA from C2C12 myoblasts and myotubes was isolated with the RNeasy mini kit (Qiagen, Hilden, Germany) according to the kit instructions. C2C12 cell RNA was isolated from 12-well plates. Where suitable, two wells with the same treatment conditions were pooled to gain higher RNA concentrations. Prior to the isolation procedure, cells were washed once with 1xPBS (Tab. 3). The PBS was aspirated completely and the extraction process was started. For cell lysis 175 µl/well RLT buffer were added to each well. Plates were put on ice for 5 minutes. Cells were completely detached from the bottom of the well with cell scrapers. Then, 175 µl

from each of the two wells to pool (= total 350 µl/pooled sample) were transferred to a QIAshredder column to further homogenize the cell lysate. The Column was centrifuged for 1 min at 13,000 rcf at RT with a table centrifuge .All further centrifugation steps were conducted with this table centrifuge at RT (Tab. 6). One volume (~350 µl) of 70 % EtOH was added to the flow-through to precipitate nucleic acids from the homogenate. 700 µl of the flow-through were then applied onto an RNeasy spin column and centrifuged for 30 sec at 13,000 rcf. The flow-through was discarded, the spin column membrane was washed once with RW1 buffer and centrifuged for 30 sec at 13.000 rcf. The flow-through was discarded and the column membrane was washed twice with RPE buffer. The Flow-through was discarded and the column was centrifuged empty to remove any residual EtOH-containing RPE buffer. Subsequently, RNA was eluted from the column by adding 30 µl of RNase-free water and centrifugation for 1 min at 13.000 rcf. RNA concentration was measured with the Nanodrop (Tab. 6) device.

3.2.4.5.2 cDNA synthesis

cDNA was synthesized from 1 µg total RNA (3.2.4.5.1) by reverse transcription PCR with the GoScript™ Reverse Transcriptase Kit (see Tab. 5). The two-step reaction was conducted as follows: 1 µg of isolated RNA were mixed with random hexanucleotide primers [final amount: 400 ng] and a nucleotide mix [final concentration: 10 µmol each dNTP] and incubated for 5 min at 65 °C to anneal random primers to the RNA. Meanwhile a reaction mix of MgCl₂ [final concentration: 2.5 mM], Transcriptase buffer and reverse transcriptase was prepared. After annealing the reaction mix was added and the synthesis was conducted in a thermocycler (Tab. 6) according to the protocol depicted in Table 21.

Table 21: cDNA synthesis incubation protocol

Step	Temperature	Time
Lid heating	40 °C	∞
Annealing	25 °C	5 min
Elongation	42 °C	60 min
Termination, enzyme inactivation	72 °C	15 min
Storage	4 °C	∞

After synthesis, cDNA samples were diluted 1:40 with nuclease-free H₂O and stored at -20 °C for further use in gene expression analysis via qRT-PCR.

3.2.4.5.3 Quantitative real-time PCR (qRT-PCR)

A relative amount of mRNA as a measure for gene expression can be calculated indirectly by measuring the amplification of a certain part of a target gene sequence of interest from cDNA by the qRT-PCR method. With this special PCR method it is possible to precisely determine the time point at which the amplification of the target gene fragment of interest reaches a defined

amount. This amount is detected as fluorescence signal coming from SYBR® Green dye that selectively intercalates into DNA molecules and is measured by the PCR machine. The Ct value (cycle of threshold) defines the time point (= amplification cycle) at which the detected fluorescence is statistically different from the baseline fluorescence. This value represents a relative measure for gene expression. Lower Ct values indicate that the gene expression of the target gene of interest is high, because due to the high amounts of mRNA of interest (respectively cDNA in the RNA transcript) in the sample, the critical fluorescence intensity was reached earlier compared to samples with higher Ct values, which would indicate lower expression levels in the sample. A commercially available GoTaq qPCR Master Mix (Tab. 5) was used. Prior to usage, 1 ml of Master Mix was supplemented with 20 µl of reference dye CXR. Gene-specific forward and reverse primers were pre-diluted 1:10 with nuclease-free H₂O. cDNA (3.2.4.5.2) from C2C12 muscle cells or primary EDL muscles was pre-diluted 1:40 in nuclease-free H₂O. The total reaction volume per sample was 10 µl. A representative reaction setup for gene expression analysis by qRT-PCR is represented in Table 22:

Table 22: qRT-PCR reaction setup

Compound	Volume	Concentration
2x GoTaq qPCR Master Mix with reference dye CXR	5 µl	1x
Forward primer (1:10 pre-diluted)	0.5 µl	10 nM
Reverse primer (1:10 pre-diluted)	0.5 µl	10 nM
cDNA (1:40 pre-diluted)	4 µl	-

qRT-PCR was run according to the following protocol depicted in Table 23:

Table 23: qRT-PCR incubation protocol

Step	Time	Temperature	Cycles
Hot Start	2 min	95 °C	1x
Denaturation	15 sec	95 °C	40x
Primer Annealing and Extension	60 sec	60 °C	
Dissociation (Melting)	-	60 – 95 °C	1x

Data evaluation was performed with the $\Delta\Delta C_t$ method. Results were expressed as relative fold changes comparing two groups of treatments with each other.

3.2.5 Statistical analysis

All generated data sets were subjected to statistical testing to identify statistically different results. The data are presented as mean values \pm standard error of the mean (SEM) with individual $n = 3$ or more data points per experimental group. The exact numbers of biological replicates are presented in the figure legends. Student's two-tailed unpaired t-test or one-way

ANOVA were performed to test the results for significance. The p-Value as measure for significance was gradually expressed in the figures as following: *p < 0.05, **p < 0.01, ***p < 0.001. All statistical analysis was performed with the GraphPad 7 software (Tab. 7).

4 Results

4.1 Impact of RabGAPs TBC1D1 and TBC1D4/AS160 on fatty acid uptake in C2C12 myotubes

It has been shown that the RabGAPs TBC1D1 and TBC1D4 are both key regulators of GLUT4 protein trafficking and glucose uptake in skeletal muscle and adipose tissue (Chadt et al., 2015; Dokas et al., 2013; Hargett et al., 2016; Szekeres et al., 2012). Relatively high expression levels of TBC1D4 protein were described in white and brown adipose tissue, while TBC1D1 protein expression in adipose cells was not detectable. In contrast, both RabGAPs were found to be expressed in a variety of murine skeletal muscle types (Chadt et al., 2008; Szekeres et al., 2012). In addition, TBC1D1 and TBC1D4 have also been shown to influence muscle lipid metabolism. It was published that knockdown or knockout of *Tbc1d1* lead to a significant increase in both, fatty acid uptake and oxidation (Chadt et al., 2015; Chadt et al., 2008). For TBC1D4 it was found that it is involved in surface recruitment of the fatty acid transport protein FAT/CD36 in cardiomyocytes (Samovski et al., 2012).

4.1.1 C2C12 myotube differentiation status

All *in vitro* cell culture experiments with cultivated murine skeletal muscle cells were conducted with myotubes that were induced to differentiate from previously seeded myoblasts. In order to ensure that the culture conditions employed for myoblast differentiation led to the formation of differentiated myotubes an initial experiment was conducted to assess the mRNA expression of two terminal markers for muscle cell differentiation. Desmin (*Des*) and Myogenin (*Myog*) have been described in literature to be terminal markers that are supposed to be highly expressed in differentiated myotubes (Mermelstein et al., 2005; Tomczak et al., 2004). Undifferentiated C2C12 myoblasts were harvested for RNA isolation (3.2.4.5.1) and cDNA synthesis (3.2.4.5.2) 24 hours after seeding. Differentiated C2C12 myotubes were harvested 6 days after the induction of differentiation. Expression levels of *Desmin* and *Myogenin* were determined using qRT-PCR (3.2.4.5.3). The results are depicted in Fig. 12. It could be shown that the expression of *Myogenin* was 2.55-fold higher in cells after 6 days of differentiation compared to cells before differentiation. Expression of *Desmin* was increased by 1.42-fold in myotubes compared with myoblasts.

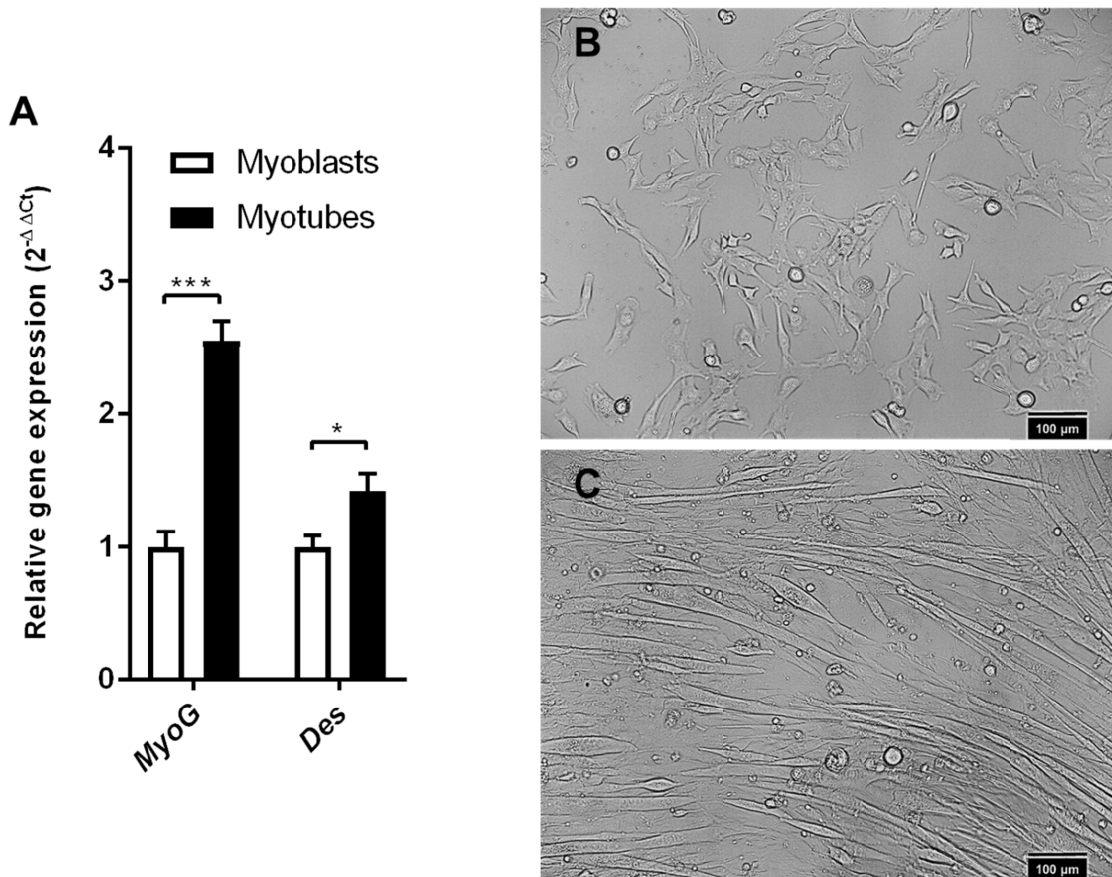


Figure 12: Differentiation status of C2C12 cells. A) Expression levels of Myogenin (*Myog*) and Desmin (*Des*) mRNA were compared between undifferentiated myoblasts (open bars) before induction of cell differentiation and 6 days after differentiation start (black bars). TATA-box binding protein (*Tbp*) was used as housekeeping gene. Values are normalized to expression levels undifferentiated myoblasts. Light microscope images of B) C2C12 myoblasts and C) differentiated C2C12 myotubes at day 6 of differentiation. Scale bar = 100 μ m. Data are presented as mean values with SEM (n = 6). Two-tailed Student's unpaired t-test with Welch's correction, *p < 0.05, ***p < 0.001.

4.1.2 Palmitic acid uptake into C2C12 myotubes after siRNA-mediated *Tbc1d1* and *Tbc1d4* knockdown

To prove that TBC1D1 is involved in skeletal muscle fatty acid metabolism, the expression levels of *Tbc1d1* were reduced by siRNA knockdown technology in C2C12 myotubes. C2C12 myoblasts were seeded and differentiated as described before (3.2.2). During differentiation the cells were transfected with siRNA specifically targeting *Tbc1d1* mRNA. Control cells were transfected with an unspecific non-target (NT) siRNA (3.2.2.1.2). To validate that siRNA treatment was successful, the expression of the target mRNA (here: *Tbc1d1*) was determined by qRT-PCR (3.2.4.5.3) (Fig. 13 A + C) Transfection of the cells with *Tbc1d1*-specific siRNA oligonucleotides reduced the mRNA expression by 83 % (\pm 12.5 %). Transfection with *Tbc1d4*-specific siRNA oligonucleotides resulted in a reduction of mRNA expression of 66.6 % (\pm 20 %) Transfected cells were used for assessing *in vitro* fatty acid uptake (Fig. 13 B + D) as described in the methods section (3.2.2.2.1). Silencing of *Tbc1d1* mRNA significantly increased C2C12

palmitate uptake by 19 % (± 8.2 %). Knocking down *Tbc1d4* mRNA led to significantly increased C2C12 cell palmitic acid uptake by 38.4 % (± 16.1 %).

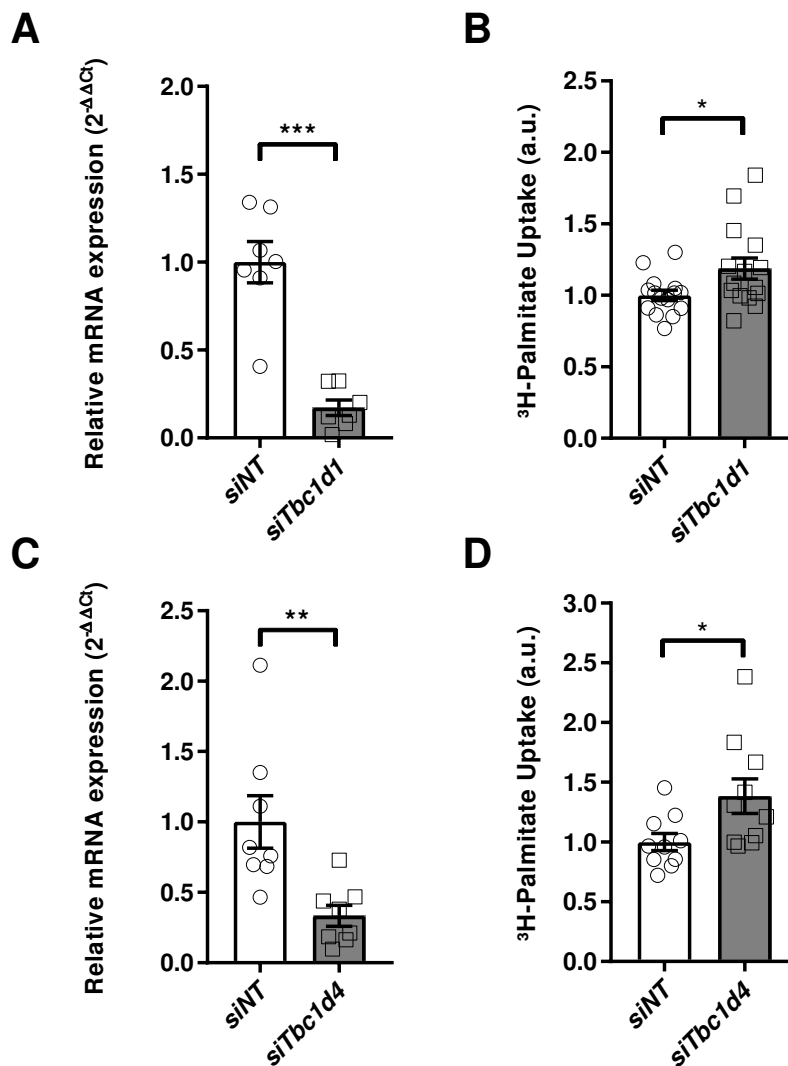


Figure 13: Palmitic Acid Uptake of C2C12 myotubes after siRNA-mediated *Tbc1d1* and *Tbc1d4* knockdown. A) and C): Relative expression of *Tbc1d1* and *Tbc1d4* mRNA after siRNA transfection. Differentiating C2C12 cells were chemically transfected with specific *Tbc1d1* (dark grey bar), or *Tbc1d4* (light grey bar) siRNA or unspecific *non-target* control siRNA on day three of differentiation. Cells were then harvested for RNA isolation and cDNA synthesis for expression analysis via qRT-PCR. Data are presented as scatter plot and mean values \pm SEM (n = 7-8). Two-tailed unpaired Student's t-test with Welch's correction, ** p < 0.01, *** p < 0.001. *Tbc1d1*: 95 % [CI: -1.12 to -0.5364], *Tbc1d4*: B) and D): *In vitro* palmitate uptake of C1C12 myotubes after siRNA-mediated knockdown of *Tbc1d1* or *Tbc1d4*. Cells that were siRNA transfected during the course of differentiation were used in *in vitro* palmitate uptake assays. Data are presented as bar-scatter plot and mean values \pm SEM (n = 10-15). Two-tailed unpaired Student's t-test with Welch's correction, * p < 0.05. *Tbc1d1*: [95 % CI: 0.01692 to 0.3587], *Tbc1d4*: [95 % CI: 0.03499 to 0.7325].

4.2 Impact of RabGAPs TBC1D1 and TBC1D4/AS160 on C2C12 skeletal muscle cell fatty acid oxidation

To demonstrate the consistency of the used cell culture model and the published principle that a lack of TBC1D1 and TBC1D4 additionally to fatty acid uptake also has an impact on fatty acid oxidation (Chadt et al. 2008), the oxidation of radioactively labeled ^{14}C -palmitate was assessed under *Tbc1d1* and *Tbc1d4* knockdown conditions. It could be shown that a siRNA-mediated reduction of *Tbc1d1* significantly increases palmitate oxidation of C2C12 myotubes by 20.4 % (± 8.2 %) (Fig. 14 A). Knockdown of *Tbc1d4* led to a statistically significant increase of palmitate oxidation by 12.3 % (± 5.2 %) (Fig. 14 B).

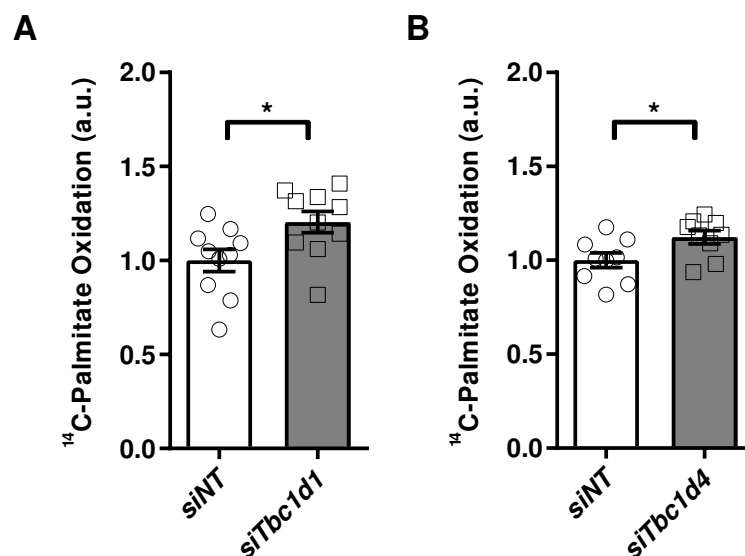


Figure 14: Impact of the RabGAPs TBC1D1 and TBC1D4/AS160 on C2C12 skeletal muscle cell fatty acid oxidation. Differentiated C2C12 cells were transfected with specific *Tbc1d1* siRNA (A; dark grey bar), specific *Tbc1d4* siRNA (B; light grey bar), or *non-target* control siRNA (A+B; open bars). Subsequently oxidation of ^{14}C -palmitate was determined indirectly by trapping released $^{14}\text{CO}_2$ with sodium hydroxide-soaked filter papers. Data are presented as bar scatter plots and means \pm SEM ($n = 9 - 10$). Two-tailed unpaired Student's t-test with Welch's correction. * $p < 0.05$. A: [95 % CI: -0.376 to -0.0316], B: [95 % CI: -0.2331 to -0.01284].

4.3 Lipid substrate specificity of the TBC1D1 and TBC1D4 effect on C2C12 myotube fatty acid uptake

The majority of experiments in this study were performed using palmitate as fatty acid substrate to assess lipid uptake into C2C12 cells. To get further insight into the observation that both, TBC1D1 and TBC1D4 seem to be critical regulatory proteins in the context of skeletal muscle lipid supply, experiments were conducted in which not palmitate (C16:0), but butyrate (C4:0) or oleate (C18:1) were used as substrate for uptake assays. The aim of these

experiments was to evaluate whether the impact of RabGAPs on lipid metabolism is dependent on chain length and/ or the grade of saturation of the administered fatty acid.

4.3.1 Impact of TBC1D1 and TBC1D4 on the uptake of short-chain and unsaturated long-chain fatty acids in C2C12 skeletal muscle cells

Subsequent to siRNA-mediated silencing of *Tbc1d1* and *Tbc1d4*, differentiated C2C12 myotubes were subjected to butyric acid or oleic acid uptake assays, respectively (Fig.15 and 16). It became evident that the uptake of short-chain butyric acid was not different between the control *non-target* and *Tbc1d1* or *Tbc1d4* knockdown cells (Fig.15). Lipid uptake was not changed under *Tbc1d1*, or *Tbc1d4*-deficient conditions. In contrast to that, a lack of *Tbc1d1* caused a significant

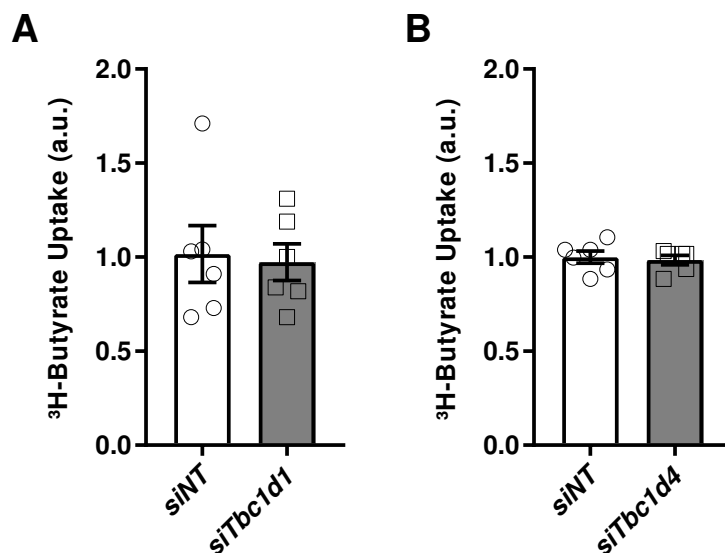


Figure 15: Short-chain fatty acid uptake into C2C12 cells under *Tbc1d1* and *Tbc1d4*-deficient conditions. A) *Tbc1d1* (dark grey bars) or B) *Tbc1d4* (light grey bars) were silenced in differentiating C2C12 myotubes. Unspecific *non-target* siRNA (siNT) was used as negative silencing control (open bars). These cells were then used further to measure short-chain butyric acid (C4:0) *in vitro*. Data are presented in bar-scatter plots as mean \pm SEM (n = 6). Two-tailed unpaired Student's t-test with Welch's correction.

Similar to the effects of *Tbc1d1* and *Tbc1d4* knockdown on ³H-butyric acid uptake, a set of experiments was performed in which *Tbc1d1* and *Tbc1d4* were silenced via siRNA technology and the uptake of unsaturated long-chain ³H-oleic acid was measured. The results show that only the uptake of oleic acid was significantly increased after *Tbc1d1* knockdown by 1.12-fold ($\pm 3.7\%$) (Fig. 16 A). *Tbc1d4* mRNA reduction increased oleic acid uptake by 1.14-fold ($\pm 5.0\%$) (Fig.16 B).

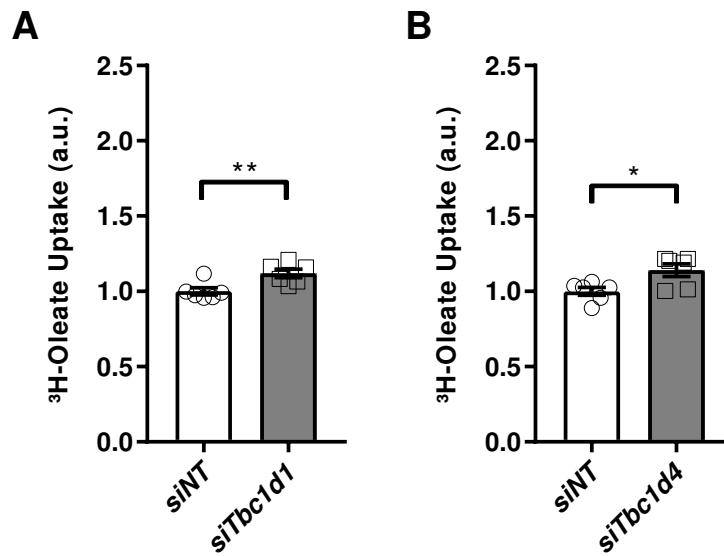


Figure 16: Unsaturated long-chain fatty acid uptake into C2C12 cells under *Tbc1d1* and *Tbc1d4*-deficient conditions. A) *Tbc1d1* (dark grey bars) or B) *Tbc1d4* (light grey bars) were silenced in differentiating C2C12 myotubes. Unspecific *non-target* siRNA (siNT) was used as negative silencing control (open bars). These cells were then used further to measure unsaturated long-chain oleic acid (C18:1 ω -9) uptake *in vitro*. Data are presented in bar-scatter plots as mean \pm SEM (n = 6). Two-tailed Student's unpaired t-test with Welch's correction, *p < 0.05, **p < 0.01. *Tbc1d1*: [95 % CI: 0.03691 to 0.2016]. *Tbc1d4*: [95 % CI: 0.02658 to 0.2535].

4.4 Expression analysis of genes involved in skeletal muscle mitochondrial biogenesis, lipid metabolism and vesicle trafficking under *Tbc1d1* knockdown conditions in C2C12 myotubes

In order to find explanations for the observed effect that a lack of either TBC1D1 or TBC1D4 has an impact on skeletal muscle cell fatty acid metabolism, an analysis of the expression of several known genes involved in cellular lipid utilization and handling, as well as transcriptional regulation was conducted. A set of targets was analyzed with regard to mRNA expression in differentiated C2C12 myotube samples that have previously been transfected with *non-target* siRNA or *Tbc1d1*-specific siRNA (3.2.2.1.2). After RNA isolation (3.2.4.5.1) from transfected myotubes and cDNA synthesis (3.2.4.5.2) the expression of candidate genes was evaluated by qRT-PCR (3.2.4.5.3).

4.4.1 Validation of *Tbc1d1* knockdown specificity after transfection with *Tbc1d1*-targeting siRNA

All following measurements were conducted with the same set of samples. To ensure that any possibly occurring differential result can be addressed to the reduction of *Tbc1d1* mRNA and to exclude that the siRNA targeting *Tbc1d1* also affects the expression of the closely related *Tbc1d4*, in a first experiment the expression of *Tbc1d1* and *Tbc1d4* was examined. As shown in Figure 17, the knockdown of *Tbc1d1* was successful. The expression in the cells could be reduced by 80.6 % (± 16 %). Additionally the siRNA-mediated knockdown with *Tbc1d1* siRNA seems to be target specific, as the expression of *Tbc1d4* was not altered after transfection.

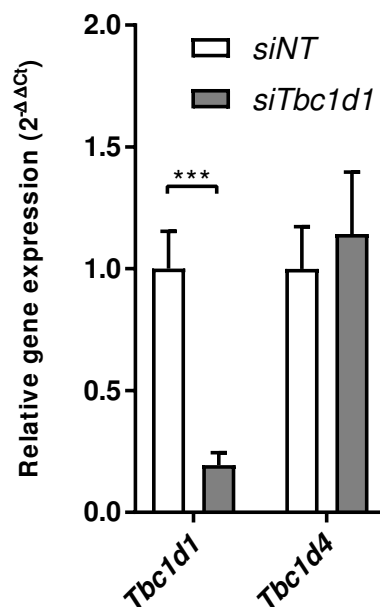


Figure 17: *Tbc1d1* knockdown efficiency and specificity. The expression of *Tbc1d1* was assessed in cDNA samples of C2C12 myotubes that have been transfected with unspecific *non-target* control siRNA (open bars) or specific *Tbc1d1* siRNA (grey bar). The mRNA expression levels of *Tbc1d1* and *Tbc1d4* were measured using qRT-PCR. Beta-actin (β -actin) was used as housekeeping gene. Values are normalized to expression levels of *non-target* control samples. Data are presented as mean values with SEM (n = 6). Two-tailed Student's unpaired t-test with Welch's correction, ***p < 0.001.

4.4.2 Analysis of mRNA expression of genes involved in fatty acid binding and uptake under *Tbc1d1* knockdown conditions in C2C12 myotubes

After having shown the efficiency and specificity of the *Tbc1d1* knockdown, the expression of genes that have been described to encode for proteins crucial for cellular fatty acid binding and fatty acid uptake was investigated. The expression of several fatty acid uptake and fatty

acid binding proteins was analyzed in cDNA from cells that had been transfected with *non-target* control siRNA compared to samples with a specific *Tbc1d1* knockdown. The results are depicted in Fig. 18. It became evident that there is no statistically significant difference in the mRNA expression of *Slc27a1* (gene that encodes for FATP1) or *Slc27a4* (gene that encodes for FATP4) due to the *Tbc1d1* deficiency. The expression levels of the two fatty acid binding protein genes *Fabp3* and *Fabp4* do not differ between the control and the *Tbc1d1*-deficient samples. In contrast, the mRNA expression of *Cd36* was significantly increased in cells with lower expression levels of *Tbc1d1* mRNA. These cells showed a 2-fold higher expression of *Cd36* compared to the control cells.

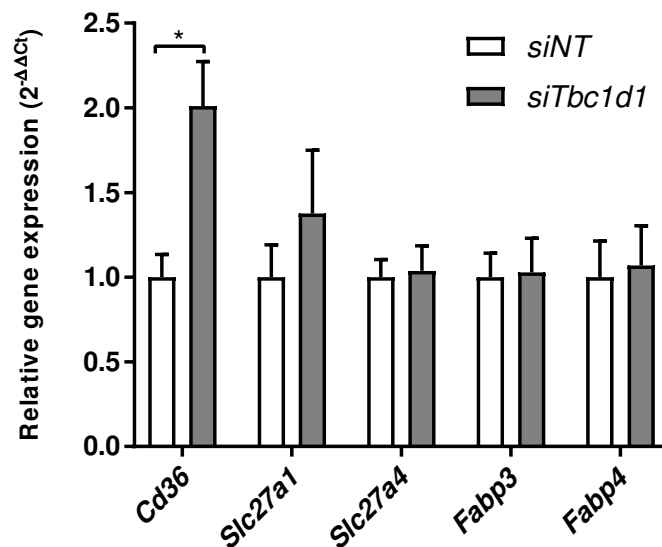


Figure 18: mRNA expression of skeletal muscle fatty acid uptake and binding proteins under *Tbc1d1*-deficient conditions. The gene expression of fatty acid transporters *Cd36*, *Slc27a1* (FATP1) and *Slc27a4* (FATP4), and the expression of fatty acid binding proteins *Fabp3* and *Fabp4* was analyzed comparing C2C12 samples transfected with unspecific *non-target* control siRNA (open bars) with samples that showed a specific siRNA-mediated *Tbc1d1* knockdown (grey bar). Beta-actin (β -actin) was used as housekeeping gene. Values are normalized to expression levels of *non-target* control samples. Data are presented as mean values with SEM (n = 6-14). Two-tailed Student's unpaired t-test with Welch's correction. *p < 0.05.

4.4.3 Analysis of mRNA expression of genes involved in lipid degradation and biosynthesis under *Tbc1d1* knockdown conditions in C2C12 myotubes

Since both, fatty acid uptake and oxidation have been reported in earlier publications to be influenced by a loss of TBC1D1 protein, in addition to genes encoding proteins that regulate the uptake of fatty acids into skeletal muscle cells, the expression of several candidate genes involved in cellular lipid degradation and biosynthesis was investigated. There was no

statistically significant difference in the mRNA expression of any of the tested targets due to the knockdown of *Tbc1d1* (Fig. 19).

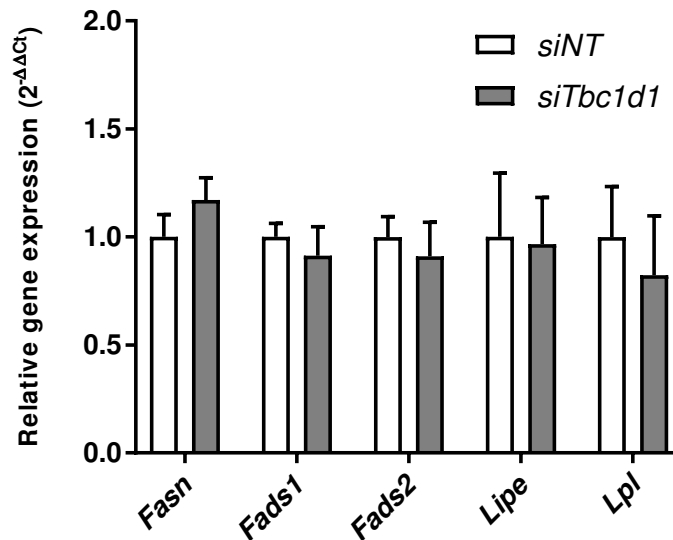


Figure 19: mRNA expression of skeletal muscle lipid degradation and synthesis proteins under *Tbc1d1*-deficient conditions. The gene expression of fatty acid synthesis genes *Fasn* (fatty acid synthase), *Fads1* and *Fads2* (fatty acid desaturase 1/2) was analyzed comparing C2C12 cDNA samples of cells transfected with unspecific *non-target* control siRNA (open bars) with samples that showed a specific siRNA-mediated *Tbc1d1* knockdown (grey bar). Beta-actin (β -actin) was used as housekeeping gene. Values are normalized to expression levels of *non-target* control samples. Data are presented as mean values with SEM (n = 5-6). Two-tailed Student's unpaired t-test with Welch's correction.

4.4.4 Analysis of mRNA expression of transcriptional regulator genes under *Tbc1d1* knockdown conditions in C2C12 myotubes

The influence of *Tbc1d1* knockdown on the expression of selected transcriptional regulators was assessed. As shown in Fig. 20, the gene expression levels of *Pparg*, *Ppard*, *Ppargc1a* and *Tfam* were not different between *non-target* siRNA and specific *Tbc1d1* siRNA transfected C2C12 myotube cDNA samples. In contrast to that, the expression levels of hypoxia-inducible factor 1-alpha (*Hif1a*) were 1.9-fold higher in cell samples that showed a reduction in *Tbc1d1* mRNA levels.

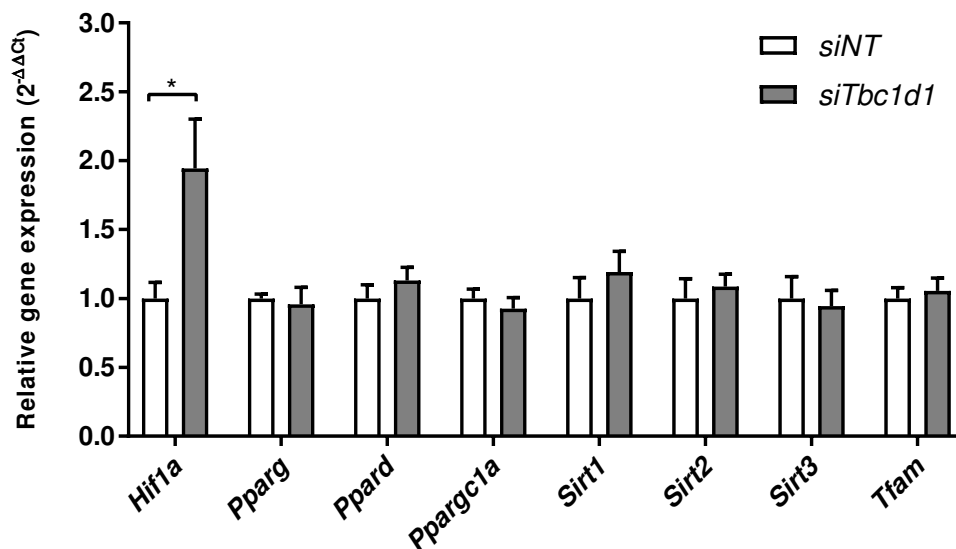


Figure 20: mRNA expression of selected skeletal muscle transcription factors after a siRNA-mediated knockdown of *Tbc1d1*. The gene expression of transcriptional regulators from the Peroxisome proliferator-activated receptor family *Pparg*, *Ppard* and the co-activator *Ppargc1a*, as well as the expression of sirtuins 1, 2 and 3 (*Sirt1*, *Sirt2*, *Sirt3*) as members of a class of histone deacetylases, and mitochondrial transcription factor A (*Tfam*) and *Hif1a* was analyzed comparing C2C12 cDNA samples of cells transfected with unspecific *non-target* control siRNA (open bars) with samples that showed a specific siRNA-mediated *Tbc1d1* knockdown (grey bar). Beta-actin (β -actin) was used as housekeeping gene. Values are normalized to expression levels of *non-target* control samples. Data are presented as mean values with SEM (n = 5-6). Two-tailed Student's unpaired t-test with Welch's correction. *p < 0.05.

4.4.5 Analysis of mRNA expression of genes implicated in mitochondrial energy metabolism under *Tbc1d1* knockdown conditions in C2C12 myotubes

On the level of the skeletal muscle mitochondria, the expression of several key regulators for fatty acid catabolism was measured. The results are depicted in following Fig. 21. Expression levels of *Cpt1b*, *Acadl*, *Hadh* and *Ucp3* were not statistically different between the C2C12 myotubes transfected with *non-target* siRNA in comparison to the cells transfected with *Tbc1d1* siRNA oligonucleotides. The mRNA expression levels of *Pdk4* were significantly different between the two groups of myotubes. *Pdk4* is expressed 1.56-fold higher in *Tbc1d1*-deficient C2C12 cells.

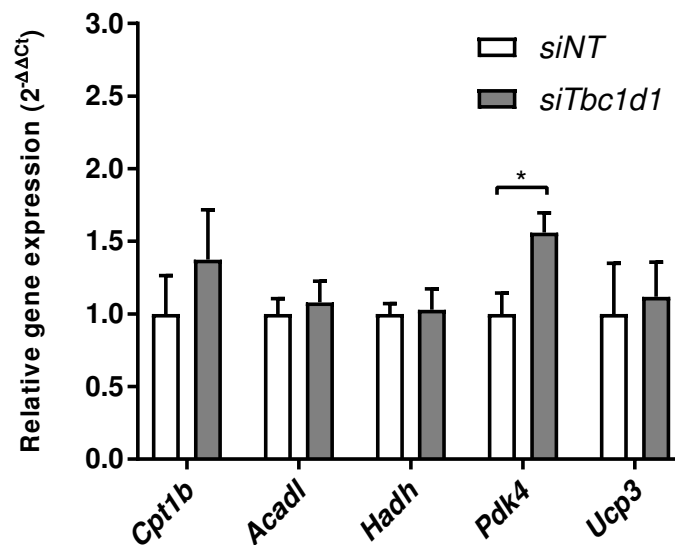


Figure 21: mRNA expression of selected skeletal muscle mitochondrial genes involved in energy metabolism after a siRNA-mediated knockdown of *Tbc1d1*. The gene expression of carnitine palmitoyltransferase 1b (*Cpt1b*), long chain –specific acyl-CoA dehydrogenase (*Acadl*), β -hydroxyacyl-CoA dehydrogenase (*Hadh*), pyruvate dehydrogenase kinase 4 (*Pdk4*) and uncoupling protein 3 (*Ucp3*) was analyzed comparing C2C12 cDNA samples of cells transfected with unspecific *non-target* control siRNA (open bars) with samples that showed a specific siRNA-mediated *Tbc1d1* knockdown (grey bar). Beta-actin (β -actin) was used as housekeeping gene. Values are normalized to expression levels of *non-target* control samples. Data are presented as mean values with SEM (n = 5-6). Two-tailed Student's unpaired t-test with Welch's correction. *p < 0.05.

4.4.6 Analysis of mRNA expression of genes encoding for proteins involved in lipid storage and lipid droplet formation under *Tbc1d1* knockdown conditions in C2C12 myotubes

To get insight into potential differences in lipid storage following *Tbc1d1* knockdown, the expression mRNAs encoding for proteins with an association to lipid storage, lipid droplet formation and degradation. The qPCR results revealed no significant differences in the gene expression of lipid storage-associated genes measured in C2C12 myotubes with or without siRNA-mediated manipulation of *Tbc1d1* expression (Fig. 22).

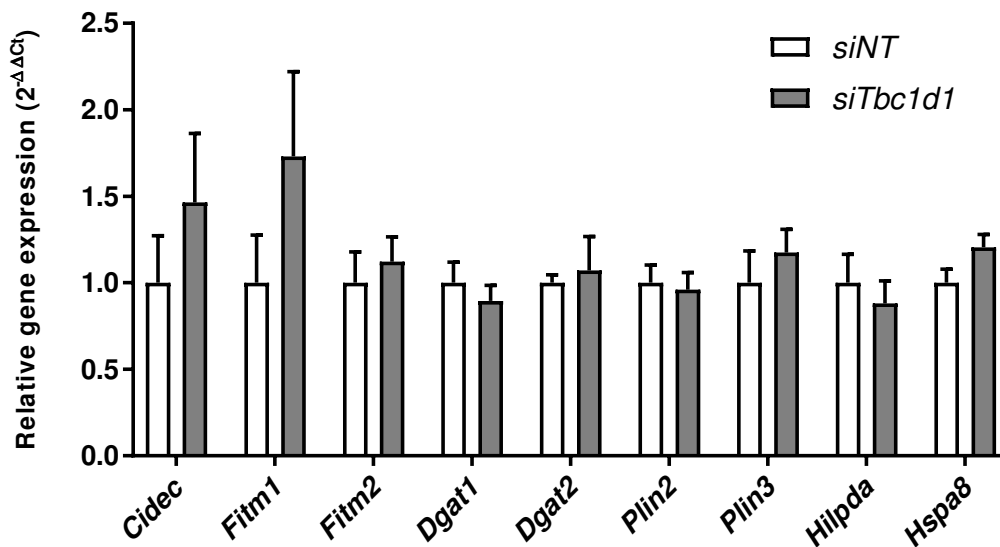


Figure 22: mRNA expression of selected skeletal muscle genes involved in lipid storage and lipid droplet formation after a siRNA-mediated knockdown of *Tbc1d1*. The gene expression of cell death activator CIDE-3 (*Cidec*), fat storage inducing transmembrane protein 1 and 2 (*Fitm1* and *Fitm2*) diacylglycerol transferase 1 and 2 (*Dgat1* and *Dgat2*), perilipin 2 and 3 (*Plin2* and *Plin3*), hypoxia-inducible lipid droplet-associated protein (*Hilpda*) and heat shock cognate protein of 70 kDa (*Hspa8*) was analyzed comparing C2C12 cDNA samples of cells transfected with unspecific *non-target* control siRNA (open bars) with samples that showed a specific siRNA-mediated *Tbc1d1* knockdown (grey bar). Beta-actin (β -actin) was used as housekeeping gene. Values are normalized to expression levels of *non-target* (*siNT*) control samples. Data are presented as mean values with SEM (n = 5-6). Two-tailed Student's unpaired t-test with Welch's correction.

4.4.7 Analysis of mRNA expression of genes encoding for direct targets of TBC1D1 under *Tbc1d1* knockdown conditions in C2C12 myotubes

The Rab GTPase activating protein (RabGAP) TBC1D1 functions as regulator of activity of small Rab GTPases. Since several members of the Rab GTPase family have been identified as *in vitro* substrates of TBC1D1 (Roach et al., 2007) and since some of these have already been described to be involved in glucose and fatty acid uptake into muscle tissues, it was investigated whether a lack of *Tbc1d1* causes changes in the expression of certain candidate Rab protein mRNAs. Here, the expression of *Rab3ip*, the GEF regulating Rab8a activation, *Dennd4c*, regulating activation of Rab10, and *Dennd6c*, the specific Rab14 GEF was assessed by qRT-PCR analysis (3.2.4.5.3). No difference in the expression of the GEF mRNA *Rab3ip*, *Dennd4c* or *Dennd6a*, or the *Rab8a*, *Rab10* and *Rab14* mRNA expression was found in *Tbc1d1*-deficient C2C12 myotubes compared to non-target transfected cells (Fig. 23).

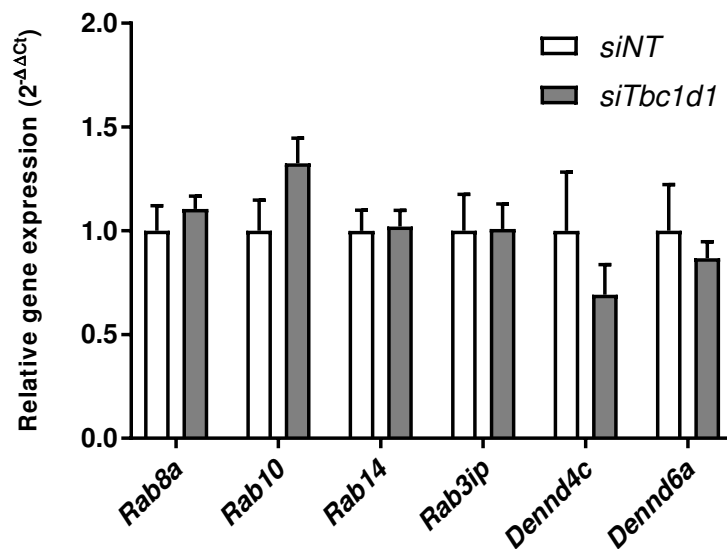


Figure 23: mRNA expression of selected Rab GTPases and guanine nucleotide exchange factors under *Tbc1d1* knockdown conditions. The gene expression of small Rab GTPases *Rab8a*, *Rab10* and *Rab14*, as well as the expression of the corresponding guanine nucleotide exchange factors (GEF) *Rab3ip* (GEF for *Rab8a*), *Dennd4c* (GEF for *Rab10*) and *Dennd6a* (GEF for *Rab14*) was analyzed comparing C2C12 cDNA samples of cells transfected with unspecific *non-target* control siRNA (open bars) with samples that showed a specific siRNA-mediated *Tbc1d1* knockdown (grey bar). Beta-actin (β -actin) was used as housekeeping gene. Values are normalized to expression levels of *non-target* (*siNT*) control samples. Data are presented as mean values with SEM (n = 5-6). Two-tailed Student's unpaired t-test with Welch's correction.

4.5 Analysis of the influence of TBC1D1 deficiency on the fatty acid profile of mouse skeletal muscle

Tbc1d-deficient myocytes display a significantly increased palmitate uptake and palmitate oxidation *in vitro* compared to control cells (see 4.1.2 and 4.2). Thus, an investigation of the fatty acid profile via a gas chromatographic approach of *Gastrocnemius* muscles from wildtype and TBC1D1 knockout animals was conducted to gain further insight into the influence of TBC1D1 on the lipid milieu and lipid processing in murine skeletal muscles.

4.5.1 Total fatty acid content of *Gastrocnemius* muscle from wildtype and D1KO mice

After determination of the fatty acid composition by a GC approach, the amounts of all detected fatty acid species that were identified (in mg/g muscle tissue) were summed up for every mouse of both genotypes to estimate the total fatty acid amount in each muscle. The analysis revealed no statistical differences in total fatty acid between WT (9.17 mg/g, ± 1.34) and D1KO (10.17 mg/g, ± 1.08) *Gastrocnemius* muscle samples (Fig. 24).

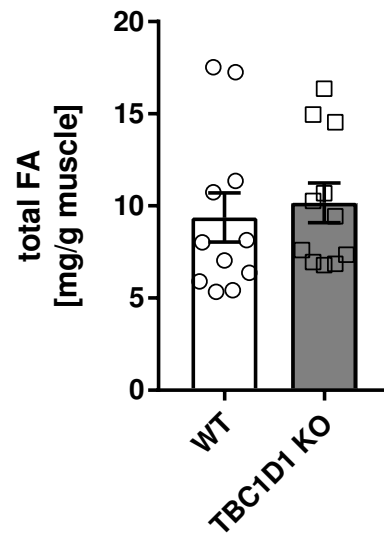


Figure 24: Total fatty acid content of WT and D1KO *Gastrocnemius* muscle samples. The total fatty acid content in mg/g muscle tissue was calculated as the sum of the amount of all fatty acids that were detected in the GC analysis of WT (open bar) and *Tbc1d1*-deficient (grey bar) *Gastrocnemius* muscle samples. Values displayed as single values and mean \pm SEM (n = 11). Two-tailed Student's unpaired t-test with Welch's correction. [95 % CI: -2.801 to 4.384].

4.5.2 Fatty acid profile of wildtype and *Tbc1d1*-deficient *Gastrocnemius* muscles

To further elucidate to what extent a lack of TBC1D1 and the consequential increase in skeletal muscle lipid uptake influence the lipid composition and intra-myocellular lipid milieu, the amount of distinct fatty acids was measured by gas chromatography in *Gastrocnemius* muscle samples of wildtype and *Tbc1d1*-deficient male mice. Since the total fatty acid content of wildtype and TBC1D1 knockout muscle samples was not different, a more resolute analysis of the individual percent amount of distinct fatty acid species within the muscle was conducted. It became evident that for four fatty acid species there were statistically significant differences between the reviewed genotypes. Mice deficient of *Tbc1d1* showed lower amounts of saturated palmitic acid (C16:0) and polyunsaturated arachidonic acid (C20:4). In contrast, the levels of monounsaturated palmitoleic acid (C16:1) and oleic acid (C18:1) were significantly increased in *Gastrocnemius* muscle samples from knockout animals.

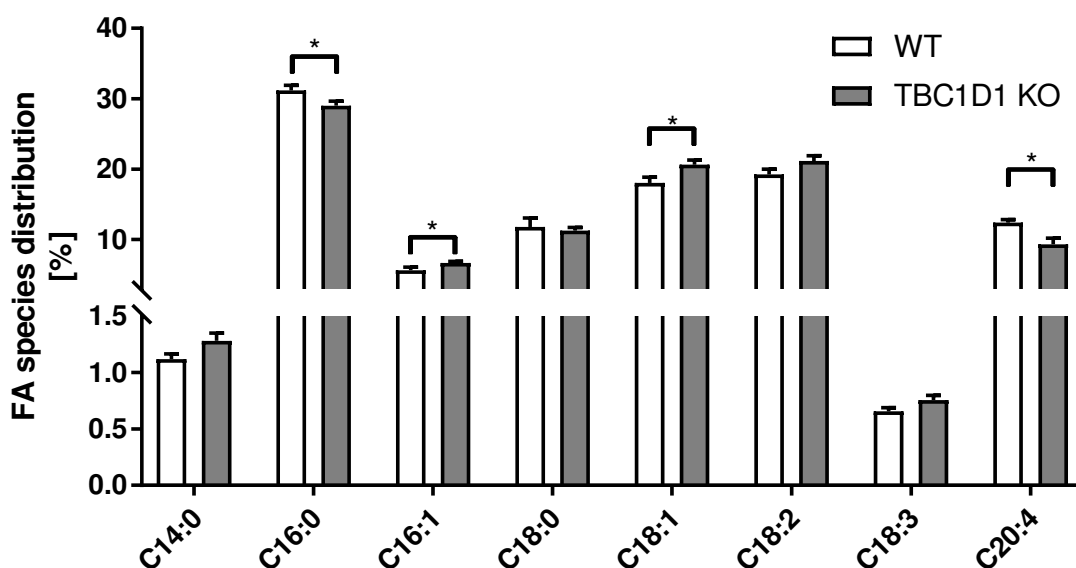


Figure 25: Fatty acid profile of Gastrocnemius muscles from wildtype and TBC1D1 KO mice. The abundance of saturated and unsaturated fatty acid species was measured via gas chromatography (GC). The fatty acids myristic acid (C14:0), palmitic acid (C16:0), palmitoleic acid (C16:1), stearic acid (C18:0), oleic acid (C18:1), linoleic acid (C18:2), α -linoleic acid (C18:3) and arachidonic acid (C20:4) were detected in the *Gastrocnemius* samples from wildtype (WT) (open bars) and TBC1D1 knockout (grey bars) male mice. Data are presented as mean percent values of total fatty acids with SEM (n = 11). Two-tailed Student's unpaired t-test with Welch's correction. *p < 0.05.

4.5.3 Fraction differences of fatty acid species classes with regard to saturation grade between wildtype and *Tbc1d1*-deficient mouse skeletal muscles

The fatty acids that have been identified in the GC analysis were clustered depending on the grade of saturation in saturated fatty acids (SFA), monounsaturated fatty acids (MUFA) and polyunsaturated fatty acids (PUFA) and compared within the cluster groups to identify genotype-specific distribution patterns. It became evident that the lack of TBC1D1 resulted in changes in the amount of fatty acid clusters within skeletal muscle cells. In comparison with wildtype (43.73 %, ± 0.88) samples, muscles from *Tbc1d1*-deficient mice (41.06 %, ± 0.8) exhibited a significantly lower amount of SFAs (Fig. 26 A). In contrast, the amount of MUFAs was significantly increased in the D1KO Gastrocnemius muscles (WT: 24.07 %, ± 1.09 ; D1KO: 27.85 %, ± 0.84) (Fig. 26 B). Parallel to that, total PUFA levels were not different between the two genotypes (Fig. 26 C). Consequently the ratio of MUFAs to SFAs that can be seen as a measure of total desaturation activity within the muscle was 1.23-fold higher in tissue samples from D1KO mice (Fig. 26 E), while no differences were found in the ratio of PUFAs to SFAs (Fig. 26 F).

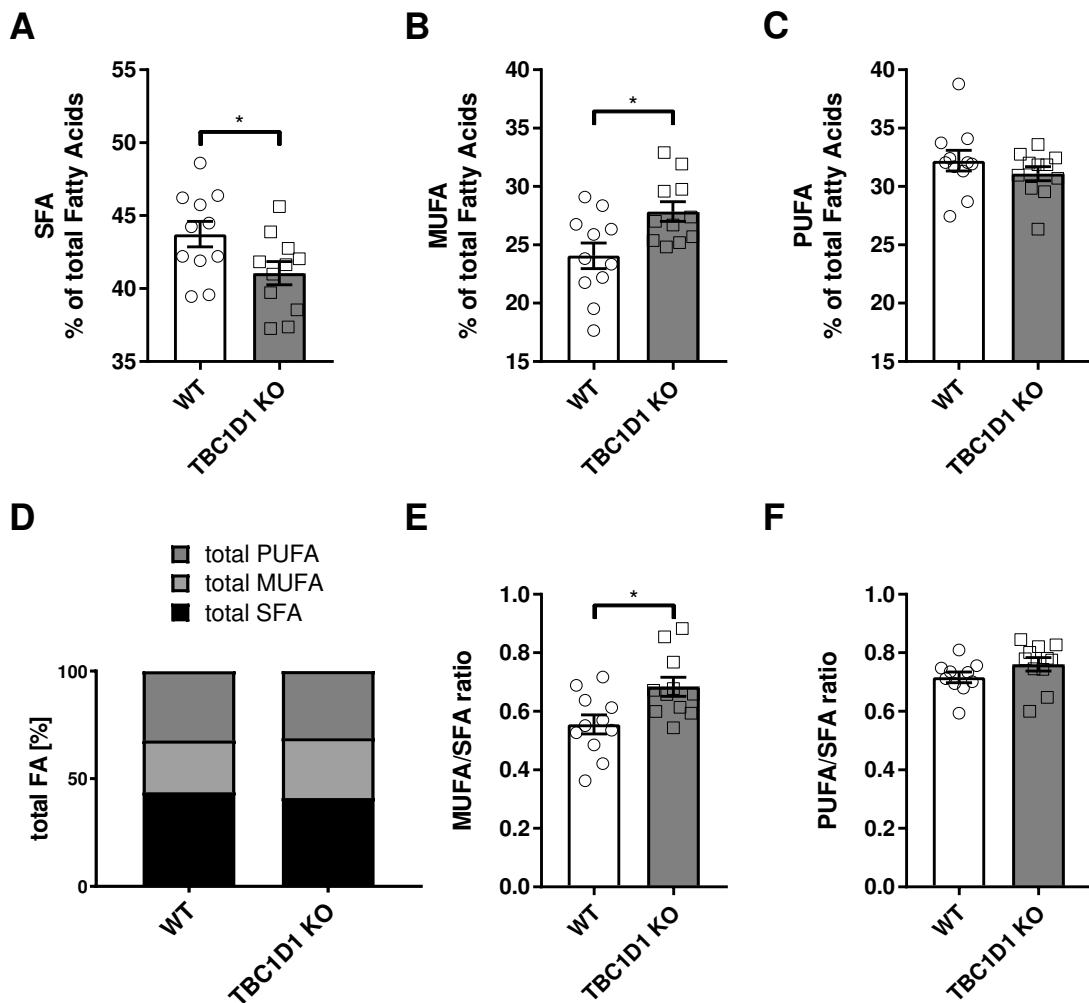


Figure 26: Distribution of fatty acid classes in wildtype and D1KO *Gastrocnemius* muscles. The amount of (A) saturated fatty acids (SFA), (B) mono unsaturated fatty acids, and (C) poly unsaturated fatty acids (PUFA) was expressed as % of total fatty acids measured in the GC analysis of wildtype (open bars) and *Tbc1d1*-deficient (grey bars) mouse *Gastrocnemius*. The results are summarized as contribution of each class to total fatty acid content (D). Based on the results the ratio of MUFAs to SFAs as measure for total desaturation activity (E), as well as the ratio of PUFAs to SFAs was calculated (F). Data are presented as mean ± SEM (n = 11). Two-tailed unpaired Student's t-test with Welch's correction. *p < 0.05. SFA: [95 % CI: -5.148 to 0.1916], MUFA: [95 % CI: 0.9006 to 6.668], MUFA/SFA: [95 % CI: 0.03247 to 0.2242].

4.5.4 FA-desaturation activities in WT and *Tbc1d1*-deficient mouse *Gastrocnemius* muscles

Since differences in the calculated total desaturase activity were found, different indexes for desaturase activity were calculated and analyzed. The results showed that the activity of $\Delta 5$ -desaturase was 0.7-fold lower in D1KO muscles compared with WT control mice (Fig. 27 A). On the other hand, the calculated $\Delta 6$ -desaturase activity did not differ between the two groups (Fig. 27 B). The cumulative $\Delta 5/\Delta 6$ -desaturase index reflected the observation of a decreased

desaturase activity and showed a 27 % reduced activity in D1KO mouse *Gastrocnemius* muscles

(Fig. 27 C). The C16 $\Delta 9$ -desaturase activity was altered inversely to the $\Delta 5$ -desaturase activity. Mice deficient for *Tbc1d1* exhibited a 27.8 % higher index for C16 desaturation (Fig. 27 D). In parallel, the $\Delta 9$ -desaturase activity towards C18 fatty acids was increased by 30.7 %. The difference was close to statistical significance ($p = 0.053$) (Fig. 27 E).

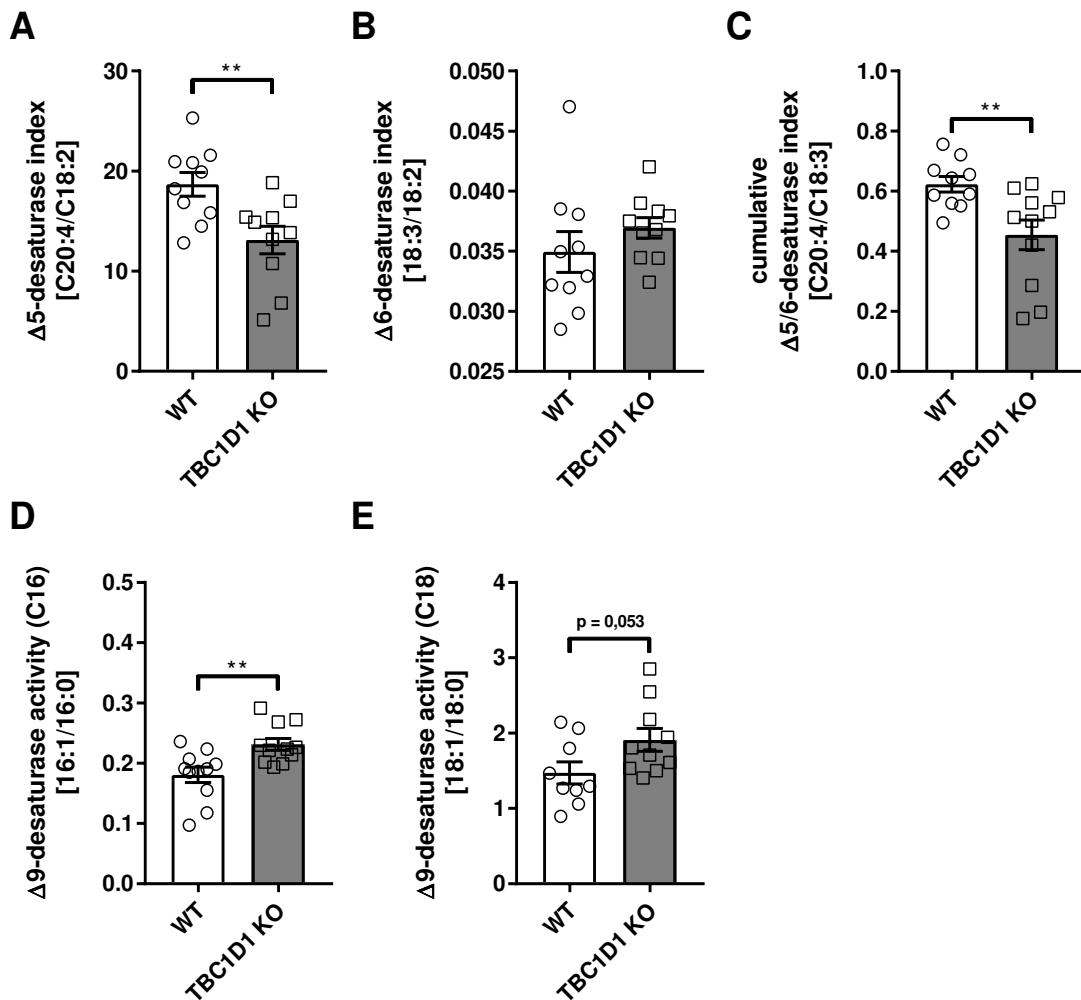


Figure 27: Comparison of calculated desaturation activity indexes in *Gastrocnemius* muscles from WT and D1KO mice. With regard to the measured fatty acid profile the activities of certain muscle desaturases were calculated for wildtype (open bars) and TBC1D1 knockout mice skeletal muscles (grey bars). $\Delta 5$ -, $\Delta 6$ -, as well as the cumulative $\Delta 5/6$ -desaturase activity indexes were calculated (A-C). Additionally, the $\Delta 9$ -desaturase activity index specific for C16 fatty acids and C18 fatty acids was evaluated (D, E). Data are presented as mean \pm SEM ($n = 10-11$). ** $p < 0.01$. A; [95 % CI: -9,388 to -1,737], C; [95 % CI: -0.2864 to -0.05049], D; [95 % CI: 0.01677 to 0.08388], E; [95 % CI: -0.006467 to 0.883].

4.5.5 FA elongation and elongase indexes of WT and TBC1D1 KO mouse *Gastrocnemius* muscles

Elongases are essential determinants of (very-) long chain fatty acid generation (Green et al., 2010; Jump, 2009). To have an indicator if a lack of TBC1D1 influences fatty acid chain elongation certain operators can be calculated to estimate overall elongase activity. No differences between WT and D1KO mice were found for SFA elongase activity (Fig. 28 A) and MUFA elongase activity (Fig. 28 B), or the palmitic acid-specific C16:0 elongation index (Fig. 28 C).

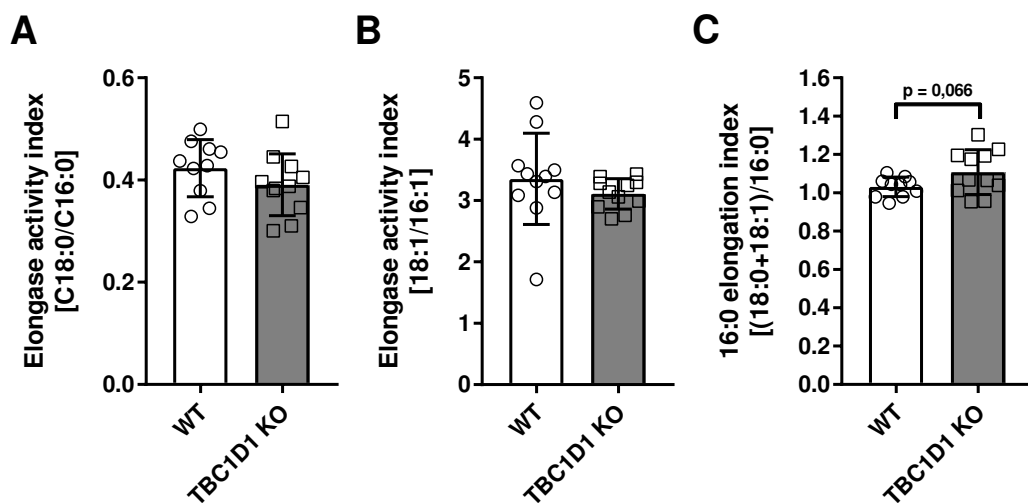


Figure 28: Comparison of elongation and elongase activity indexes in *Gastrocnemius* muscles from WT and *Tbc1d1*-deficient mice. From the data gained by FA profiling of WT (open bars) and D1KO (grey bars) *Gastrocnemius* muscles measures were calculated to estimate muscle SFA elongase activity (A), MUFA elongase activity (B) and the palmitic acid-specific 16:0 elongation index (C). Data presented as single values and means \pm SEM (n = 11). Two-tailed unpaired Student's t test with Welch's correction.

4.5.6 Thioesterase and *de novo* lipogenesis indexes of WT and TBC1D1 KO mouse *Gastrocnemius* muscles

Hydrolases from the thioesterase family participate in fatty acid synthesis (Chirala et al., 2001). Another measure for fatty acid synthesis is the *de novo* lipogenesis index. The thioesterase index was decreased by 18 % in *Tbc1d1*-deficient mouse muscles in comparison to WT muscles (Fig. 29 A). Similarly, the *de novo* lipogenesis index was 15.4 % lower in samples from D1KO mice compared to WT littermates (Fig. 29 B).

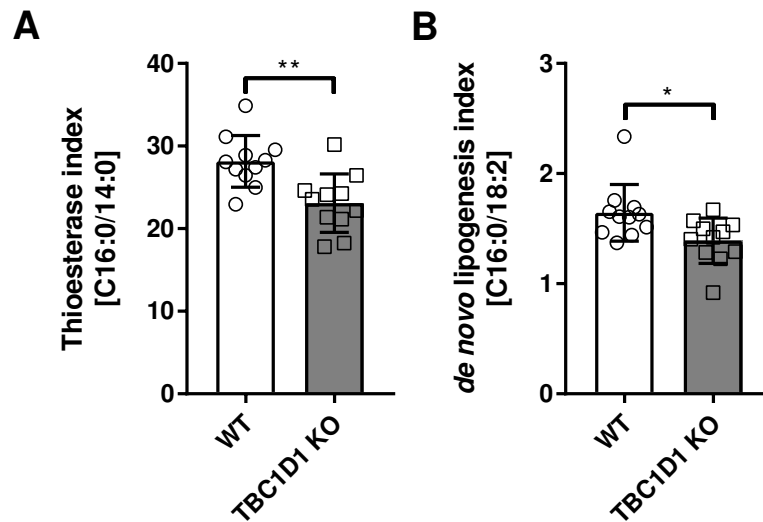


Figure 29: Comparison of indexes for lipid synthesis in *Gastrocnemius* muscle samples from WT and D1KO mice. Fatty acid profiling data from wildtype (open bars) and *Tbc1d1*-deficient (grey bars) mouse *Gastrocnemius* muscle samples were used to calculate the thioesterase index (A) and the de novo lipogenesis index (B) as measures for skeletal muscle lipid synthesis. Data presented as single values and means \pm SEM ($n = 11$). Two-tailed unpaired Student's *t* test with Welch's correction. * $p < 0.05$, ** $p < 0.01$. A: [95 % CI: -8.052 to -2.101], B: [95 % CI: -0.4609 to -0.04576].

4.6 Malonyl- and acetyl-CoA levels of wildtype and *Tbc1d1*-deficient *Gastrocnemius* muscles

One approach was to evaluate the levels of malonyl-CoA and acetyl-CoA in skeletal muscle samples from WT and D1KO mice. Malonyl-CoA has been described to regulate mitochondrial fatty acid oxidation. Analysis was performed in unstimulated *Gastrocnemius* muscles and muscles from mice that received an i.p. injection of AICAR prior to muscle dissection. It became evident that in the tested samples neither under basal, nor under AICAR-stimulated conditions malonyl-CoA levels were different between WT and *Tbc1d1*-deficient muscle samples (Fig. 30 A). In accordance to that, no differences were found in the acetyl-CoA levels between the genotypes (Fig. 30 B).

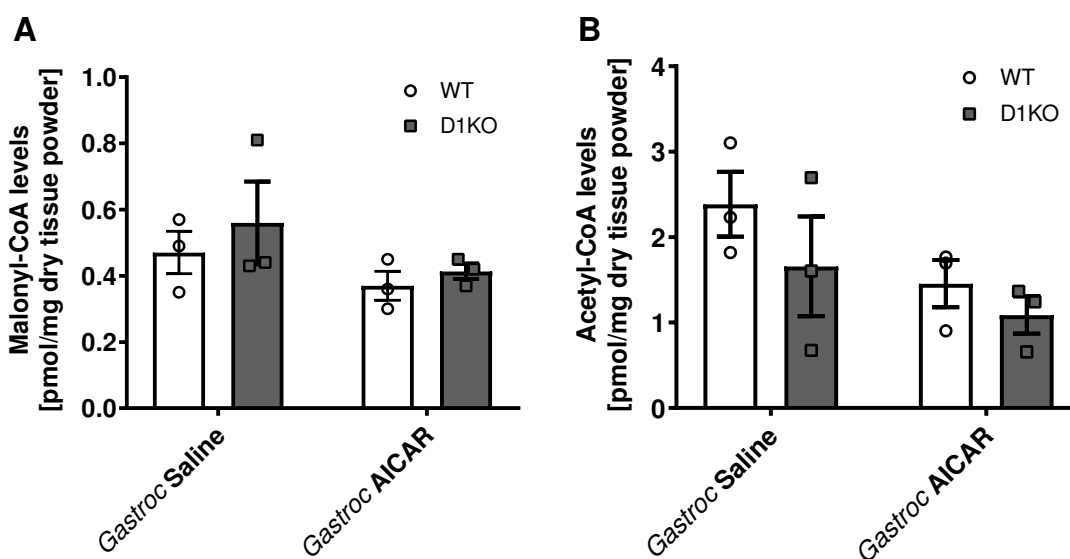


Figure 30: Levels of malonyl- and acetyl-CoA of wildtype and *Tbc1d1*-deficient mouse *Gastrocnemius* muscles. *Gastrocnemius* muscles of unstimulated, Saline-injected muscles and AICAR pre-injected wildtype (open circles and bars) and D1KO (grey squares and bars) mice were subjected to a LC-MS/MS measurement to evaluate muscle malonyl- (A) and acetyl-CoA (B) levels. Data displayed as single values and mean \pm SEM (n = 3). Two-way ANOVA with Sidak's multiple comparison test.

4.7 Role of Rab GTPases as protein downstream targets of TBC1D1 and TBC1D4 in *in vitro* C2C12 myotube fatty acid uptake

Small Rab GTPases (RAB proteins) are the main downstream targets of RabGAPs such as TBC1D1 and TBC1D4. As RAB proteins are involved in numerous different intracellular vesicle transport processes and some Rab GTPases have been already described as regulators of GLUT4 trafficking, it was tested in how far some candidate RABs influence palmitic acid uptake into C2C12 myotubes following siRNA-mediated knockdown of RAB candidates.

4.7.1 FA elongation and elongase indexes of WT and TBC1D1 KO mouse *Gastrocnemius* muscles

Experiments were conducted in C2C12 myotubes after 6 days of cell differentiation. Cells were chemically transfected with RAB-specific siRNA oligonucleotides on day 3 in the course of differentiation (3.2.2.1.2). To validate that the transfection of the myotubes was sufficient and led to a measurable decrease in target gene expression, RNA was isolated from cells either after transfection with a non-target (*siNT*) control, or *Rab* gene-specific siRNA oligonucleotides (*siRab*) and gene expression levels were analyzed by qRT-PCR (3.2.4.5.3). In comparison with

siNT control cells, expression levels of *Rab8a* were reduced by 46 %, of *Rab8b* by 72 %, of *Rab10* by 45 %, of *Rab12* by 74 %, of *Rab14* by 50 %, of *Rab28* by 59 % and of *Rab40b* by 89 % in cells transfected with target-specific siRNA.

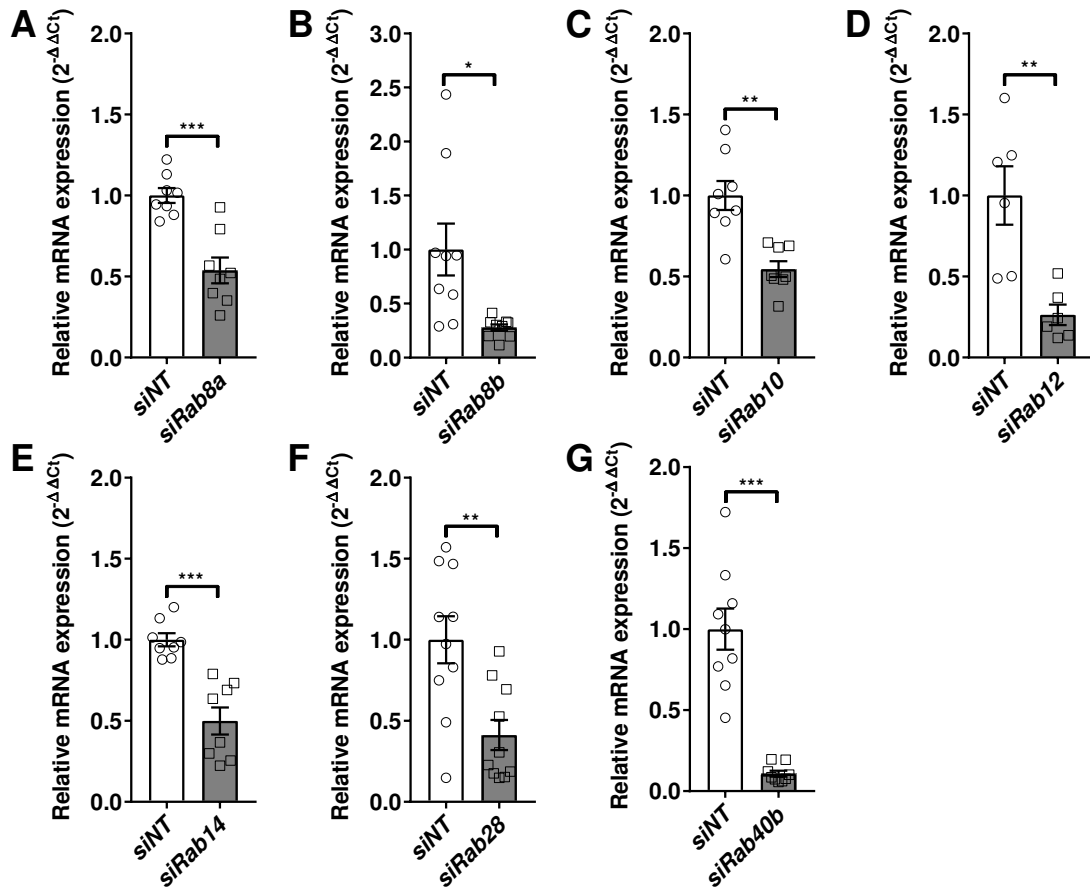


Figure 31: Validation of siRNA-mediated knockdown of target candidate Rab GTPase genes in C2C12 myotubes. Differentiating C2C12 myotubes were chemically transfected with Rab target-specific siRNA oligonucleotides on day 3 of cell differentiation. On day 6 of differentiation RNA was isolated and transcribed into cDNA. Expression levels were analyzed by SYBR green qRT-PCR and expressed as fold values calculated by the $2^{-\Delta\Delta C_t}$ method. Comparison is made between non-target siRNA (open bars) and Rab-specific siRNA (dark grey bars) transfected cells. Data presented as single values and means \pm SEM (n = 6 – 10). Two-tailed unpaired Student's t test with Welch's correction. *p < 0.05, **p < 0.01, ***p < 0.001. *Rab8a*: [95 % CI: -0.6629 to -0.2618]; *Rab8b*: [95 % CI: -1.277 to -0.1674]; *Rab10*: [95 % CI: -0.6788 to -0.23]; *Rab12*: [95 % CI: -1.201 to -0.2726]; *Rab14*: [95 % CI: -0.7067 to -0.2954]; *Rab28*: [95 % CI: -0.955 to -0.2204]; *Rab40b*: [95 % CI: -1.187 to -0.5974].

4.7.2 Impact of distinct Rab GTPases on *in vitro* fatty acid uptake in C2C12 myotubes

After having validated a successful knockdown of target Rab candidate genes, the differentiated C2C12 myotubes were utilized to measure the influence of Rab protein expression manipulations on the ^3H -palmitate uptake. All candidate Rab proteins used

throughout this study have previously been shown to be *in vitro* substrates of TBC1D1 and TBC1D4

(Miinea et al., 2005; Roach et al., 2007). Some of them have been described to be associated with GLUT4 trafficking in muscle and adipose tissue (see 1.5.1). It could be shown that the knockdown of *Rab8a* led to a 27 % reduced fatty acid uptake in comparison with non-target siRNA transfected cells (Fig. 32 A). Silencing of *Rab8b*, a closely related isoform of *Rab8a*, had an effect on C2C12 lipid uptake as well, as *Rab8b* knockdown led to a significant 12 % reduction in palmitic acid uptake (Fig. 32 B). Knockdown of *Rab10* caused a 27 % lower palmitic acid uptake (Fig. 32 C), while fatty acid uptake was decreased by 24 % after *Rab14* knockdown (Fig. 32 E). A novel Rab candidate, *Rab40b*, which has so far not been described in the context of muscle energy metabolism, was silenced as well and caused a decrease in palmitic acid uptake of 19 % in comparison with the control cells (Fig. 32 G). In opposition to the Rab GTPases that were shown to be involved in cellular lipid uptake, knocking down the expression of *Rab12* and *Rab28*, two proteins that have also been shown to be substrates for TBC1D1, did not have any effect on C2C12 myotube palmitate uptake (Fig. 32 D + F). Triple silencing of *Rab8a*, *Rab10* and *Rab14* in parallel decreased fatty acid uptake by 34 % (Fig. 32 H).

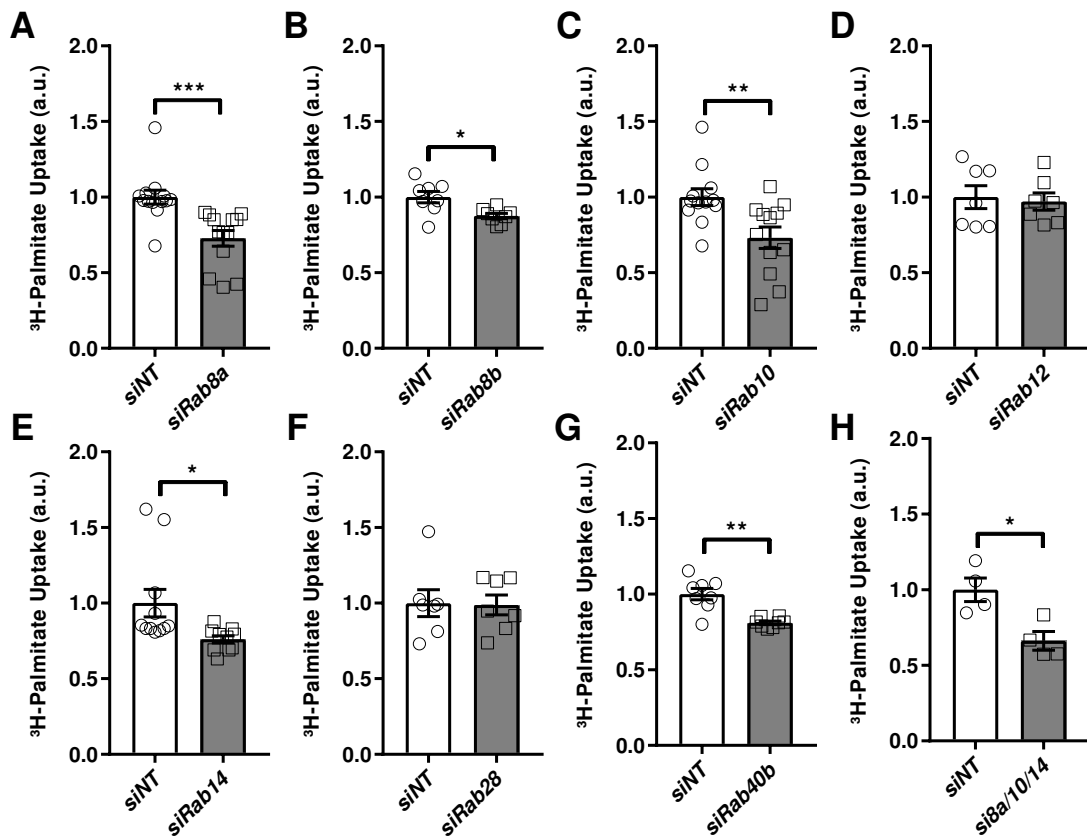


Figure 32: Role of distinct Rab GTPases in C2C12 myotube fatty acid uptake. RabGAP substrate Rab GTPases Rab8a, Rab8b, Rab10, Rab12, Rab14, Rab28 and Rab40b were separately silenced in C2C12 myotubes via siRNA technology. After 6 days of differentiation cells were utilized for ³H-palmitic acid uptake assays. Cells in which one of the Rab candidates was knocked down (dark grey bars) were compared with cells transfected with control non-target siRNA. Data expressed as single values and mean \pm SEM (n = 4 – 13). Two-tailed unpaired Student's t test with Welch's correction. *p < 0.05, **p < 0.01, ***p < 0.001. *Rab8a*: [95 % CI: -0.4146 to -0.1305]; *Rab8b*: [95 % CI: -0.2177 to -0.03197]; *Rab10*: [95 % CI: -0.4563 to -0.08162]; *Rab14*: [95 % CI: -0.4447 to -0.03496]; *Rab40b*: [95 % CI: -0.2796 to -0.09841] *triple Rab8a/Rab10/Rab14*: [-0.5834 to -0.9123].

4.7.3 Impact of insulin-stimulation on C2C12 myotube fatty acid uptake (FAU) after independent single silencing of *Rab8a*, *Rab10* and *Rab14*

Insulin is able to increase cellular fatty acid uptake, likely through stimulating the surface recruitment of cellular fatty acid transport proteins (Dimitriadis et al., 2011; Stahl et al., 2002). To elucidate if the main candidate Rab proteins Rab8a, Rab10 and Rab14 may be involved in the cell surface translocation of any fatty acid transport protein, the respective Rab GTPases were silenced in C2C12 myotubes using siRNA technology (3.2.2.1.2) (Fig. 31). Subsequently, the amount of fatty acid uptake was evaluated under basal conditions and after a 15 min stimulation phase with 120 nM insulin. Under basal conditions, silencing of either one of the Rab genes encoding for *Rab8a*, *Rab10* or *Rab14* led to significant reductions in ³H-palmitate uptake (*siRab8a*: -39 %; *siRab10*: -35 %; *siRab14*: -26 %) in comparison with cells that were

transfected with *non-target* control siRNA (*siNT*). In control cells, insulin stimulation increased fatty acid uptake by 22 %. Similar to the basal situation, the rate of fatty acid uptake was significantly lower under knockdown conditions of *Rab8a*, *Rab10* and *Rab14* (*siRab8a*: -20 %; *siRab10*: -18 %; *siRab14*: -22 %) in comparison to insulin-stimulated control siRNA (*siNT*) transfected cells. Insulin stimulation increased fatty acid uptake when comparing basal and insulin-stimulated cells after siRNA-mediated Rab knockdown. Under *Rab8a* knockdown conditions the insulin-stimulated FAU was 41 % higher than in the basal state. Similar results were found after *Rab10* and *Rab14* silencing, where exposure to insulin caused a +47 %, respectively +25 % increase in fatty acid uptake due to the Rab protein deficiency. Comparing basal control cells with insulin-stimulated Rab knockdown cells no difference was found. The fatty acid uptake levels were comparable.

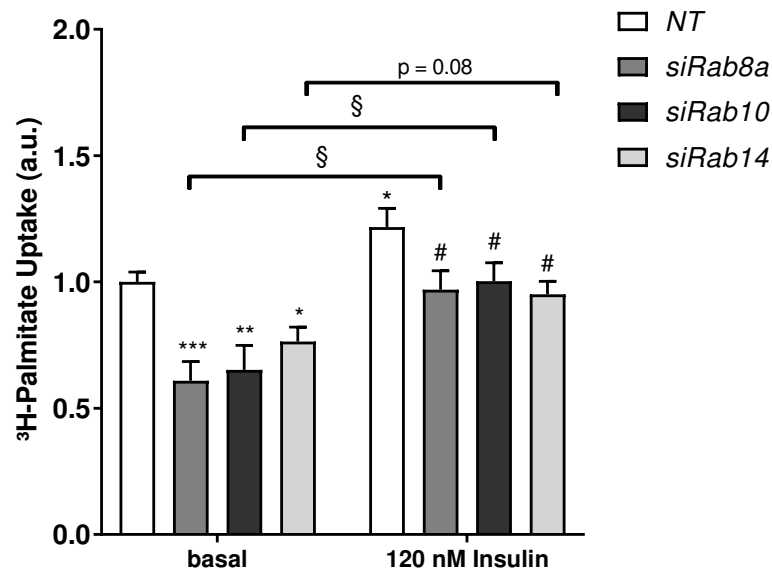


Figure 33: Influence of insulin stimulation on C2C12 myotube fatty acid uptake under candidate Rab knockdown conditions. RabGAP substrate Rab GTPases *Rab8a* (grey bars), *Rab10* (dark grey bars) and *Rab14* (light grey bars) were silenced independently in C2C12 myotubes via siRNA technology. After 6 days of differentiation cells were utilized for ^3H -palmitic acid uptake assays. Fatty acid uptake was either measured under basal conditions, or after 15 min stimulation with 120 nm insulin. Cells in which the Rab candidates were knocked down were compared with cells transfected with control *non-target* siRNA (open bars). Data expressed as mean \pm SEM (n = 5 – 11). One-way ANOVA. * vs. NT basal, *p < 0.05, **p < 0.01, ***p < 0.001; # vs. NT insulin, #p < 0.05; § *siRab* basal vs. *siRab* insulin.

4.8 The Role of Rab GTPases as protein downstream targets of TBC1D1 and TBC1D4 in *ex vivo* mouse *EDL* and *Soleus* muscle fatty acid oxidation

Several Rab GTPases have been shown previously to be downstream substrates of the RabGAPs TBC1D1 and TBC1D4. To further elucidate the role of the Rab proteins in

myocellular lipid metabolism, the two RAB proteins RAB8a and RAB10 which had the largest impact on C2C12 cell lipid utilization (see Fig. 31 and 32) were further tested in relation to their influence on lipid oxidation *ex vivo*. C57BL/6J mice hind limbs were injected with sterile saline solution, containing specific siRNA oligonucleotides targeting one of the Rab proteins. Mouse muscles were electrically transfected with the siRNA molecules by *in vivo* electrotransfection (IVE) (3.2.1.1). After one week of maintenance, *EDL* and *Soleus* muscle were dissected and used further for *ex vivo* fatty acid oxidation assays (3.2.1.3).

4.8.1 Role of Rab8a in *ex vivo* EDL and Soleus fatty acid oxidation (FAO)

EDL and *Soleus* muscles that have previously been transfected with either *non-target* control siRNA or *Rab8a*-specific siRNA oligonucleotides were dissected and subjected to a ^3H -palmitate oxidation assay. Successful siRNA-mediated knockdown was quantified on protein level with a RAB8-specific antibody (Fig. 34 A). Importantly, only muscle samples with a minimum Rab8 protein reduction of 20 % were considered for further functional analysis. *Rab8a* silencing had no effect on the fatty acid oxidation of *EDL* muscles (Fig. 34 B), while the FAO of *Soleus* muscles with reduced Rab8a protein expression was 23.8 % lower in comparison to muscles transfected with control siRNA (Fig. 34 C).

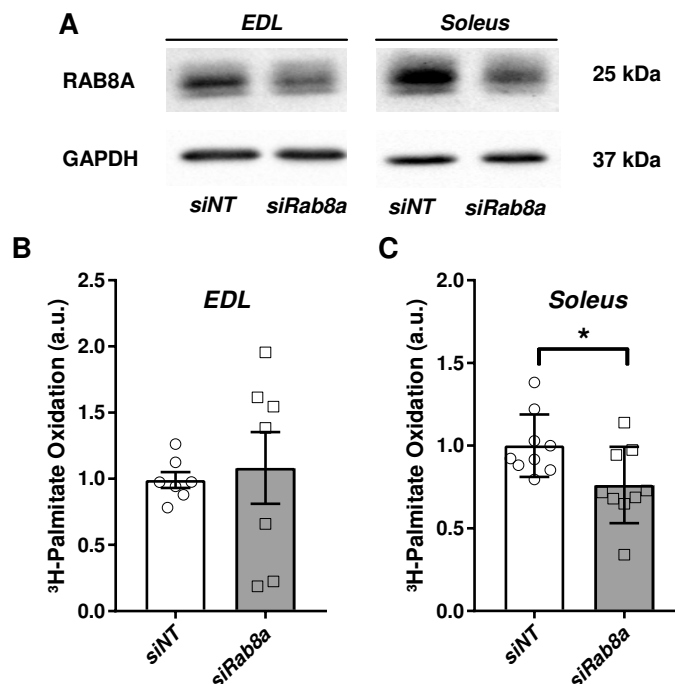


Figure 34: Impact of Rab8a on *EDL* and *Soleus* muscle *ex vivo* fatty acid oxidation. Mouse hind limbs were *in vivo* electrotransfected with the IVE method with either *non-target* control siRNA (open bars), or *Rab8a*-specific siRNA (grey bars). One week after transfection muscles were dissected and used for *ex vivo* fatty acid oxidation assays. Aliquots of muscle lysates were used for western blot analysis of knockdown efficiency on protein level (A). Quantification of fatty acid oxidation was performed for *EDL* (B) and *Soleus* (C) from samples that showed at least 20 % reduction of RAB8a protein expression. Data are

presented as mean \pm SEM (*EDL*: n = 7; *Soleus*: n = 9). Two-tailed unpaired Student's t test with Welch's correction. *p < 0.05.

4.8.2 Role of Rab10 in *ex vivo* *EDL* and *Soleus* fatty acid oxidation (FAO)

EDL and *Soleus* muscles were transfected with either *non-target* control or *Rab10*-specific siRNA oligonucleotides (Tab. 9). After one week, muscles were dissected and subjected to a ^3H -palmitate oxidation assay (3.2.1.3). Successful siRNA-mediated knockdown was quantified on protein level with a RAB10-specific antibody (Fig. 35 A). Importantly, only muscle samples with a minimum Rab10 protein reduction of 20 % were considered for analysis. *Rab10* silencing had no effect on either the fatty acid oxidation of *EDL* muscles (Fig. 35 B), or *Soleus* muscles (Fig. 35 C) in C57BL/6J mice compared to non-target control siRNA transfected muscles.

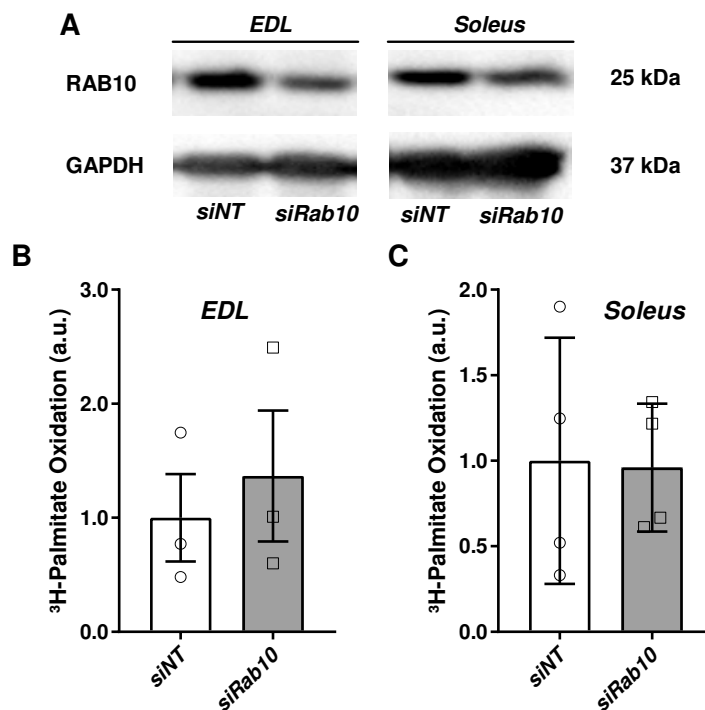


Figure 35: Impact of Rab10 on *EDL* and *Soleus* muscle *ex vivo* fatty acid oxidation. Mouse hind limbs were in vivo electrotransfected with the IVE method with either *non-target* control siRNA (open bars), or *Rab10*-specific siRNA (grey bars). One week after transfection muscles were dissected and used for *ex vivo* fatty acid oxidation assays. Aliquots of muscle lysates were used for western blot analysis of knockdown efficiency on protein level (A). Quantification of fatty acid oxidation was performed for *EDL* (B) and *Soleus* (C) from samples that showed at least 20 % reduction of RAB10 protein expression. Data are presented as mean \pm SEM (*EDL*: n = 7; *Soleus*: n = 9). Two-tailed unpaired Student's t test with Welch's correction. *p < 0.05.

4.9 Role of fatty acid transport proteins FATP1, FATP4 and FAT/CD36 in fatty acid uptake (FAU) in C2C12 myotubes

Regulated fatty acid uptake is likely to be regulated by specific proteins that facilitate binding and translocation of lipids into the cell. FATP1, FATP4 and FAT/CD36 are described to be expressed in skeletal muscle cells. To evaluate the contribution of the single transporters to palmitate uptake into myotubes, siRNA-mediated silencing experiments were conducted to reduce mRNA and protein expression of the respective lipid transporters (3.2.2.1.2), followed by *in vitro* ³H-palmitate uptake assays (3.2.2.2.1). To assure that the knockdown of the transporters was successful, total RNA was isolated from a part of the siRNA-transfected cells and expression of transporter gene mRNA was assessed by qRT-PCR (3.2.4.5.3). *Fatp1* was expressed at a 0.64-fold lower level in *siFatp1* transfected cells compared to non-target control cells (Fig. 36 A). *Fatp4* expression was 0.6-fold lower after *siFatp4* intervention (Fig. 36 B). *Cd36* expression was 0.56-fold reduced after *Cd36* silencing with siRNA (Fig. 36 C).

From all transporter tested in the cultured muscle cells, *Cd36* knockdown showed the mildest effect on FAU. Due to *Cd36* silencing, fatty acid uptake was reduced by 4 % compared to control cells. In contrast, a reduction of *Fatp1* expression levels resulted in an 11 % lower palmitate uptake in comparison to reference cells. Only the knockdown of *Fatp4* reached statistical significance in the presented data set. *Fatp4* knockdown resulted in a 13 % lower lipid uptake of the cells in contrast to the non-target siRNA transfected control cells (Fig. 36 D).

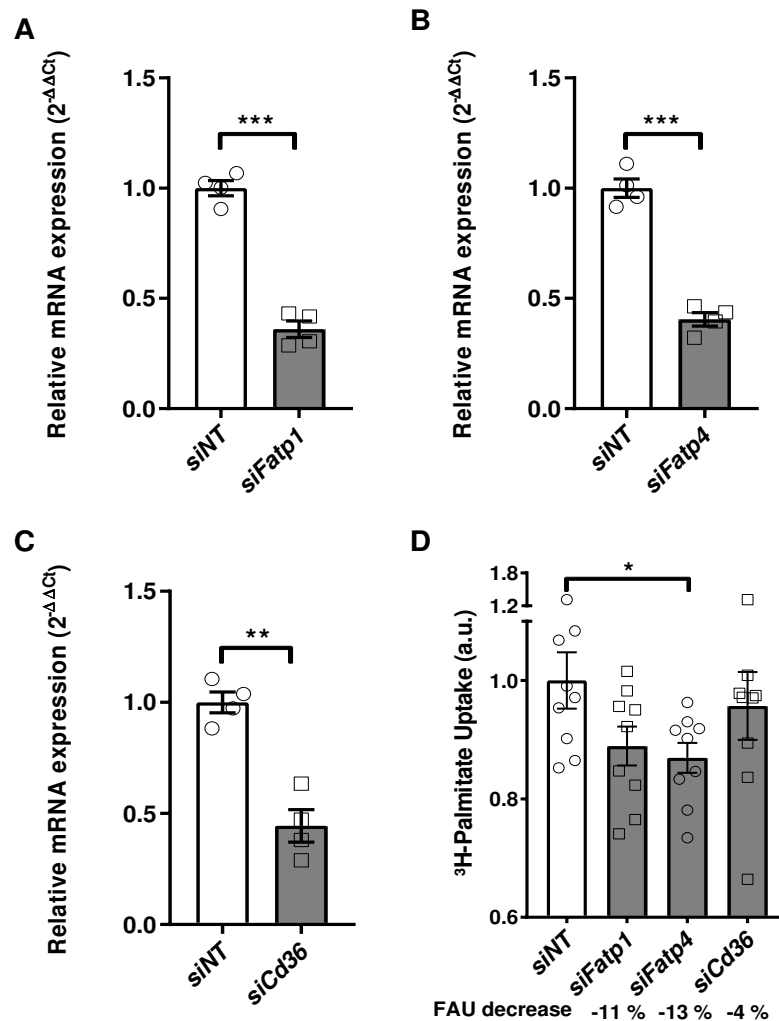


Figure 36: Influence of FATP1, FATP4 and FAT/CD36 on C2C12 myotube fatty acid uptake. Candidate fatty acid transport proteins were silenced via siRNA technology (grey bars). As reference, cells were transfected with non-target siRNA (siNT) (open bars). Knockdown was validated on qRT-PCR level (A-C). Fatty acid uptake was measured in vitro by evaluating the incorporated ³H-palmitate (D). Data presented as mean ± SEM (n = 4 – 9). Two-tailed Student's t test with Welch's correction (knockdowns) and one-way ANOVA (fatty acid uptake). *p < 0.05, ***p < 0.001.

4.10 TBC1D1 and its influence on the expression of fatty acid metabolism-relevant proteins

In the context of glucose metabolism it has been shown that *Tbc1d1*- and *Tbc1d4*-deficiency has impact on skeletal muscle glucose homeostasis. The impairment in insulin-stimulated glucose uptake may derive from marked reductions in GLUT4 protein content due to the RabGAP deficiency, e.g. in the *EDL* muscle. As expression analysis of several candidate genes in this study revealed *Tbc1d1*-deficiency has an impact on the expression of some of the tested genes with relation to lipid metabolism. Further experiments were conducted to

investigate a potential role of TBC1D1 on target protein expression. Here, the expression levels of fatty acid translocase FAT/CD36, and pyruvate dehydrogenase kinase isoform 4 (PDK4), which both were differentially expressed on mRNA level between *non-target* siRNA-transfected and *Tbc1d1*-deficient C2C12 myotubes, as well as the protein expression of FATP4, which has been described to be translocated to the cell surface from intracellular storage compartments and is one fatty acid transport protein responsible for skeletal muscle lipid uptake, were analyzed under varying conditions in wildtype and D1KO *EDL* muscles.

4.10.1 Influence of *Tbc1d1*-deficiency on FATP4, PDK4 and FAT/CD36 protein expression in mouse *EDL* muscles under palmitate stimulation

Wildtype and D1KO male mice were starved for 16 h before muscle dissection. One *EDL* muscle from each mouse was immediately frozen after extraction. The other muscle was incubated in a KHB-BSA buffer supplemented with 600 μ M palmitate for two hours before muscle lysis and protein preparation. Muscle protein lysates were subjected to SDS gel electrophoresis and subsequently subjected to Western blot analysis (3.2.4.3). For fatty acid transport protein isoform 4 (FATP4) it was found that, independent from *ex vivo* challenging the muscles with palmitate, D1KO *EDL* muscles showed an increased expression of FATP4 (1.39-fold w/o palmitate, 1.26-fold w/ palmitate) on protein level in comparison to wildtype muscles (Fig. 37 A). In contrast to that, FAT/CD36 protein levels were not different between the two genotypes with or without the palmitate incubation (Fig. 37 B). For pyruvate dehydrogenase kinase isoform 4 (PDK4), protein expression without palmitate stimulation was increased 1.45-fold in *EDL* muscles from *Tbc1d1*-deficient mice in comparison to wildtype *EDL* samples. For samples that underwent the 2 h palmitate incubation, it was found that PDK4 protein levels were 1.27-fold higher in D1KO *EDL* muscles than in *EDL* muscles from wildtype mice (Fig. 37 C).

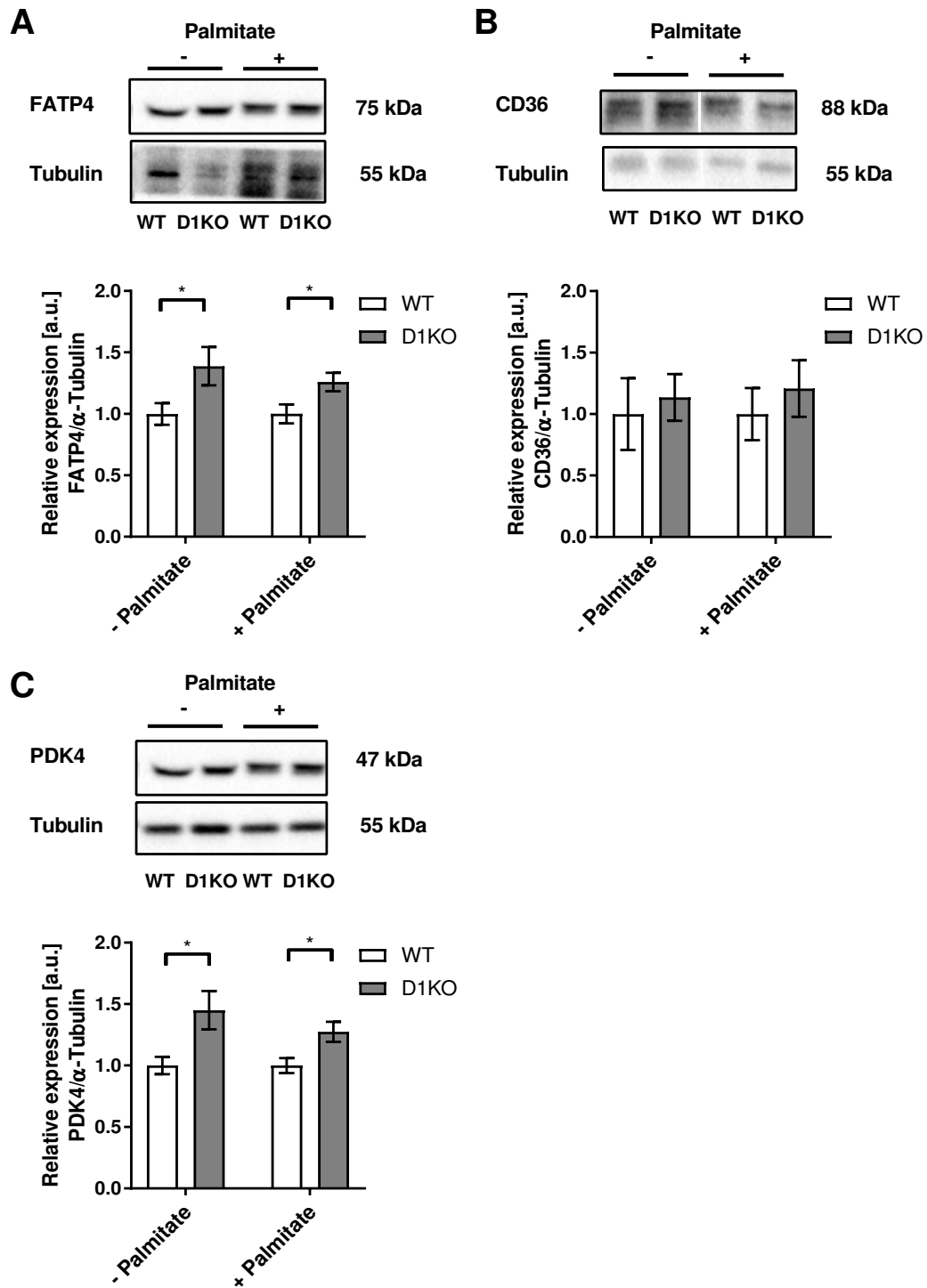


Figure 37: Western blot analysis of FATP4, CD36 and PDK4 in wildtype and D1KO EDL muscle samples after *ex vivo* palmitate stimulation. EDL muscles from wildtype (WT) and *Tbc1d1*-deficient (D1KO) male mice were dissected and either directly processed for western blot analysis (- Palmitate), or, stimulated with 600 μ M palmitate for 2 h *ex vivo* (+ Palmitate). Tubulin was used as reference protein. Protein detection was performed for FATP4 (A), CD36 (B) and PDK4 (C). Data are expressed as mean folds of wildtype \pm SEM ($n = 6 - 11$). Two-tailed Student's *t* test with Welch's correction. * $p < 0.05$.

4.10.2 Influence of *Tbc1d1*-deficiency on FATP4, PDK4 and FAT/CD36 protein expression in mouse *EDL* muscles under fasting and refeeding conditions

To investigate to what extent food supply and intake affects the expression of target proteins FATP4, CD36 and PDK4 in WT and D1KO mouse skeletal muscles, mice were either fed *ad libitum*, fasted for 16 h, or fasted for 16 h followed by a 4 h refeeding phase with a chow diet prior to animal sacrificing and muscle dissection. Isolated *EDL* muscles were prepared for SDS-PAGE and subsequent western blot analysis (3.2.4.3). It became evident that in random fed animals no difference between wildtype and *Tbc1d1*-deficient mice with regard to either FATP4 (Fig. 38 A), PDK4 (Fig. 38 B), or FAT/CD36 (Fig. 38 C) was found. In contrast, prior fasting for 16 h resulted in a 1.93-fold increase in the expression of FATP4 and a 1.93-fold increased protein expression of PDK4, while FAT/CD36 levels were unchanged. Similar to random feeding, a 4 h refeeding after 16 h of fasting revealed no differences between the investigated genotypes for any of the proteins of interest.

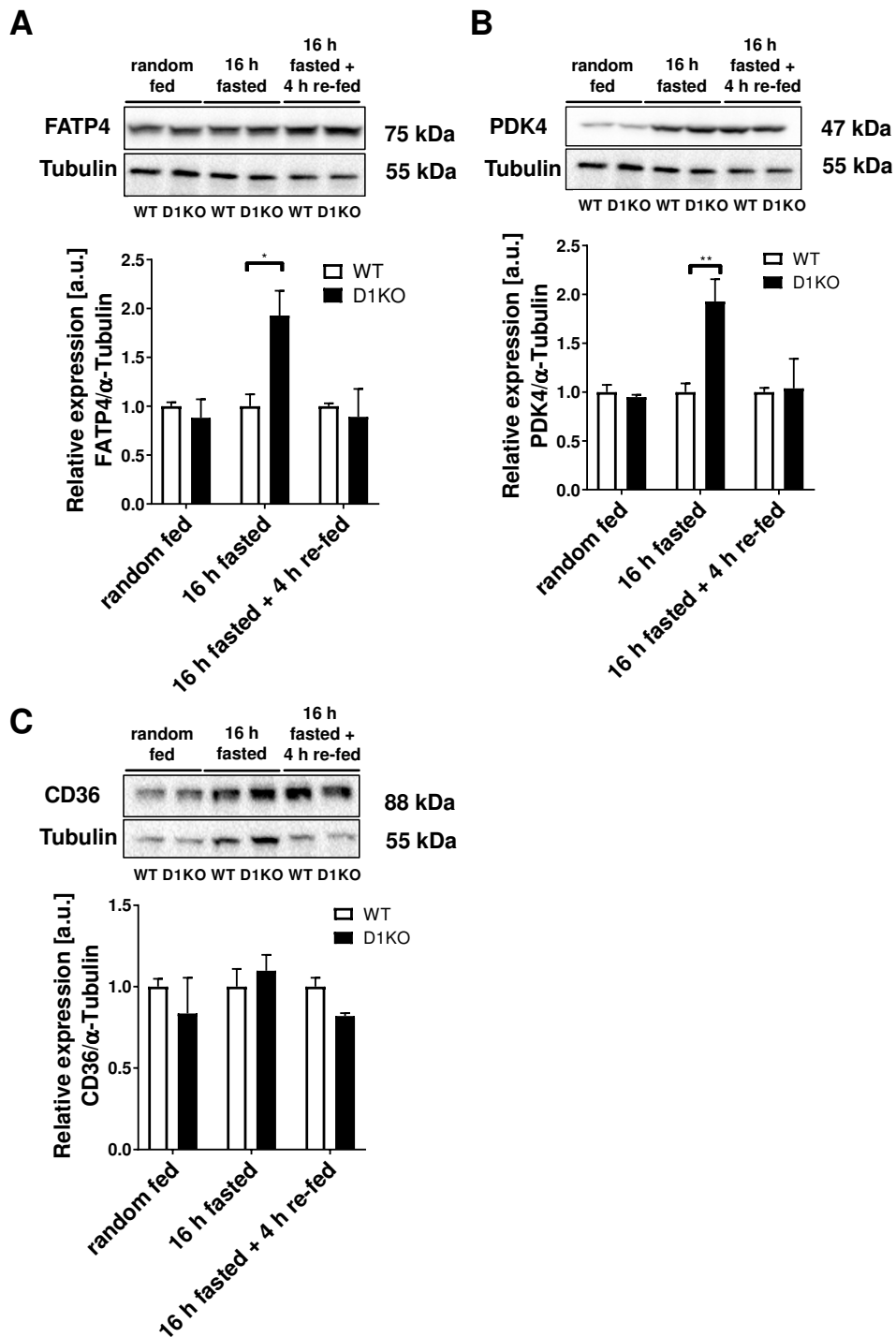


Figure 38: Influence of fasting and feeding on the protein expression levels of FATP4, PDK4 and CD36 in WT and D1KO mouse *EDL* muscles. *EDL* muscles from wildtype (WT) and *Tbc1d1*-deficient (D1KO) male mice that were either random fed, fasted for 16 h, or fasted for 16 h and re-fed for 4 h prior to muscle dissection were processed for western blot analysis. Tubulin was used as reference protein. Protein detection was performed for FATP4 (A), CD36 (B) and PDK4 (C). Data are expressed as mean folds of wildtype \pm SEM ($n = 4$). Two-tailed Student's *t* test with Welch's correction. * $p < 0.05$, ** $p < 0.01$.

4.11 The connection of TBC1D1 and TBC1D4 with the fatty acid translocase FAT/CD36 in *ex vivo* skeletal muscle fatty acid uptake (FAU)

In vitro studies revealed that the RabGAPs TBC1D1 and TBC1D4 are important regulators of skeletal muscle fatty acid uptake and oxidation. Moreover, published data (Chadt et al., 2015; Chadt et al., 2008) also stress the role of both proteins in *ex vivo* skeletal muscle lipid oxidation and whole-body lipid utilization. To further elucidate the mechanism responsible for the increase in fatty acid utilization, an experiment measuring *ex vivo* ^3H -palmitic acid uptake was conducted (3.2.1.2). For that purpose, intact *EDL* and *Soleus* muscles from genetically modified mice lacking *Tbc1d1* (D1KO), *Tbc1d4* (D4KO), the fatty acid translocase *Cd36* (CD36KO), or a double- and triple-deficient combination of these knockouts (D1-CD36KO, D4-CD36KO, D1-D4-CD36KO) were utilized and compared to wildtype mice.

For *EDL* muscles (Fig. 39 A) it became evident that both, D1KO and D4KO mice displayed a 1.32-fold higher palmitate uptake compared to wildtype control mice. In contrast to that, mice lacking FAT/CD36 had a 0.8-fold lower FAU. To evaluate if CD36 is responsible for the observations of the RabGAPs with regard to fatty acid uptake, RabGAP-CD36 double- and triple knockout mice were included into the study. The combination of D1KO-CD36KO caused an increase of fatty acid uptake of 1.6-fold. The combined knockout of *Cd36* and *Tbc1d4* (D4KO-CD36KO) led to a milder but significant increase of palmitate uptake of 1.18-fold. D1/4KO-CD36 triple deficiency caused a 1.37-fold increase in FAU. For *Soleus* muscle (Fig. 39 B), the experiments revealed that in comparison with wildtype control mice, the D1KO showed a 1.14-fold, but not statistically significant increased FAU, while no changes were found for D4KO, CD36KO, D1-CD36KO, or D1-D4-CD36KO mice. In contrast, mice lacking TBC1D1 and FAT/CD36 (D1KO-CD36KO) exhibited a significant 1.52-fold increase of fatty acid uptake in the co-absence of both proteins.

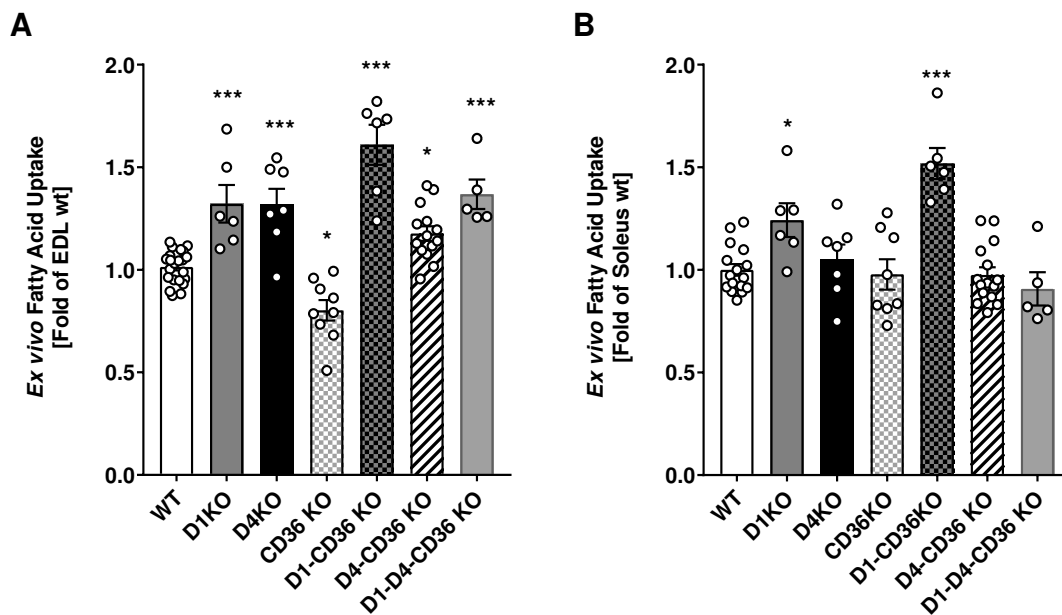


Figure 39: The role of TBC1D1, TBC1D4 and FAT/CD36 on *ex vivo* fatty acid uptake in mouse *EDL* and *Soleus* muscle. *Ex vivo* studies were conducted with dissected *EDL* (A) and *Soleus* (B) skeletal muscles from wildtype (WT; open bars), *Tbc1d1*- (D1KO; dark grey bars), *Tbc1d4*- (D4KO; black bars), and *Cd36*-deficient (CD36KO; open light grey plaid bars) mice, and *Tbc1d1*-*Cd36*-double- (D1-CD36KO; dark grey black plaid bars), *Tbc1d4*-*Cd36*-double- (D4-CD36KO; open striated bar), and *Tbc1d1*-*Tbc1d4*-*Cd36*-triple-deficient (D1-D4-CD36KO; light grey bars) mice. Data are presented as single values and mean \pm SEM (n = 6 – 22). One-way ANOVA with Tukey's multiple comparison test vs. WT control mice. *p < 0.05, ***p < 0.001. *EDL*: D1KO [95 % CI: -0.5216 to -0.09478], D4KO [95 % CI: -0.505 to -0.1029], CD36KO [95 % CI: 0.02726 to 0.394], D1-CD36KO [95 % CI: -0.8094 to -0.3825], D4-CD36KO [95 % CI: -0.3218 to -0.004939], D1-D4-CD36KO [95 % CI: -0.5842 to -0.125]. *Soleus*: D1KO [-0.4829 to -0.002656], D1-CD36KO [95 % CI: -0.7576 to -0.2797].

4.12 Interplay of TBC1D1, TBC1D4 and FATP4 with regard to C2C12 myotube fatty acid uptake

To gain further insight into the mechanism that may be responsible for the effect of *Tbc1d1*- and *Tbc1d4*- deficiency on skeletal muscle fatty acid metabolism, co-silencing experiments utilizing siRNA technology were performed. As FATP4 was found to be increased on protein level in D1KO mouse *EDL* muscles, it was investigated to what extent FATP4 has an impact on C2C12 ^3H -palmitate uptake in relation to a reduced expression of *Tbc1d1* and *Tbc1d4* mRNA. For that purpose, C2C12 myotubes were co-transfected with siRNA oligonucleotides selectively targeting either *Tbc1d1* (*siD1*) or *Tbc1d4* (*siD4*) and *Fatp4* (*siFatp4*) (Tab. 9). Knockdown efficiencies were analyzed by qRT-PCR (3.2.4.5.3). It could be shown that *siFatp4* transfection of myotubes reduced the expression of *Fatp4* by 90 % compared with cells transfected with *non-target* control siRNA (*siNT*) (Fig. 40 A + B). In cells with co-knockdown of *Tbc1d1*, the *Tbc1d1* mRNA expression levels were reduced by 88 % (Fig. 40 A). Similarly, *Tbc1d4* gene expression levels were reduced by 66 % in relation to the control samples (Fig. 40 B). C2C12

cells that were co-transfected with siRNA targeting one of the RabGAPs and *Fatp4* to achieve a double target deficiency were further used for *in vitro* fatty acid uptake assays. It was found that a combined deficiency of *Fatp4* and *Tbc1d1* did not alter ^3H -palmitate uptake of C2C12 myotubes in comparison with control cells (Fig. 40 C). Cells with a reduced expression of *Fatp4* and *Tbc1d4* also did not display changes in fatty acid uptake compared to control cell (Fig. 40 C).

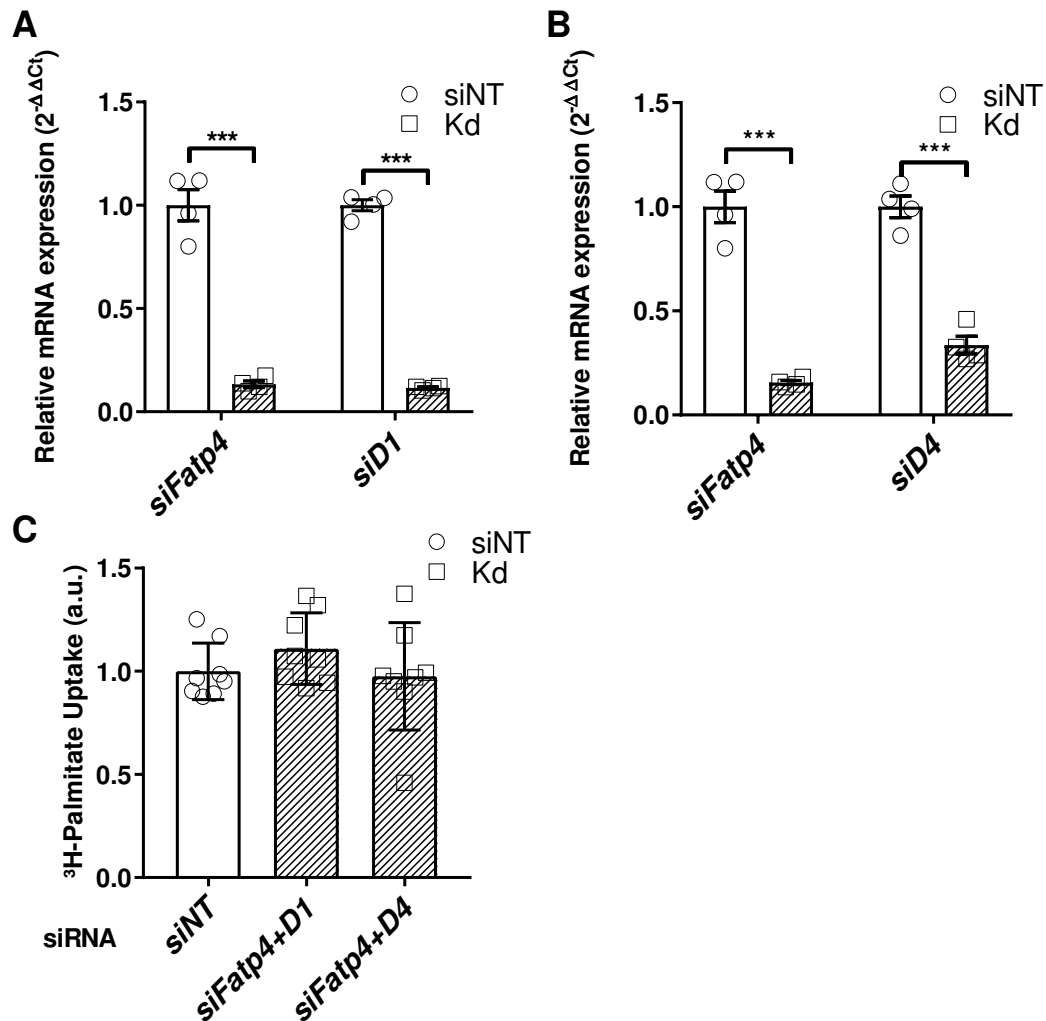


Figure 40: TBC1D1, TBC1D4 and FATP4 in regulating C2C12 myotube fatty acid uptake. Differentiating C2C12 myotubes were transfected with *non-target* control siRNA (*siNT*) (open bars; circle symbols), or a combination of siRNA oligonucleotides targeting the expression of *Fatp4* and *Tbc1d1* (*siFatp4+D1*), or *Fatp4* and *Tbc1d4* (*siFatp4+D4*) (both: striped bars; square symbols for specific knockdowns). Cells were further differentiated and subsequently used for ^3H -palmitate uptake assays (FAU) (C). Efficiency of double knockdown (Kd) was confirmed by qRT-PCR (A + B). Data are presented as single values and mean \pm SEM (Kd: n = 4, FAU: n = 8). Two-tailed unpaired Student's t test with Welch's correction. ***p < 0.001.

5 Discussion

The present study focusses on the influence of the RabGAPs TBC1D1 and TBC1D4 on the regulation of skeletal muscle cell lipid metabolism. Since it was widely unknown at which level the GAPs regulate fatty acid metabolism in muscle cells and which of them drive the switch from glucose to lipid utilization upon *Tbc1d1*-deficiency a multilateral experimental approach was conducted. Whether the D1 and D4 effect is a general effect that applies to all kinds of fatty acids or if the observation accounts more for a certain group of fatty acid species was investigated in an *in vitro* cell culture approach. To assess, in how far a deficiency for *Tbc1d1* may influence skeletal muscle gene and protein expression, a large scale screening was performed on the expression levels of distinct candidate genes that were reported in literature to interplay with skeletal muscle lipid metabolism at different levels. Further, it was investigated if TBC1D1 may affect the cellular lipid remodeling and composition by comparing the fatty acid profiles of *ex vivo* skeletal muscle samples of wildtype and D1KO mice. Beyond this, experiments were conducted to elucidate if TBC1D1/TBC1D4 downstream Rab GTPase substrates interfere with muscle lipid utilization. In this context it was also examined to what extend TBC1D1 and TBC1D4 may interfere with the muscle cell surface recruitment of specific fatty acid transport proteins. While only a few studies were conducted focusing on the regulation of lipid metabolism and RabGAPs, in the past several studies have linked TBC1D1 and TBC1D4/AS160 to muscle glucose uptake and GLUT4 translocation. Moreover, it could be shown that both GAPs also are involved in the regulated utilization of fatty acids. Studies from our working group could show that both, TBC1D1 and TBC1D4 function as molecular substrate preference switches that regulate the choice of either glucose, or fatty acids as metabolic energy source. Thus, the goal of this study was to add conclusive information on how RabGAPs directly or indirectly control skeletal muscle fatty acid utilization.

5.1 TBC1D1 and TBC1D4 regulate skeletal muscle fatty acid metabolism, depending on fatty acid chain length, by promoting fatty acid transport protein translocation, but also by altering gene expression

A novel finding is that in differentiated C2C12 cells the closely related GAP TBC1D4 also influences *in vitro* lipid metabolism. The model of *Tbc1d1*-deficient C2C12 myotubes that were used for *in vitro* palmitate uptake and oxidation studies could be re-established in the presented study, where a knockdown of *Tbc1d1* resulted in a similarly increased fatty acid uptake and oxidation. Here, it could be shown that silencing *Tbc1d4* had similar increasing effects in both, lipid uptake and lipid oxidation as it was reported for *Tbc1d1*-deficiency. This finding is interesting, as it is in accordance with the proposed complementary role of both proteins that

has been reported in the context of GLUT4 vesicle translocation before (Chen et al., 2008). A more recent study found similar effects for *Tbc1d4*-deficiency in the rat L6 myocyte cell line (Miklosz et al., 2016). A study performed in our working group investigated the effect of genetic knockouts of *Tbc1d1*, *Tbc1d4* and both GAPs on the *ex vivo* fatty acid oxidation of different mouse skeletal muscles. It became evident that in the glycolytic *EDL* muscle a lack of either TBC1D1, TBC1D4 or both proteins in parallel resulted in a significantly increased basal palmitate oxidation, while in the oxidative *Soleus* muscle only the D4KO led to an increase in lipid oxidation (Chadt et al., 2015). These results and the results generated during the presented study in C2C12 myotubes are in accordance with published data on C2C12 cells. For this muscle model cell line it was found that these cells predominantly express glycolytic fibers (Meissner et al., 2007). It seems that especially in glycolytic muscles TBC1D1 and TBC1D4 play comparable roles, while oxidative fibers might be more dependent on TBC1D4, as shown in *ex vivo* assays (Chadt et al., 2015).

The present study is the first one to date that links TBC1D4 in addition to TBC1D1 to alterations on *in vitro* C2C12 myotube fatty acid utilization. Here, it could be shown that the effect of silencing *Tbc1d1* and *Tbc1d4* mRNA expression with regard to increasing C2C12 myotube fatty acid uptake strongly depends on the chain length of the fatty acid administered to the cells. On the one hand this illustrates that the D1 and D4 impact on muscle cell lipid utilization depends on the chain-length of the fatty acid, and on the other hand it shows, that the degree of saturation among the long-chain fatty acids seems to be irrelevant for the impact of TBC1D1 and TBC1D4. Mechanistically, this leads to the conclusion that TBC1D1 and TBC1D4 mediate their influence upon lipid uptake by regulating the translocation of fatty acid transport proteins, similar to the translocation of GLUT4. This hypothesis is supported by the finding of Samovski et al. who showed a direct connection of the RabGAP TBC1D4 with the cell surface content of CD36 in cardiomyocytes (Samovski et al., 2012). When the uptake of fatty acids is studied in experimental approaches long-chain fatty acids, especially palmitic acid (C16:0), are commonly used as lipid substrates (Chadt et al., 2008; Son et al., 2018; Stanford et al., 2018). This is also the case in most experiments of the presented study. It has been proposed that approximately 90 % of cellular long-chain fatty acid uptake is facilitated by certain protein-mediated transport processes (Stahl et al., 2002). The proteins that are involved in skeletal muscle fatty acid uptake have been characterized in the past extensively. CD36, FATP1 and FATP4 were found to facilitate skeletal muscle long-chain fatty acid uptake (Bandyopadhyay et al., 2006; Bonen et al., 1999; Febbraio et al., 1999; Kiens et al., 2004). For short-chain fatty acids not very much is known about the uptake into skeletal muscle cells. Literature describes proteins of the monocarboxylate transporter (MCT) family to be involved in brain and intestinal uptake of short-chain fatty acids (Moschen et al., 2012; Van Rymenant et al., 2017). However, no distinct transporter for short-chain fatty acids was found so far in skeletal muscle cells. It was

only reported that CD36 exclusively transports long-chain fatty acids, but does not bind short-chain fatty acids (J. F. Glatz et al., 2010).

Nevertheless, beyond governing the ongoing of intracellular transportation events, it is also possible that, as a secondary event, increased lipid uptake could influence gene expression. It was found in the present study that the mRNA expression of *Pdk4* was significantly higher in C2C12 myotubes with *Tbc1d1*-deficiency. To further explain how TBC1D1 influences fatty acid oxidation, the expression of selected mitochondrial genes encoding for lipid metabolism-relevant proteins was compared in control and *Tbc1d1*-deficient C2C12 muscle cells. Further, in the present study it could be shown that PDK4 protein abundance was significantly higher in isolated *EDL* muscles from fasted D1KO mice compared to wildtype littermates. This increase in PDK4 protein expression was found to be independent of challenging the muscles *ex vivo* with palmitate. Instead, it exclusively occurred after starvation. Besides candidates that are part of lipid catabolism, expressional changes were also observed for *Cd36* and *Fatp4*. Only for *Cd36* a significant increase in mRNA after knockdown of *Tbc1d1* was found. However, CD36 protein expression was not altered by starvation or palmitate incubation and remained on the same level as the respective wildtype control. Several studies stress the important role of CD36 in muscle lipid uptake (J. F. C. Glatz & Luiken, 2018; Silverstein & Febbraio, 2009). However, it was published that *Cd36* expression levels are higher in muscles rich of oxidative red fibers and consequently rather low in glycolytic muscles (Bonon et al., 1998). Facing the fact that C2C12 myocytes mainly contain glycolytic fibers (Meissner et al., 2007) and since the gene expression of other muscle fatty acid transport proteins and binding proteins (*Fatp1*, *Fatp4*, *Fabp3*, *Fabp4*) was not altered by knocking down *Tbc1d1*, it remains unclear to what extent CD36 contributes to fatty acid metabolism in this particular *in vitro* cell culture model. In contrast, CD36 protein levels were not altered in *ex vivo* *EDL* muscle samples of D1KO mice compared to wildtype control muscles. Other expression data in the present study suggested that in skeletal muscle FATP4 might potentially be another important facilitator of lipid supply. Expression analysis revealed that *Fatp4* expression was not affected in C2C12 cells on mRNA level. The present study also revealed that D1KO muscles expressed significantly higher protein levels of FATP4. This effect was only visible in the samples from mice that were starved for 16 h, but neither in the random fed, nor in the muscles from mice that were refed for 4 h after 16 h of fasting, similar to the protein expression results of PDK4.

PDK4 is widely expressed in metabolically relevant tissues and is the most abundant PDK isoform in glycolytic and oxidative skeletal muscles in humans and rodents (Holness & Sugden, 2003). *Pdk4* expression is a complex and highly regulated process that involves multiple transcription factors and molecules with the ability to enhance or inhibit the *Pdk4* promoter (Connaughton et al., 2010). This is of importance because PDK4 is a central regulator of cellular carbohydrate metabolism. It was reported that, besides other factors, the expression is regulated by Type 2 *Diabetes mellitus*, fasting, and other conditions that may promote switching

the energy substrate (Connaughton et al., 2010; Feige & Auwerx, 2007). It was found that PDK4 is a central mediator of metabolic flexibility in skeletal muscle cells (S. Zhang et al., 2014). Liu and colleagues further reported that *Pdk4* knockdown led to a switch in human trophoblast carbohydrate metabolism from glycolysis towards oxidative phosphorylation (OXPHOS) (Liu et al., 2017).

During the early characterization of *Tbc1d1*-deficient mice it has already been described that the knockout mice show a reduction in insulin-stimulated glucose uptake, and an increased lipid uptake and oxidation already under basal conditions (Chadt et al., 2008). Based on the present data it seems that *Tbc1d1*-deficiency causes an induction of PDK4 protein expression and *Pdk4* gene expression. This dataset is the first scientific link of TBC1D1 and FATP4 on protein level. The question how TBC1D1 causes increased FATP4 expression remains unclear, because so far a direct regulatory function of the GAP was not described. However, there needs to be a mechanism with the aim to influence skeletal muscle lipid uptake without involving CD36. Summermatter and colleagues stated that the protein expression of several fatty acid uptake facilitators (CD36, FATP4) strongly corresponds to the mRNA expression levels of *Ppargc1a* (encoding for PGC1 α) (Summermatter et al., 2010). *Ppargc1a* was not differentially expressed between control and *Tbc1d1*-deficient C2C12 cells. Also further studies could focus on the role of FATP1 in this context. Due to the lack of a working commercially available FATP1 antibody, no data on the expression of this particular protein in skeletal muscle tissue could be produced in the present study. Interestingly, Miklosz and colleagues found in rat L6 myotubes that silencing *Tbc1d4* increased the expression of CD36, FATP1 and FATP4 on protein level (Miklosz et al., 2017; Miklosz et al., 2016). It could be speculated that the physiological influence of a lack of *Tbc1d1* to shift metabolism from glucose towards fatty acid utilization might be rather a preventive step of the muscle tissue as a consequence of increased lipid influx then a direct gene expression regulation mechanism. It may be that the increased influx of lipids results in an increase of lipid oxidation. This could be a strategy to prevent lipid accumulation and lipotoxic disturbances of muscle integrity. This explanation seems favorable since *Tbc1d1*-deficient muscles in the present study show no signs of lipid accumulation or huge changes with regard to mitochondria. Supplementary data from Chadt et al. reveal that a RabGAP-deficiency did not alter mitochondrial copy number or citric synthase activity compared to wildtype mouse muscles (Chadt et al., 2015). None of the measured mitochondrial genes in the present study, except *Pdk4*, was differentially expressed. Maher and colleagues reported decreased fatty acid oxidation and decreased β -HAD (*Hadh*) activity in skeletal muscles overexpressing *Tbc1d1*. They further speculate that the reduced enzyme activity might derive from reduced protein levels of β -HAD, but may also have different reasons (Maher et al., 2014). Under *Tbc1d1*-deficient conditions the mRNA expression level of *Hadh* was not affected. The β -HAD protein expression was not assessed in the present study. However, it remains questionable to what extend the statement of Maher et al. that *Tbc1d1* overexpression alters β -

HAD protein levels which finally causes a reduction in total enzyme activity due to a sheer difference in the amount of the protein can serve as the final explanation. Since the enzyme content in the present study seems not to be affected by manipulating the amount of muscle cell *Tbc1d1*, it may be possible that TBC1D1 affects enzyme activity rather than expression. This also argues towards the direction that the increases in PDK4 protein and gene expression may rather be indirect consequences of an increased fatty acid flux, than direct consequences of gene expression regulation. Interestingly, the difference in glycolytic *EDL* muscle PDK4 expression only became significant after 16 h of fasting the mice prior to muscle dissection. It could be possible that glucose became depleted during fasting which created a state of demanding an alternative energy source. Thus, PDK4 expression may have been promoted, which then led to the inhibition of the pyruvate dehydrogenase complex and a subsequent shift towards lipid fuel substrates. Indeed, fasting was described as one of the triggers of PDK4 induction (Connaughton et al., 2010; Feige & Auwerx, 2007). At least in the context of TBC1D1, fasting alone may not be sufficient to explain rising PDK4 protein and *Pdk4* mRNA levels, because results from unfasted C2C12 myotubes deficient for *Tbc1d1* showed that even without starvation the mRNA expression of *Pdk4* was increased compared to control cells. To find a more comprehensive answer, further studies could focus on the interplay of *Pdk4* and *Tbc1d1* by introducing the PDK4 inhibitor DCA (dichloroacetate) (H. Park & Jeoung, 2016) into the experimental setups to elucidate if the mentioned effects of the GAP in muscle cells are still present when PDK4 activity is blocked.

To date no published study could show that TBC1D1 might act as a direct regulator of gene and protein expression. To explain the effect of TBC1D1 on the regulation of gene and protein expression in skeletal muscle cells a few mechanisms may be considered. These potential mechanisms point towards a rather indirect role of TBC1D1. A phenomenon known as metabolic reprogramming was described to take place upon an increase in intracellular lipid content and involves transcription factors from the PPAR family and PGC1 α (Muoio & Koves, 2007). Varga et al. describe the members of the PPAR transcription factor family as specifically regulated by lipids that control lipid metabolism (Varga et al., 2011). Al-Khami and colleagues report that the uptake of exogenous lipids into myeloid-derived suppressor cells induces a drastic functional and metabolic reprogramming of the cells which results in the induction of lipid binding and transport proteins (e.g. CD36) and a further increased lipid uptake (Al-Khami et al., 2017). In the context of muscle cells it was found that physiological stimulation by endurance training caused upregulation of several genes involved in myocellular lipid metabolism in human *tibialis anterior* (Schmitt et al., 2003). Furuyama and colleagues could show that one of the transcription factors that regulates the expression of PDK4 is FOXO1. They state that FOXO1 induces PDK4 in skeletal muscle during starvation (Furuyama et al., 2003). This is the physiological reaction to switch energy metabolism from glucose towards lipid catabolism. These observations fit in part to the results that were obtained as presented here. An increase

of PDK4 in wildtype and *Tbc1d1*-deficient mouse muscles was observed only in starved mice. However, since the induction of PDK4 protein expression was smaller in wildtype littermate control animals, it may only be a part of the explanation of the regulatory function of TBC1D1. The increase in fatty acid uptake could be another reason for observing changes in gene and protein expression upon *Tbc1d1*-deficiency. As Varga et al. state, PPAR family transcription factors are inducible by fatty acids (Varga et al., 2011). Amongst other factors PPAR α was described to induce transcription of PDK4 (Pilegaard & Neufer, 2004), PPAR γ can induce FATP4 transcription via NEFA-inducible transcription factor (Schaiff et al., 2005). Thus, it could be assumed that with the increase in fatty acid uptake into the muscle cells upon a lack of the RabGAP a brief accumulation of lipids within the cell occurs that induces upregulation of genes that are involved in lipid handling and lipid degradation. Houten et al. reported that a synergistic interplay of AMPK and fatty acids is responsible for the induction of PDK4 expression in skeletal muscles (Houten et al., 2009). A study from Armoni et al. provides a link of regulatory free fatty acids and the repression of gene and protein expression in cardiac muscle cells (Armoni et al., 2005). This finding is interesting in the field of TBC1D1 research, because it was published that *RabGAP*-deficient mice exhibited reduced levels of GLUT4 protein in their skeletal muscles, while they switched their metabolism towards uptake and oxidation of fatty acids (Chadt et al., 2015). Based on the Armoni study, it could be speculated that the fatty acids are responsible for a degradation of GLUT4 in muscles lacking functional TBC1D1. However, this hypothesis needs to be further validated. Hence, the reduction of GLUT4 may be counteracted by increasing FATP4 to ensure a sufficient supply of the muscle cells with energy substrates. The data from Armoni and colleagues however stress the assumption that the RabGAP effect on gene expression is rather indirect by promoting increased lipid uptake in the first place which then may result in altered gene expression by inducing several FA-responsive transcriptional regulators.

5.2 *Tbc1d1*-deficiency has an influence on skeletal muscle cell lipid composition, lipid processing, but not lipid storage and the content of the AMPK-malonyl-CoA signaling axis for β -oxidation

Since the fate of lipids that are taken up by skeletal muscle cells remained unknown a qRT-PCR screening approach was conducted to search for candidate genes involved in lipid storage, degradation and procession that may be differentially expressed under *Tbc1d1*-deficient conditions. Additionally, a comparative GC determination of the fatty acid content and composition of *Gastrocnemius* muscles from C57BL/6J wildtype control mice and D1KO mice was performed.

Based on the fact that skeletal muscle cells deficient for *Tbc1d1* display a markedly increased uptake of long-chain fatty acids *in vitro* and *ex vivo* it could have been assumed that an increase in intracellular lipids might lead to a chronically increased lipid content of these muscles. However, the data from the GC fatty acid profiling of WT and D1KO *Gastrocnemius* muscles reveal that the total amount of fatty acids measured in this approach did not differ between the investigated genotypes. This finding is supported by the results of Chadt and colleagues who found that plasma triglycerides and plasma NEFA levels were unaffected by a lack of TBC1D1 (Chadt et al., 2015). Although these data summarize findings with regard to circulating lipids, they may reflect the situation within the skeletal muscles because the mice lacking *Tbc1d1* not only display elevated lipid uptake levels in isolated skeletal muscles, but they also show an increased whole-body lipid metabolism (Chadt et al., 2015; Chadt et al., 2008). The finding of a comparable intramyocellular lipid content is promoted further by the results obtained in the C2C12 myotube expression screening of *non-target* control siRNA-transfected (*siNT*) and *siTbc1d1*-transfected cells. The qRT-PCR results revealed that genes encoding for fat storage-inducing transmembrane proteins (*Fitm1*, *Fitm2*), diacylglycerol transferases (*Dgat1*, *Dgat2*), which are associated with lipid droplet formation (Markgraf et al., 2016) and perilipins (*Plin2*, *Plin3*), that were associated with lipid droplet formation, coating and storage were not differentially expressed between *non-target* siRNA control transfected and *siTbc1d1* transfected C2C12 cells. Also, the expression of hormone-sensitive lipase (*Lipe*) and lipoprotein lipase (*Lpl*), two genes involved in triglyceride breakdown and triglyceride generation were not affected by knocking down *Tbc1d1*. Although the fatty acid profiling showed that the measured total fatty acid content did not differ between the WT and D1KO samples, the distribution of fatty acid species was significantly different. It was found that muscles lacking *Tbc1d1* contain less palmitic acid (C16:0) and arachidonic acid (C20:4), while they seem to have increased levels of mono-unsaturated fatty acids palmitoleic acid (C16:1) and oleic acid (C18:1) in comparison with WT control muscles. Interestingly, it was published that palmitoleic acid is involved in counteracting the p38 MAP kinase-mediated skeletal muscle insulin resistance (Talbot et al., 2014). Other studies describe beneficial effects of dietary palmitoleic acid or palmitoleic acid released by adipose tissue on skeletal muscle insulin sensitivity of obese and diabetic mice, as well as increased glucose uptake and oxidation in both *in vitro* and *ex vivo* studies in mice (Dimopoulos et al., 2006; Guo et al., 2012; Souza et al., 2014; Yang et al., 2011). For oleic acid it was published that it prevents saturated fatty acid-induced skeletal muscle insulin-resistance and ER stress (Alkhateeb & Qnais, 2017; Salvado et al., 2013). Lim and colleagues could link oleic acid to the induction of fatty acid oxidation in C2C12 myotubes through a protein kinase A-dependent activation of a sirtuin1-PGC1 α complex (Lim et al., 2013). In this study, however, it was found that, at least on mRNA level, no differences occurred in the expression of PGC1 α (*Ppargc1a*) or muscle-relevant sirtuins (*Sirt1*, *Sirt2*, *Sirt3*) between control and *Tbc1d1*-deficient C2C12 myotubes. To what extent changes in the amount of palmitoleic and oleic acid can be explained as compensatory mechanism to compensate for the disturbed

insulin response of the deficient muscles remains unclear. However, in the context of a whole-body switch from carbohydrate metabolism towards lipid utilization, this explanation seems to be rather unlikely.

The presented study found that absence of TBC1D1 resulted in a decreased calculated $\Delta 5$ -desaturase activity, while the mRNA expression of the corresponding gene (*Fads1*) was unchanged. The knockout mice show significantly reduced levels of the PUFA arachidonic acid (AA) which may be attributed to the fact that $\Delta 5$ -desaturase activity was lower in these mice compared to wildtype littermates. Literature associates an increased plasma occurrence of arachidonic acid due to an increased $\Delta 5$ -desaturase activity with Type 2 *Diabetes mellitus* (Imamura et al., 2014). If this is true, this would be in line with the non-diabetic characteristics of D1KO mice that were shown to respond normally during glucose and insulin tolerance tests, although isolated *EDL* muscles from these knockout mice displayed an absence of insulin-stimulated glucose uptake, a reduced GLUT4 protein expression and a reduced GLUT4 cell surface content upon insulin stimulation (Chadt et al., 2015). The plasma fatty acid composition of wildtype and *Tbc1d1*-deficient mice was not measured in the present study, but could add more information on the influence of the RabGAP on circulating lipids. Beyond this, the activities of $\Delta 9$ -desaturases could also be shown to be different between the investigated genotypes. It was assessed that the activities of $\Delta 9$ -desaturases responsible for the conversion of palmitic acid (C16:0) to palmitoleic acid (C16:1) and for converting stearic acid (C18:0) into oleic acid (C18:1) seem to be elevated in *Gastrocnemius* muscles from *Tbc1d1*-deficient mice compared to wildtype littermates. Other differences between wildtype and D1KO animals could be found for thioesterase activity and the calculated *de novo* lipogenesis. Skeletal muscles have the ability to perform lipogenesis (Funai et al., 2013). As part of the cellular fatty acid synthase (FAS) complex, thioesterases are responsible for terminating the synthesis reaction and releasing the fatty acid (Del Puerto et al., 2017). The fatty acid profiling showed that muscles deficient for *Tbc1d1* have a lower thioesterase activity than wildtype control muscles. Similarly, the calculated *de novo* lipogenesis was also lower in these muscles. The results presented in this paragraph indicate that TBC1D1 may participate in the regulation of enzymes involved in fatty acid degradation and fatty acid conversion. Although little is known about how TBC1D1 may regulate enzyme activities, a study from Maher et al. demonstrated that overexpressing the RabGAP in mouse *Soleus* muscles reduced the oxidation of palmitic acid by inhibiting the activity of the mitochondrial β -oxidation enzyme β -hydroxyacyl-CoA dehydrogenase (β -HAD) (Maher et al., 2014). Decreased thioesterase and lipogenesis indexes support the assumption that *RabGAP*-deficiency rather promotes fatty acid catabolism, than synthesizing or accumulating fatty acids. Dokas et al. reported that *Tbc1d1*-deficiency even protects from obesity in a *leptin*-deficient mouse model (Dokas et al., 2016). This further points towards a catabolic instead of a storage phenotype mediated by TBC1D1.

Based on these indications it may be postulated that the fatty acids that are taken up by skeletal muscles from D1KO mice are not stored in intracellular lipid droplets but may be metabolized directly. This is supported by the finding of the present work and other studies that *Tbc1d1*-deficiency also causes increased lipid oxidation and energy expenditure (Dokas et al., 2016; Hargett et al., 2015). None of the published studies links the *Tbc1d1*-deficiency-derived lipid uptake to changes in intracellular lipid content. Further investigations may be needed to address the question how exactly TBC1D1 affects the activities of enzymes involved in fatty acid promotion and degradation to explain the differences found in the fatty acid profiling. Moreover, upcoming experiments could examine the role of TBC1D4 on the fatty acid profile of skeletal muscle and plasma.

At least in the context of TBC1D1 the AMPK-malonyl-CoA signaling axis may be less important. Malonyl-CoA is a crucial inhibitor of CPT1, a key enzyme shuttling activated acyl-CoA long-chain fatty acids into mitochondria (Saha et al., 1997; Schmidt & Herpin, 1998). Beyond, the levels of malonyl-CoA and acetyl-CoA did not differ between WT and D1KO *Gastrocnemius* muscles under basal and AICAR-stimulated conditions. One possible explanation for the observed effects of *Tbc1d1* could have been differences in cellular malonyl-CoA levels. One could have expected that the increased fatty acid oxidation of muscle cells deficient for *Tbc1d1* might have been a direct consequence of decreased levels of malonyl-CoA. On the other hand it could have been speculated about the levels of acetyl-CoA, a molecule from which malonyl-CoA can be synthesized by acyl-CoA carboxylase (ACC), or be converted into by malonyl-CoA decarboxylase (MCD) (Abu-Elheiga et al., 2001; van Weeghel et al., 2018). If TBC1D1 mediated its influence on lipid catabolism on the level of mitochondrial β -oxidation via regulating long-chain fatty acid shuttling into mitochondria then decreased levels of malonyl-CoA would have been measured in *Tbc1d1*-deficient muscles, while acetyl-CoA levels could have been elevated. Nevertheless, even stimulating the mice with AICAR before muscle dissection did not affect levels of both substances in the knockout mice. AICAR acts via the AMPK signaling cascade as an inhibitor of ACC by phosphorylating it, which ultimately leads to a decrease in malonyl-CoA levels (Scudiero et al., 2016; Thomson & Winder, 2009). These results stress the hypothesis that TBC1D1 may not directly act on mitochondrial fatty acid uptake via CPT1, but might rather regulate related mitochondrial enzyme activities and general cellular lipid uptake. To complete the image of the ACC-malonyl-CoA lipid oxidation axis, further studies could investigate if *Tbc1d1*-scarcity changes the phosphorylation pattern of skeletal muscle ACC.

5.3 Small Rab GTPases as direct downstream targets of TBC1D1 and TBC1D4 have a direct impact on skeletal muscle cell fatty acid metabolism

In the present study, it was found that the RABs described to regulate GLUT4 translocation also seem to be involved in regulating the uptake of fatty acids into muscle cells. Several Rab proteins have been shown to be *in vitro* substrates of TBC1D1 and TBC1D4 (Miinea et al., 2005; Roach et al., 2007). Of these, especially RAB8a, RAB10, RAB14 and RAB28 were of interest because these have been shown in several studies to participate in cell surface recruitment of GLUT4 (Brewer et al., 2016; Bruno et al., 2016; Ishikura et al., 2007; Z. Li et al., 2017; Sano et al., 2008; Sun et al., 2014; Zhou et al., 2017). Here, it was found that reducing the expression of RAB8a, RAB8b, RAB10, RAB14 and RAB40b in differentiating C2C12 myotubes led to significant reductions of palmitic acid separate from each other.

It is likely that more than the well-described RABs that were shown to regulate GLUT4 translocation in literature and in the present study to be involved in cellular fatty acid uptake since intracellular transportation processes are complex and of importance for cell survival and development. Thus, it was not surprising that novel Rab GTPases, which participate in C2C12 myotube lipid uptake could be identified in this study. RAB8b and RAB40b were shown to be *in vitro* substrates of TBC1D1 in in-house screenings and other studies (Roach et al., 2007). RAB8b, a close relative of the well-known RAB8a, was published to be associated with several secretion and recycling events in different cell types, such as the transport of particles from the West Nile virus from recycling endosomes (Kobayashi et al., 2016), apical transport in ciliated cells (Sato et al., 2014), calveolar endocytosis (Demir et al., 2013), or the regulation of secretory processes in pituitary gland tumor cells (Chen et al., 2001). So far, no data are available with regard to (muscle) cell energy metabolism and energy substrate uptake. Regarding the function of RAB40b, only little is found in literature. So far, it was attributed to participate in cancer cell invasion and metastasis (Jacob et al., 2013; Jacob et al., 2016; Li et al., 2015). Similarly to RAB8b, no data are available linking RAB40b to (myo)cellular energy and lipid substrate metabolism.

Ex vivo, whole *EDL* and *Soleus* muscles transfected with siRNA oligonucleotides targeting the expression of *Rab8a* and *Rab10* showed in part different results. For *Rab8a*-deficiency, it was found that in oxidative *Soleus*, but not in glycolytic *EDL* knocking down *Rab8a* expression significantly reduced *ex vivo* palmitic acid oxidation. For *Rab10* no differences in palmitic acid oxidation were found after knockdown of the Rab GTPase. These findings are interesting, as it has been shown for RABs 8a, 10 and 14 that they also are associated with GLUT4 translocation. Moreover, it was reported that lipid uptake facilitating proteins such as CD36, FATP1 and FATP4 are translocated in a comparable fashion as shown for GLUT4 (J. F. Glatz et al., 2016; Luiken et al., 2003). If this is the case, the intracellular movement of vesicles

containing either one of the lipid transporters also needs to be tightly regulated by Rab GTPases. Samovski et al. could show a first link of RAB protein action and fatty acid transporter translocation. They claimed that RAB8a is involved in cardiomyocyte surface recruitment of CD36 (Samovski et al., 2012). Around 60-70 different Rab GTPases have been identified in mammalian organisms (Kiral et al., 2018; Shi et al., 2017). Knowing that, it is logically consistent to assume that one cellular RAB protein has to fulfil multiple functions as there are more than 60-70 distinct trafficking steps occurring in a single cell, that all need to be coordinated. However, it remains unclear why RABs that regulate GLUT4 trafficking also participate in regulating long-chain fatty acid uptake. An additive experiment in which the three most prominent RAB protein were co-silenced revealed that silencing RAB8a, RAB10 and RAB14 in parallel did not have an additive effect on C2C12 cell fatty acid uptake. An interpretation of these findings could be that every RAB regulates only a part of the way of a transporter-containing vesicles. These consecutive steps between which the vesicles are handed over from one RAB to the other seem to depend on each other. Any disturbance at any stage of the translocation path will result in a reduction in the cell surface transporter content that eventually leads to a decrease in cellular fatty acid uptake. Studies in neurons showing the interplay of different Rab GTPases during ESCRT pathways, as well as other studies support this theory (Hutagalung & Novick, 2011; Sheehan et al., 2016). Thus, the presented non-additive effect of silencing several RAB candidates in parallel that resulted in effect sizes comparable to single RAB manipulations could be explained in a similar way as the ESCRT pathway paper showed. It seems to be the case that one missing candidate RAB in a chain of consecutively acting proteins that may mediate the different steps of cellular vesicle trafficking is sufficient to disturb prosecution of vesicle movement. It is then possible that vesicles cannot be passed from one RAB to the other, which would ultimately result in a lack of vesicles that may be preceded by following RABs. As a consequence a simultaneous reduction of the expression of several RAB proteins involved in lipid transporter vesicle translocation would not add effect size to the *in vitro* lipid uptake because at least some of the RAB proteins may act after each other at different points of intracellular vesicle movement and rather not in parallel. Thus, it could be concluded that the first reduced RAB in the transportation chain may already be determinant for the effect size.

Another interesting finding is, that *ex vivo* data presented in this study that were generated after silencing *Rab8a* and *Rab10* *in vivo* were divergent from the cell culture data. The differences between the results obtained for the effect of *Rab8a* and *Rab10* silencing *in vitro* in C2C12 myotubes and *ex vivo* in *EDL* and *Soleus* muscle in terms of fatty acid metabolism need to be discussed as well. Silencing of *Rab8a* and *Rab10* in C2C12 myotubes caused a significant reduction in palmitic acid uptake. Silencing *Rab10* via *in vivo* electrotransfection (IVE) had no impact on *ex vivo* lipid oxidation. However, IVE-mediated *Rab8a* silencing caused a reduced fatty acid oxidation only in the *Soleus* muscles. One explanation may be that *Soleus* as

an oxidative muscle strongly depends on a constant supply with fatty acids. If RAB8a might be involved in the regulation of translocation of several of the expressed fatty acid transporter proteins it could be that a reduced uptake in *Rab8a*-deficient *Soleus* muscles may consequently result in a reduced lipid oxidation. Alternatively, one publication revealed that in liver a regulatory network of RAB8a and TBC1D4, together with other factors, controls lipid droplet formation (L. Wu et al., 2014). Further studies could investigate if *Rab8a*-deficient skeletal muscles may also exhibit improper lipid storage in addition to disturbed uptake of lipids, which may cause a reduced availability of lipids for mitochondrial fatty acid oxidation and a reduction in fatty acid catabolism. The IVE method needs particular revision. For the present study the IVE was conducted in a minimal-invasive way (see 3.2.1.1). Saline containing a siRNA-oligonucleotide dilution was injected through the skin and the connective tissue in regions of the hind limbs of mice to most likely target the *EDL* and *Soleus* muscles. On the one hand, this way of administering the siRNA is less wearing for the animals as they do not have to recover from a surgery that lays open the muscle to have access for a direct injection into the muscle. On the other hand the experimenter can only carefully guess where to inject the siRNA. This will affect transfection efficiency. Efficiency is further affected by the sheer size and three-dimensional structure of the muscle. A homogenous distribution of the oligonucleotide solution is almost impossible to achieve. This leads then to a rather poor overall knockdown efficiency. This is also the reason why for the *Rab10*-knockdown only an N of 3-4 could be used for the final analysis, because only this low number of muscles showed a minimum of 20 % reduction of RAB10 protein expression in the knockdown validation blot. The IVE technique offers great opportunities for manipulating gene expression *in vivo*. However, the method needs to be optimized to achieve better knockdown results and to reduce the number of animals necessary for statistical analysis.

The present study could show a direct responsiveness of RAB protein action to insulin stimulation. In independent experiments it could be shown that insulin caused a 20 % increase in fatty acid uptake compared to control cells. Cells that underwent *Rab*-targeted siRNA transfection showed for all three investigated Rab GTPases *Rab8a*, *Rab10* and *Rab14* a significantly increased basal to insulin-stimulated palmitic acid uptake. The strength of the increase was comparable for all three tested RAB proteins. However, among the insulin-stimulated cells the pattern of decreased fatty acid uptake, which was observed under basal conditions after silencing, was similar. The idea of hormone-regulated translocation events is an interesting link between the actions of RAB proteins and the physiologically regulated recruitment of lipid transport proteins. Andreas Stahl and colleagues described that fatty acid transport proteins FATP1 and FATP4 are being translocated from intracellular storage compartments to the cell surface upon insulin stimulation in adipocytes (Stahl et al., 2002). In the same year, Luiken et al. published that insulin also triggers translocation of CD36 towards the cell surface in murine skeletal muscles, as well as a redistribution of CD36 in murine

cardiomyocytes. In their study, where a total hind-limb perfusion was performed, the authors found an approximately 50 % increase in surface CD36 content (Luiken, Dyck, et al., 2002; Luiken, Koonen, et al., 2002). It is assumed that the action of insulin on lipid uptake is conducted via an increase in the translocation of fatty acid transport proteins, such as CD36, and members of the FATP family, FATP1 and FATP4 (J. F. Glatz et al., 2002; Luiken, Dyck, et al., 2002; Luiken, Koonen, et al., 2002; Samovski et al., 2012; Stahl et al., 2002). Samovski et al. could link the action of the RabGAP TBC1D4 and RAB8a to insulin-stimulated cell surface recruitment of CD36 in cardiomyocytes (Samovski et al., 2012). Thus, it is possible that also in the skeletal muscle Rab GTPases participate in the stimulus-mediated shuttling of fatty acid uptake facilitators between the cell surface and intracellular storage sites. For the three most prominent RAB proteins with established associations to GLUT4 translocation in muscle and adipose tissue, RAB8a, RAB10 and RAB14 (Ishikura et al., 2007; Sano et al., 2008). This illustrates the influence of insulin on RAB protein-mediated regulation of muscle cell lipid supply. Further, it points to the potential involvement of translocated fatty acid uptake facilitators and their enrichment at the cell surface upon insulin stimulation. Further experiments could focus on the impact of RAB proteins in combination with physiological stimuli, such as insulin or AICAR, to visualize a direct interaction of a RabGAP (TBC1D1, TBC1D4), a Rab GTPase and a candidate lipid transporter surface translocation, similar as done elsewhere (Samovski et al., 2012). This could directly link GAP action on its downstream Rab GTPase targets with a physiological response (regulated fatty acid uptake).

5.3.1 FATP4, rather than CD36 is mainly responsible for the observed lipid-preferring metabolic switch caused by *Tbc1d1*-deficiency in skeletal muscle

In order to elucidate which of the candidate fatty acid transporters that is expressed in skeletal muscle is/are responsible for the observation, that *Tbc1d1*- and *Tbc1d4*-deficiency causes increases in long-chain fatty acid uptake, a series of *in vitro* and *ex vivo* experiments was conducted. The idea was to find candidates that may be regulated in their intracellular translocation by the RabGAPs and one or more of the Rab GTPases that were previously shown to influence muscle cell lipid uptake.

Besides the mouse models deficient for *Tbc1d1* (D1KO) and *Tbc1d4* (D4KO), a mouse line deficient for *Cd36* was available as well. Crossbreeding these animals with each other resulted in mouse strains double deficient for one of the GAPs and *Cd36* (double knockout), and mice lacking both GAPs and *Cd36* (triple knockout). These mice were utilized to assess *ex vivo* palmitic acid uptake. For the experiments the mice were fasted for 16 h prior to muscle dissection and *ex vivo* incubations. The single knockout animals gave results that meet the expectations of published literature (Chadt et al., 2015; Febbraio et al., 1999). As presented in

this study, *D1*- and *D4*- deficiency resulted in increased lipid uptake and oxidation *in vitro*. These uptake results could be recapitulated in *EDL* muscle *ex vivo* experiments. It was found that *D1KO* and *D4KO* *EDL* muscles took up significantly more palmitic acid compared with wildtype littermate control mice. In contrast, *CD36KO* mice showed a 21 % reduced fatty acid uptake compared with control *EDL*s. This result can also cope with literature. Bonen et al. measured a roughly 25 % reduced whole-hind limb FA uptake in *CD36KO* mice compared with control animals (Bonen et al., 2007). This finding also underlines that *CD36* may not be the only protein important for muscle lipid utilization, as a total knockout of this protein reduces the fatty acid uptake by only 25 %. The double knockout *EDL* muscles, that combined one of the *GAP* knockouts with a *CD36* knockout revealed results that were similar to the results obtained with the single *D1KO* and *D4KO*. Comparable results were seen with the triple *D1-D4-CD36*-deficient animals. All double- and triple-deficient genotypes showed an increased lipid uptake compared to control muscles. This in turn argues against an inimitably important role of the fatty acid translocase *CD36* in the *TBC1D1*- and *TBC1D4*-driven lipid uptake phenotype. At least in this particular animal models, which display an increased whole-body lipid metabolism (Dokas et al., 2013), as well as increased lipid catabolism in isolated skeletal muscles (Chadt et al., 2015), it may be possible to address the metabolic phenotype to other lipid uptake proteins than *CD36*.

In comparison with wildtype mice, *D1KO* and *D1-CD36KO* mice showed increased levels of fatty acid uptake into the oxidative *Soleus* muscle. Chadt et al. found that *Soleus* muscle only involves *TBC1D1* in regulating basal fatty acid oxidation. They describe a significant basal oxidative increase in *Soleus* from *D1KO* mice, but not from *D4KO* mice (Chadt et al., 2015). This effect was found in a comparable fashion for *ex vivo* fatty acid uptake. Similar to the published results for *ex vivo* lipid oxidation (Chadt et al., 2015), neither *Tbc1d4*-, nor *Tbc1d1-Tbc1d4-Cd36*-deficiency changed palmitate uptake in comparison with wildtype control *Soleus* muscles. Interestingly, in *Soleus Cd36*-deficiency did not alter fatty acid uptake. An explanation could be that *CD36* knockout mice increase the protein expression of *FATP1* and, even stronger, of *FATP4* (Bonen et al., 2007). This could be due to a compensatory mechanism. *Soleus* is a muscle consisting mainly of oxidative muscle fibers. As such, it preferentially uses fatty acids as source of energy. The lack of *CD36* in this muscle type could be compensated by increasing the expression of other muscle cell lipid uptake proteins, such as *FATP1* and *FATP4*. This may be necessary for this type of muscle to maintain the full capacity of energy metabolism. A reason why this is not seen in the *EDL* may be that *EDL* is a glycolytic muscle. Bonen et al. found that the white part of the *Gastrocnemius* muscle, consisting of similar glycolytic fibers as the *EDL*, did not show an induction of *FATP1* or *FATP4* protein expression (Bonen et al., 2007). Over all, the present data suggest that in the *Soleus* the *RabGAP* effect on fatty acid uptake is also not conceived by *CD36*, since the double knockout of *Tbc1d1* and *Cd36* did not diminish palmitic acid uptake.

To further clarify to what extent the most abundant fatty acid transport proteins in skeletal muscle, CD36, FATP1, FATP4 (Jain et al., 2015), contribute to fatty acid uptake into muscle cells, the expression of *Cd36*, *Fatp1* and *Fatp4* was reduced by siRNA technology in C2C12 myotubes to assess the individual influence on FA uptake. It could be shown that *Cd36* silencing reduced the C2C12 cell palmitic acid uptake rate by only 4 %. In contrast, knocking down *Fatp1* resulted in a decrease of FA uptake by 11 %, compared to *non-target* siRNA transfected reference cells. Only silencing *Fatp4* resulted in a statistically significant reduction of palmitate uptake of 13 %. Although the expression of *Cd36* mRNA could be shown to be increased with *Tbc1d1*-deficiency in C2C12 cells, the impression arises that CD36 alone certainly participates in skeletal muscle fatty acid uptake, but its role is only one among others. Hence, these *in vitro* data suggest that, at least in cell culture, FATP4 might be the lipid uptake facilitating protein with the largest impact. The reason to take a cell culture model for these investigations is of practical nature. The *Cd36*-deficient mouse model was available and used for other experiments in the present study. A *Fatp1* knockout mouse can be purchased but was not available for the present study due to time issues with quarantine and breeding (Kim et al., 2004). However, a whole-body knockout of *Fatp4* was shown to be embryonically lethal due to severe developmental dermopathy (Herrmann et al., 2005). Thus, it was a suitable option to conduct the experiments in C2C12 myotubes *in vitro*.

As discussed, CD36 seems not to be the fatty acid transport protein that is responsible for increased lipid uptake upon RabGAP knockout or knockdown. However, FATP4 gained interest as it could be shown in the present study to be probably the most important fatty acid uptake protein in cultured skeletal muscle cells and to be upregulated on protein level in D1KO *EDL* muscles. Thus, a first *in vitro* trial was conducted to reveal a potential connection of the RabGAPs TBC1D1 and TBC1D4 with FATP4. This study is the first to show that a double-deficiency of either *Tbc1d1-Fatp4*, or *Tbc1d4-Fatp4* had no influence on C2C12 myotube palmitate uptake, while the single *Tbc1d1*- and *Tbc1d4*-knockdowns resulted in significantly increased palmitate uptake. On the other hand, silencing *Fatp4* caused a reduction of lipid uptake into the muscle cells *in vitro*. The effect seen when silencing either one of the proteins seem to be abolished when the *GAPs* and *Fatp4* are reduced in the cells. This may indicate that both proteins depend on each other and conceive their action in a coordinated way. If the two proteins were independent from each other, results as achieved for *Cd36*- and *Tbc1d1*- or *Tbc1d4*-deficiency could have been expected. In the *ex vivo* FA uptake studies. *GAP-Cd36* double knockdowns resulted in an effect that was comparable to the effect achieved with *GAP* silencing alone. Because the results for *GAP-Fatp4* silencing look different a regulatory association of TBC1D1, TBC1D4 and FATP4 may exist. It could be speculated that the RabGAPs regulate the activity of Rab GTPases that may be involved in the translocation of FATP4-containing vesicles. These vesicles may fuse with the plasma membrane and increase the surface amount of FATP4. Consequently, FATP4 facilitates fatty acid uptake. Additionally,

as discussed previously, the GAPs may indirectly regulate the expression of FATP4 by already initially increasing the uptake of fatty acids which subsequently may lead to specific transcription factor activations to manifest the switch from glucose towards lipid metabolism on the molecular and protein level.

5.4 Conclusion and Outlook

In the present study, the role of the Rab GTPase-activating proteins TBC1D1 and TBC1D4 in skeletal muscle fatty acid metabolism was investigated. More in detail, research was conducted to clarify how the RabGAPs mediate their action, since information about this were only subject of a few publications. It could be shown that the effects on skeletal muscle metabolism deriving from manipulations of the TBC1D1 and TBC1D4 can be subdivided into a more indirect and a direct way of impact. In terms of direct actions of D1 and D4, it could be shown in this study, that deficiency of a number of RAB GTPases that have been shown to be *in vitro* substrates of TBC1D1 and TBC1D4 act negatively on fatty acid uptake in *in vitro* C2C12 myotubes, as well as in *ex vivo* mouse skeletal muscles. This part of RabGAP influencing skeletal muscle lipid homeostasis can be categorized as direct effect, because the key feature of GTPase activating proteins is to regulate the activity state of downstream target proteins such as RAB proteins. The Rab proteins are a huge family of proteins mediating intracellular vesicle trafficking. These events include translocation of vesicles harboring transport proteins relevant for cellular energy substrate uptake. The present study also asked the question which of the several skeletal muscle fatty acid transport facilitators may be of essential importance for mediating the observed GAP effect on fatty acid uptake. It could be shown that in contrast to several other studies that stressed the importance of CD36 as the major skeletal muscle fatty acid transporter, this protein seems not to be relevant in association with the observation that *Tbc1d1*- and *Tbc1d4*-deficiency causes a switch from glucose to lipid metabolism, accompanied by a significant increase in cellular lipid uptake. Evidence from the present study indicates that FATP4 is the fatty acid transporter that is mainly responsible for this effect. Moreover, the present study is the first to demonstrate a potential connection of TBC1D1, or TBC1D4 with FATP4, at least *in vitro*. Another novelty is the finding that the GAP-deficiency effect seems to exclusively be restricted to the transporter-associated uptake of long-chain fatty acids.

As indirect effects of *RabGAP*-deficiency, first of all the increased lipid uptake should be taken into account. Studies reported that fatty acids have the potential to induce certain transcription factors that in turn trigger gene expression. In particular, this study could show that the mRNA and protein expression of PDK4 were strongly increased in *Tbc1d1*-deficient cells and mice. PDK4 is a master regulator of cellular fuel selection. Its induction causes a shift from glucose to lipid metabolism, e.g. in muscle cells. A direct impact of TBC1D1 or TBC1D4 on gene expression is unknown. The finding argues for a rather indirect effect as fuel selection is

an essential part of metabolic flexibility and thus may be a consequence of increased lipid availability upon an increased lipid uptake. From this point of view, the increased skeletal muscle lipid oxidation also seems to be rather a secondary effect of a higher fatty acid availability. However, in this context it was reported previously that TBC1D1 has the ability to influence mitochondrial β -HAD activity, which in turn causes alterations in lipid oxidation. Findings from the present study support the assumption that enzyme activity may depend on GAPs. A fatty acid profiling revealed that the composition of lipids in muscles from D1KO mice differs from the one of wildtype littermates, while the total fatty acid content of the genetically different muscles is the same. Theoretical calculations based on the composition showed that several cellular enzymes differed in relation to their activity between the two groups of animals.

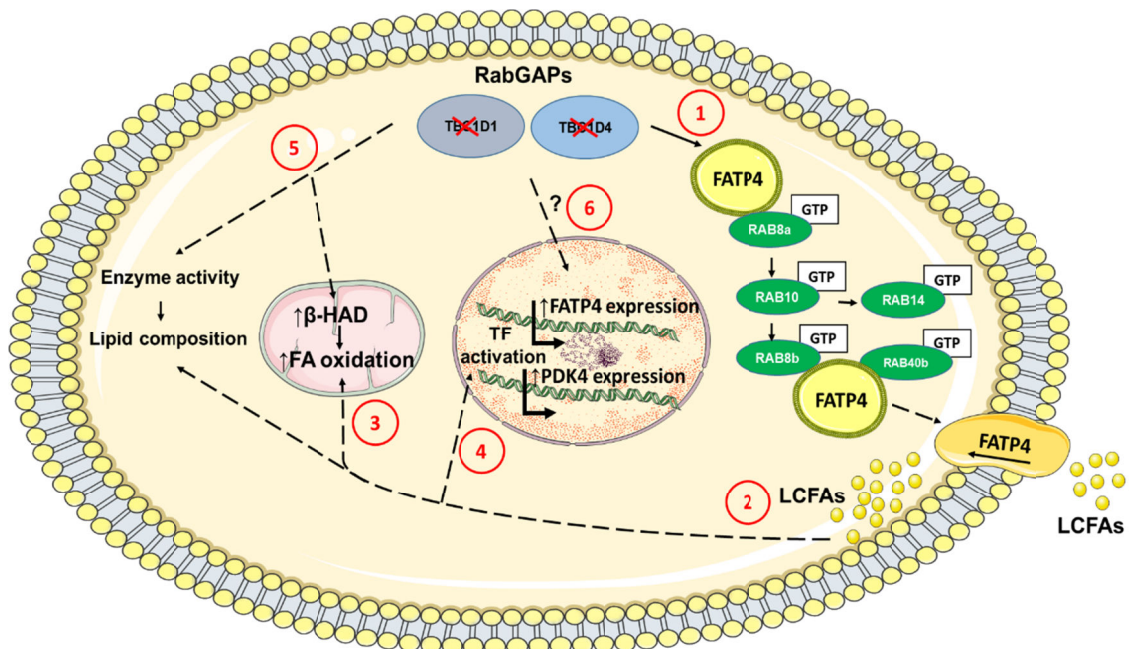


Figure 41: Summary of the action of *RabGAP*-deficiency on lipid metabolism of skeletal muscle cells. Concluding the presented results, TBC1D1 and TBC1D4 mediate their action via both, direct and indirect mechanisms. Muscle cells deficient for one of the RabGAPs may exhibit an increased translocation of FATP4 from intracellular storage sites to the cell surface, mediated by a series of direct GAP targets (Rab GTPases) RAB8a, RAB8b, RAB10, RAB14, RAB40b (1). This leads to an increase in long-chain FA uptake (2) which is accompanied by an increase in mitochondrial β -oxidation (3). Under *Tbc1d1*-deficient conditions skeletal muscle cells display alterations in the expression of genes involved in FA uptake (*Fatp4*) and the myocellular switch from glucose to lipid metabolism (*Pdk4*) which was also found on protein expression level. This may be an indirect consequence of initially increased long-chain fatty acid uptake (4). RabGAP-deficiency also may cause changes in the activity of key β -oxidation enzymes (e.g. β -HAD), as well as enzymes that are involved in the cellular diversification of fatty acid species which in turn changes lipid composition in the GAP knockout muscle cells (5). A direct impact of TBC1D1 and TBC1D4 on gene expression was not found so far, but cannot be excluded finally (6).

The presented study shows that the cellular response to RabGAPs is complex and most likely result of several primary and secondary events. Further studies could focus on the one

hand on the primary effects. It is possible that more than the RAB proteins described in this study participate in muscle cell fatty acid uptake. In this study at least two novel candidate RABs regulating lipid uptake, RAB8b and RAB40b, could be identified and it is likely that there may be more. Additionally, studies could focus more on the role of FATP4, and potential other interesting candidate FATPs, such as FATP1. This present study gives initial evidence that FATP4 is an important candidate. Further, *in vivo* studies involving AAVs could be conducted to selectively reduce FATP4 expression in mouse muscles and to evaluate its role on GAP-dependent lipid utilization *ex vivo*. Given that the *Fatp1*-deficient mice would be available, similar crossbreeding strategies could be followed as it was done for *Cd36*-deficient mice. These mice could be used to generate genetically modified mice offspring that carry the described combinations of *RabGAP*-deficiency with a *Fatp1*-deficiency to clarify if FATP1 may participate in the GAP-mediated alterations of skeletal muscle lipid uptake as well. Other more mechanistic studies could focus in the role of TBC1D1 and TBC1D4 on altering enzyme activities as these were shown to be present in this study and other publications.

6 Literature

- Abe, T., Hirasaka, K., Kohno, S., Tomida, C., Haruna, M., Uchida, T., . . . Nikawa, T. (2016). Capric Acid Up-Regulates UCP3 Expression without PDK4 Induction in Mouse C2C12 Myotubes. *J Nutr Sci Vitaminol (Tokyo)*, *62*(1), 32-39. doi: 10.3177/jnsv.62.32
- Abu-Elheiga, L., Matzuk, M. M., Abo-Hashema, K. A., & Wakil, S. J. (2001). Continuous fatty acid oxidation and reduced fat storage in mice lacking acetyl-CoA carboxylase 2. *Science*, *291*(5513), 2613-2616. doi: 10.1126/science.1056843
- Abumrad, N. A., el-Maghrabi, M. R., Amri, E. Z., Lopez, E., & Grimaldi, P. A. (1993). Cloning of a rat adipocyte membrane protein implicated in binding or transport of long-chain fatty acids that is induced during preadipocyte differentiation. Homology with human CD36. *J Biol Chem*, *268*(24), 17665-17668.
- ADA. (2010). Diagnosis and classification of diabetes mellitus. *Diabetes Care*, *33 Suppl 1*, S62-69. doi: 10.2337/dc10-S062
- ADA. (2016). 2. Classification and Diagnosis of Diabetes. *Diabetes Care*, *39 Suppl 1*, S13-22. doi: 10.2337/dc16-S005
- Adeva-Andany, M. M., Carneiro-Freire, N., Seco-Filgueira, M., Fernandez-Fernandez, C., & Mourino-Bayolo, D. (2018). Mitochondrial beta-oxidation of saturated fatty acids in humans. *Mitochondrion*. doi: 10.1016/j.mito.2018.02.009
- Al-Khami, A. A., Zheng, L., Del Valle, L., Hossain, F., Wyczechowska, D., Zabaleta, J., . . . Ochoa, A. C. (2017). Exogenous lipid uptake induces metabolic and functional reprogramming of tumor-associated myeloid-derived suppressor cells. *Oncoimmunology*, *6*(10), e1344804. doi: 10.1080/2162402X.2017.1344804
- Alarcon, G., Roco, J., Medina, A., Van Nieuwenhove, C., Medina, M., & Jerez, S. (2016). Stearoyl-CoA desaturase indexes and n-6/n-3 fatty acids ratio as biomarkers of cardiometabolic risk factors in normal-weight rabbits fed high fat diets. *J Biomed Sci*, *23*, 13. doi: 10.1186/s12929-016-0235-6
- Albaugh, V. L., Banan, B., Ajouz, H., Abumrad, N. N., & Flynn, C. R. (2017). Bile acids and bariatric surgery. *Mol Aspects Med*, *56*, 75-89. doi: 10.1016/j.mam.2017.04.001
- Albu, J. B., Murphy, L., Frager, D. H., Johnson, J. A., & Pi-Sunyer, F. X. (1997). Visceral fat and race-dependent health risks in obese nondiabetic premenopausal women. *Diabetes*, *46*(3), 456-462.
- Ali, B. R., Wasmeier, C., Lamoreux, L., Strom, M., & Seabra, M. C. (2004). Multiple regions contribute to membrane targeting of Rab GTPases. *J Cell Sci*, *117*(Pt 26), 6401-6412. doi: 10.1242/jcs.01542

- Alkhateeb, H., & Qnais, E. (2017). Preventive effect of oleate on palmitate-induced insulin resistance in skeletal muscle and its mechanism of action. *J Physiol Biochem*, *73*(4), 605-612. doi: 10.1007/s13105-017-0594-9
- Anderson, C. M., & Stahl, A. (2013). SLC27 fatty acid transport proteins. *Mol Aspects Med*, *34*(2-3), 516-528. doi: 10.1016/j.mam.2012.07.010
- Araki, S., Kikuchi, A., Hata, Y., Isomura, M., & Takai, Y. (1990). Regulation of reversible binding of smg p25A, a ras p21-like GTP-binding protein, to synaptic plasma membranes and vesicles by its specific regulatory protein, GDP dissociation inhibitor. *J Biol Chem*, *265*(22), 13007-13015.
- Araya, J., Rodrigo, R., Pettinelli, P., Araya, A. V., Poniachik, J., & Videla, L. A. (2010). Decreased liver fatty acid delta-6 and delta-5 desaturase activity in obese patients. *Obesity (Silver Spring)*, *18*(7), 1460-1463. doi: 10.1038/oby.2009.379
- Armoni, M., Harel, C., Bar-Yoseph, F., Milo, S., & Karnieli, E. (2005). Free fatty acids repress the GLUT4 gene expression in cardiac muscle via novel response elements. *J Biol Chem*, *280*(41), 34786-34795. doi: 10.1074/jbc.M502740200
- Bajaj, P., Reddy, B., Jr., Millet, L., Wei, C., Zorlutuna, P., Bao, G., & Bashir, R. (2011). Patterning the differentiation of C2C12 skeletal myoblasts. *Integr Biol (Camb)*, *3*(9), 897-909. doi: 10.1039/c1ib00058f
- Bandyopadhyay, G. K., Yu, J. G., Ofrecio, J., & Olefsky, J. M. (2006). Increased malonyl-CoA levels in muscle from obese and type 2 diabetic subjects lead to decreased fatty acid oxidation and increased lipogenesis; thiazolidinedione treatment reverses these defects. *Diabetes*, *55*(8), 2277-2285. doi: 10.2337/db06-0062
- Banerji, M. A., Chaiken, R. L., Gordon, D., Kral, J. G., & Lebovitz, H. E. (1995). Does intra-abdominal adipose tissue in black men determine whether NIDDM is insulin-resistant or insulin-sensitive? *Diabetes*, *44*(2), 141-146.
- Barbosa, A. D., & Siniossoglou, S. (2017). Function of lipid droplet-organelle interactions in lipid homeostasis. *Biochim Biophys Acta*, *1864*(9), 1459-1468. doi: 10.1016/j.bbamcr.2017.04.001
- Barr, F., & Lambright, D. G. (2010). Rab GEFs and GAPs. *Curr Opin Cell Biol*, *22*(4), 461-470. doi: 10.1016/j.ceb.2010.04.007
- Baus, D., Heermeier, K., De Hoop, M., Metz-Weidmann, C., Gassenhuber, J., Dittrich, W., . . . Tennagels, N. (2008). Identification of a novel AS160 splice variant that regulates GLUT4 translocation and glucose-uptake in rat muscle cells. *Cell Signal*, *20*(12), 2237-2246. doi: 10.1016/j.cellsig.2008.08.010

- Bazhan, N. M., Baklanov, A. V., Piskunova, J. V., Kazantseva, A. J., & Makarova, E. N. (2017). Expression of genes involved in carbohydrate-lipid metabolism in muscle and fat tissues in the initial stage of adult-age obesity in fed and fasted mice. *Physiol Rep*, 5(19). doi: 10.14814/phy2.13445
- Befroy, D. E., Petersen, K. F., Dufour, S., Mason, G. F., de Graaf, R. A., Rothman, D. L., & Shulman, G. I. (2007). Impaired mitochondrial substrate oxidation in muscle of insulin-resistant offspring of type 2 diabetic patients. *Diabetes*, 56(5), 1376-1381. doi: 10.2337/db06-0783
- Bjerregaard, P., Pedersen, H. S., & Mulvad, G. (2000). The associations of a marine diet with plasma lipids, blood glucose, blood pressure and obesity among the inuit in Greenland. *Eur J Clin Nutr*, 54(9), 732-737.
- Bonen, A., Han, X. X., Habets, D. D., Febbraio, M., Glatz, J. F., & Luiken, J. J. (2007). A null mutation in skeletal muscle FAT/CD36 reveals its essential role in insulin- and AICAR-stimulated fatty acid metabolism. *Am J Physiol Endocrinol Metab*, 292(6), E1740-1749. doi: 10.1152/ajpendo.00579.2006
- Bonen, A., Luiken, J. J., Liu, S., Dyck, D. J., Kiens, B., Kristiansen, S., . . . Glatz, J. F. (1998). Palmitate transport and fatty acid transporters in red and white muscles. *Am J Physiol*, 275(3 Pt 1), E471-478.
- Bonen, A., Miskovic, D., & Kiens, B. (1999). Fatty acid transporters (FABPpm, FAT, FATP) in human muscle. *Can J Appl Physiol*, 24(6), 515-523.
- Boren, J., Taskinen, M. R., Olofsson, S. O., & Levin, M. (2013). Ectopic lipid storage and insulin resistance: a harmful relationship. *J Intern Med*, 274(1), 25-40. doi: 10.1111/joim.12071
- Bosma, M. (2016). Lipid droplet dynamics in skeletal muscle. *Exp Cell Res*, 340(2), 180-186. doi: 10.1016/j.yexcr.2015.10.023
- Brewer, P. D., Habtemichael, E. N., Romenskaia, I., Coster, A. C., & Mastick, C. C. (2016). Rab14 limits the sorting of Glut4 from endosomes into insulin-sensitive regulated secretory compartments in adipocytes. *Biochem J*, 473(10), 1315-1327. doi: 10.1042/BCJ20160020
- Brons, C., & Grunnet, L. G. (2017). MECHANISMS IN ENDOCRINOLOGY: Skeletal muscle lipotoxicity in insulin resistance and type 2 diabetes: a causal mechanism or an innocent bystander? *Eur J Endocrinol*, 176(2), R67-R78. doi: 10.1530/EJE-16-0488
- Bruno, J., Brumfield, A., Chaudhary, N., Iaea, D., & McGraw, T. E. (2016). SEC16A is a RAB10 effector required for insulin-stimulated GLUT4 trafficking in adipocytes. *J Cell Biol*, 214(1), 61-76. doi: 10.1083/jcb.201509052

- Burant, C. F., Takeda, J., Brot-Laroche, E., Bell, G. I., & Davidson, N. O. (1992). Fructose transporter in human spermatozoa and small intestine is GLUT5. *J Biol Chem*, *267*(21), 14523-14526.
- Campbell, P. J., & Carlson, M. G. (1993). Impact of obesity on insulin action in NIDDM. *Diabetes*, *42*(3), 405-410.
- Capilla, E., Diaz, M., Hou, J. C., Planas, J. V., & Pessin, J. E. (2010). High basal cell surface levels of fish GLUT4 are related to reduced sensitivity of insulin-induced translocation toward GGA and AS160 inhibition in adipocytes. *Am J Physiol Endocrinol Metab*, *298*(2), E329-336. doi: 10.1152/ajpendo.00547.2009
- Cartee, G. D. (2015). Mechanisms for greater insulin-stimulated glucose uptake in normal and insulin-resistant skeletal muscle after acute exercise. *Am J Physiol Endocrinol Metab*, *309*(12), E949-959. doi: 10.1152/ajpendo.00416.2015
- Cersosimo, E., Triplitt, C., Solis-Herrera, C., Mandarino, L. J., & DeFronzo, R. A. (2000). Pathogenesis of Type 2 Diabetes Mellitus. In L. J. De Groot, G. Chrousos, K. Dungan, K. R. Feingold, A. Grossman, J. M. Hershman, C. Koch, M. Korbonits, R. McLachlan, M. New, J. Purnell, R. Rebar, F. Singer & A. Vinik (Eds.), *Endotext*. South Dartmouth (MA)
- Chabowski, A., Coort, S. L., Calles-Escandon, J., Tandon, N. N., Glatz, J. F., Luiken, J. J., & Bonen, A. (2005). The subcellular compartmentation of fatty acid transporters is regulated differently by insulin and by AICAR. *FEBS Lett*, *579*(11), 2428-2432. doi: 10.1016/j.febslet.2004.11.118
- Chadt, A., Immisch, A., de Wendt, C., Springer, C., Zhou, Z., Stermann, T., . . . Al-Hasani, H. (2015). "Deletion of both Rab-GTPase-activating proteins TBC1D1 and TBC1D4 in mice eliminates insulin- and AICAR-stimulated glucose transport [corrected]. *Diabetes*, *64*(3), 746-759. doi: 10.2337/db14-0368
- Chadt, A., Leicht, K., Deshmukh, A., Jiang, L. Q., Scherneck, S., Bernhardt, U., . . . Al-Hasani, H. (2008). Tbc1d1 mutation in lean mouse strain confers leanness and protects from diet-induced obesity. *Nat Genet*, *40*(11), 1354-1359. doi: 10.1038/ng.244
- Chadt, A., Scherneck, S., Joost, H. G., & Al-Hasani, H. (2018). Molecular links between Obesity and Diabetes: "Diabesity". In L. J. De Groot, G. Chrousos, K. Dungan, K. R. Feingold, A. Grossman, J. M. Hershman, C. Koch, M. Korbonits, R. McLachlan, M. New, J. Purnell, R. Rebar, F. Singer & A. Vinik (Eds.), *Endotext*. South Dartmouth (MA)
- Charney, A. N., Micic, L., & Egnor, R. W. (1998). Nonionic diffusion of short-chain fatty acids across rat colon. *Am J Physiol Gastrointest Liver Physiol*, *274*(3), G518-G524. doi: 10.1152/ajpgi.1998.274.3.G518
- Chavrier, P., Parton, R. G., Hauri, H. P., Simons, K., & Zerial, M. (1990). Localization of low molecular weight GTP binding proteins to exocytic and endocytic compartments. *Cell*, *62*(2), 317-329.

- Chen, S., Liang, M. C., Chia, J. N., Ngsee, J. K., & Ting, A. E. (2001). Rab8b and its interacting partner TRIP8b are involved in regulated secretion in AtT20 cells. *J Biol Chem*, *276*(16), 13209-13216. doi: 10.1074/jbc.M010798200
- Chen, S., Murphy, J., Toth, R., Campbell, D. G., Morrice, N. A., & Mackintosh, C. (2008). Complementary regulation of TBC1D1 and AS160 by growth factors, insulin and AMPK activators. *Biochem J*, *409*(2), 449-459. doi: 10.1042/BJ20071114
- Chirala, S. S., Jayakumar, A., Gu, Z. W., & Wakil, S. J. (2001). Human fatty acid synthase: role of interdomain in the formation of catalytically active synthase dimer. *Proc Natl Acad Sci U S A*, *98*(6), 3104-3108. doi: 10.1073/pnas.051635998
- Chitraju, C., Trotsmuller, M., Hartler, J., Wolinski, H., Thallinger, G. G., Lass, A., . . . Spener, F. (2012). Lipidomic analysis of lipid droplets from murine hepatocytes reveals distinct signatures for nutritional stress. *J Lipid Res*, *53*(10), 2141-2152. doi: 10.1194/jlr.M028902
- Chomentowski, P., Coen, P. M., Radikova, Z., Goodpaster, B. H., & Toledo, F. G. (2011). Skeletal muscle mitochondria in insulin resistance: differences in intermyofibrillar versus subsarcolemmal subpopulations and relationship to metabolic flexibility. *J Clin Endocrinol Metab*, *96*(2), 494-503. doi: 10.1210/jc.2010-0822
- Colicelli, J. (2004). Human RAS superfamily proteins and related GTPases. *Sci STKE*, *2004*(250), RE13. doi: 10.1126/stke.2502004re13
- Collins, J. M., Neville, M. J., Pinnick, K. E., Hodson, L., Ruyter, B., van Dijk, T. H., . . . Frayn, K. N. (2011). De novo lipogenesis in the differentiating human adipocyte can provide all fatty acids necessary for maturation. *J Lipid Res*, *52*(9), 1683-1692. doi: 10.1194/jlr.M012195
- Connaughton, S., Chowdhury, F., Attia, R. R., Song, S., Zhang, Y., Elam, M. B., . . . Park, E. A. (2010). Regulation of pyruvate dehydrogenase kinase isoform 4 (PDK4) gene expression by glucocorticoids and insulin. *Mol Cell Endocrinol*, *315*(1-2), 159-167. doi: 10.1016/j.mce.2009.08.011
- Craighead, J. E. (1978). Current views on the etiology of insulin-dependent diabetes mellitus. *N Engl J Med*, *299*(26), 1439-1445. doi: 10.1056/NEJM197812282992605
- Daemen, S., van Polanen, N., & Hesselink, M. K. C. (2018). The effect of diet and exercise on lipid droplet dynamics in human muscle tissue. *J Exp Biol*, *221*(Pt Suppl 1). doi: 10.1242/jeb.167015
- Dal Bosco, A., Mugnai, C., Ruggeri, S., Mattioli, S., & Castellini, C. (2012). Fatty acid composition of meat and estimated indices of lipid metabolism in different poultry genotypes reared under organic system. *Poult Sci*, *91*(8), 2039-2045. doi: 10.3382/ps.2012-02228

- Dash, S., Langenberg, C., Fawcett, K. A., Semple, R. K., Romeo, S., Sharp, S., . . . Savage, D. B. (2010). Analysis of TBC1D4 in patients with severe insulin resistance. *Diabetologia*, *53*(6), 1239-1242. doi: 10.1007/s00125-010-1724-x
- Dash, S., Sano, H., Rochford, J. J., Semple, R. K., Yeo, G., Hyden, C. S., . . . Savage, D. B. (2009). A truncation mutation in TBC1D4 in a family with acanthosis nigricans and postprandial hyperinsulinemia. *Proc Natl Acad Sci U S A*, *106*(23), 9350-9355. doi: 10.1073/pnas.0900909106
- de la Rosa Rodriguez, M. A., & Kersten, S. (2017). Regulation of lipid droplet-associated proteins by peroxisome proliferator-activated receptors. *Biochim Biophys Acta*, *1862*(10 Pt B), 1212-1220. doi: 10.1016/j.bbaliip.2017.07.007
- DeFronzo, R. A., Jacot, E., Jequier, E., Maeder, E., Wahren, J., & Felber, J. P. (1981). The effect of insulin on the disposal of intravenous glucose. Results from indirect calorimetry and hepatic and femoral venous catheterization. *Diabetes*, *30*(12), 1000-1007.
- Del Puerto, M., Cabrera, M. C., & Saadoun, A. (2017). A Note on Fatty Acids Profile of Meat from Broiler Chickens Supplemented with Inorganic or Organic Selenium. *Int J Food Sci*, *2017*, 7613069. doi: 10.1155/2017/7613069
- Delprato, A., Merithew, E., & Lambright, D. G. (2004). Structure, exchange determinants, and family-wide rab specificity of the tandem helical bundle and Vps9 domains of Rabex-5. *Cell*, *118*(5), 607-617. doi: 10.1016/j.cell.2004.08.009
- Demir, K., Kirsch, N., Beretta, C. A., Erdmann, G., Ingelfinger, D., Moro, E., . . . Boutros, M. (2013). RAB8B is required for activity and caveolar endocytosis of LRP6. *Cell Rep*, *4*(6), 1224-1234. doi: 10.1016/j.celrep.2013.08.008
- Demonbreun, A. R., Biersmith, B. H., & McNally, E. M. (2015). Membrane fusion in muscle development and repair. *Semin Cell Dev Biol*, *45*, 48-56. doi: 10.1016/j.semcdb.2015.10.026
- Deng, B., Zhu, X., Zhao, Y., Zhang, D., Pannu, A., Chen, L., & Niu, W. (2018). PKC and Rab13 mediate Ca(2+) signal-regulated GLUT4 traffic. *Biochem Biophys Res Commun*, *495*(2), 1956-1963. doi: 10.1016/j.bbrc.2017.12.064
- Dimitriadis, G., Mitrou, P., Lambadiari, V., Maratou, E., & Raptis, S. A. (2011). Insulin effects in muscle and adipose tissue. *Diabetes Res Clin Pract*, *93 Suppl 1*, S52-59. doi: 10.1016/S0168-8227(11)70014-6
- Dimopoulos, N., Watson, M., Sakamoto, K., & Hundal, H. S. (2006). Differential effects of palmitate and palmitoleate on insulin action and glucose utilization in rat L6 skeletal muscle cells. *Biochem J*, *399*(3), 473-481. doi: 10.1042/BJ20060244
- Dokas, J., Chadt, A., Joost, H. G., & Al-Hasani, H. (2016). Tbc1d1 deletion suppresses obesity in leptin-deficient mice. *Int J Obes (Lond)*, *40*(8), 1242-1249. doi: 10.1038/ijo.2016.45

- Dokas, J., Chadt, A., Nolden, T., Himmelbauer, H., Zierath, J. R., Joost, H. G., & Al-Hasani, H. (2013). Conventional knockout of *Tbc1d1* in mice impairs insulin- and AICAR-stimulated glucose uptake in skeletal muscle. *Endocrinology*, *154*(10), 3502-3514. doi: 10.1210/en.2012-2147
- Duran, R. V., & Hall, M. N. (2012). Regulation of TOR by small GTPases. *EMBO Rep*, *13*(2), 121-128. doi: 10.1038/embor.2011.257
- Eathiraj, S., Pan, X., Ritacco, C., & Lambright, D. G. (2005). Structural basis of family-wide Rab GTPase recognition by rabenosyn-5. *Nature*, *436*(7049), 415-419. doi: 10.1038/nature03798
- Eaton, S. (2002). Control of mitochondrial beta-oxidation flux. *Prog Lipid Res*, *41*(3), 197-239.
- Eiselein, L., Schwartz, H. J., & Rutledge, J. C. (2004). The challenge of type 1 diabetes mellitus. *ILAR J*, *45*(3), 231-236.
- Endemann, G., Stanton, L. W., Madden, K. S., Bryant, C. M., White, R. T., & Protter, A. A. (1993). CD36 is a receptor for oxidized low density lipoprotein. *J Biol Chem*, *268*(16), 11811-11816.
- Febbraio, M., Abumrad, N. A., Hajjar, D. P., Sharma, K., Cheng, W., Pearce, S. F., & Silverstein, R. L. (1999). A null mutation in murine CD36 reveals an important role in fatty acid and lipoprotein metabolism. *J Biol Chem*, *274*(27), 19055-19062.
- Feige, J. N., & Auwerx, J. (2007). Transcriptional coregulators in the control of energy homeostasis. *Trends Cell Biol*, *17*(6), 292-301. doi: 10.1016/j.tcb.2007.04.001
- Ferrannini, E., Bjorkman, O., Reichard, G. A., Jr., Pilo, A., Olsson, M., Wahren, J., & DeFronzo, R. A. (1985). The disposal of an oral glucose load in healthy subjects. A quantitative study. *Diabetes*, *34*(6), 580-588.
- Flowers, M. T. (2009). The delta9 fatty acid desaturation index as a predictor of metabolic disease. *Clin Chem*, *55*(12), 2071-2073. doi: 10.1373/clinchem.2009.135152
- Foster, D. W. (2012). Malonyl-CoA: the regulator of fatty acid synthesis and oxidation. *J Clin Invest*, *122*(6), 1958-1959.
- Frasa, M. A., Koessmeier, K. T., Ahmadian, M. R., & Braga, V. M. (2012). Illuminating the functional and structural repertoire of human TBC/RABGAPs. *Nat Rev Mol Cell Biol*, *13*(2), 67-73. doi: 10.1038/nrm3267

- Fukuda, M. (2011). TBC proteins: GAPs for mammalian small GTPase Rab? *Biosci Rep*, *31*(3), 159-168. doi: 10.1042/BSR20100112
- Funai, K., Song, H., Yin, L., Lodhi, I. J., Wei, X., Yoshino, J., . . . Semenkovich, C. F. (2013). Muscle lipogenesis balances insulin sensitivity and strength through calcium signaling. *J Clin Invest*, *123*(3), 1229-1240. doi: 10.1172/JCI65726
- Furuyama, T., Kitayama, K., Yamashita, H., & Mori, N. (2003). Forkhead transcription factor FOXO1 (FKHR)-dependent induction of PDK4 gene expression in skeletal muscle during energy deprivation. *Biochem J*, *375*(Pt 2), 365-371. doi: 10.1042/BJ20030022
- Galgani, J. E., Moro, C., & Ravussin, E. (2008). Metabolic flexibility and insulin resistance. *Am J Physiol Endocrinol Metab*, *295*(5), E1009-1017. doi: 10.1152/ajpendo.90558.2008
- Gemmink, A., Bosma, M., Kuijpers, H. J., Hoeks, J., Schaart, G., van Zandvoort, M. A., . . . Hesselink, M. K. (2016). Decoration of intramyocellular lipid droplets with PLIN5 modulates fasting-induced insulin resistance and lipotoxicity in humans. *Diabetologia*, *59*(5), 1040-1048. doi: 10.1007/s00125-016-3865-z
- Gerhart, J., Elder, J., Neely, C., Schure, J., Kvist, T., Knudsen, K., & George-Weinstein, M. (2006). MyoD-positive epiblast cells regulate skeletal muscle differentiation in the embryo. *J Cell Biol*, *175*(2), 283-292. doi: 10.1083/jcb.200605037
- Gibbons, C. H., & Goebel-Fabbri, A. (2017). Microvascular Complications Associated With Rapid Improvements in Glycemic Control in Diabetes. *Curr Diab Rep*, *17*(7), 48. doi: 10.1007/s11892-017-0880-5
- Gimeno, R. E., Ortegon, A. M., Patel, S., Punreddy, S., Ge, P., Sun, Y., . . . Stahl, A. (2003). Characterization of a heart-specific fatty acid transport protein. *J Biol Chem*, *278*(18), 16039-16044. doi: 10.1074/jbc.M211412200
- Glatz, J. F., Bonen, A., & Luiken, J. J. (2002). Exercise and insulin increase muscle fatty acid uptake by recruiting putative fatty acid transporters to the sarcolemma. *Curr Opin Clin Nutr Metab Care*, *5*(4), 365-370.
- Glatz, J. F., Luiken, J. J., & Bonen, A. (2010). Membrane fatty acid transporters as regulators of lipid metabolism: implications for metabolic disease. *Physiol Rev*, *90*(1), 367-417. doi: 10.1152/physrev.00003.2009
- Glatz, J. F., Nabben, M., Heather, L. C., Bonen, A., & Luiken, J. J. (2016). Regulation of the subcellular trafficking of CD36, a major determinant of cardiac fatty acid utilization. *Biochim Biophys Acta*, *1861*(10), 1461-1471. doi: 10.1016/j.bbaliip.2016.04.008
- Glatz, J. F. C., & Luiken, J. (2018). Dynamic role of the transmembrane glycoprotein CD36 (SR-B2) in cellular fatty acid uptake and utilization. *J Lipid Res*. doi: 10.1194/jlr.R082933

- Goodpaster, B. H., He, J., Watkins, S., & Kelley, D. E. (2001). Skeletal muscle lipid content and insulin resistance: evidence for a paradox in endurance-trained athletes. *J Clin Endocrinol Metab*, *86*(12), 5755-5761. doi: 10.1210/jcem.86.12.8075
- Goodpaster, B. H., Krishnaswami, S., Resnick, H., Kelley, D. E., Haggerty, C., Harris, T. B., . . . Newman, A. B. (2003). Association between regional adipose tissue distribution and both type 2 diabetes and impaired glucose tolerance in elderly men and women. *Diabetes Care*, *26*(2), 372-379.
- Goodpaster, B. H., & Sparks, L. M. (2017). Metabolic Flexibility in Health and Disease. *Cell Metab*, *25*(5), 1027-1036. doi: 10.1016/j.cmet.2017.04.015
- Gorgens, S. W., Benninghoff, T., Eckardt, K., Springer, C., Chadt, A., Melior, A., . . . Eckel, J. (2017). Hypoxia in Combination With Muscle Contraction Improves Insulin Action and Glucose Metabolism in Human Skeletal Muscle via the HIF-1alpha Pathway. *Diabetes*, *66*(11), 2800-2807. doi: 10.2337/db16-1488
- Gower, B. A., Nagy, T. R., & Goran, M. I. (1999). Visceral fat, insulin sensitivity, and lipids in prepubertal children. *Diabetes*, *48*(8), 1515-1521.
- Grarup, N., Moltke, I., Albrechtsen, A., & Hansen, T. (2015). Diabetes in Population Isolates: Lessons from Greenland. *Rev Diabet Stud*, *12*(3-4), 320-329. doi: 10.1900/RDS.2015.12.320
- Green, C. D., Ozguden-Akkoc, C. G., Wang, Y., Jump, D. B., & Olson, L. K. (2010). Role of fatty acid elongases in determination of de novo synthesized monounsaturated fatty acid species. *J Lipid Res*, *51*(7), 1871-1877. doi: 10.1194/jlr.M004747
- Greenberg, A. S., Coleman, R. A., Kraemer, F. B., McManaman, J. L., Obin, M. S., Puri, V., . . . Mashek, D. G. (2011). The role of lipid droplets in metabolic disease in rodents and humans. *J Clin Invest*, *121*(6), 2102-2110. doi: 10.1172/JCI46069
- Greising, S. M., Gransee, H. M., Mantilla, C. B., & Sieck, G. C. (2012). Systems biology of skeletal muscle: fiber type as an organizing principle. *Wiley Interdiscip Rev Syst Biol Med*, *4*(5), 457-473. doi: 10.1002/wsbm.1184
- Gross, D. A., Zhan, C., & Silver, D. L. (2011). Direct binding of triglyceride to fat storage-inducing transmembrane proteins 1 and 2 is important for lipid droplet formation. *Proc Natl Acad Sci U S A*, *108*(49), 19581-19586. doi: 10.1073/pnas.1110817108
- Guo, X., Li, H., Xu, H., Halim, V., Zhang, W., Wang, H., . . . Wu, C. (2012). Palmitoleate induces hepatic steatosis but suppresses liver inflammatory response in mice. *PLoS One*, *7*(6), e39286. doi: 10.1371/journal.pone.0039286
- Han, R. H., Wang, M., Fang, X., & Han, X. (2013). Simulation of triacylglycerol ion profiles: bioinformatics for interpretation of triacylglycerol biosynthesis. *J Lipid Res*, *54*(4), 1023-1032. doi: 10.1194/jlr.M033837

- Hargett, S. R., Walker, N. N., Hussain, S. S., Hoehn, K. L., & Keller, S. R. (2015). Deletion of the Rab GAP Tbc1d1 modifies glucose, lipid, and energy homeostasis in mice. *Am J Physiol Endocrinol Metab*, *309*(3), E233-245. doi: 10.1152/ajpendo.00007.2015
- Hargett, S. R., Walker, N. N., & Keller, S. R. (2016). Rab GAPs AS160 and Tbc1d1 play nonredundant roles in the regulation of glucose and energy homeostasis in mice. *Am J Physiol Endocrinol Metab*, *310*(4), E276-288. doi: 10.1152/ajpendo.00342.2015
- Hayes, M., Choudhary, V., Ojha, N., Shin, J. J., Han, G. S., Carman, G. M., . . . Levine, T. (2017). Fat storage-inducing transmembrane (FIT or FITM) proteins are related to lipid phosphatase/phosphotransferase enzymes. *Microb Cell*, *5*(2), 88-103. doi: 10.15698/mic2018.02.614
- Henique, C., Mansouri, A., Fumey, G., Lenoir, V., Girard, J., Bouillaud, F., . . . Cohen, I. (2010). Increased mitochondrial fatty acid oxidation is sufficient to protect skeletal muscle cells from palmitate-induced apoptosis. *J Biol Chem*, *285*(47), 36818-36827. doi: 10.1074/jbc.M110.170431
- Henne, W. M., Reese, M. L., & Goodman, J. M. (2018). The assembly of lipid droplets and their roles in challenged cells. *EMBO J*, *37*(12). doi: 10.15252/embj.201898947
- Henriksson, J. (1995). Muscle fuel selection: effect of exercise and training. *Proc Nutr Soc*, *54*(1), 125-138.
- Herrmann, T., Grone, H. J., Langbein, L., Kaiser, I., Gosch, I., Bennemann, U., . . . Stremmel, W. (2005). Disturbed epidermal structure in mice with temporally controlled fatp4 deficiency. *J Invest Dermatol*, *125*(6), 1228-1235. doi: 10.1111/j.0022-202X.2005.23972.x
- Hirschey, M. D., Shimazu, T., Goetzman, E., Jing, E., Schwer, B., Lombard, D. B., . . . Verdin, E. (2010). SIRT3 regulates mitochondrial fatty-acid oxidation by reversible enzyme deacetylation. *Nature*, *464*(7285), 121-125. doi: 10.1038/nature08778
- Holland, W. L., Brozinick, J. T., Wang, L. P., Hawkins, E. D., Sargent, K. M., Liu, Y., . . . Summers, S. A. (2007). Inhibition of ceramide synthesis ameliorates glucocorticoid-, saturated-fat-, and obesity-induced insulin resistance. *Cell Metab*, *5*(3), 167-179. doi: 10.1016/j.cmet.2007.01.002
- Holness, M. J., & Sugden, M. C. (2003). Regulation of pyruvate dehydrogenase complex activity by reversible phosphorylation. *Biochem Soc Trans*, *31*(Pt 6), 1143-1151. doi: 10.1042/
- Hossain, P., Kavar, B., & El Nahas, M. (2007). Obesity and diabetes in the developing world--a growing challenge. *N Engl J Med*, *356*(3), 213-215. doi: 10.1056/NEJMp068177
- Houten, S. M., Chegary, M., Te Brinke, H., Wijnen, W. J., Glatz, J. F., Luiken, J. J., . . . Wanders, R. J. (2009). Pyruvate dehydrogenase kinase 4 expression is synergistically induced by AMP-activated protein kinase and fatty acids. *Cell Mol Life Sci*, *66*(7), 1283-1294. doi: 10.1007/s00018-009-9066-x

- Houten, S. M., & Wanders, R. J. (2010). A general introduction to the biochemistry of mitochondrial fatty acid beta-oxidation. *J Inherit Metab Dis*, *33*(5), 469-477. doi: 10.1007/s10545-010-9061-2
- Hruz, P. W., & Mueckler, M. M. (2001). Structural analysis of the GLUT1 facilitative glucose transporter (review). *Mol Membr Biol*, *18*(3), 183-193.
- Hutagalung, A. H., & Novick, P. J. (2011). Role of Rab GTPases in membrane traffic and cell physiology. *Physiol Rev*, *91*(1), 119-149. doi: 10.1152/physrev.00059.2009
- Huynh, F. K., Green, M. F., Koves, T. R., & Hirschey, M. D. (2014). Measurement of fatty acid oxidation rates in animal tissues and cell lines. *Methods Enzymol*, *542*, 391-405. doi: 10.1016/B978-0-12-416618-9.00020-0
- Imamura, S., Morioka, T., Yamazaki, Y., Numaguchi, R., Urata, H., Motoyama, K., . . . Inaba, M. (2014). Plasma polyunsaturated fatty acid profile and delta-5 desaturase activity are altered in patients with type 2 diabetes. *Metabolism*, *63*(11), 1432-1438. doi: 10.1016/j.metabol.2014.08.003
- Ishikura, S., Bilan, P. J., & Klip, A. (2007). Rabs 8A and 14 are targets of the insulin-regulated Rab-GAP AS160 regulating GLUT4 traffic in muscle cells. *Biochem Biophys Res Commun*, *353*(4), 1074-1079. doi: 10.1016/j.bbrc.2006.12.140
- Jacob, A., Jing, J., Lee, J., Schedin, P., Gilbert, S. M., Peden, A. A., . . . Prekeris, R. (2013). Rab40b regulates trafficking of MMP2 and MMP9 during invadopodia formation and invasion of breast cancer cells. *J Cell Sci*, *126*(Pt 20), 4647-4658. doi: 10.1242/jcs.126573
- Jacob, A., Linklater, E., Bayless, B. A., Lyons, T., & Prekeris, R. (2016). The role and regulation of Rab40b-Tks5 complex during invadopodia formation and cancer cell invasion. *J Cell Sci*, *129*(23), 4341-4353. doi: 10.1242/jcs.193904
- Jain, S. S., Chabowski, A., Snook, L. A., Schwenk, R. W., Glatz, J. F., Luiken, J. J., & Bonen, A. (2009). Additive effects of insulin and muscle contraction on fatty acid transport and fatty acid transporters, FAT/CD36, FABPpm, FATP1, 4 and 6. *FEBS Lett*, *583*(13), 2294-2300. doi: 10.1016/j.febslet.2009.06.020
- Jain, S. S., Luiken, J. J., Snook, L. A., Han, X. X., Holloway, G. P., Glatz, J. F., & Bonen, A. (2015). Fatty acid transport and transporters in muscle are critically regulated by Akt2. *FEBS Lett*, *589*(19 Pt B), 2769-2775. doi: 10.1016/j.febslet.2015.08.010
- Jain, S. S., Snook, L. A., Glatz, J. F., Luiken, J. J., Holloway, G. P., Thurmond, D. C., & Bonen, A. (2012). Munc18c provides stimulus-selective regulation of GLUT4 but not fatty acid transporter trafficking in skeletal muscle. *FEBS Lett*, *586*(16), 2428-2435. doi: 10.1016/j.febslet.2012.05.061

- Janssen, I., Heymsfield, S. B., Wang, Z. M., & Ross, R. (2000). Skeletal muscle mass and distribution in 468 men and women aged 18-88 yr. *J Appl Physiol (1985)*, *89*(1), 81-88. doi: 10.1152/jappl.2000.89.1.81
- Jayasinghe, I. D., & Launikonis, B. S. (2013). Three-dimensional reconstruction and analysis of the tubular system of vertebrate skeletal muscle. *J Cell Sci*, *126*(Pt 17), 4048-4058. doi: 10.1242/jcs.131565
- Jayasinghe, I. D., Lo, H. P., Morgan, G. P., Baddeley, D., Parton, R. G., Soeller, C., & Launikonis, B. S. (2013). Examination of the subsarcolemmal tubular system of mammalian skeletal muscle fibers. *Biophys J*, *104*(11), L19-21. doi: 10.1016/j.bpj.2013.04.029
- Jorgensen, M. E., Borch-Johnsen, K., Stolk, R., & Bjerregaard, P. (2013). Fat distribution and glucose intolerance among Greenland Inuit. *Diabetes Care*, *36*(10), 2988-2994. doi: 10.2337/dc12-2703
- Jump, D. B. (2009). Mammalian fatty acid elongases. *Methods Mol Biol*, *579*, 375-389. doi: 10.1007/978-1-60761-322-0_19
- Kahn, S. E., Hull, R. L., & Utzschneider, K. M. (2006). Mechanisms linking obesity to insulin resistance and type 2 diabetes. *Nature*, *444*(7121), 840-846. doi: 10.1038/nature05482
- Kalra, S. (2013). Diabesity. *J Pak Med Assoc*, *63*(4), 532-534.
- Kamp, F., & Hamilton, J. A. (2006). How fatty acids of different chain length enter and leave cells by free diffusion. *Prostaglandins Leukot Essent Fatty Acids*, *75*(3), 149-159. doi: 10.1016/j.plefa.2006.05.003
- Kaushik, S., & Cuervo, A. M. (2015). Degradation of lipid droplet-associated proteins by chaperone-mediated autophagy facilitates lipolysis. *Nat Cell Biol*, *17*(6), 759-770. doi: 10.1038/ncb3166
- Kelley, D. E. (2005). Skeletal muscle fat oxidation: timing and flexibility are everything. *J Clin Invest*, *115*(7), 1699-1702. doi: 10.1172/JC125758
- Kelley, D. E., Goodpaster, B., Wing, R. R., & Simoneau, J. A. (1999). Skeletal muscle fatty acid metabolism in association with insulin resistance, obesity, and weight loss. *Am J Physiol*, *277*(6 Pt 1), E1130-1141.
- Kelley, D. E., He, J., Menshikova, E. V., & Ritov, V. B. (2002). Dysfunction of mitochondria in human skeletal muscle in type 2 diabetes. *Diabetes*, *51*(10), 2944-2950.
- Kelley, D. E., & Mandarino, L. J. (2000). Fuel selection in human skeletal muscle in insulin resistance: a reexamination. *Diabetes*, *49*(5), 677-683.

- Kern, A., Dikic, I., & Behl, C. (2015). The integration of autophagy and cellular trafficking pathways via RAB GAPs. *Autophagy*, *11*(12), 2393-2397. doi: 10.1080/15548627.2015.1110668
- Kiens, B., Roepstorff, C., Glatz, J. F., Bonen, A., Schjerling, P., Knudsen, J., & Nielsen, J. N. (2004). Lipid-binding proteins and lipoprotein lipase activity in human skeletal muscle: influence of physical activity and gender. *J Appl Physiol* (1985), *97*(4), 1209-1218. doi: 10.1152/jappphysiol.01278.2003
- Kim, J. K., Gimeno, R. E., Higashimori, T., Kim, H. J., Choi, H., Punreddy, S., . . . Shulman, G. I. (2004). Inactivation of fatty acid transport protein 1 prevents fat-induced insulin resistance in skeletal muscle. *J Clin Invest*, *113*(5), 756-763. doi: 10.1172/JCI18917
- Kiral, F. R., Kohrs, F. E., Jin, E. J., & Hiesinger, P. R. (2018). Rab GTPases and Membrane Trafficking in Neurodegeneration. *Curr Biol*, *28*(8), R471-R486. doi: 10.1016/j.cub.2018.02.010
- Kobayashi, S., Suzuki, T., Kawaguchi, A., Phongphaew, W., Yoshii, K., Iwano, T., . . . Sawa, H. (2016). Rab8b Regulates Transport of West Nile Virus Particles from Recycling Endosomes. *J Biol Chem*, *291*(12), 6559-6568. doi: 10.1074/jbc.M115.712760
- Kosfeld, A., Kreuzer, M., Daniel, C., Brand, F., Schafer, A. K., Chadt, A., . . . Weber, R. G. (2016). Whole-exome sequencing identifies mutations of TBC1D1 encoding a Rab-GTPase-activating protein in patients with congenital anomalies of the kidneys and urinary tract (CAKUT). *Hum Genet*, *135*(1), 69-87. doi: 10.1007/s00439-015-1610-1
- Kotronen, A., Seppanen-Laakso, T., Westerbacka, J., Kiviluoto, T., Arola, J., Ruskeepaa, A. L., . . . Oresic, M. (2010). Comparison of lipid and fatty acid composition of the liver, subcutaneous and intra-abdominal adipose tissue, and serum. *Obesity (Silver Spring)*, *18*(5), 937-944. doi: 10.1038/oby.2009.326
- Kraegen, E. W., Cooney, G. J., & Turner, N. (2008). Muscle insulin resistance: a case of fat overconsumption, not mitochondrial dysfunction. *Proc Natl Acad Sci U S A*, *105*(22), 7627-7628. doi: 10.1073/pnas.0803901105
- Lambernd, S., Taube, A., Schober, A., Platzbecker, B., Gorgens, S. W., Schlich, R., . . . Eckel, J. (2012). Contractile activity of human skeletal muscle cells prevents insulin resistance by inhibiting pro-inflammatory signalling pathways. *Diabetologia*, *55*(4), 1128-1139. doi: 10.1007/s00125-012-2454-z
- Lamboley, C. R., Murphy, R. M., McKenna, M. J., & Lamb, G. D. (2014). Sarcoplasmic reticulum Ca²⁺ uptake and leak properties, and SERCA isoform expression, in type I and type II fibres of human skeletal muscle. *J Physiol*, *592*(6), 1381-1395. doi: 10.1113/jphysiol.2013.269373

- Langenberg, C., & Lotta, L. A. (2018). Genomic insights into the causes of type 2 diabetes. *Lancet*, *391*(10138), 2463-2474. doi: 10.1016/S0140-6736(18)31132-2
- Larson-Meyer, D. E., Newcomer, B. R., Ravussin, E., Volaufova, J., Bennett, B., Chalew, S., . . . Sothorn, M. (2011). Intrahepatic and intramyocellular lipids are determinants of insulin resistance in prepubertal children. *Diabetologia*, *54*(4), 869-875. doi: 10.1007/s00125-010-2022-3
- Lebovitz, H. E. (1999). Type 2 diabetes: an overview. *Clin Chem*, *45*(8 Pt 2), 1339-1345.
- Li, H., Ou, L., Fan, J., Xiao, M., Kuang, C., Liu, X., . . . Xu, Y. (2017). Rab8A regulates insulin-stimulated GLUT4 translocation in C2C12 myoblasts. *FEBS Lett*, *591*(3), 491-499. doi: 10.1002/1873-3468.12555
- Li, Y., Jia, Q., Wang, Y., Li, F., Jia, Z., & Wan, Y. (2015). Rab40b upregulation correlates with the prognosis of gastric cancer by promoting migration, invasion, and metastasis. *Med Oncol*, *32*(4), 126. doi: 10.1007/s12032-015-0562-6
- Li, Z., Yue, Y., Hu, F., Zhang, C., Ma, X., Li, N., . . . Niu, W. (2017). Electrical pulse stimulation induces GLUT4 glucose transporter translocation in C2C12 myotubes that depends on Rab8A, Rab13 and Rab14. *Am J Physiol Endocrinol Metab*, aipendo001032017. doi: 10.1152/ajpendo.00103.2017
- Lillioja, S., Mott, D. M., Spraul, M., Ferraro, R., Foley, J. E., Ravussin, E., . . . Bogardus, C. (1993). Insulin resistance and insulin secretory dysfunction as precursors of non-insulin-dependent diabetes mellitus. Prospective studies of Pima Indians. *N Engl J Med*, *329*(27), 1988-1992. doi: 10.1056/NEJM199312303292703
- Lim, J. H., Gerhart-Hines, Z., Dominy, J. E., Lee, Y., Kim, S., Tabata, M., . . . Puigserver, P. (2013). Oleic acid stimulates complete oxidation of fatty acids through protein kinase A-dependent activation of SIRT1-PGC1alpha complex. *J Biol Chem*, *288*(10), 7117-7126. doi: 10.1074/jbc.M112.415729
- Liu, X., Zuo, R., Bao, Y., Qu, X., Sun, K., & Ying, H. (2017). Down-regulation of PDK4 is Critical for the Switch of Carbohydrate Catabolism during Syncytialization of Human Placental Trophoblasts. *Sci Rep*, *7*(1), 8474. doi: 10.1038/s41598-017-09163-8
- Luiken, J. J., Bonen, A., & Glatz, J. F. (2002). Cellular fatty acid uptake is acutely regulated by membrane-associated fatty acid-binding proteins. *Prostaglandins Leukot Essent Fatty Acids*, *67*(2-3), 73-78.
- Luiken, J. J., Coort, S. L., Willems, J., Coumans, W. A., Bonen, A., van der Vusse, G. J., & Glatz, J. F. (2003). Contraction-induced fatty acid translocase/CD36 translocation in rat cardiac myocytes is mediated through AMP-activated protein kinase signaling. *Diabetes*, *52*(7), 1627-1634.
- Luiken, J. J., Dyck, D. J., Han, X. X., Tandon, N. N., Arumugam, Y., Glatz, J. F., & Bonen, A. (2002). Insulin induces the translocation of the fatty acid transporter FAT/CD36 to the

- plasma membrane. *Am J Physiol Endocrinol Metab*, 282(2), E491-495. doi: 10.1152/ajpendo.00419.2001
- Luiken, J. J., Koonen, D. P., Willems, J., Zorzano, A., Becker, C., Fischer, Y., . . . Glatz, J. F. (2002). Insulin stimulates long-chain fatty acid utilization by rat cardiac myocytes through cellular redistribution of FAT/CD36. *Diabetes*, 51(10), 3113-3119.
- Luquet, S., Gaudel, C., Holst, D., Lopez-Soriano, J., Jehl-Pietri, C., Fredenrich, A., & Grimaldi, P. A. (2005). Roles of PPAR delta in lipid absorption and metabolism: a new target for the treatment of type 2 diabetes. *Biochim Biophys Acta*, 1740(2), 313-317. doi: 10.1016/j.bbadis.2004.11.011
- Mafakheri, S., Chadt, A., & Al-Hasani, H. (2018). Regulation of RabGAPs involved in insulin action. *Biochem Soc Trans*, 46(3), 683-690. doi: 10.1042/BST20170479
- Maher, A. C., McFarlan, J., Lally, J., Snook, L. A., & Bonen, A. (2014). TBC1D1 reduces palmitate oxidation by inhibiting beta-HAD activity in skeletal muscle. *Am J Physiol Regul Integr Comp Physiol*, 307(9), R1115-1123. doi: 10.1152/ajpregu.00014.2014
- Maier, T., Leibundgut, M., & Ban, N. (2008). The crystal structure of a mammalian fatty acid synthase. *Science*, 321(5894), 1315-1322. doi: 10.1126/science.1161269
- Marat, A. L., Dokainish, H., & McPherson, P. S. (2011). DENN domain proteins: regulators of Rab GTPases. *J Biol Chem*, 286(16), 13791-13800. doi: 10.1074/jbc.R110.217067
- Markgraf, D. F., Al-Hasani, H., & Lehr, S. (2016). Lipidomics-Reshaping the Analysis and Perception of Type 2 Diabetes. *Int J Mol Sci*, 17(11). doi: 10.3390/ijms17111841
- Markgraf, D. F., Klemm, R. W., Junker, M., Hannibal-Bach, H. K., Ejsing, C. S., & Rapoport, T. A. (2014). An ER protein functionally couples neutral lipid metabolism on lipid droplets to membrane lipid synthesis in the ER. *Cell Rep*, 6(1), 44-55. doi: 10.1016/j.celrep.2013.11.046
- Martin, S., & Parton, R. G. (2006). Lipid droplets: a unified view of a dynamic organelle. *Nat Rev Mol Cell Biol*, 7(5), 373-378. doi: 10.1038/nrm1912
- Martino, G., Mugnai, C., Compagnone, D., Grotta, L., Del Carlo, M., & Sarti, F. (2014). Comparison of Performance, Meat Lipids and Oxidative Status of Pigs from Commercial Breed and Organic Crossbreed. *Animals (Basel)*, 4(2), 348-360. doi: 10.3390/ani4020348
- McMahon, D. K., Anderson, P. A., Nassar, R., Bunting, J. B., Saba, Z., Oakeley, A. E., & Malouf, N. N. (1994). C2C12 cells: biophysical, biochemical, and immunocytochemical properties. *Am J Physiol*, 266(6 Pt 1), C1795-1802. doi: 10.1152/ajpcell.1994.266.6.C1795

- Meissner, J. D., Umeda, P. K., Chang, K. C., Gros, G., & Scheibe, R. J. (2007). Activation of the beta myosin heavy chain promoter by MEF-2D, MyoD, p300, and the calcineurin/NFATc1 pathway. *J Cell Physiol*, *211*(1), 138-148. doi: 10.1002/jcp.20916
- Mermelstein, C. S., Amaral, L. M., Rebello, M. I., Reis, J. S., Borojevic, R., & Costa, M. L. (2005). Changes in cell shape and desmin intermediate filament distribution are associated with down-regulation of desmin expression in C2C12 myoblasts grown in the absence of extracellular Ca²⁺. *Braz J Med Biol Res*, *38*(7), 1025-1032. doi: /S0100-879X2005000700005
- Miinea, C. P., Sano, H., Kane, S., Sano, E., Fukuda, M., Peranen, J., . . . Lienhard, G. E. (2005). AS160, the Akt substrate regulating GLUT4 translocation, has a functional Rab GTPase-activating protein domain. *Biochem J*, *391*(Pt 1), 87-93. doi: 10.1042/BJ20050887
- Miklosz, A., Lukaszuk, B., Zendzian-Piotrowska, M., Branska-Januszewska, J., Ostrowska, H., & Chabowski, A. (2017). Challenging of AS160/TBC1D4 Alters Intracellular Lipid milieu in L6 Myotubes Incubated With Palmitate. *J Cell Physiol*, *232*(9), 2373-2386. doi: 10.1002/jcp.25632
- Miklosz, A., Lukaszuk, B., Zendzian-Piotrowska, M., Kurek, K., & Chabowski, A. (2016). The Effects of AS160 Modulation on Fatty Acid Transporters Expression and Lipid Profile in L6 Myotubes. *Cell Physiol Biochem*, *38*(1), 267-282. doi: 10.1159/000438628
- Minokoshi, Y., Toda, C., & Okamoto, S. (2012). Regulatory role of leptin in glucose and lipid metabolism in skeletal muscle. *Indian J Endocrinol Metab*, *16*(Suppl 3), S562-568. doi: 10.4103/2230-8210.105573
- Mitchell, K. J., Pannerec, A., Cadot, B., Parlakian, A., Besson, V., Gomes, E. R., . . . Sassoon, D. A. (2010). Identification and characterization of a non-satellite cell muscle resident progenitor during postnatal development. *Nat Cell Biol*, *12*(3), 257-266. doi: 10.1038/ncb2025
- Moltke, I., Grarup, N., Jorgensen, M. E., Bjerregaard, P., Treebak, J. T., Fumagalli, M., . . . Hansen, T. (2014). A common Greenlandic TBC1D4 variant confers muscle insulin resistance and type 2 diabetes. *Nature*, *512*(7513), 190-193. doi: 10.1038/nature13425
- Morales, P. E., Bucarey, J. L., & Espinosa, A. (2017). Muscle Lipid Metabolism: Role of Lipid Droplets and Perilipins. *J Diabetes Res*, *2017*, 1789395. doi: 10.1155/2017/1789395
- Moschen, I., Broer, A., Galic, S., Lang, F., & Broer, S. (2012). Significance of short chain fatty acid transport by members of the monocarboxylate transporter family (MCT). *Neurochem Res*, *37*(11), 2562-2568. doi: 10.1007/s11064-012-0857-3
- Mu, J., Brozinick, J. T., Jr., Valladares, O., Bucan, M., & Birnbaum, M. J. (2001). A role for AMP-activated protein kinase in contraction- and hypoxia-regulated glucose transport in skeletal muscle. *Mol Cell*, *7*(5), 1085-1094.

- Mueckler, M., & Thorens, B. (2013). The SLC2 (GLUT) family of membrane transporters. *Mol Aspects Med*, 34(2-3), 121-138. doi: 10.1016/j.mam.2012.07.001
- Muoio, D. M., & Koves, T. R. (2007). Skeletal muscle adaptation to fatty acid depends on coordinated actions of the PPARs and PGC1 alpha: implications for metabolic disease. *Appl Physiol Nutr Metab*, 32(5), 874-883. doi: 10.1139/H07-083
- Murakami, K., Sasaki, S., Takahashi, Y., Uenishi, K., Watanabe, T., Kohri, T., . . . Suzuki, J. (2008). Lower estimates of delta-5 desaturase and elongase activity are related to adverse profiles for several metabolic risk factors in young Japanese women. *Nutr Res*, 28(12), 816-824. doi: 10.1016/j.nutres.2008.08.009
- Nakamura, M. T., Yudell, B. E., & Loor, J. J. (2014). Regulation of energy metabolism by long-chain fatty acids. *Prog Lipid Res*, 53, 124-144. doi: 10.1016/j.plipres.2013.12.001
- Ng, J. M., Azuma, K., Kelley, C., Pencek, R., Radikova, Z., Laymon, C., . . . Kelley, D. E. (2012). PET imaging reveals distinctive roles for different regional adipose tissue depots in systemic glucose metabolism in nonobese humans. *Am J Physiol Endocrinol Metab*, 303(9), E1134-1141. doi: 10.1152/ajpendo.00282.2012
- Nickerson, J. G., Alkhateeb, H., Benton, C. R., Lally, J., Nickerson, J., Han, X. X., . . . Bonen, A. (2009). Greater transport efficiencies of the membrane fatty acid transporters FAT/CD36 and FATP4 compared with FABPpm and FATP1 and differential effects on fatty acid esterification and oxidation in rat skeletal muscle. *J Biol Chem*, 284(24), 16522-16530. doi: 10.1074/jbc.M109.004788
- Novick, P. (2016). Regulation of membrane traffic by Rab GEF and GAP cascades. *Small GTPases*, 7(4), 252-256. doi: 10.1080/21541248.2016.1213781
- Ottenheijm, C. A., & Granzier, H. (2010). Lifting the nebula: novel insights into skeletal muscle contractility. *Physiology (Bethesda)*, 25(5), 304-310. doi: 10.1152/physiol.00016.2010
- Pan, X., Eathiraj, S., Munson, M., & Lambright, D. G. (2006). TBC-domain GAPs for Rab GTPases accelerate GTP hydrolysis by a dual-finger mechanism. *Nature*, 442(7100), 303-306. doi: 10.1038/nature04847
- Park, H., & Jeoung, N. H. (2016). Inflammation increases pyruvate dehydrogenase kinase 4 (PDK4) expression via the Jun N-Terminal Kinase (JNK) pathway in C2C12 cells. *Biochem Biophys Res Commun*, 469(4), 1049-1054. doi: 10.1016/j.bbrc.2015.12.113
- Park, S. Y., Jin, W., Woo, J. R., & Shoelson, S. E. (2011). Crystal structures of human TBC1D1 and TBC1D4 (AS160) Rab GTPase-activating protein (RabGAP) domains reveal critical elements for GLUT4 translocation. *J Biol Chem*, 286(20), 18130-18138. doi: 10.1074/jbc.M110.217323

- Pedersen, B. K. (2013). Muscle as a secretory organ. *Compr Physiol*, 3(3), 1337-1362. doi: 10.1002/cphy.c120033
- Petersen, K. F., Dufour, S., & Shulman, G. I. (2005). Decreased insulin-stimulated ATP synthesis and phosphate transport in muscle of insulin-resistant offspring of type 2 diabetic parents. *PLoS Med*, 2(9), e233. doi: 10.1371/journal.pmed.0020233
- Pfeffer, S. (2005). Filling the Rab GAP. *Nat Cell Biol*, 7(9), 856-857. doi: 10.1038/ncb0905-856
- Pfeffer, S. R. (2005). Structural clues to Rab GTPase functional diversity. *J Biol Chem*, 280(16), 15485-15488. doi: 10.1074/jbc.R500003200
- Pilegaard, H., & Neufer, P. D. (2004). Transcriptional regulation of pyruvate dehydrogenase kinase 4 in skeletal muscle during and after exercise. *Proc Nutr Soc*, 63(2), 221-226.
- Ponnampalam, E. N., Lewandowski, P. A., Fahri, F. T., Burnett, V. F., Dunshea, F. R., Plozza, T., & Jacobs, J. L. (2015). Forms of n-3 (ALA, C18:3n-3 or DHA, C22:6n-3) Fatty Acids Affect Carcass Yield, Blood Lipids, Muscle n-3 Fatty Acids and Liver Gene Expression in Lambs. *Lipids*, 50(11), 1133-1143. doi: 10.1007/s11745-015-4070-4
- Prasad, R. B., & Groop, L. (2015). Genetics of type 2 diabetes-pitfalls and possibilities. *Genes (Basel)*, 6(1), 87-123. doi: 10.3390/genes6010087
- Precechtelova, J., Borsanyiiova, M., Sarmirova, S., & Bopegamage, S. (2014). Type I diabetes mellitus: genetic factors and presumptive enteroviral etiology or protection. *J Pathog*, 2014, 738512. doi: 10.1155/2014/738512
- Reddy, J. K., & Hashimoto, T. (2001). Peroxisomal beta-oxidation and peroxisome proliferator-activated receptor alpha: an adaptive metabolic system. *Annu Rev Nutr*, 21, 193-230. doi: 10.1146/annurev.nutr.21.1.193
- Richieri, G. V., Anel, A., & Kleinfeld, A. M. (1993). Interactions of long-chain fatty acids and albumin: determination of free fatty acid levels using the fluorescent probe ADIFAB. *Biochemistry*, 32(29), 7574-7580.
- Richter, E. A., & Hargreaves, M. (2013). Exercise, GLUT4, and skeletal muscle glucose uptake. *Physiol Rev*, 93(3), 993-1017. doi: 10.1152/physrev.00038.2012
- Roach, W. G., Chavez, J. A., Miinea, C. P., & Lienhard, G. E. (2007). Substrate specificity and effect on GLUT4 translocation of the Rab GTPase-activating protein Tbc1d1. *Biochem J*, 403(2), 353-358. doi: 10.1042/BJ20061798
- Rumsey, S. C., Kwon, O., Xu, G. W., Burant, C. F., Simpson, I., & Levine, M. (1997). Glucose transporter isoforms GLUT1 and GLUT3 transport dehydroascorbic acid. *J Biol Chem*, 272(30), 18982-18989.

- Ruoslahti, E., & Reed, J. C. (1994). Anchorage dependence, integrins, and apoptosis. *Cell*, *77*(4), 477-478.
- Saha, A. K., Vavvas, D., Kurowski, T. G., Apazidis, A., Witters, L. A., Shafrir, E., & Ruderman, N. B. (1997). Malonyl-CoA regulation in skeletal muscle: its link to cell citrate and the glucose-fatty acid cycle. *Am J Physiol*, *272*(4 Pt 1), E641-648. doi: 10.1152/ajpendo.1997.272.4.E641
- Sakamoto, K., & Holman, G. D. (2008). Emerging role for AS160/TBC1D4 and TBC1D1 in the regulation of GLUT4 traffic. *Am J Physiol Endocrinol Metab*, *295*(1), E29-37. doi: 10.1152/ajpendo.90331.2008
- Salvado, L., Coll, T., Gomez-Foix, A. M., Salmeron, E., Barroso, E., Palomer, X., & Vazquez-Carrera, M. (2013). Oleate prevents saturated-fatty-acid-induced ER stress, inflammation and insulin resistance in skeletal muscle cells through an AMPK-dependent mechanism. *Diabetologia*, *56*(6), 1372-1382. doi: 10.1007/s00125-013-2867-3
- Samovski, D., Su, X., Xu, Y., Abumrad, N. A., & Stahl, P. D. (2012). Insulin and AMPK regulate FA translocase/CD36 plasma membrane recruitment in cardiomyocytes via Rab GAP AS160 and Rab8a Rab GTPase. *J Lipid Res*, *53*(4), 709-717. doi: 10.1194/jlr.M023424
- Samuel, V. T., Petersen, K. F., & Shulman, G. I. (2010). Lipid-induced insulin resistance: unravelling the mechanism. *Lancet*, *375*(9733), 2267-2277. doi: 10.1016/S0140-6736(10)60408-4
- Samuel, V. T., & Shulman, G. I. (2016). The pathogenesis of insulin resistance: integrating signaling pathways and substrate flux. *J Clin Invest*, *126*(1), 12-22. doi: 10.1172/JCI77812
- Sano, H., Roach, W. G., Peck, G. R., Fukuda, M., & Lienhard, G. E. (2008). Rab10 in insulin-stimulated GLUT4 translocation. *Biochem J*, *411*(1), 89-95. doi: 10.1042/BJ20071318
- Sato, T., Iwano, T., Kunii, M., Matsuda, S., Mizuguchi, R., Jung, Y., . . . Harada, A. (2014). Rab8a and Rab8b are essential for several apical transport pathways but insufficient for ciliogenesis. *J Cell Sci*, *127*(Pt 2), 422-431. doi: 10.1242/jcs.136903
- Schaffer, J. E., & Lodish, H. F. (1994). Expression cloning and characterization of a novel adipocyte long chain fatty acid transport protein. *Cell*, *79*(3), 427-436.
- Schaiff, W. T., Bildirici, I., Cheong, M., Chern, P. L., Nelson, D. M., & Sadovsky, Y. (2005). Peroxisome proliferator-activated receptor-gamma and retinoid X receptor signaling regulate fatty acid uptake by primary human placental trophoblasts. *J Clin Endocrinol Metab*, *90*(7), 4267-4275. doi: 10.1210/jc.2004-2265
- Schenk, S., Saberi, M., & Olefsky, J. M. (2008). Insulin sensitivity: modulation by nutrients and inflammation. *J Clin Invest*, *118*(9), 2992-3002. doi: 10.1172/JCI34260

- Schmidt, I., & Herpin, P. (1998). Carnitine palmitoyltransferase I (CPT I) activity and its regulation by malonyl-CoA are modulated by age and cold exposure in skeletal muscle mitochondria from newborn pigs. *J Nutr*, *128*(5), 886-893. doi: 10.1093/jn/128.5.886
- Schmitt, B., Fluck, M., Decombaz, J., Kreis, R., Boesch, C., Wittwer, M., . . . Hoppeler, H. (2003). Transcriptional adaptations of lipid metabolism in tibialis anterior muscle of endurance-trained athletes. *Physiol Genomics*, *15*(2), 148-157. doi: 10.1152/physiolgenomics.00089.2003
- Schonfeld, P., & Wojtczak, L. (2016). Short- and medium-chain fatty acids in energy metabolism: the cellular perspective. *J Lipid Res*, *57*(6), 943-954. doi: 10.1194/jlr.R067629
- Schwenk, R. W., Holloway, G. P., Luiken, J. J., Bonen, A., & Glatz, J. F. (2010). Fatty acid transport across the cell membrane: regulation by fatty acid transporters. *Prostaglandins Leukot Essent Fatty Acids*, *82*(4-6), 149-154. doi: 10.1016/j.plefa.2010.02.029
- Schwer, B., Bunkenborg, J., Verdin, R. O., Andersen, J. S., & Verdin, E. (2006). Reversible lysine acetylation controls the activity of the mitochondrial enzyme acetyl-CoA synthetase 2. *Proc Natl Acad Sci U S A*, *103*(27), 10224-10229. doi: 10.1073/pnas.0603968103
- Scudiero, O., Nigro, E., Monaco, M. L., Oliviero, G., Polito, R., Borbone, N., . . . Piccialli, G. (2016). New synthetic AICAR derivatives with enhanced AMPK and ACC activation. *J Enzyme Inhib Med Chem*, *31*(5), 748-753. doi: 10.3109/14756366.2015.1063622
- Sharp, S. A., Weedon, M. N., Hagopian, W. A., & Oram, R. A. (2018). Clinical and research uses of genetic risk scores in type 1 diabetes. *Curr Opin Genet Dev*, *50*, 96-102. doi: 10.1016/j.gde.2018.03.009
- Sheehan, P., Zhu, M., Beskow, A., Vollmer, C., & Waites, C. L. (2016). Activity-Dependent Degradation of Synaptic Vesicle Proteins Requires Rab35 and the ESCRT Pathway. *J Neurosci*, *36*(33), 8668-8686. doi: 10.1523/JNEUROSCI.0725-16.2016
- Shi, M. M., Shi, C. H., & Xu, Y. M. (2017). Rab GTPases: The Key Players in the Molecular Pathway of Parkinson's Disease. *Front Cell Neurosci*, *11*, 81. doi: 10.3389/fncel.2017.00081
- Shulman, G. I. (2000). Cellular mechanisms of insulin resistance. *J Clin Invest*, *106*(2), 171-176. doi: 10.1172/JCI110583
- Silverstein, R. L., & Febbraio, M. (2009). CD36, a scavenger receptor involved in immunity, metabolism, angiogenesis, and behavior. *Sci Signal*, *2*(72), re3. doi: 10.1126/scisignal.272re3

- Smathers, R. L., & Petersen, D. R. (2011). The human fatty acid-binding protein family: evolutionary divergences and functions. *Hum Genomics*, 5(3), 170-191.
- Son, N. H., Basu, D., Samovski, D., Pietka, T. A., Peche, V. S., Willecke, F., . . . Goldberg, I. J. (2018). Endothelial cell CD36 optimizes tissue fatty acid uptake. *J Clin Invest*. doi: 10.1172/JCI99315
- Souza, C. O., Teixeira, A. A., Lima, E. A., Batatinha, H. A., Gomes, L. M., Carvalho-Silva, M., . . . Rosa Neto, J. C. (2014). Palmitoleic acid (n-7) attenuates the immunometabolic disturbances caused by a high-fat diet independently of PPARalpha. *Mediators Inflamm*, 2014, 582197. doi: 10.1155/2014/582197
- Stahl, A., Evans, J. G., Pattel, S., Hirsch, D., & Lodish, H. F. (2002). Insulin causes fatty acid transport protein translocation and enhanced fatty acid uptake in adipocytes. *Dev Cell*, 2(4), 477-488.
- Stahl, A., Hirsch, D. J., Gimeno, R. E., Punreddy, S., Ge, P., Watson, N., . . . Lodish, H. F. (1999). Identification of the major intestinal fatty acid transport protein. *Mol Cell*, 4(3), 299-308.
- Stanford, K. I., Lynes, M. D., Takahashi, H., Baer, L. A., Arts, P. J., May, F. J., . . . Goodyear, L. J. (2018). 12,13-diHOME: An Exercise-Induced Lipokine that Increases Skeletal Muscle Fatty Acid Uptake. *Cell Metab*, 27(6), 1357. doi: 10.1016/j.cmet.2018.04.023
- Stellingwerff, T., Boon, H., Jonkers, R. A., Senden, J. M., Spriet, L. L., Koopman, R., & van Loon, L. J. (2007). Significant intramyocellular lipid use during prolonged cycling in endurance-trained males as assessed by three different methodologies. *Am J Physiol Endocrinol Metab*, 292(6), E1715-1723. doi: 10.1152/ajpendo.00678.2006
- Stenmark, H. (2009). Rab GTPases as coordinators of vesicle traffic. *Nat Rev Mol Cell Biol*, 10(8), 513-525. doi: 10.1038/nrm2728
- Stermann, T., Menzel, F., Weidlich, C., Jeruschke, K., Weiss, J., Altenhofen, D., . . . Al-Hasani, H. (2018). Deletion of the RabGAP TBC1D1 Leads to Enhanced Insulin Secretion and Fatty Acid Oxidation in Islets From Male Mice. *Endocrinology*, 159(4), 1748-1761. doi: 10.1210/en.2018-00087
- Stockli, J., Fazakerley, D. J., & James, D. E. (2011). GLUT4 exocytosis. *J Cell Sci*, 124(Pt 24), 4147-4159. doi: 10.1242/jcs.097063
- Summermatter, S., Baum, O., Santos, G., Hoppeler, H., & Handschin, C. (2010). Peroxisome proliferator-activated receptor {gamma} coactivator 1{alpha} (PGC-1{alpha}) promotes skeletal muscle lipid refueling in vivo by activating de novo lipogenesis and the pentose phosphate pathway. *J Biol Chem*, 285(43), 32793-32800. doi: 10.1074/jbc.M110.145995

- Sun, Y., Chiu, T. T., Foley, K. P., Bilan, P. J., & Klip, A. (2014). Myosin Va mediates Rab8A-regulated GLUT4 vesicle exocytosis in insulin-stimulated muscle cells. *Mol Biol Cell*, 25(7), 1159-1170. doi: 10.1091/mbc.E13-08-0493
- Sun, Y., Jaldin-Fincati, J., Liu, Z., Bilan, P. J., & Klip, A. (2016). A complex of Rab13 with MICAL-L2 and alpha-actinin-4 is essential for insulin-dependent GLUT4 exocytosis. *Mol Biol Cell*, 27(1), 75-89. doi: 10.1091/mbc.E15-05-0319
- Sylow, L., Kleinert, M., Richter, E. A., & Jensen, T. E. (2017). Exercise-stimulated glucose uptake - regulation and implications for glycaemic control. *Nat Rev Endocrinol*, 13(3), 133-148. doi: 10.1038/nrendo.2016.162
- Szekeres, F., Chadt, A., Tom, R. Z., Deshmukh, A. S., Chibalin, A. V., Bjornholm, M., . . . Zierath, J. R. (2012). The Rab-GTPase-activating protein TBC1D1 regulates skeletal muscle glucose metabolism. *Am J Physiol Endocrinol Metab*, 303(4), E524-533. doi: 10.1152/ajpendo.00605.2011
- Sztalryd, C., & Brasaemle, D. L. (2017). The perilipin family of lipid droplet proteins: Gatekeepers of intracellular lipolysis. *Biochim Biophys Acta*, 1862(10 Pt B), 1221-1232. doi: 10.1016/j.bbali.2017.07.009
- Sztalryd, C., & Kimmel, A. R. (2014). Perilipins: lipid droplet coat proteins adapted for tissue-specific energy storage and utilization, and lipid cytoprotection. *Biochimie*, 96, 96-101. doi: 10.1016/j.biochi.2013.08.026
- Talbot, N. A., Wheeler-Jones, C. P., & Cleasby, M. E. (2014). Palmitoleic acid prevents palmitic acid-induced macrophage activation and consequent p38 MAPK-mediated skeletal muscle insulin resistance. *Mol Cell Endocrinol*, 393(1-2), 129-142. doi: 10.1016/j.mce.2014.06.010
- Taylor, E. B., An, D., Kramer, H. F., Yu, H., Fujii, N. L., Roeckl, K. S., . . . Goodyear, L. J. (2008). Discovery of TBC1D1 as an insulin-, AICAR-, and contraction-stimulated signaling nexus in mouse skeletal muscle. *J Biol Chem*, 283(15), 9787-9796. doi: 10.1074/jbc.M708839200
- Thomas, C. C., & Philipson, L. H. (2015). Update on diabetes classification. *Med Clin North Am*, 99(1), 1-16. doi: 10.1016/j.mcna.2014.08.015
- Thomson, D. M., & Winder, W. W. (2009). AMP-activated protein kinase control of fat metabolism in skeletal muscle. *Acta Physiol (Oxf)*, 196(1), 147-154. doi: 10.1111/j.1748-1716.2009.01973.x
- Toledo, F. G. S., Johannsen, D. L., Covington, J. D., Bajpeyi, S., Goodpaster, B., Conley, K. E., & Ravussin, E. (2018). Impact of prolonged overfeeding on skeletal muscle mitochondria in healthy individuals. *Diabetologia*, 61(2), 466-475. doi: 10.1007/s00125-017-4496-8

- Tomczak, K. K., Marinescu, V. D., Ramoni, M. F., Sanoudou, D., Montanaro, F., Han, M., . . . Beggs, A. H. (2004). Expression profiling and identification of novel genes involved in myogenic differentiation. *FASEB J*, *18*(2), 403-405. doi: 10.1096/fj.03-0568fje
- Turcotte, L. P., Swenberger, J. R., Tucker, M. Z., Yee, A. J., Trump, G., Luiken, J. J., & Bonen, A. (2000). Muscle palmitate uptake and binding are saturable and inhibited by antibodies to FABP(PM). *Mol Cell Biochem*, *210*(1-2), 53-63.
- van Belle, T. L., Coppieters, K. T., & von Herrath, M. G. (2011). Type 1 diabetes: etiology, immunology, and therapeutic strategies. *Physiol Rev*, *91*(1), 79-118. doi: 10.1152/physrev.00003.2010
- Van Belle, T. L., Juntti, T., Liao, J., & von Herrath, M. G. (2010). Pre-existing autoimmunity determines type 1 diabetes outcome after Flt3-ligand treatment. *J Autoimmun*, *34*(4), 445-452. doi: 10.1016/j.jaut.2009.11.010
- van Herpen, N. A., & Schrauwen-Hinderling, V. B. (2008). Lipid accumulation in non-adipose tissue and lipotoxicity. *Physiol Behav*, *94*(2), 231-241. doi: 10.1016/j.physbeh.2007.11.049
- Van Rymenant, E., Abranko, L., Tumova, S., Grootaert, C., Van Camp, J., Williamson, G., & Kerimi, A. (2017). Chronic exposure to short-chain fatty acids modulates transport and metabolism of microbiome-derived phenolics in human intestinal cells. *J Nutr Biochem*, *39*, 156-168. doi: 10.1016/j.jnutbio.2016.09.009
- van Weeghel, M., Abdurrachim, D., Nederlof, R., Argmann, C. A., Houtkooper, R. H., Hagen, J., . . . Houten, S. M. (2018). Increased cardiac fatty acid oxidation in a mouse model with decreased malonyl-CoA sensitivity of CPT1B. *Cardiovasc Res*, *114*(10), 1324-1334. doi: 10.1093/cvr/cvy089
- Varga, T., Czimmerer, Z., & Nagy, L. (2011). PPARs are a unique set of fatty acid regulated transcription factors controlling both lipid metabolism and inflammation. *Biochim Biophys Acta*, *1812*(8), 1007-1022. doi: 10.1016/j.bbadis.2011.02.014
- Vork, M. M., Glatz, J. F., & Van Der Vusse, G. J. (1993). On the mechanism of long chain fatty acid transport in cardiomyocytes as facilitated by cytoplasmic fatty acid-binding protein. *J Theor Biol*, *160*(2), 207-222. doi: 10.1006/jtbi.1993.1014
- Vorum, H., Brodersen, R., Kragh-Hansen, U., & Pedersen, A. O. (1992). Solubility of long-chain fatty acids in phosphate buffer at pH 7.4. *Biochim Biophys Acta*, *1126*(2), 135-142.
- Wang, F., & Tong, Q. (2009). SIRT2 suppresses adipocyte differentiation by deacetylating FOXO1 and enhancing FOXO1's repressive interaction with PPARgamma. *Mol Biol Cell*, *20*(3), 801-808. doi: 10.1091/mbc.E08-06-0647

- Wasik, A. A., & Lehtonen, S. (2018). Glucose Transporters in Diabetic Kidney Disease-Friends or Foes? *Front Endocrinol (Lausanne)*, *9*, 155. doi: 10.3389/fendo.2018.00155
- Weisberg, S. P., McCann, D., Desai, M., Rosenbaum, M., Leibel, R. L., & Ferrante, A. W., Jr. (2003). Obesity is associated with macrophage accumulation in adipose tissue. *J Clin Invest*, *112*(12), 1796-1808. doi: 10.1172/JCI19246
- Welte, M. A. (2015). Expanding roles for lipid droplets. *Curr Biol*, *25*(11), R470-481. doi: 10.1016/j.cub.2015.04.004
- Wendel, A. A., Lewin, T. M., & Coleman, R. A. (2009). Glycerol-3-phosphate acyltransferases: rate limiting enzymes of triacylglycerol biosynthesis. *Biochim Biophys Acta*, *1791*(6), 501-506. doi: 10.1016/j.bbalip.2008.10.010
- Whitmore, C. (2010). Type 2 diabetes and obesity in adults. *Br J Nurs*, *19*(14), 880, 882-886. doi: 10.12968/bjon.2010.19.14.49041
- WHO. (2016). Global Report on Diabetes. 1 - 88.
- Wieringa, G., Zerah, S., Jansen, R., Simundic, A. M., Queralto, J., Solnica, B., . . . European Communities Confederation of Clinical, C. (2012). The EC4 European syllabus for post-graduate training in clinical chemistry and laboratory medicine: version 4--2012. *Clin Chem Lab Med*, *50*(8), 1317-1328.
- Wu, L., Xu, D., Zhou, L., Xie, B., Yu, L., Yang, H., . . . Li, P. (2014). Rab8a-AS160-MSS4 regulatory circuit controls lipid droplet fusion and growth. *Dev Cell*, *30*(4), 378-393. doi: 10.1016/j.devcel.2014.07.005
- Wu, Q., Ortegon, A. M., Tsang, B., Doege, H., Feingold, K. R., & Stahl, A. (2006). FATP1 is an insulin-sensitive fatty acid transporter involved in diet-induced obesity. *Mol Cell Biol*, *26*(9), 3455-3467. doi: 10.1128/MCB.26.9.3455-3467.2006
- Wu, Y., Ding, Y., Tanaka, Y., & Zhang, W. (2014). Risk factors contributing to type 2 diabetes and recent advances in the treatment and prevention. *Int J Med Sci*, *11*(11), 1185-1200. doi: 10.7150/ijms.10001
- Xu, H., Barnes, G. T., Yang, Q., Tan, G., Yang, D., Chou, C. J., . . . Chen, H. (2003). Chronic inflammation in fat plays a crucial role in the development of obesity-related insulin resistance. *J Clin Invest*, *112*(12), 1821-1830. doi: 10.1172/JCI19451
- Yaffe, D., & Saxel, O. (1977). Serial passaging and differentiation of myogenic cells isolated from dystrophic mouse muscle. *Nature*, *270*(5639), 725-727.
- Yang, Z. H., Miyahara, H., Takemura, S., & Hatanaka, A. (2011). Dietary saury oil reduces hyperglycemia and hyperlipidemia in diabetic KKAy mice and in diet-induced obese C57BL/6J mice by altering gene expression. *Lipids*, *46*(5), 425-434. doi: 10.1007/s11745-011-3553-1

- Yasa, I. C., Gunduz, N., Kilinc, M., Guler, M. O., & Tekinay, A. B. (2015). Basal Lamina Mimetic Nanofibrous Peptide Networks for Skeletal Myogenesis. *Sci Rep*, *5*, 16460. doi: 10.1038/srep16460
- Ye, X., Li, M., Hou, T., Gao, T., Zhu, W. G., & Yang, Y. (2017). Sirtuins in glucose and lipid metabolism. *Oncotarget*, *8*(1), 1845-1859. doi: 10.18632/oncotarget.12157
- Zacharewicz, E., Hesselink, M. K. C., & Schrauwen, P. (2018). Exercise counteracts lipotoxicity by improving lipid turnover and lipid droplet quality. *J Intern Med*. doi: 10.1111/joim.12729
- Zhang, C., & Liu, P. (2017). The lipid droplet: A conserved cellular organelle. *Protein Cell*, *8*(11), 796-800. doi: 10.1007/s13238-017-0467-6
- Zhang, S., Hulver, M. W., McMillan, R. P., Cline, M. A., & Gilbert, E. R. (2014). The pivotal role of pyruvate dehydrogenase kinases in metabolic flexibility. *Nutr Metab (Lond)*, *11*(1), 10. doi: 10.1186/1743-7075-11-10
- Zhou, Z., Menzel, F., Benninghoff, T., Chadt, A., Du, C., Holman, G. D., & Al-Hasani, H. (2017). Rab28 is a TBC1D1/TBC1D4 substrate involved in GLUT4 trafficking. *FEBS Lett*, *591*(1), 88-96. doi: 10.1002/1873-3468.12509
- Zierath, J. R., & Hawley, J. A. (2004). Skeletal muscle fiber type: influence on contractile and metabolic properties. *PLoS Biol*, *2*(10), e348. doi: 10.1371/journal.pbio.0020348
- Zurlo, F., Larson, K., Bogardus, C., & Ravussin, E. (1990). Skeletal muscle metabolism is a major determinant of resting energy expenditure. *J Clin Invest*, *86*(5), 1423-1427. doi: 10.1172/JCI114857

7 Appendix

7.1 Index of figures

Figure	Title	Page
Figure 1	Structural composition of skeletal muscles	4
Figure 2	Model representation of insulin signaling and insulin- and contraction induced GLUT4 translocation	6
Figure 3	Key reactions of fatty acid β -oxidation	10
Figure 4	Skeletal muscle metabolic flexibility	12
Figure 5	Peripheral lipid accumulation and the development of diabetes	14
Figure 6	Activity regulation of small Rab-GTPases	17
Figure 7	Domain structure and AKT/AMPK phosphorylation sites of mouse TBC1D1 and TBC1D4	19
Figure 8	Schematic overview over the IVE principle	36
Figure 9	C2C12 cell culture and usage time line	40
Figure 10	<i>In vitro</i> fatty acid oxidation assay	43
Figure 11	Representative GC fatty acid profiling result	49
Figure 12	Differentiation status of C2C12 cells	57
Figure 13	Palmitic Acid Uptake of C2C12 myotubes after siRNA-mediated <i>Tbc1d1</i> and <i>Tbc1d4</i> knockdown	58
Figure 14	Impact of the RabGAPs TBC1D1 and TBC1D4/AS160 on C2C12 skeletal muscle cell fatty acid oxidation	59
Figure 15	Short-chain fatty acid uptake into C2C12 cells under <i>Tbc1d1</i> and <i>Tbc1d4</i> -deficient conditions	60
Figure 16	Unsaturated long-chain fatty acid uptake into C2C12 cells under <i>Tbc1d1</i> and <i>Tbc1d4</i> -deficient conditions	61
Figure 17	<i>Tbc1d1</i> knockdown efficiency. and specificity	62
Figure 18	mRNA expression of skeletal muscle fatty acid uptake and binding proteins under <i>Tbc1d1</i> -deficient conditions	63
Figure 19	mRNA expression of skeletal muscle lipid degradation and	64

Figure	Title	Page
	synthesis proteins under <i>Tbc1d1</i>-deficient conditions	
Figure 20	mRNA expression of selected skeletal muscle transcription factors after a siRNA-mediated knockdown of <i>Tbc1d1</i>	65
Figure 21	mRNA expression of selected skeletal muscle mitochondrial genes involved in energy metabolism after a siRNA-mediated knockdown of <i>Tbc1d1</i>	66
Figure 22	mRNA expression of selected skeletal muscle genes involved in lipid storage and lipid droplet formation after a siRNA-mediated knockdown of <i>Tbc1d1</i>	67
Figure 23	mRNA expression of selected Rab GTPases and guanine nucleotide exchange factors under <i>Tbc1d1</i> knockdown conditions	68
Figure 24	Total fatty acid content of WT and D1KO <i>Gastrocnemius</i> muscle samples	69
Figure 25	Fatty acid profile of <i>Gastrocnemius</i> muscles from wildtype and TBC1D1 KO mice	70
Figure 26	Distribution of fatty acid classes in wildtype and D1KO <i>Gastrocnemius</i> muscles	71
Figure 27	Comparison of calculated desaturation activity indexes in <i>Gastrocnemius</i> muscles from WT and D1KO mice	72
Figure 28	Comparison of elongation and elongase activity indexes in <i>Gastrocnemius</i> muscles from WT and <i>Tbc1d1</i> -deficient mice	73
Figure 29	Comparison of indexes for lipid synthesis in <i>Gastrocnemius</i> muscle samples from WT and D1KO mice	74
Figure 30	Levels of malonyl- and acetyl-CoA of wildtype and <i>Tbc1d1</i> -deficient mouse <i>Gastrocnemius</i> muscles	75
Figure 31	Validation of siRNA-mediated knockdown of target candidate Rab GTPase genes in C2C12 myotubes	76
Figure 32	Role of distinct Rab GTPases in C2C12 myotube fatty acid uptake	78
Figure 33	Influence of insulin stimulation on C2C12 myotube fatty acid uptake under candidate Rab knockdown conditions	79

Figure	Title	Page
Figure 34	Impact of Rab8a on <i>EDL</i> and <i>Soleus</i> muscle <i>ex vivo</i> fatty acid oxidation	80
Figure 35	Impact of Rab10 on <i>EDL</i> and <i>Soleus</i> muscle <i>ex vivo</i> fatty acid oxidation	81
Figure 36	Influence of FATP1, FATP4 and FAT/CD36 on C2C12 myotube fatty acid uptake	83
Figure 37	Western blot analysis of FATP4, CD36 and PDK4 in wildtype and D1KO <i>EDL</i> muscle samples after <i>ex vivo</i> palmitate stimulation	85
Figure 38	Influence of fasting and feeding on the protein expression levels of FATP4, PDK4 and CD36 in WT and D1KO mouse <i>EDL</i> muscles	87
Figure 39	The role of TBC1D1, TBC1D4 and FAT/CD36 on <i>ex vivo</i> fatty acid uptake in mouse <i>EDL</i> and <i>Soleus</i> muscle	89
Figure 40	TBC1D1, TBC1D4 and FATP4 in regulating C2C12 myotube fatty acid uptake	90
Figure 41	Summary of the action of <i>RabGAP</i> -deficiency on lipid metabolism of skeletal muscle cells	107

7.2 Index of tables

Table	Title	Page
Table 1	Skeletal and cardiac muscle fatty acid binding and transport proteins	9
Table 2	Summary over the utilized experimental mouse strains	23
Table 3	Chemicals	24
Table 4	Radiochemicals	25
Table 5	Commercial reaction kits	26
Table 6	Utilized devices and tools	26
Table 7	Software used for measurements and quantifications	28
Table 8	Buffers, cell culture media and solutions	28
Table 9	siRNA oligonucleotides	29
Table 10	Utilized primary and secondary Western Blot antibodies	30
Table 11	Disposable material	30
Table 12	qRT-PCR Primer sequences	31
Table 13	Genotyping primers	34
Table 14	Seeding densities of C2C12 myoblasts prior to differentiation	39
Table 15	Reaction setup for genotyping D1KO mice	44
Table 16	Reaction setup for genotyping D4KO mice	45
Table 17	Reaction setup for genotyping CD36KO mice	45
Table 18	Genotyping thermocycler programs	45
Table 19	SDS-polyacrylamide gel preparation	47
Table 20	Fatty acid reference standard for gas chromatography	49
Table 21	cDNA synthesis incubation protocol	53
Table 22	qRT-PCR reaction setup	54
Table 23	qRT-PCR incubation protocol	54

7.3 Abbreviations

%	percent
≥	greater or equal than
°C	degree Celsius
Δ	delta
AA	arachidonic acid
AAV	adeno-associated virus
ACAD	acyl-CoA dehydrogenase
ACC	acyl-CoA carboxylase
AICAR	5-aminoimidazole-4-carboxamide-1-β-D-ribofuranoside
approx.	approximately
APS	ammonium persulfate
ATP	adenosine triphosphate
bp	base pair
Ca ²⁺	calcium ion
CaCl ₂	calcium chloride
CBD	calmodulin-binding domain
cDNA	complementary DNA
CH	Switzerland
CI	confidence interval
CoA	coenzyme A
CPT	carnitine palmitoyltransferase
Ct	cycle of threshold
D1/4KO	TBC1D1/TBC1D4 double knockout
D1KO	TBC1D1 knockout
D4KO	TBC1D4 knockout
ddH ₂ O	double distilled water
DGAT	diacylglycerol acyltransferase
DMEM	Dulbecco's modified eagle medium

DNL	<i>de novo</i> lipogenesis
EDL	<i>Musculus extensor digitorum longus</i>
e.g.	for example (<i>latin: exemplum gratum</i>)
ER	endoplasmic reticulum
FADH ₂	reduced flavin adenine dinucleotide
FAS	fatty acid synthase
FCS	fetal calf serum
FFA	free fatty acid
Fig.	Figure
Fwd	forward
GAP	GTPase activating protein
Gastroc	<i>Musculus gastrocnemius</i>
GC	gas chromatography
GEF	guanine nucleotide exchange factor
HRP	horseradish peroxidase
HS	horse serum
Hz	Hertz
i.p.	<i>intra peritoneal</i>
IRS	insulin receptor substrate
Kd	knockdown
KH ₂ PO ₄	potassium dihydrogenphosphate
KHB	Krebs-Henseleit buffer
KO	knockout
KRH	Krebs-Ringer-HEPES buffer
LC-MS/MS	liquid chromatography-mass spectrometry/mass spectrometry
LD	lipid droplet
LPL	lipoprotein lipase

M.	musculus (latin: muscle)
MAG	monoacylglycerol
MCD	malonyl-CoA decarboxylase
MeOH	methanol
Mg ²⁺	magnesia ion
MgSO ₄	magnesium sulfate
MilliQ	Millipore-filtered water
min	minute
ms	milli second
MT-ND2	Mitochondrial encoded NADH dehydrogenase 2
MUFA	mono unsaturated fatty acid
NADH	reduced nicotinamide adenine dinucleotide
NaHCO ₃	sodium hydrogen carbonate
NaOH	sodium hydroxide
NT	non-target
OXPHOS	oxidative phosphorylation
p	statistical probability value
P/S	Penicillin Streptomycin
pA	peak area
PBS	phosphate buffered saline
PCR	polymerase chain reaction
PDC	pyruvate dehydrogenase complex
PDPK1	3-phosphoinositide-dependent protein kinase 1
P _i	inorganic phosphate
PI3K	phosphatidylinositol-3-kinase
PM	plasma membrane
pmol	pico mole
PTB	phosphotyrosine-binding domain
PUFA	poly unsaturated fatty acid
qRT-PCR	quantitative real-time PCR

Rab	R as-related in b rain; small Rab GTPases
RabGAP	Rab GTPase activating protein
rcf	relative centrifugal force
Rev	reverse
RQ	respiratory quotient
RT	room temperature
SD	standard deviation
SDS	sodium dodecyl sulfate
SEM	standard error of the mean
Ser	serine
SFA	short chain fatty acid
si	siRNA
Soleus	<i>Musculus soleus</i>
t	time
T1DM	Type 1 <i>diabetes mellitus</i>
T2DM	Type 2 <i>diabetes mellitus</i>
TA	<i>Musculus tibialis anterior</i>
TBS-T	Tris-buffered saline with Tween-20
TEMED	tetramethylethylenediamine
Temp.	temperature
TG	triglycerides
Thr	threonine
V	Volt
VLDL	very low density lipoprotein
vol%	volume percent
w/	with
w/o	without
w/v	weight per volume
WHO	World Health Organization

7.4 Contribution to publications

- a) Zhou Z, Menzel F, **Benninghoff T**, Chadt A, Du C, Holman GD, Al-Hasani H (2016) “**Rab28 is a TBC1D1/TBC1D4 substrate involved in GLUT4 trafficking**”. FEBS Letters, doi: 10.1002/1873-3468.12509

Contribution: Co-performance of *ex vivo* glucose uptake assays (Fig. 3); co-performance of GLUT4 translocation assays (Fig. 4).

- b) Görgens SW, **Benninghoff T**, Eckardt K, Springer C, Chadt A, Melior A, Wefers J, Cramer A, Jensen J, Birkeland KI, Drevon CA, Al-Hasani H, Eckel J (2017) “**Hypoxia in combination with muscle contraction improves insulin action and glucose metabolism in human skeletal muscle via the HIF-1 α pathway**”. Diabetes, doi:10.2337/db16-1488

Contribution: Mouse hind limb *in vivo* electrotransfection (IVE) with *Hif1a*-specific siRNA; dissection of mouse *Soleus* muscle and performance of *ex vivo* glucose uptake assays (Supplementary Fig. 4).

- c) Goeddeke S, Knebel B, Fahlbusch P, Hörbelt T, Poschmann G, van de Velde F, **Benninghoff T**, Al-Hasani H, Jacob S, van Nieuwenhove Y, Lapauw B, Lehr S, Ouwens DM, Kotzka J (2018) “**CDH13 abundance interferes with adipocyte differentiation and is a novel biomarker for adipose tissue health**”. International Journal of Obesity, doi: 10.1038/s41366-018-0022-4

Contribution: Performance and supportive analysis of *in vitro* fatty acid uptake assays (Fig. 2B).

- d) Stermann T, Menzel F, Weidlich C, Jeruschke K, Weiss J, Altenhofen D, **Benninghoff T**, Pujol A, Bosch F, Rustenbeck I, Ouwens DM, Thoresen GH, de Wendt C, Lebek S, Schallschmidt T, Kragl M, Lammert E, Chadt A, Al-Hasani H (2018) “**Deletion of the RabGAP TBC1D1 leads to enhanced insulin secretion and fatty acid oxidation in islets from male mice**”. Endocrinology, doi: 10.1210/en.2018-00087

Contribution: Performance of *ex vivo* fatty acid oxidation assays with isolated primary mouse islets (Fig. 6A and 6B).

Further, parts of this thesis shall be published in a separate paper. The manuscript is currently under preparation:

- e) **Benninghoff T**, Zeinert I, Sinowenka I, Schöndeling C, Batchelor H, Zhou Z, Chadt A, Al-Hasani H (in preparation) Working title: **“The control of the RabGAP TBC1D1 over skeletal muscle lipid metabolism is specific for long-chain fatty acids and dependent on fatty acid transporter FATP4”**.

7.5 Acknowledgements

Meine persönliche Danksagung ist nicht Gegenstand meiner wissenschaftlichen Arbeit.
Ich sehe daher für diesen Abschnitt von einer Veröffentlichung ab.

Eidesstattliche Erklärung

Hiermit erkläre ich, dass ich die vorliegende Dissertation selbstständig und ohne fremde Hilfe unter Beachtung der „Grundsätze zur Sicherung guter wissenschaftlicher Praxis an der Heinrich-Heine-Universität Düsseldorf“ verfasst habe. Es wurden nur die angegebenen Quellen und Hilfsmittel benutzt. Wörtlich und inhaltlich übernommene Gedanken wurden als solche kenntlich gemacht.

Düsseldorf, den 05. Dezember 2019

Tim Benninghoff